Effect of space conditions on neuronal plasticity and connectivity

Giuseppe Pani

2013

ISBN 978-9-0598962-4-6

Effect of space conditions on neuronal plasticity and connectivity

Giuseppe Pani

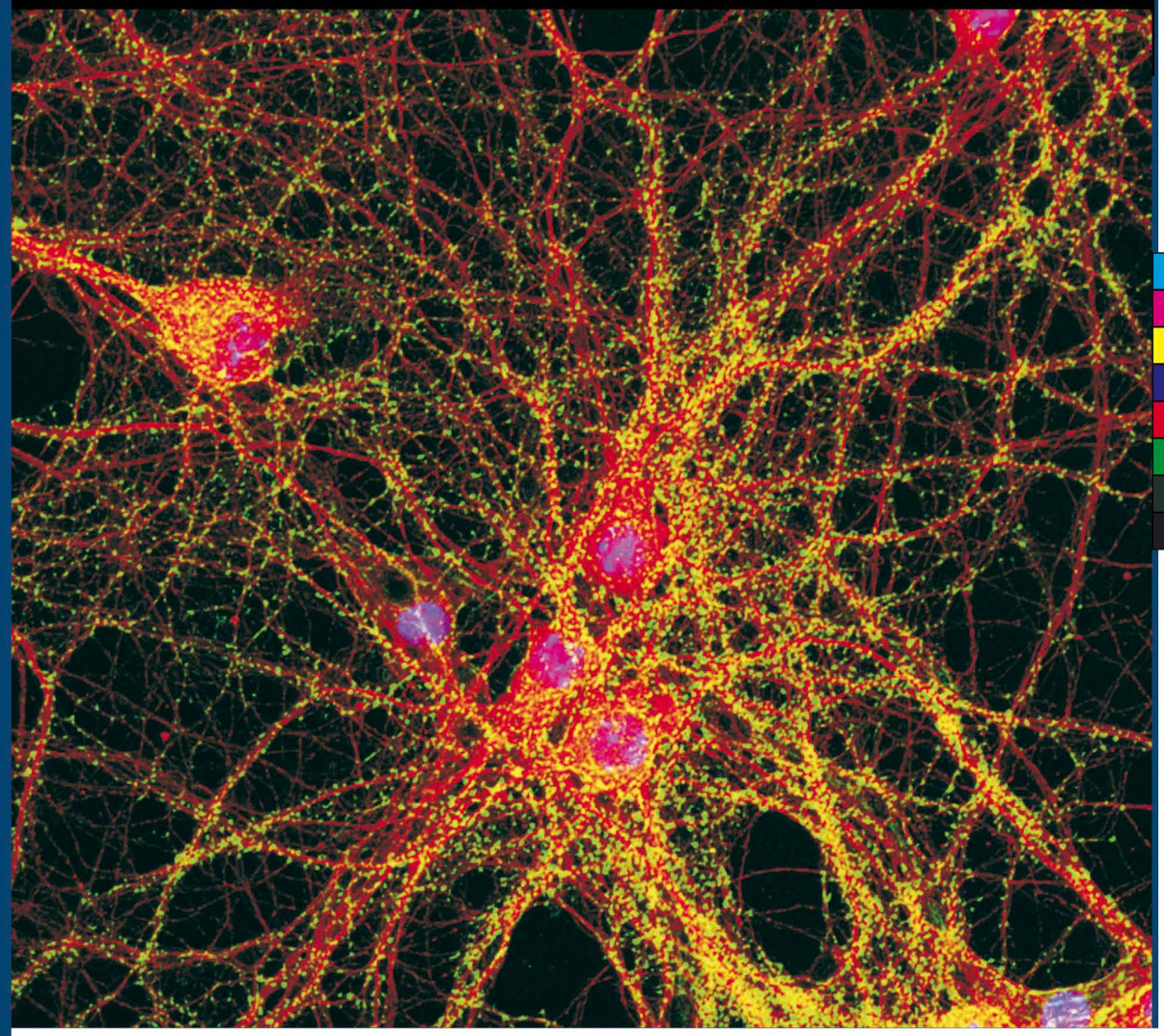

UNIVERSITEIT GENT

FACULTEIT BIO-INGENIEURSWETENSCHAPPEN

Talvolta è meglio perdersi sulla strada di un viaggio impossibile piuttosto che non partire mai.

Sometimes it is better to get lost on the way of an impossible journey rather than to have never left.

Giorgio Faletti

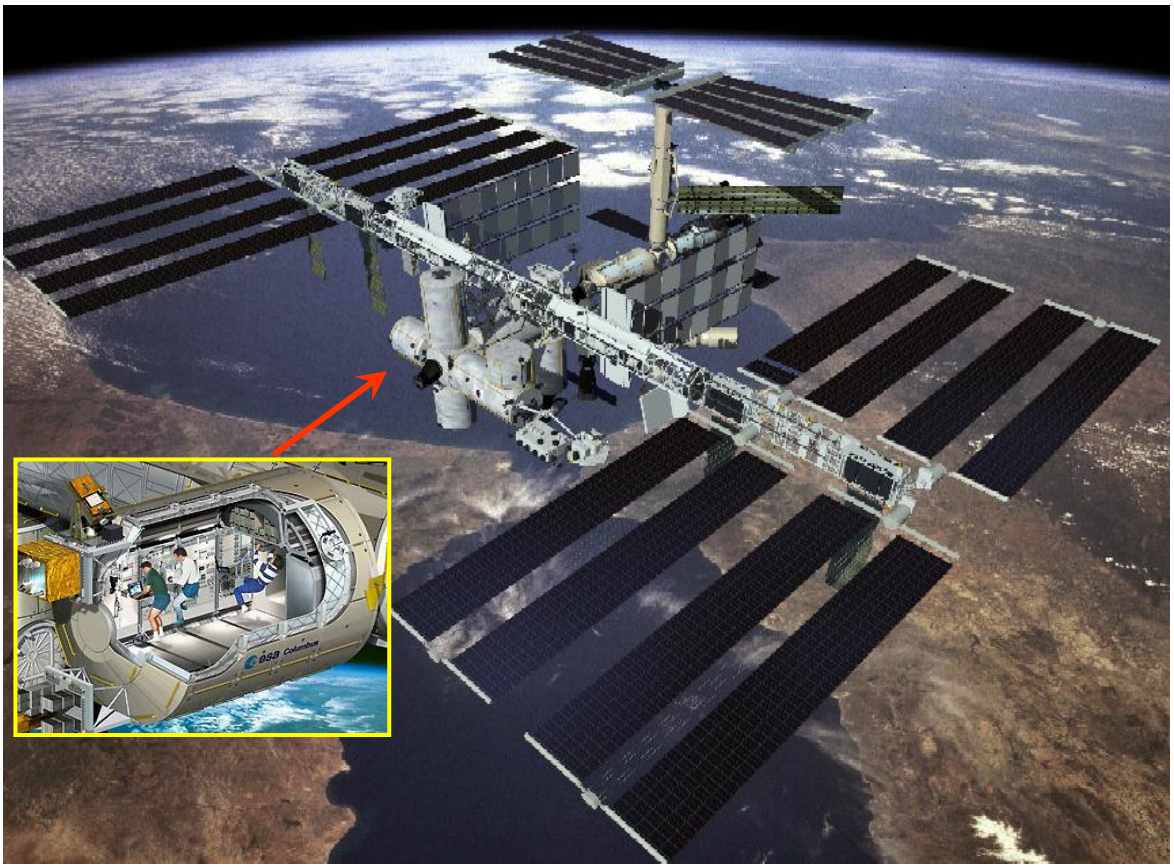

Promoters:

Prof. Dr. Sarah Baatout
Radiobiology Unit
Belgian Nuclear Research Centre
SCK•CEN
Boeretang 200
B-2400 Mol
sbaatout@sckcen.be

Bio-imaging and Cytometry (BW14)
Department of Molecular Biotechnology
Faculty of Bioscience Engineering
653 Coupure Links
B-9000 Ghent

Prof. Dr. Patrick Van Oostveldt
Bio-imaging and Cytometry (BW14)
Department of Molecular Biotechnology
Coupure links 653
B-9000 Ghent
patrick.vanoostveldt@ugent.be

Dr. Mohammed Abderrafi Benotmane
Radiobiology Unit
Belgian Nuclear Research Centre
SCK•CEN
Boeretang 200
B-2400 Mol
abenotma@sckcen.be

SCK•CEN Co-mentor:

Dr. Louis de Saint-Georges
Radiobiology Unit
Belgian Nuclear Research Centre
SCK•CEN
Boeretang 200
B-2400 Mol

Dean: Prof. Dr. Ir. Guido VAN HUYLENBROECK

Rector: Dr. Paul Van CAUWENBERGE

Regione autonoma della Sardegna

Effect of space conditions

on

neuronal plasticity and connectivity

Giuseppe Pani

Thesis submitted in fulfilment of the requirements for the degree of Doctor (PhD)

in Applied Biological Sciences

Cover illustration

Mouse cortex primary neurons cultured for 10 days were stained for the post-synaptic protein PSD-95 (green), as well as for the cytoskeleton protein β-Tubulin III (red) and nuclei (blue). Staining and acquisition were performed by Giuseppe Pani.

This image has been submitted to the International Antibody Image Competition organized by Sigma Aldrich and was selected so far for the semifinal that includes the best 12 pictures received. The results of the final will be known at the end of June 2013.
Cover art design by Giuseppe Pani

Giuseppe Pani (2013). Effect of space conditions on neuronal plasticity and connectivity. PhD Thesis. Ghent University.

ISBN: 978-90-5989-624-6

Members of the Examination Committee

Prof. Dr. Sarah Baatout (Promoter)
Radiobiology Unit, Belgian Nuclear Research Centre (SCK•CEN)
Bio-imaging and Cytometry, Department of Molecular Biotechnology, Faculty of Bioscience Engineering

Prof. Dr. Patrick Van Oostveldt (Promoter)
Bio-imaging and Cytometry, Department of Molecular Biotechnology, Faculty of Bioscience Engineering, Ghent University

Dr. Mohammed Abderrafi Benotmane (Co-promoter)
Radiobiology Unit, Belgian Nuclear Research Centre (SCK•CEN)

Prof. Dr. Ir. Frank Devlieghere (Chairman)
Department of Food Safety and Food Quality, Faculty of Bioscience Engineering, Ghent University

Prof. Dr. Ir. Tom van de Wiele (Secretary)
LabMET, Biochemical and Microbial Technology, Faculty of Bioscience Engineering, Ghent University

Dr. Daniela Santucci
Section of Behavioural Neurosciences, Department of Cell Biology and Neurosciences, Istituto Superiore di Sanità, Rome, Italy

Prof. Dr. Evelyne Meyer
Department of Pharmacology, Toxicology and Biochemistry, Faculty of Veterinary Medicine, Ghent University

Prof. Dr. Luc Leybaert
Department of Basic Medical Sciences, Faculty of Medicine and Health Sciences, Ghent University

Prof. Dr. Ir. Sofie Bekaert
Clinical Research Centre, Faculty for Medicine and Health Sciences, Ghent University

Dr. Ir. Winnok H. De Vos
Bio-imaging and Cytometry, Department of Molecular Biotechnology, Faculty of Bioscience Engineering, Ghent University

Prof. Dr. Jo Lambert
Department of Dermatology, Faculty of Medicine and Health Sciences, Ghent University

Table of contents

Table of figures

List of tables

Abbreviations

Ann V	Annexin V
ARS	Acute Radiation Syndrome
BASC	Brca1-associated surveillance complex
BDNF	Derived neurotrophic factor
BER	Base excision repair
BSA	Bovine serum albumin
β-tub 3	β-tubulin 3
Cdks	Cyclin-dependent protein kinases
CMEs	Coronal mass ejections
CNS	Central nervous system
CRS	Chronic radiation syndrome
CT	Computational tomography
DNA	Deoxyribonucleic acid
DSBs.	Double strand breaks
EDF	Extended Depth of Focus
ESA	European Space Agency
FD N°	Flight day N°
FITC	Fluorescein isothiocyanate
GC	Ground Control samples
GCRs	Galactic cosmic rays
GO	Gene ontology
Gy	Gray
HR	Homologous recombination
HZE	High-Z and high-energy particles
ICRP	International Commission on Radiation Protection
IL-2	Interleukin-2
IR	Ionizing radiation
IRIF	Ionizing radiation-induced foci
ISS	International Space Station
Kibo	Japanese Experimental Module
LEO	Low-Earth’s orbit
LET	Linear energy transfer
LiMiD	Light Microscopy Division
LNT	Linear non-threshold
LTD	Long-term depression
LTP	Mechanisms, long-term potentiation
MDS	Mice Drawer System
MIA	Motion and InterAct
MMR	Mismatch repair
MNN	MorphoNeuroNet

MnSOD	Manganese-containing superoxide dismutase
MRI	Magnetic resonance imaging
NER	Nucleotide excision repair
NF	Neurofilament
NGF	Neuron growth factor
NHEJ	Non-homologous end joining
PBLs	Neripheral blood lymphocytes
PBS	Phosphate buffered saline
PC12	Rat pheochromocytoma
PFA	Paraformaldehyde
PI	Propidium iodide
PMMA	Polymethylmethacrylate
PNS	Peripheral nervous system
PSD	Postsynaptic density
RIN	RNA Integrity Number
RNA	Ribonucleic acid
ROI	Region of interest
ROS	Reactive oxygen species
RPM	Random Positioning Machine
RWV	Rotating Wall Vessel
SAS	Space Adaptation Syndrome
SCK•CEN	Belgian Nuclear Research Centre
SD	Spreading depression
SH-SY5Y	Cell lines as human neuroblastoma
SI	International System of Units
SMS	Space Motion Sickness
SNR	Signal-to-noise ratio
SPEs	Solar particle events
SSBs	Single strand breaks
Sv	Sievert
TLD	Thermoluminescent dosimetry
UV	Ultraviolet
VITO	Flemish Institute for Technological Research
wT	Tissue weighting factor
γ-H2AX	Phosphorylated histone 2AX

Chapter I | Introduction

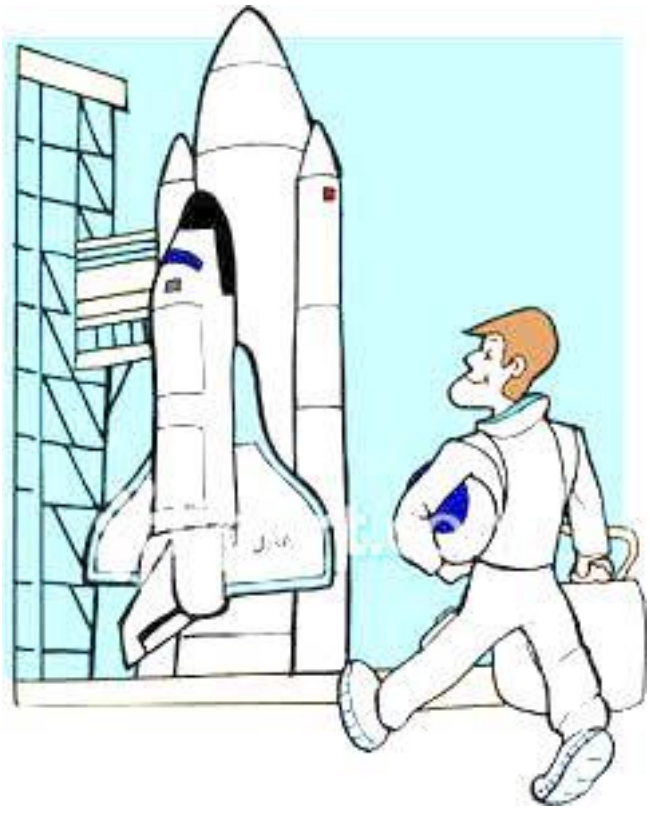

Introduction

1. Human spaceflight

On October 4, 1957, the Soviet satellite Sputnik was launched from the cosmodrome of Baikonur. Opening the space exploration age, the Sputnik was the world's first artificial satellite and the first man-made object to be placed into the Earth's orbit.

On November of the same year, the dog Laika was the first animal in orbit on board the Sputnik II, launched from the cosmodrome of Baikonur. On April 12, 1961, Yuri Gagarin, a Soviet cosmonaut, took off to the space aboard the Vostok for the first human space flight, closing the mission 108 minutes later. As the first human being in space, doing a full turn of the Earth, he showed that humans can fly over the atmosphere.

Although the first human space flight was in 1961, space biology is a relatively young discipline. It was born with the first dedicated space missions and the use of space vectors designed for the biological experiments to be performed in weightlessness conditions:

- SpaceLab SL-1, first American space lab placed aboard the Space Shuttle (1983)
- Salyut 7, first Russian space laboratory aboard the automated bio-satellite (1983)
- Sounding rockets, Maser (1989) and Maxus (1991)

The building of space stations as Salyut (1971-1986), Skylab (1973-1979), Mir (1986-2000) and the International Space Station (ISS; 2000 - Present) offered new opportunities for space research since these allowed to increase the permanence in space until six or more months. During the permanence in space, astronauts are exposed to the two main space conditions, known as microgravity and cosmic radiations. Since the first human space flight, researchers tried to understand the effects of space environment on human physiology and to develop appropriate countermeasures. These effects can be really deleterious for human health, in

particular in future long term space missions, such as towards Mars, during which astronauts will be exposed to the deep space radiations and microgravity for more than one year.

1.1. Low gravity conditions

To demonstrate that the falling time of bodies was independent of their mass, Galileo dropped balls of the same material, but of different masses, from the Leaning Tower of Pisa. Later he determined the gravity acceleration, namely the "attraction force of bodies" which is the fall towards the Earth centre. The estimated gravitational acceleration was, and still is 9,82 m/s^2.

The "gravitational field" law, deduced by Isaac Newton in 1666, stated that forces which keep planets in their orbits must be reciprocal to the squares of their distances from the centres about which they revolve [1]. Therefore, the further away bodies are situated from the Earth the least they feel gravity acceleration; indeed, in deep space the gravitational acceleration is theoretically close to 0.

1.1.1. Real and simulated microgravity facilities and instruments

To presume the presence of weightlessness condition in orbiting spacecrafts because they are "in space" or "outside the Earth's atmosphere" is a common mistake. Indeed, although it might seem that they are "far" away enough from the Earth, they are actually only 300-500 km in orbit around the planet surface.

All the satellites, which orbit around our planet, are continuously attracted by the Earth and if they did not have any motion of their own, they would fall back to the ground. Practically, satellites move along a linear trajectory that keeps them away from the Earth, pushed by a certain power (e.g. ISS speed is about 28000 km/h) proportional to their mass and the distance from the planet centre: the trajectory is constantly curved towards the Earth allowing satellites to orbit around the planet. The typical gravity on board satellites or spacecrafts at an altitude of 350 km is still 9.08 m/s^2, 8% less than the gravitational acceleration on the Earth, but since they move

along the propulsion trajectory, with the centrifugal force making the condition created aboard, a continuous free fall, known also as “microgravity” or “low gravity” condition is taking place (Fig. 1). Therefore, the gravity condition generated into the spacecraft or the ISS is similar but not equal to the weightlessness condition, which is available only in deep space where gravity forces are absent [2]. The first thought which expressed the “free fall condition” was made by Albert Einstein in 1907. As written in "the happiest thought of my life", he realized that a body which is falling down experiences no gravitational field, therefore, gravitation was exactly equivalent to acceleration.

More than 200 European experiments have been carried aboard the ISS until 2008. That year, a new ESA module, the **Columbus** laboratory, was connected to the station. The Columbus

Figure 1: Scheme representing the gravitational force (green arrow) and propulsion force (blue arrow) which both act on satellites to generate the satellite orbit (red arrow). (Drawn by G. Pani)

module is equipped with a suite of flexible multiuser facilities that offer extensive research capabilities to perform medical, biological and physics experiments [3]. ESA developed for the Columbus module a range of research racks to offer European scientists full access to a low gravity environment which cannot be reproduced on Earth. Furthermore, other facilities from NASA, Canadian, Russian and Japanese agencies are available aboard the Station.

Other orbital research platforms used also for biological experiments are the Russian **Foton** and **Bion** types of recoverable unmanned capsules [4]. A typical Foton mission lasts about 12–18 days and all experiments on board have to be fully automated with telemetry allowing for up and downlink capabilities for command and control of payloads as well as experiment parameters. All the experiments are placed in the spacecraft’s Re-entry Module [4].

Non-orbital low gravity platforms like sounding rockets, parabolic flight airplanes and drop towers are also available to conduct experiments on reduced gravity conditions. The **sounding rockets** were originally developed to "sound" the upper atmosphere and are used since the late 1950's. The rocket goes up until the moment it falls back to the Earth. The low gravity period, between 6 and 15 minutes, is just before the re-entry phase and the free fall ends when it re-enters into the atmosphere. Here as well, all the experiments should be partially or fully automated [4]. The **parabolic flights** are performed by airplanes which perform up to 30 parabolas, reproducing the gravitational acceleration of 0.16 g for approximately 23 s or 0.38 g for approximately 30 s per parabola. Each low gravity period is preceded and followed by 20 s of hypergravity (1.8-2 g). These parabolic flights are used not only to train astronauts or test instruments before spaceflights but also to allow researchers to directly perform medical, biological or physical experiments in such environment [4]. **Drop towers** give the opportunity to perform a variety of experiments requiring only a limited exposure (few seconds) to low gravity. In this facility, a capsule falls down into a 146 m dropping tower [4].

To model the gravity on Earth, methods, like bed rest or tail suspension, or facilities, like free fall machines or clinostats, have been developed to provide reproducible and low cost alternatives. In particular, the **bed rest** method is used to simulate the effect of microgravity on the human body. The physiological effects, like bone or muscle mass loss or fluid shift are obtained in bed tilted at 6° for a long period with the feet higher than the head, and are simulating microgravity effects observed in astronauts during space flight [5, 6]. The **tail suspension** is a method to replace the bed rest where the study is performed on rodents. Rodents are partially suspended for a long period by their tails wrapped with adhesive tape [7]. Experiments on small animals or cell cultures can also be performed using 2D or 3D clinostats. These facilities continuously and randomly change the gravity vectors modifying the direction of rotation. The **2D clinostat** rotates only along one axis and can reproduce, like in the Rotating Wall Vessel (RWV), a continuous free fall condition of sedimentation and of gravity. The 3D

Random Positioning Machine (RPM) (Dutch Space) (Fig. 2) allows to modify the gravity vector by random rotations along 2 axes. The RPM is based on the principle of 'gravity-vector-averaging' and in its centre, the gravity vector (resulting from such random rotation) is reduced by a factor around 10^{-3}-10^{-4}. A broad number of experiments performed with RPM or RWV have similar results as in space conditions [8]. The selection of the device to perform experiments in simulated microgravity is related to the experiment itself [8].

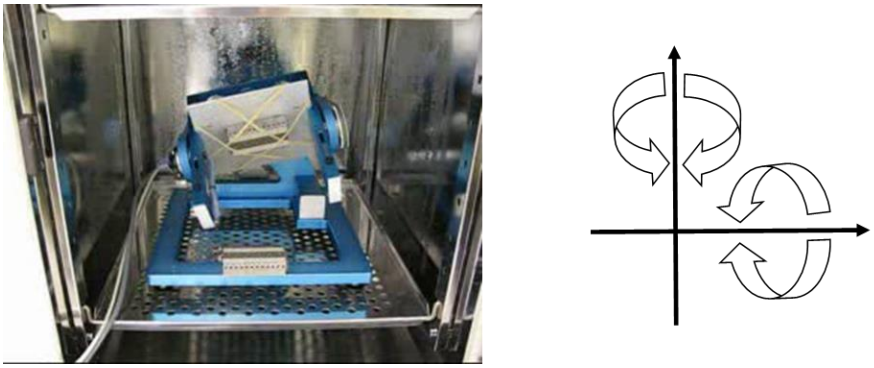

Figure 2: Desktop Random Positioning Machine.
Left: the RPM inside the incubator. Right: sketch of the 3D rotation along 2 axes. (picture taken and drawing by G. Pani)

1.1.2. Human body response to the gravitational change

During space journeys in spacecraft's, astronauts are constantly exposed to space conditions (cosmic rays and microgravity). Exposure to microgravity has been shown to adversely affect several aspects of human physiology. To identify physiological disorders that it can induce, astronaut's health was monitored throughout daily work or under routinely physical exercises. Specific tests on muscles, bones, heart, lungs, immune system, neuronal system and the sense organs have been performed to better understand the human body response to microgravity conditions.

The first response of human body to space environment is Space Motion Sickness (SMS), which is experienced by more than 70% of astronauts during their first spaceflights and less in trained astronauts [9]. SMS is a cumulative response of body changes. It occurs from the first hours of spaceflight onwards and it shows several symptoms as postural illusion, visual

disturbances, nausea and headaches, neuromuscular fatigue and weakness as well as postural imbalance and ataxia [1][10]. After 3-5 days, most astronauts have recovered or begun to recover from the "acute symptoms" that appeared during short-term exposure, and are able to move without feeling weakened [10]. Throughout the long spaceflight missions, "sopite symptoms" as chronic drowsiness, fatigue, mood and personality changes persist. After acute space sickness symptoms disappear, these sopite ones might affect for a long time the astronaut's skills to execute sophisticated tasks [11].

Throughout spaceflights, several systems (out of which musculoskeletal, sensory-motor, cardiovascular and immune systems) are affected due to the reduced gravity (Table 1 page 13).

1.1.2.1. Musculoskeletal system.

In the past decades, the musculoskeletal system represented one of the most studied microgravity research topics. Since the first spaceflights, muscular atrophy and decreased bone mass (which lead to the early onset of osteoporosis) were reported in astronauts [12-15].

Within the first days in microgravity, a reduction in muscle activity is already detectable and progresses throughout the whole duration in space [16]. Microgravity affects muscles that play a postural role in ground gravity condition, and are known as antigravity muscles [17-19]. Other studies showed that also extensor [19] and flexor [20] muscles are affected by microgravity. However, all the skeletal muscles appeared to be proportionally affected by low gravity during long space missions [21]. Although the level of muscle reduction is dependent to the muscle activity, microgravity affects muscle fibres with different proportion [16]. Studies on animals and humans reported that type I fibres (slow and resistant to fatigue) as well as type II fibres (type IIa, fast and resistant to fatigue, and type IIb, fast and sensitive to fatigue) are affected by microgravity [17, 19, 20, 22]. Kalb and Solomon [19] proposed that the observed muscle reduction in microgravity can be induced by three sets of factors. The first is the probable decrease of muscle gene expression and protein production due to the reduction of the gravity

[1] Ataxia is a neurological sign consisting of lack of voluntary coordination of muscle movements.

load. The second is the impairment in neural drive to the muscle. The third set is represented by systemic factors as hormone alteration and changes in metabolism [19, 23]. Upon return to Earth, astronauts need time to recover from a space environment experiencing weakness and delayed onset muscle soreness. Myopathology of muscles as interstitial oedema, macrophage activities and fibre necrosis have also been reported several days after landing [19].

Bone is an active tissue in continuous remodelling, bone architecture being directly related to the mechanical stresses which are exerted on it. In reduced gravity conditions, these stresses are of less magnitude or non-existent and induce a severe instability between bone formation and bone resorption. It is approximately estimated that 1-2% of total bone mass is removed and lost in a month under low gravity conditions [15]. In long-term spaceflight (180 days) all bone formation parameters were decreased whilst bone resorption markers were increased [14]. Decrease of bone formation and increase of bone demineralization were primarily found on weight-bearing bones [13, 15]. Therefore, astronauts perform daily exercises with special gymnastic machines as countermeasure to muscle atrophy and bone mass reduction.

1.1.2.2. Sensory-motor system

The sensory motor neurons are one of the most critical systems affected by the reduction of gravity during spaceflight. Throughout long space travel, the sensory motor system partially recovers from exposure to low gravity and this may have some effects both on the astronauts and on the final result of the mission. The reorganization of the three main sources of spatial information (visual, somatosensory and vestibular systems) is necessary for human beings to adapt to the new space environment.

It was reported that in reduced gravity conditions, signals from the central vestibular system, peripheral pressure receptors and visual cues become misleading to a point where disorientation occurs. Therefore, visual reference aboard the spacecraft becomes important for astronaut orientation [24]. The incoming input conflict experienced by astronauts induces a

condition known as Space Adaptation Syndrome (SAS) which is the major cause of Space Motion Sickness (SMS). The perception of position and locomotion are the final result of the central nervous system ability to merge the auditory and visual signals with vestibular input and proprioceptive information as motion, temperature and pressure in muscles and skin [19, 25].

1.1.2.3. Cardiovascular system

The cardiovascular system includes the heart, the circulatory system as well as blood and is linked to the lymphatic system. It is responsible for the supply of oxygen and energy to the organs and tissues and for the removal of the metabolic waste products [26]. Spaceflight induces significant effects on the cardiovascular system. The loss of gravitational forces that occurs throughout space travels causes a fluid shift from the lower to the upper part of the body which induces the characteristic facial oedema within the first days of microgravity conditions [26]. The head-ward fluid redistribution induces thin legs [26] (Fig. 3). Furthermore, due to the fluid shift, cranial veins dilate misleading the blood volume sensors which interpret this event as an increase of the blood volume followed by hypervolemia activation [27]. Indeed, decreased blood

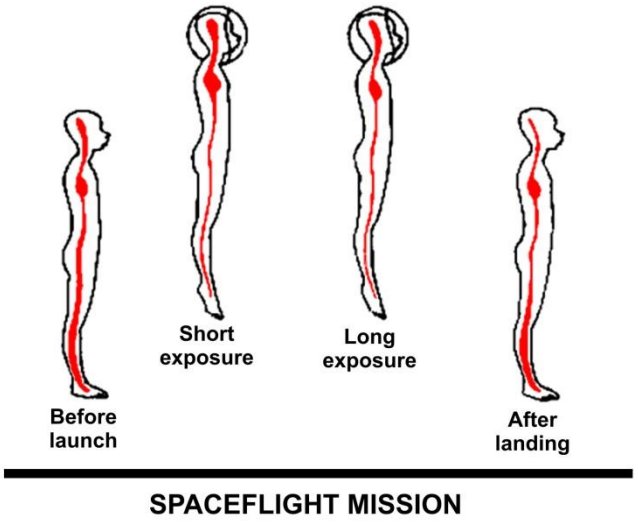

Figure 3: Fluid distribution in the human body during a spaceflight.
(a) On Earth, gravity exerts a downward force to keep fluids flowing to the lower body. (b) In space, the fluid tends to redistribute towards the chest and the upper body. At this point, the body detects an "overflow" in and around the heart. (c) The body rids itself of this perceived "excess" fluid. The body functions with less fluid and the heart becomes smaller. (d) Upon return to Earth, gravity again pulls the fluid downward, but there is not enough fluid to function normally on Earth (Drawing modified from *[26]* by G. Pani).

volume (hypovolemia) was reported after spaceflight in conjunction with orthostatic intolerance [28] and the plasma volume was shown to be decreased of about 10-17 % [29]. In addition, studies in animals and astronauts found a consistent decrease in heart rate during spaceflight [30, 31]. Finally, blood analysis showed reduction of plasma catecholamines which are linked to the muscle sympathetic activity and also correlated to diastolic pressure and heart rate [32, 33].

1.1.2.4. Immune system

The immune system consists in immunological cells, lymph nodes and organs which are also altered under space conditions. Regulation and efficiency changes can have important effects on the ability to protect the human body from invasion of foreign pathogens. Impairment of the immune system can induce secondary immunodeficiency and raise the risk of developing bacterial or viral infections [34]. In the last 30 years a large variety of experiments on lymphocytes reported that immune system cells are influenced by space environment with a reduction in proliferation and cytokine production [35, 36]. An impaired mitogenic activation in microgravity was also reported [35, 37]. The cell-to-cell interaction of lymphocytes with associated cells as monocytes plays an important role in their activation. Indeed, the reduced activation of lymphocytes might be due to the impaired monocyte motility under low gravity [38]. Furthermore, an increase in apoptosis level was observed in T-lymphocytes exposed to real or simulated low gravity [39]. Gene expression and proteomic analysis underline a decreased secretion of IL-1 and IL-2, interferon and other cytokines [40-42] and a reduced production of α-chain of interleukin 2 receptor [36]. Studies on rats and mice exposed to microgravity reported a hypoplasia[2] of lymphoid organs like thymus, lymph nodes and spleen, subsequently associated with a reduced number of lymphocytes and erythrocytes [41, 43, 44].

The immune system is also involved in repeated wounds. During these events, blood enters the wound site and brings with it cellular elements and plasmic constituents [45-47]. Studies on

[2] Hypoplasia is underdevelopment or incomplete development of a tissue or organ. Sometimes it refers to an inadequate or below-normal number of cells.

intrinsic wound healing in rats reported that matrix formation in induced subcutaneous injuries was significantly inhibited under spaceflight conditions [48]. Additionally, an altered capacity to produce an adequate population of macrophages and a reduced collagen concentration in the wound has been reported. Due to the importance of collagen for wound strength, migration of certain cell types and angiogenesis, the reduced wound collagen content might affect the ability of a wound to heal successfully under spaceflight conditions [48].

In addition to microgravity, immune system impairment can be increased by other stress factors such as radiation, anxiety, heavy work load and sleep deprivation [41, 49]. Modified diet and physical exercises are considered as a countermeasure to immune deficiency induced by spaceflight environment and in a group of female volunteers subjected for 60 days to the bed rest test, an increased production of primary antibody was observed [50].

1.1.3. Cell response to the gravitational change

Since basic life is developed in a gravitational environment and that the majority of cell processes are influenced by gravitational field, an adaptive process is expected in cells exposed to microgravity. One of the aims of space cell biology programs is to understand the mechanisms involved in the perception and the translation of mechanical signals as gravity.

Several investigations performed in real or simulated microgravity reported morphological and functional changes in cells. As observed, microgravity can induce a certain variety of changes related to proliferation, differentiation, adhesion, cytoskeleton, migration and cell death [35, 38, 51, 52]. The first biological experiments took place in 1985 aboard the SpaceLab and reported a drastic reduction in lymphocyte proliferation [35, 53]. Further studies on other cell types, adherent and non-adherent, exposed to real or simulated microgravity confirmed a general reduction in proliferation [12, 54, 55].

In all adherent cells, cell shape, adhesion and motility are important for growth and cell-to-cell interaction. Furthermore, these three processes are cytoskeleton-dependent. The organization

and the production of the three main structures of cytoskeleton, microfilaments, microtubules and intermediate filaments, are altered in low gravity [38, 51, 56] and it induces several changes in cell shape, adhesion and motility [57-59]. Therefore, it has been hypothesized that cytoskeleton is one of the sensing cell systems directly linked to gravitational changes [60]. Moreover, it seems that microgravity plays an important role in the signalling pathways activated by growth factors, adhesion integrin's and Rho signalling [61-63]. Additionally, Rho Gases regulate motility related functions as well as proliferation and gene expression.

Another important factor observed in low gravity is the increased cell death [64-66], described in both *in vivo* and *in vitro* studies [67, 68]. Cell death has also been reported to be induced by oxidative stress [66] and development of premature senescence [69-71] in microgravity conditions.

Table 1. Effects of microgravity on systems and cells

Systems	**Cells**
• Decreased bone mass • Decreased muscle mass • Deconditioning of posture and gait control • Deconditioning of motion sensors and loss of balance • Deconditioning of the somatosensory system • Changes of cardiovascular activity and decreased plasma volume followed by hypovolemia • Head-ward fluid redistribution • Impaired immune system • Impaired wound healing	• Impaired proliferation • Changes in differentiation • Reduced cell motility • Cytoskeletal alterations • Apoptosis • Down- and up-regulation of genes

1.2. Space radiations

1.2.1. Cosmic and solar radiations

In the 1960's scientists became aware of ionizing space radiation generated from three different origins: cosmos, sun and Earth. The early developments of electroscopes described in the pioneering works of Pierre Curie allowed the assessment of microcurrents of particles

crossing the atmosphere. In 1910, the Italian physicist Pacini suggested that electroscopes measured the background noise due to the Earth ground [72]. In the following years, Wulf demonstrated that at the top of the Eiffel tower half of the radiation emitted by the Earth ground had disappeared. Later, with a balloon experiment, Hess reported that the natural radiation in the atmosphere gradually decreased up to 1 km and increased again above 1.8 km, suggesting an income of extra-terrestrial radiations. Furthermore, he demonstrated that the increase of radiations is time independent and almost absent during solar eclipse events. The existence of radiations generated by cosmos was demonstrated for the first time in 1947 and the term "cosmic rays" was used lately by Millikan [73].

Gilbert, Gauss and Poincaré hypothesized that charged particles may be influenced by the Earth's magnetism and that it exists as a ring around the Earth. The experimental proofs came with the Explorer I satellite and thereafter Pioneer IV. In 1958, these experiments allowed Van Allen and Franck to point out the existence of the Earth's radiation belt named "Van Allen belt" and the fact that this belt acts as a shield against charged particles [74, 75].

It is actually known that the Earth is continuously hit by high-energy ionized particles coming from outer space and it is protected by the magnetic belt and the atmosphere. The average dose from cosmic radiation on Earth's surface is merely 0.3 mSv/year. This dose is relatively low compared to the average Belgian dose of 4.6 mSv/year generated by natural and man-made sources of radiation (medical exposures, atomic bombs, nuclear accidents, etc…) [76]. However, an elevated dose of ionizing radiation with high energy (0.2 mSv/day) is received by astronauts in space [77]. Therefore, cosmic rays represent an important barrier to exploration of the solar system by human beings, since high-energy space radiations may have deleterious biological effects. The environmental radiation in space is typified by a wide variety of primary particles covering an extended range of energies. When passing through the mass of a spacecraft and its contents, these particles can participate in a number of different types of nuclear

interactions, producing a complex complement of both charged and neutral secondary particles [78].

The three principal sources of primary ionizing radiation in space are: (1) galactic cosmic rays (GCRs), (2) energetic electrons and protons of the Earth's trapped radiation belts, and (3) solar particle events (SPEs) [78]. Space radiations are composed of particles with a wide range of charges and energies which are produced mainly by GCRs (Fig. 4).

Between 1960's and 1970's the technological developments of particle counters allowed to determine the composition of cosmic radiation reporting that primary cosmic rays consist in very energetic (10^8-10^{20} eV) protons and nuclear particles of atomic numbers and heavy ions up to 40 MeV [79-82].

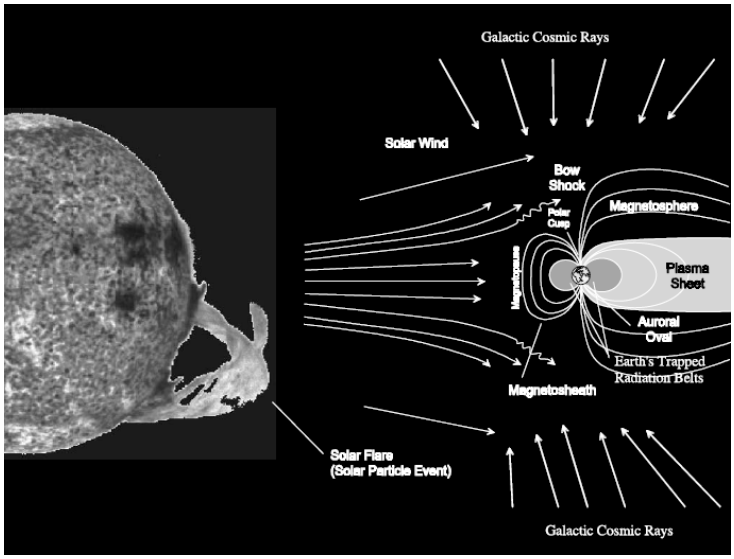

Figure 4: The three principal sources of space radiation: galactic cosmic radiation, solar wind and solar flare. The Earth magnetic field affects space radiations protecting the Earth [82].

Galactic cosmic rays (GCRs) are high energy particles coming from far away in the galaxy flowing into our solar system. The intensity of the GCRs is partly decreased by the magnetic field associated with the Sun's solar wind and by the Earth's magnetic field. There is no information about their source direction since these particles are scrambled by irregular interstellar magnetic fields on their way towards our planet. Due to their high energies, up to 10^{20} eV, they most probably originate from supernova explosions, neutron stars, pulsars or other sources where high energetic phenomena are involved [78, 83]. The energy spectrum of the

GCRs peaks at about 85% of the speed of light, or 1 GeV per nucleon in energy units, and consequently these particles are so penetrating that shielding can only partially reduce the doses absorbed by the crew [84]. Approximately 87% of the particles composing the GCR are protons, 12% are helium nuclei and 1% are particles heavier than helium as high-Z and high-energy (HZE) particles. Iron ions, with 18%, as well as protons, with 24%, make a major contribution to the equivalent dose and their energy spectrum goes from 100 to 1000 MeV/nucleon [83, 85].

The Earth is surrounded by intense region of energetic protons and electrons known as Van Allen Belts or **Earth's trapped radiation belts**. These particles are trapped by the geomagnetic field where they follow a complex motion named cyclotron motion. The particle motion is not uniform and the field lines converge close to the poles. This induces charged particles to move back and forth along the belt lines, changing their direction at the points close to the poles [78]. **Trapped electrons** are organized in two belts or zones; the inner belt electron energies are less than 5 MeV and the outer is above than 7 MeV. Most of the low energy electrons are stopped by the spacecraft shield. Electrons with energies about 10 MeV become very important due to their dangerousness but since they are in the outer belt, which is above the low-Earth's orbit (LEO; max altitude about 2000 km), it means that aboard the ISS trapped electrons represent a small risk for human health [78]. **Trapped protons** are disposed in a single belt where the intensity distribution decreases proportionally to the distance from Earth. The energy spectrum of trapped protons extends from several MeV up to several hundreds MeV, with a board peak between 150 and 250 MeV and the majority of these protons is beyond the ISS orbit. However, due to the fact that the Earth magnetic field axis is displaced from its rotation axis, there is a region of the Brasilian coast, named South Atlantic Anomaly, where the geomagnetic field drops unusually close to the Earth. In this area, at the altitude of 400 km along the ISS orbit, half of the ionizing radiation dose is from trapped protons and the other half is from GCR's [78].

The **solar wind** is the continuous emission of particles from the sun and is mainly constituted by protons and electrons. The intensities of these particles are between 10^{10} and 10^{12}

particles $cm^{-2}*s^{-1}*sr^{-1}$ and they are characterized by a speed between 300 and 800 $km*s^{-1}$. Furthermore, the energies are so low (100-3500 eV) that they can be blocked by the first micrometres of skin; therefore they do not have an impact on human health. Large amount of energies can be occasionally released from the sun surface as unexpected explosion of gamma rays, hard and soft X-rays and radio waves. These types of events are named solar particle events (SPEs) and the produced particles are trapped by the interplanetary magnetic field. The SPE particles emitted have a wide variability in number and energy spectrum of particles and they have the potential to expose space crew to life threatening doses [83].

Most of the energy loss experienced by primary particles as they pass through a spacecraft will cause ionization. However, the energies of many of these particles are sufficiently high and the amount of shielding represented by the spacecraft is sufficiently large so that a fraction of these primary particles will undergo nuclear interactions with the constituent nuclei of the spacecraft and its contents, producing **secondary particles**. These secondaries can include knockout protons, neutrons and α-particles, as well as recoil heavy nuclei. While the number of different particle species is large and the energy spectrum which they occupy is quite broad, their fluxes are often low (Fig. 5). Rare events associated with solar flares and coronal mass ejections

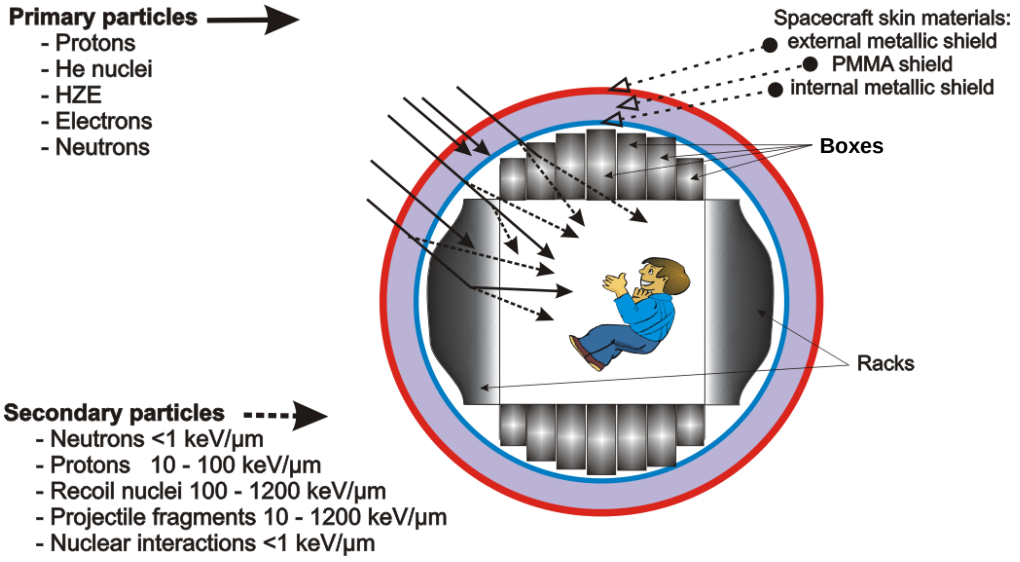

Figure 5: Primary and secondary particles inside the spacecraft.
Primary particles (plain thick arrows) through the spacecraft structure skin and components (racks and boxes) and the generated secondary particles (dashed thick arrows). (Drawn by G. Pani)

(CMEs) can produce sudden and dramatic increase in flux. Spaceship shielding is thus one of the most important factors in determining the characteristics of the ionizing space radiation inside a spaceship [78].

1.2.2. Shielding materials (Target)

Protecting the astronauts from cosmic radiations during space missions is of crucial importance but shielding a spacecraft is more complicated than shielding a nuclear reactor or particle accelerators, due to obvious mass constraints. The spacecraft hull is mainly made out of aluminium and polyethylene and the practical shielding thicknesses are insufficient to stop most of the incident GCR particles. Most of the energy loss experienced by primary particles causes ionization passing through a spacecraft skin. However, the energies of many of these particles are sufficiently high and the amount of shielding represented by the spacecraft is adequately large that only a fraction of these primary particles will undergo nuclear interactions with the constituent nuclei of the spacecraft hull and its components. These interactions cause fragmentation of the incident ions into lighter charged particles and neutrons, producing secondary particles [86, 87]. In many reactions, the resulting fragments have more biological significance than the incident ions [88]. In the last decade, several analyses and experiments on shielding materials of ISS have been performed. These investigations using 1 GeV/nucleon iron ions showed that for metallic targets and thin polymethylmethacrylate it was possible to measure the fluences of the primary beam and produced fragments, while for the metallic targets and thick polymethylmethacrylate (PMMA) targets it was only possible to measure the iron fluence [87]. In 2006 was launched Genesis 1, a new inflatable module designed and produced by Bigelow Aerospace. Due to the light material and the reduced space when is deflated it allows to be easily transported into space. Differently from traditional modules, primary envelope of this type of payload is made from non-metallic soft materials, therefore, into these habitats, the

radiation dose is lower due to the significant reduction of scattering effect and the secondary particle production.

With the actual method used to shield spacecrafts, astronauts will be exposed to dangerous doses of radiation from cosmic rays during interplanetary voyages.

The geomagnetic field produced by the Earth was a strong inspiration to design a new spacecraft shield. Innovative research has begun to examine the use of superconducting magnet technology to protect astronauts from radiation during long-duration spaceflights creating a magnetic field around the spacecraft. It could be that next generation of spacecraft will be implemented with this technology, allowing to build safer and lighter spaceships [89].

1.2.3. Space dosimetry

Measurements of cosmic rays have been performed in space by using active and passive devices during all manned missions [90, 91]. During various shuttle flights, on Apollo, Skylab, MIR and ISS [20], the effective doses varied with altitude and inclination of each flight. Highest values were observed during the high altitude shuttle flights at low inclinations with a radiation dose up to 4 mSv/day, and during the Apollo Program, with about 3 mSv/day. Early measurements on the Mir Orbit Station taken during a period of eleven years (1986 to 1997) showed dose rates from 162 to 508 μGy/day [78]. For an ISS type orbit (51.6° inc., 320-450 km altitude), it was estimated that the neutron contribution to an astronaut's total equivalent dose was in a range from 30% to 60% [78]. In the BASE-A flight experiment performed in September 2006, on board of ISS (ca. 400 km altitude) (Soyuz Mission 13S), were TLD dosimeters (passive dosimeters) placed that measured cosmic radiation for 11 days. These dosimeters indicated an average dose of 180 μGy/day [92]. The Matroshka-MOSFET dosimetry mission provided a large quantity of radiation dose data inside the ISS for the period of January 2006 to April 2007, showing an effective 30 days and annual doses of 18 and 219 mSv, respectively [93].

1.2.4. Simulating accelerated space particles on Earth

Cosmic rays are a pool of various accelerated particles and investigating the effects of space radiation is crucial for future deep long space travel. One of the methods used on Earth to study the effects of cosmic radiation is the use of a **stratospheric balloon** which allows to transport samples at an altitude up to 40 km for a few days and to expose them to the wide variety of accelerated particles coming from space.

To obtain accelerated particles on the Earth, two ways are known: the use of natural sources or special facilities to produce and accelerate ions.

The use of particle accelerators can deliver beams with high quality of many elements. Particle accelerators can be divided into two main groups: **linear accelerators**, which produce low energy beams (below 50 MeV), or **synchrotron** and **cyclotron**, which produce high energy beams (up to 2 GeV). These types of accelerators are available at the European centres GSI Helmholtz Centre for Heavy Ion Research (German: GSI Helmholtzzentrum für Schwerionenforschung GmbH; Darmstadt, Germany) and Grand Accélérateur National d'Ions Lourds (GANIL; Caen, France). Furthermore, many European centres, in collaboration with ESA are also able to perform experiments related to space radiations. Other irradiation facilities are located at ESA/ESTEC (Noordwijk, the Netherlands) and at the Belgian Nuclear Centre SCK•CEN in Mol, Belgium, where natural gamma sources, as Cobalt-60 and Cesium-137, and neutron sources, as Californium 252, are used as an alternative to the conventional particle accelerator to simulate cosmic radiation.

1.2.5. Radiation protection

1.2.5.1. Dose

In radiation biology, it is crucial to be aware of the radiation dose. Indeed, the induced damage is proportional to the received dose, the energy and the number of ionizations. The Gray (Gy) is the reference unit for the **absorbed dose** which corresponds to the absorption of one

Joule of ionizing radiation by one kilogram of matter. A deterministic effect is induced by high doses; therefore, an increase for radiation dose induces a proportional change in the observed effect. However, the frequency and the intensity of the effects induced by low doses, below 0.5 Sv, can also be stochastic. In its 1990 recommendations [94], the International Commission on Radiation Protection (ICRP) introduced another radiation unit used in radiation biology which is the Sievert (Sv), that is the International System of Units (SI) derived unit of **equivalent radiation dose**. Quantities that are measured in Sieverts are designed to represent the stochastic biological effects of ionizing radiation. In the same year ICRP also defined the quantity **effective dose** as the sum of the equivalent doses in the principal tissues and organs, each weighted by a tissue weighting factor (wT) [94]. Furthermore ICRP emphasises that the effective dose provides a measure of radiation detriment for protection purposes only; it should not be used for epidemiological evaluations and does not provide an individual-specific dose.

Up to now, the risk related to ionising irradiation has been predominantly estimated by a linear non-threshold (LNT) model. For extrapolation on the effect of low doses, few models were proposed to estimate the induced effects. The LNT model was proposed to infer the best relationship between stochastic and deterministic effects. However, this model might under or over-estimate the radiation-induced effects [95]. Indeed, the observed phenomena of hyper-radiosensitivity in the low dose range, the inducible radioresistance, the bystander effects [96],

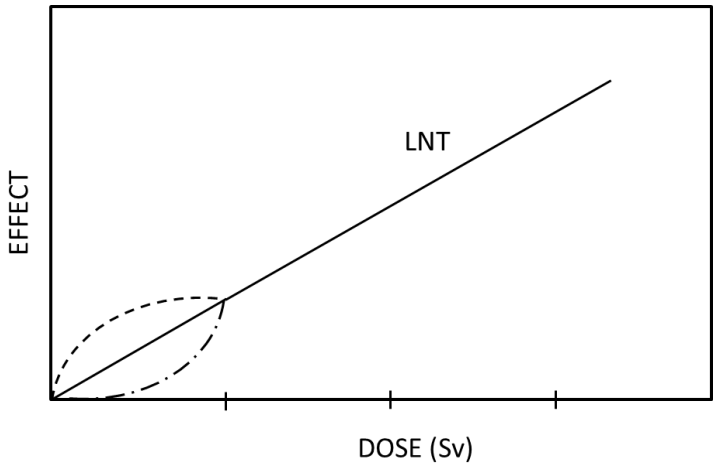

Figure 6: Graph of models proposed to evaluate the risks associated with low dose radiation.
The linear non-threshold (LNT) model (continuous line), overestimation model (upper curve) and underestimation model (lower curve). (Drawn by G. Pani)

genomic instability and adaptive response show a differentiated relationship between the effective radiation risk and equivalent doses below 0.5 Sv (Fig. 6).

1.2.5.2. Dose rate

Another important notion in radiation biology is the dose rate. Indeed, it expresses the received dose (Sv or Gy) in a certain time period (seconds, minutes, hours, days, ……). Therefore, exposing an organism to a high dose for a short time induces effects that can be already observed within a short period and followed throughout a long time after irradiation. On the contrary, exposure to the same dose throughout longer time might allow the organism to activate different strategies to repair the induced damage [97] or to adapt to the new situation, if it does not undergo death process.

1.2.5.3. Radiosensitivity

It is known that patients can display hypersensitivity to ionising radiation after radiation therapies. Development of side-effects after radiation therapy in normal tissues has been reported in 5–7% of cancer patients and referred as "clinical radiation reactions"; such effects may be either acute or late [98]. Among the factors leading to severe normal tissue reactions after ionizing radiation exposure, the individual radiosensitivity is considered of utmost importance. The patients with equivalent radiotherapy treatment developed acute or late reactions in normal tissues underlying three types of sensitivity: **low**, **moderate** or **high** radiosensitivity. Different individual radiosensitivity might allow an adaptation to the maximal tolerable dose with an overall increase in the cure rate [99]. Moreover, a different radiosensitivity at the single organ level has been reported. Therefore, to provide a better basis for radioprotection purposes, the organ radiosensitivity (effective dose) was taken into account and the tissue weighting factors (equivalent dose) were introduced by the ICRP [100]. Furthermore, for organ radiosensitivity other factors such as cell type, age, organ proliferation status and microenvironment, all having a critical role should also be taken into account [101, 102].

1.2.5.4. Linear energy transfer (LET)

Another important parameter that should be taken into consideration is the linear energy transfer or LET. The LET of a heavy ion particle indicates the rate of energy deposition in the linear dimension of the absorbing material and it is a measure of the energy transferred to the material. A Bragg peak is produced when the transferred beam energy increases the passing through the material. In the Bragg peak the LET is defined as "high LET" and the biological effects of radiations are well observed. On the contrary, less biological effects are observed during the initial energy transfer, and in this case the LET is defined as low [103].

With regard to spaceflight, these varying track structures can arise when primary high LET particles in space interact with spacecraft-shielding material and the human body, resulting in secondary radiation like neutrons and charged particles [104].

1.2.6. Biological effects of ionizing radiations

It is known that exposure to space radiations can affect human health, thus it is important for the safety of crew members to estimate the possible effects incurred during space missions. In fact, radiation exposure is one of the principal risks for astronauts on extended space missions, such as a long permanence aboard the ISS or future missions to Mars. After ionizing radiation exposure, several effects at the cellular level, as DNA damage, oxidative stress, arrest in cell cycle, apoptosis, change in cell motility and senescence, have been reported.

1.2.6.1. Oxidative stress

The cell damage induced by an excess of oxidants as reactive oxygen species (ROS, e.g., oxygen ions, free radicals, and peroxides) are known as **oxidative stress**. Low amounts of ROS are naturally produced in cells and are necessary for important cellular functions, but they are also harmful in excess. Certain cell types produce ROS to kill invading microbes; furthermore, ROS are also involved in cell signaling [105]. Finally, oxidative stress is known to play a role in

cellular processes, such as aging and apoptosis. It has also been linked to some diseases like Alzheimer's disease [106] or in atherosclerosis that can lead to cardiovascular diseases [107].

Ionizing radiations, as well as other factors, can induce a state of oxidative stress. Ionizing radiation can induce cellular damage and stress both directly, by energetic disruption of DNA integrity, and indirectly, as a result of the formation of intracellular free radicals from water. DNA damage can also be indirectly induced by cytoplasm irradiation, as demonstrated in an experiment with free radical scavengers, where the DNA damage is dependent on ROS generation [108, 109]. As a result of irradiation, ROS can be produced by cells for several minutes or even hours after exposure; in parallel to ROS production, cells are induced to raise their antioxidant expression [108]. The higher production of antioxidants may play a role in the radioadaptive response [108]. Indeed, it has been observed that the *in vitro* or *in vivo* use of exogenous antioxidants as N-acetylcysteine, ascorbic acid, sodium ascorbate, α-lipoic acid, co-enzyme Q10, L-selenomethionine [110], or enzymes such as the manganese-containing superoxide dismutase (MnSOD) [111] reduce the indirect damage induced by radiation generated ROS, thus playing an important role in the radioprotection of organisms.

Actually, the spacecraft shielding against space radiation is not fully efficient yet. Indeed, it has been suggested to integrate into the astronaut diet additional antioxidants to decrease the risk related to oxidative stress throughout long-term journeys in space [112, 113] .

1.2.6.2. DNA damage

Due to environmental factors and normal metabolic processes inside the cell, DNA damage occurs at a rate of 1,000 to 1,000,000 molecular lesions per cell per day.

Endogenous sources of DNA damage include hydrolysis, oxidation, alkylation, and mismatch of DNA bases, while sources of exogenous DNA damage include ionizing radiation, ultraviolet (UV) radiation, and various chemical agents. At the cellular level, damaged DNA that is not properly repaired can lead to genomic instability, apoptosis or senescence, which can

greatly affect the organism development and ageing processes. More importantly, loss of genomic integrity predisposes the organism to immunodeficiency, neurological disorders, cardiovascular diseases and cancer. Therefore, it is essential for cells to efficiently respond to DNA damage through coordinated and integrated DNA-damage checkpoints and repair pathways [103, 114]. The vast majority of DNA damage affects the primary structure of the double helix as single (SSBs) or double strand breaks (DSBs). The DNA damage repair pathways include the direct reversal, the mismatch repair (MMR), the nucleotide excision repair (NER), the base excision repair (BER), the homologous recombination (HR) as well as the non-homologous end joining (NHEJ) pathways.

Radiations can directly induce two major types of DNA damage, SSBs and DSBs [115], and are directly proportional to the radiation dose. When DSBs occur, H2AX histones in the vicinity of the break becomes phosphorylated on residue serine 139, leading to the formation of so-called γ-H2AX foci [116]. Phosphorylated histone 2AX (γ-H2AX) is used as marker of induced DSBs [114] and can be detected and estimated through immunofluorescence staining and image analysis [117]. The final effect can be related to the LET of the irradiation. In fact, samples exposed to low LET present less damage than biological samples exposed to high LET [103]. The distribution of H2AX foci is also related to the source or the facility used to irradiate (Fig. 7) [114]. X-ray tube and natural sources produce a beam cone inducing a homogenous distribution of DSBs into the nucleus (Fig, 7 A). On the contrary, particle accelerators produce lines of DSBs in exposed nuclei (Fig. 7 B-C).

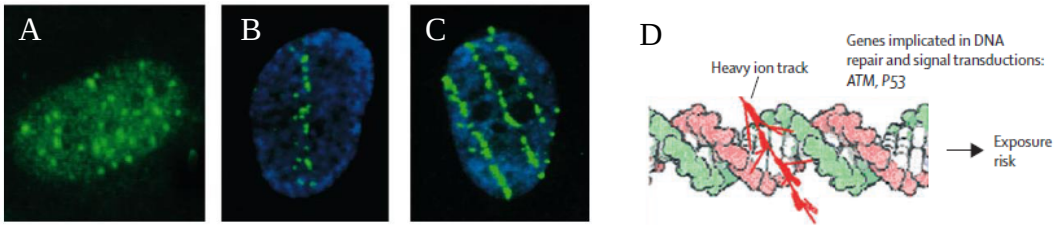

Figure 7: Different distributions of γ-H2AX related to the ionizing radiation sources.
A) 2 Gy of gamma-rays, B) 0.5 Gy at 54 KeV/µm of accelerated silicon ions, C) 0.5 Gy at 176 KeV/µm of accelerated iron ions, D) Model of DNA damage induced by ionizing radiations [114].

1.2.6.3. Cell cycle checkpoints

Changes in DNA integrity activate the cell cycle checkpoint processes in order to allow time for repairing the damage before proceeding to mitosis. For successful long-term cell proliferation two processes should be performed correctly. First, the chromosome replication–division cycle has to occur in a correct order. Second, the events of chromosomal synthesis have to be repeated with a period equal to the mass doubling time. The first processes are necessary to maintain the DNA integrity and the second processes are necessary to maintain the cell nucleo-cytoplasmic ratio within viable bounds. The correct sequence of events is a robust characteristic of the chromosome cycle. The cell cycle arrest due to DNA damage suggests that cell replication steps are sequence dependent. Pre- and mitosis process can be stopped by deterrent factors like the DNA replication block due to drugs, the cell growth block induced by nutrient deprivation or the DNA damage caused by internal or external factors.

The eukaryotic cell cycle has three main checkpoints: at the end of G1, at the end of G2 and between metaphase and anaphase (Fig. 8). If the conditions for a successful cell division are not reached, the chromosome cycle can be blocked in one of the three checkpoints (Fig. 8). The core components of the eukaryotic cell cycle engine are cyclin-dependent protein kinases (Cdks) and their regulatory subunits (cyclin). Three different complexes as G1 cyclin–Cdk, S cyclin–Cdk and M cyclin–Cdk complexes are important for progression through the next event. Furthermore, S cyclin–Cdk complexes are responsible for initiating and completing DNA replication and the M cyclin–Cdk complexes drive eukaryotes into mitosis and restrain re-entry into G1 phase.

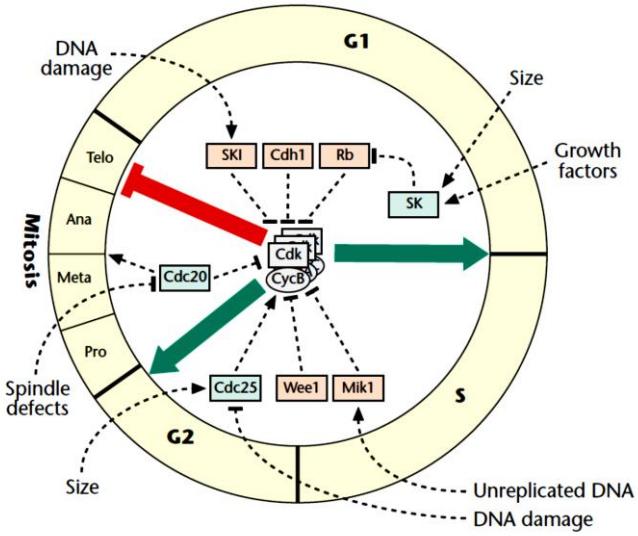

Figure 8: Cell cycle checkpoint accelerators (green) and breaks (red) of the cell cycle engine. Checkpoint pathways (dashed lines) modulate the activities of the accelerators and breaks. Pro, prophase; Meta, metaphase; Ana, anaphase; Telo, telophase [118].

The DNA damage modulates the signal arresting the cell cycle at specific checkpoints by inactivating Cdks [118, 119]. In mammalian cells, ionizing radiation generates double-stranded breaks in DNA, which modulates phosphorylation with following activation of ATM. Certain number of substrates involved in DNA repair, apoptotic death and cell cycle arrest are phosphorylated by ATM. ATM phosphorylates and inactivates MDM2, which is involved in the degradation of p53 protein by the ubiquitin–proteasome pathway. Therefore, p53 accumulates in response to DNA damage induced by radiation. p53 promotes the transcription of several genes, like the inhibitors of all cyclin–Cdk complexes and proteins involved in the DNA repair. Finally, p53 can also be involved in the cell suicide programme (apoptosis), presumably if the DNA damage is not repairable. Moreover, ATM activates protein kinases like Chk1 and Chk2, which then phosphorylate and stabilize p53, thereby enhancing the effects of p53 in response to DNA damage. Chk1 and Chk2 can also activate Cdc25, which is an activator of cyclin-Cdks (Fig. 8). The G1-arrest state is enhanced by the quick degradation of Cdc25A which is involved in the activation of CycA–Cdk2 and CycE–Cdk2 [120]. Another target of ATM is BASC (Brca1-associated surveillance complex). The activation of this particular complex triggers the DNA repair and arrests DNA replication.

Throughout these pathways, ATM plays an important role in cell cycle arrest, genome repair and apoptosis in response to DNA damage directly or indirectly induced by radiation.

1.2.6.4. Apoptosis

Apoptosis, or programmed cell death, is one of the major controlled cellular processes. During this event cells can undergo self-destruction in case of unrepairable damage. Apoptosis is also involved in modulating the cell number and proliferation in normal growth and development. When cell responses to DNA damage, hypoxia, or other types of stress are induced, p53 is partly responsible for leading to cell-cycle arrest, senescence and cell death. The levels and activities of p53 proteins are involved in apoptosis process and are carefully regulated in normal cells.

All molecular processes involved in radiation-induced apoptosis are not completely known. The involved mechanisms probably change according to the cell type or the received radiation dose [121-123]. Upon radiation-induced DNA damage, mechanisms involved in cell cycle arrest, as ATM and DNA-PK activation and reduced degradation of p53 due to MDM2 inhibition, allow cells to repair the genome. On the contrary, if the genome is not repairable, p53 concentration increases and induces $p21^{waf1/cip1}$, a protein involved in cell-cycle arrest, to up-regulate Bax, Noxa and p53 up-regulated apoptosis modulator (PUMA). In addition, p53 down-regulates the expression of anti-apoptotic proteins as Bcl-2 and Bcl-X_L. ATM is also involved in the phosphorylation of E2F1 which up-regulates pro-apoptotic proteins like through p73, Apaf-1 and a few caspases. Apoptosis can be induced also by membrane-derived signals, as sphingomyelin, ceramide [124, 125] and Daxx, a CD95-binding protein [126] which can activate pro-apoptotic SAPK/JNK pathways. Targets of SAPK/JNK include p53, Bax, c-Jun and caspases [126-129] from which activation can lead to apoptosis. The total amount of cell damage seems to be an important element to lead the cell to repair the damage and survive, or to undergo apoptosis.

1.2.6.5. Senescence

In 1961, Hayflick and colleagues reported that normal human fibroblasts have limited number of replicative cycles [130]. Human fibroblasts arrested the cell cycle and exhibited different cell morphology. This stable cell state is known as **replicative** or **cellular senescence**. Generally cellular senescence reflects few changes that occur throughout the ageing of organisms. The difference between pre-senescent and senescent cells lies in multiple aspects of cellular physiology [131, 132]; for example, senescent cells present changes in gene expression [133]. Senescent cells frequently secrete enzymes and cytokines that can induce death of neighbouring cells or tissue damage contributing to the age-related decline in tissue and/or the genesis of certain age-related pathologies [134, 135].

At the molecular level, cellular senescence may involve various mechanisms which are not completely understood. Numerous studies suggest that telomere shortening is one of the main reason for replicative senescence [136]. It has been considered that telomere shortening over a certain point might modulate the DNA damage response activating one of the cell cycle checkpoints [132]. Another reported sign of senescence is an increase of lysosomal β-galactosidase, observed by SA β-gal histochemical staining performed in tissues or cells [137]. Indeed, this method is used as a marker to detect senescence induced by oxidative stress.

Cellular senescence can be induced by a variety of extrinsic factors, such as ionizing radiation, UV and hydrogen peroxide [138]. The extrinsic senescence occurs when cells still have functional telomeres and the potential to proliferate under suitable culture conditions. In this case, signals to senesce originate from sources independent of telomeres. In a few experiments it was reported that low doses of ionizing radiations can induce senescence in cultured cells [139, 140].

1.2.6.6. Cell motility

Cell motility is required for many important physiological processes during development, such as cell migration during gastrulation, embryological development, tissue regeneration and

axon growth. The basis for most of the active movements exhibited by cells is the cytoskeleton. In some instances motility is simply generated by its regulated assembly and disassembly. In other cases, motility results from the activities of 'motor' proteins which interact with the different cytoskeletal elements.

Several investigations on cancer irradiation therapies reported that ionizing radiation can induce different effects on metastatic capabilities of malignant tumour cells. In these studies cell adhesion capability to extracellular matrix, cell migration and cell invasive capability were taken into account. High doses of X-rays and protons reduce human fibrosarcoma cell adherence to substrates like fibronectin, laminin, and vitronectin; on the contrary, cells exposed to 4Gy of carbon-ions showed a significantly higher attachment to fibronectin [141]. Furthermore, it was observed that migration capability of human fibrosarcoma cells decreased after proton as well as carbon ion low dose irradiations. On the other hand, low doses of X-rays (0.5Gy) increase cell motility in the same cell type [141]. In other cell types like AsPC-1, BxPC-3 and MIAPaCa-2, C-ion irradiation (2 Gy) suppressed the migration of cells, and diminished MIAPaCa-2 cell invasion [102]. On the other hand 2 Gy C-irradiation induced invasiveness in the PANC-1 cells, without altering their migration ability [102]. Furthermore, changes in distribution and expression of cytoskeletal proteins were observed in cells exposed to ionizing radiation [142-144]. Therefore, cell motility changes induced by ionizing radiation might be linked to the cell types and to the accelerated particle types used.

1.3. Biological effectiveness of combined conditions

In the previous sections, the two main space conditions, microgravity and cosmic radiations, and their respective effects, were separately described. In real space conditions both weightlessness and ionizing radiation are simultaneously experienced. Hence, it is important to understand the combined effects of the two conditions in order to estimate the risk for astronauts

during a long-term mission. Concerning the effects induced by both stressors, three main theories with supporting experiments have been developed and performed.

The first hypothesis proposes a synergistic effect when the two stressors are combined. Within the studies on lymphocytes exposed to simulated low gravity combined with gamma radiations, it was observed that DNA repair dynamics were delayed following these stressors (Fig. 9) [145]; furthermore, an increase of apoptosis was observed in simulated low gravity after irradiation [145].

The second hypothesis proposes an antithetical effect due to combination of both space stressors. It is known that radiation or microgravity can induce apoptosis, on the contrary the combination of the two stressors showed a decrease in radiation-induced apoptosis [146] and cell cycle arrest in G2 phase [147] upon low gravity. A pertinent hypothesis was proposed by Manti [148] proposing that cells exposed to microgravity might tolerate higher DNA damage, inducing a better adaptation with lower level of radiation-induced apoptosis and cell cycle arrest. However, more damaged cells would survive but it might increase the mutation rate due to higher error during repair mechanisms and in absence of G2 phase block [149].

The third hypothesis proposes uncorrelated effects with the combined space conditions. Human fibroblasts exposed to 5-10 Gy of X-rays before spaceflight did not show any difference compared to the controls in the survival curves and in the DNA repair kinetics [150].

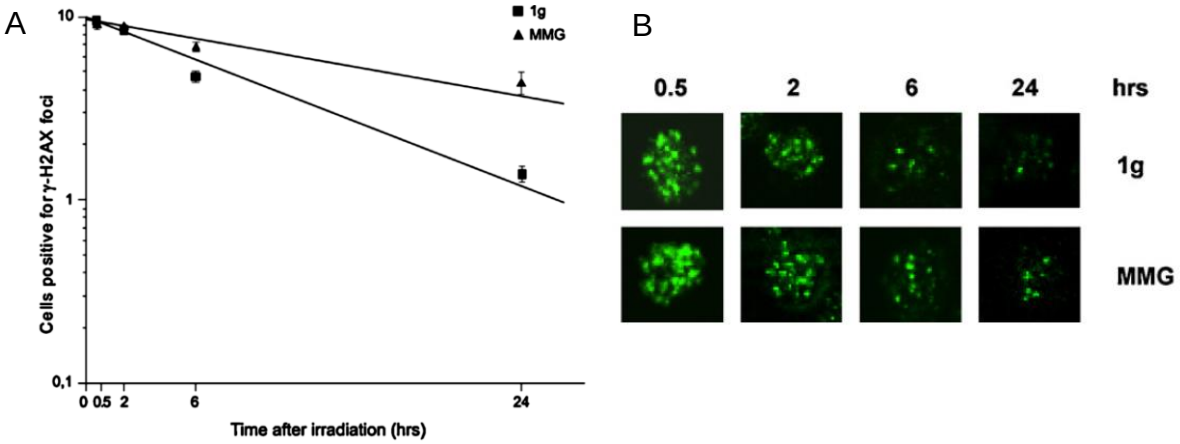

Figure 9: Kinetics of γ-H2AX foci in peripheral blood lymphocytes (PBLs) irradiated with 5 Gy of γ-rays and incubated at 1×g or in MMG (μg) during repair time.
(A) Fraction of cells positive for γ-H2AX foci, determined by counting 300–500 cells for each experiment [149].

2. **Central nervous system: a system in continuous reorganization.**

The nervous system consists of two main divisions: the **central nervous system** (CNS), which is composed of the brain and the spinal cord, and the peripheral nervous system. The **peripheral nervous system** (PNS) consists in the nerves that bring information from the outside world via the sensory systems, and the nerves that carry information from the body's interior to the spinal cord and brain. The brain is the dominant structure of the nervous system. It is the master controller of all body functions, and the analyser and interpreter of complex information and behaviour patterns. Neurons are considered as the most important cells in the nervous system [151]. The main property that makes neurons unique is their capability to send signals to specific target cells over long distances. Observing neurons, three main morphological structures can be recognized: the **soma** or cell body, the surrounding short extensions named **dendrites** and a few long extensions named **axons** (Fig. 10 A). Axons and dendrites together are named **neurites**. The tips of developing axons are enlarged structures called **outgrowth cones** (Fig. 10 B). These exhibit a highly active, ameboid-like array of filamentous processes that extend and retract continuously. The direction of outgrowth of these processes determines the direction of the axon extension and hence the direction of axon pathway formation. The outgrowth cone motility and the direction of pathway formation is influenced by diffusible attractant or repellent substances secreted by their intermediate or final destinations. [152].

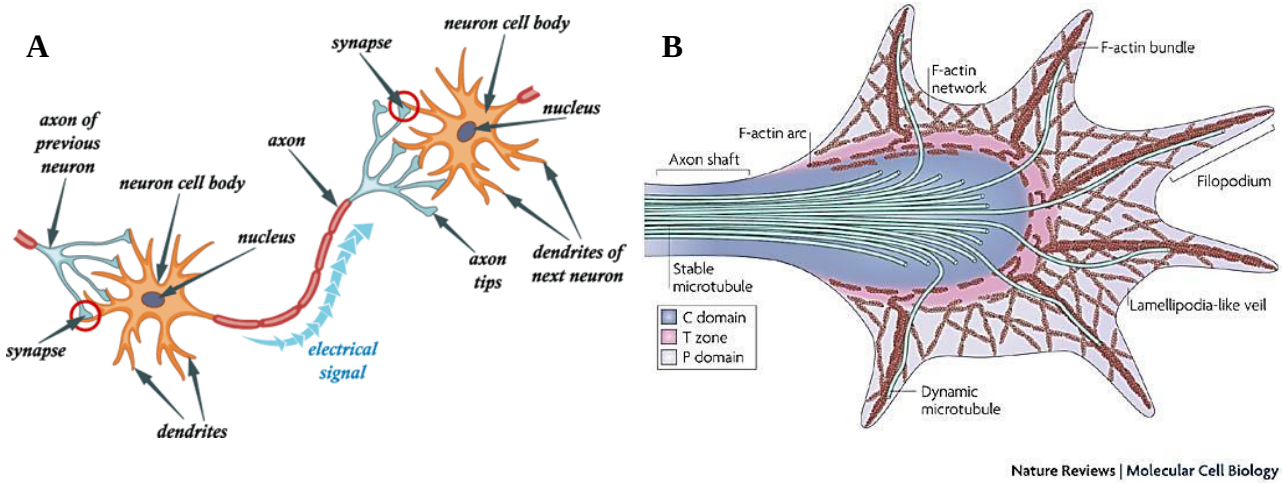

Figure 10: Neuron morphology (http://www.superinterestingfacts.com/top-ten-neuron-facts/) (A) and neurite outgrowth cone (B).
Stable microtubules are available in the neurite shaft and F-actin network, F-actin bundle and dynamic microtubules are available in the cortical zone (peripheral area of cells with high density of microfilaments) [152].

2.1. Neuronal network plasticity

Throughout the developmental stages, neuron precursors are able to move and extend dendrites and axon to establish synapses with target cells and become mature neuron. Plasticity is the final phenomenon which occurs in the developing brain whereas **neuronal network plasticity**, or **neuroplasticity**, is an ability of the adult brain to reorganize connections between neurons. Basically, the term "neuroplasticity" is related to the neuronal capability to modify some functional processes in response to the alterations in incoming information [153]. Moreover, plasticity is an intrinsic property of the nervous system maintained throughout life enabling to include important physiological changes allowing modification of functions and structures in response to environmental changes via the strengthening, weakening, pruning, or adding of synaptic connections as well as by promoting neurogenesis [154]. Furthermore, it has been shown that environmental changes can alter cognition and behaviour by modifying connections between existing neurons in the hippocampus, cortex and other parts of the brain [155].

In the neuronal network, remodelling the outgrowth cone activities plays an important role in modifying and increasing the terminal arborisation of the axon. Modification in the axonal

arborisation is not the only activity involved in the neuroplasticity; also formation of new dendritic spines is also important in this process. The dendritic spines are short extensions at the side of the dendrites which are involved in the process of synapsis creation. They are the postsynaptic sites to which the presynaptic buttons have contact. They have a complex ultrastructure and come in a large variety of shapes [156]. Furthermore, spines are not static but can undergo rapid shape changes [157, 158] that are influenced by neuronal activities [159].

As previously reported, space conditions can alter cell motility reducing the capability of cells to migrate on substrates and since the outgrowth cone is regulated by cell locomotion roles, hence, it might be that the remodelling of neuronal network is affected by reduced gravity and ionizing radiations.

2.2. Synaptic plasticity or connectivity

A single neuron generally receives multiple synaptic inputs from different neurons and processes these excitatory and inhibitory inputs through temporal and spatial summation. The number of neurons with a synaptic connection to a single neuron and the plasticity of these connections are the most basic features underlying the construction of neuronal circuits and circuit plasticity. The synaptic connections to one cell are, in general, highly selective. In addition to these selective mechanisms, the activity-dependent increase in synaptic connections is also indispensable to maintain the brain function over life.

The adult brain is capable of remodelling its neuronal arborisation. The term **synaptic plasticity** refers to the neural activities which can also modify the behaviour of neural circuits by one of the three mechanisms: first by modifying the strength or efficacy of synaptic transmission at pre-existing synapses, second by eliciting the growth of new synaptic connections or the pruning away of existing ones and third by modulating the excitability properties of individual neurons. The neuronal network activity can enhance or depress the synaptic transmission and these changes can induce modifications that may persist for days or weeks or perhaps even

longer. Transient forms of synaptic plasticity have been associated with short-term adaptations to sensory inputs, transient changes in behavioural states, and short-lasting forms of memory. More lasting changes are thought to play important roles in the construction of neural circuits during development and with long-term forms of memory in the mature nervous system. Some of the forms of synaptic plasticity found at the excitatory synapses in the mammalian brain are **short-term mechanisms**, **long-term potentiation** (LTP) and **long-term depression** (LTD) **mechanisms** [160-164].

As reported in sections 4.1 and 4.2, experiments performed in real or modulated microgravity or using ionizing radiations showed activity and distribution changes in synapses. In particular, the potential action, the number of synapses, the signal wave and their propagation velocity were affected during or after exposure to space conditions [165-167]. Moreover, it has been observed that the SMS, which is also due to the misleading of information coming from the environment to the CNS, appears within the first hours of spaceflight with a decrease of symptoms over the permanence in space. Therefore, space conditions might induce initially long-term depression in the central nervous system followed by long-term potentiation in order to adapt to the new environment.

2.3. Neurogenesis

Adult neurogenesis is the process to generate new neurons which will integrate into formed neuronal networks after postnatal development. Investigations on rodents exposed to microgravity or ionizing radiations, as heavy ions, reported that both conditions influenced the neurogenesis and the migration of new neurons to the final destination during development as well as in adult stages [168, 169] reducing the capability of generating or regenerating processes in the CNS.

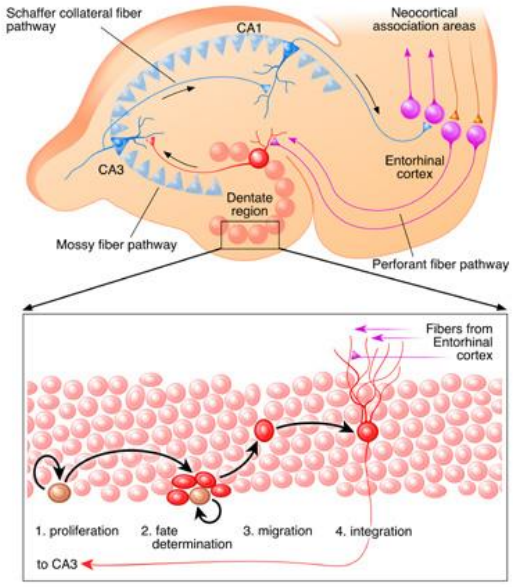

Figure 11: Neurogenesis in adult brain (http://www4.utsouthwestern.edu/HsiehLab/research.html).
New neurons generate from stem cells in the ventricle and move towards the inner part until they reach the final destination.

2.4. In vitro models

Several studies on neuronal networks and synapsis plasticity, neurogenesis and their modulation by external stimuli or compounds have been performed on adult laboratory animals like mice, rats or rabbits. Today, these investigations can be partially performed using facilities such as magnetic resonance imaging (MRI) or computational tomography (CT) without sacrifying animals. Most of the time images obtained by CT and MRI have low resolution and these techniques require anaesthesia or markers inducing stress in animals, therefore histological methods for deeper investigations are required. To study certain events which occur in neurons, *in vitro* models should be used. To obtain an *in vitro* model two types of cells can be used: cell lines or primary neurons. Cell lines as human neuroblastoma (SH-SY5Y) and rat pheochromocytoma (PC12) cells can be differentiated in post-mitotic neurons and used to study phenomena linked to neuronal physiology and morphology or events involved in neurodegeneration induced by exogenous factors (drugs, infections, temperature or radiations)

[170-172]. To study neuronal differentiation mesenchymal stem cells can be cultured and stimulated to differentiate into neurons [173]. Furthermore, primary neurons from hippocampus, cortex and cerebellum can be cultured after dissection and dissociation of tissues. This type of cell culture is more sensitive than cell lines, in particular if compounds are tested to determine their effect on the outgrowth cone [174].

Most of the studies are performed on non-dense neuronal networks in which immature neurons are not yet well connected and that makes them easier to investigate processes linked to the outgrowth cone and the extension of neurites. In other cases, neurons need to be well connected in order to obtain mature neurons in culture. It was reported that immature neurons, available in non-dense neuronal networks, and mature neurons, available in dense neuronal networks, differ in action potential activities, spontaneous synaptic currents, number of synapses and neurite growth speed [175, 176]. It was also described that synaptic protein distribution and associated vesicles are partially dependent on the acquisition of functional synaptic transition [175]. Additionally, recent studies suggest that GABA and glycin neurotransmitters have inhibitory activity on mature but excitatory activity on immature cortical neurons [177, 178]. Furthermore, it was reported that mature neurons are less sensitive to external compounds or agents than immature neurons [179, 180]. It is also known that cognitive dysfunction and memory impairment at adult age can be induced by neurological disease as well as external events like toxic compounds or radiations.

Investigations on neuron connectivity in cells cultured for a long period of time showed an increase of connections between neurons over time following a non-linear correlation. Indeed, the neuronal network and the number of connections increase fast until a reasonable stage of connectivity; thereafter, the growth rate slows down [176]. Therefore, to test several compounds or external events and evaluate the induced effects, long-term cultured neurons extending neurites much slower than young neuron cultures are preferable.

3. Cytoskeleton and cell motility in adherent cells

The **motility** is the major characteristic of living organisms, and it is expressed as movement of cells or movement of molecules within the cells themselves. The major part of the active movements exhibited by eukaryotic cells is mostly based on the **cytoskeleton**. In some instances motility (developed in section 4.2) is simply generated by regulation of assembly and disassembly of cytoskeletal structures. In other cases, motility is the result of "motor" proteins activities, interacting with cytoskeletal elements.

Cytoskeleton plays an important role in cell adhesion, cell shape and cell migration as well as other cellular functions like internal organization, transport and cell division [181]. Cytoskeleton is composed of three main protein structures: **microfilaments**, **microtubules** and **intermediate filaments**. They are linked and connected to cellular organelles and cytoplasmic membranes by several associated proteins like vinculin, talin, myosin and others. Furthermore, it is known that cytoskeletal proteins are directly or indirectly associated to cell growth, metabolism and signal transduction [182].

Microfilaments or **actin filaments** are the thinnest filaments of the cytoskeleton. Actin participates in many important cellular processes including muscle **contraction**, **cell motility**, **cell division** and **cytokinesis**, **vesicle** and **organelle movement**, **cell signaling**, and the **establishment** and **maintenance** of **cell junctions** and **cell shape**. Many of these processes are mediated by extensive and intimate interactions of actin with cellular membranes.

Since the first cell imaging investigations on adherent cells, it has been observed that microfilament distribution is altered and the induced changes are related to the increase or decrease of gravity forces. As observed in experiments performed on adherent cells in hypergravity, the density of microfilaments increases in the cytosol [183]. On the contrary, experiments performed aboard the ISS and on RPM showed that the concentration of

microfilaments in the cytosol is drastically reduced [184] and an increase of gel-like network of microfilaments was observed in the proximity of the cell cortex [38, 59].

Microtubules are long and cylindrical structures with 25 nm of external diameter and 15 nm of internal diameter. They are composed of polymerised **α**- and **β-tubulin dimers**, globular proteins which polymerise in protofilaments by end-to-end junctions. Finally, protofilaments form a tube by the lateral association of 13 protofilaments. Microtubules are involved in the internal transport, locomotion and cell shape [185].

Axons and dendrites extending from a cell body in nerve cells provide a good example of the role of stable microtubules in determining cell polarity (Fig. 12). However, the microtubules in axons and dendrites are organized differently. In axons, the microtubules are all oriented with their plus ends away from the cell body and in dendrites, the microtubules are oriented in both directions; some plus ends point towards the cell body and some point towards the cell periphery.

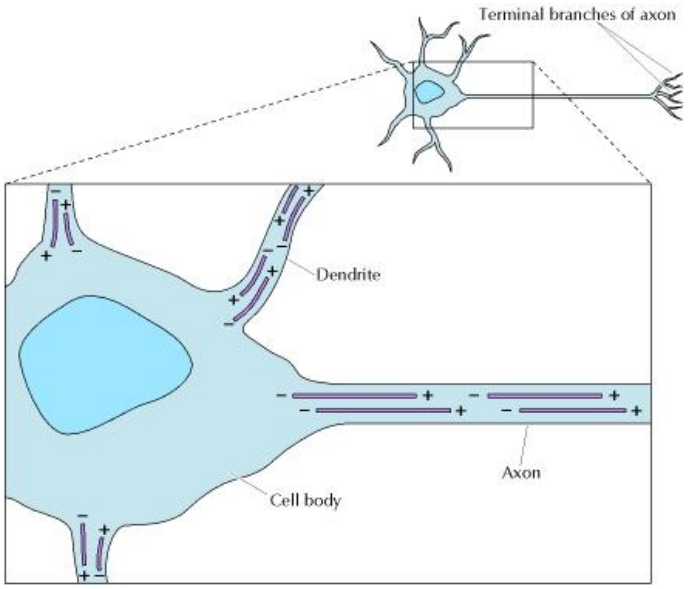

Figure 12: Organization of microtubules in nerve cells.
Two distinct types of processes extend from the cell body of nerve cells (neurons). Stable microtubules in both axons and dendrites terminate in the cytoplasm rather than being anchored in the centrosome. In dendrites, microtubules are oriented in both directions, with their plus ends pointing both towards and away from the cell body. In contrast, all of the axon microtubules are oriented with their plus ends pointing towards the tip of the axon [227] .

As reported in sections 1.1 and 4.1, microtubule distribution can be altered by changes of gravity. Within the first hour of RPM conditions, microtubules change in distribution moving towards the centrosome surrounding the nucleus and thereafter re-establishing the microtubular network in the cytosol appearing highly arborized without reaching the cell cortex [38]. Since stable microtubules are located in neuronal extensions (Fig. 12), their destabilisation due to gravity change might alter their morphology.

Intermediate filaments have a diameter of about 10 nm, and are not directly involved in cell movement; on the contrary, they appear to play a structural role by providing mechanical strength to cells and tissues. Intermediate filaments are composed of a variety of proteins that are expressed in different types of cells. More than 50 different intermediate filament proteins have been identified and classified into different groups (type I to VI) [186].

Cells exhibit a wide range of movements which are triggered by cytoskeleton changes. Examples of cell motility include movements of cells from one location to another during development or during wound healing, neurite outgrowth cone movements during neuron migration or neurite extension, contraction of a muscle cell, movements of chromosomes during mitosis and separation into two daughter cells during cell division or movements of membrane-bound vesicles into cells.

It has been reported that microgravity can also influence cell motility increasing it in suspension cells, as lymphocytes during sounding rocket experiments [187], or reducing cell motility in adherent cells, as monocytes exposed to ISS environment for 24 h [59]. Cell motility and the capability of cells to adhere to the matrix are directly linked to cytoskeleton. Indeed, experiments on cytoskeletal proteins have reported their alteration when cells are cultured in different gravity conditions [38, 51, 59, 183]. Moreover it has been reported that the organization of microtubules and microfilaments is altered by short exposure to simulated microgravity at the level of the outgrowth cone [188].

4. The central nervous system and in space conditions

4.1. CNS and microgravity

During spaceflights and immediately after landing, one of the first effects that astronauts experience is postural instability from which they gradually recover within the following days after landing [189]. Several studies illustrate that visual and proprioperceptive sensory feedback information is used for postural control with reliance to vestibular function [190-192]. Therefore, the perception of position and locomotion in reduced gravity is the result of the brain ability to integrate auditory and visual signs with vestibular input and proprioceptive information [19, 25]. If the input from these sensors is altered by the gravity condition changes, the central nervous system is forced to interpret the new stimuli and therefore develop alternative strategies to supplement the altered stimuli by increasing neuroplastic activity [10, 25]. However, if these strategies do not develop in a short time, astronauts are affected by SAS and, consequently, by SMS.

Experiments performed within Biosatellite program and Space Shuttle missions reported changes in rodent CNS areas as somatosensory and visual cortex and caudate nucleus which receive extero-, proprioceptive and vestibular inputs. Other areas as the hypothalamus, the posterior cortex, the pons and the medulla werereported to also be changed [193]. Spaceflight and ground-based experiments made on rodents revealed functional and adaptive changes, in particular at the synapsis level. It was hypothesized that this synaptic response represents an adjustment of the CNS to the altered sensory input coming from the vestibular system [194].

Attention has been directed to suggest that the neural development can be affected by changes in gravity fields. Since these processes are regulated by both chemical and mechanical factors, gravity may play a crucial role as a stimulus for proper development of the nervous system. Therefore, during the Cosmos 1514 flight, pups were exposed to space conditions *in*

utero and brains were thereafter morphologically and histochemically examined [168]. Quantitative analysis of the cytoarchitecture of the neocortex showed signs of delayed migration of neuronal elements (neurogenesis). In addition, ultrastructural studies revealed some delay in neuroblastic differentiation as well as in cytoskeletal changes in unmyelinated fibres and in outgrowth cones of axons and dendrites in the hypothalamic supraoptic nuclei [168]. Furthermore, experiments performed on rats during the Space Flight Science 1 and 2 reported changes in ribbon synaptic plasticity. In particular, it was demonstrated that gravity sensor hair cells have an extraordinary ability to change number, type and distribution of synapses. Additionally, it was observed at the flight day 2 (FD2) that the number of synapsis increased in type I and II hair cells of the rat utricular macula, continuing to increase over the time as observed at the FD 14 [165] . Experiments on chicken eye-cup during parabolic flight revealed that the wave propagation velocity of spreading depression (SD) was reduced in low gravity and the latency between the stimulus and the start of the wave increased. On the contrary, the wave propagation velocity of SD increased in hypergravity, leading to the conclusion that the signal propagation in the CNS is gravity-dependent [166].

Since all organisms evolved and developed on Earth, the gravity plays and important role in cell motility. Several experiments on adherent cells exposed to real or simulated low gravity reported morphological alterations, reduced cell locomotion and cytoskeletal changes [15, 38, 54-56, 59, 64, 195]. Therefore, modelled gravity may alter neuroplasticity acting mainly at the cytoskeleton level, reducing the outgrowth cone motility and inducing changes at the synapsis level. The lack of adequate flight hardware to sustain neurons in culture, and the complexity of studying neurons in such a complex situation are some of the causes of our extremely limited knowledge on the effects of microgravity on neurons. Nevertheless a few experiments were performed to increase this knowledge. *In vitro* experiments, performed with well-connected motor-neurons and myocytes exposed for 24 h to clinostat reported that neuromuscular synapses were affected by the reduced gravity [58]. Concomitantly, the similar setup showed a reduced

number of *ex-novo* synapses in co-culture exposed to modelled low gravity compared to controls [58]. Additionally, changes in neuron morphology such as altered cytoskeleton or neurite swelling were described [196]. Studies on outgrowth cone in altered gravity reported an enhancement of actin-dependent lamellar protrusion and cell spreading after parabolic flight or hypergravity [188]. On the contrary, neuroblastoma cells treated with taxol and exposed to simulated low gravity showed outgrowth cones with irregular microtubule structures appearing densely packed and forming loops [188]. Studies on primary cortical neurons reported that dissociated cells firstly exposed for 24 h to the RWV and plated thereafter on coverslips and cultured in ground conditions form cluster and develop more astrocytes than the controls. Moreover, no difference was observed in resting membrane potential between controls and RWV exposed neurons [57]. Ground-based experiments performed on mice using the hindlimb-upload method to simulate microgravity reported a down regulation of Itga3 in brain tissue. This gene encodes for the alpha3 subunit of the transmembrane heterodimeric complex (integrin) which is important for adhesion, locomotion and the organization of sub-membrane actin cytoskeleton [197]. Recent *in vivo* experiments on mice exposed to the ISS environment for 91 days into the new life support system for small animal named Mice Drawer System (MDS) (Fig. 13) [198] reported a possible reduced expression of neuron growth factor (NGF) and brain derived neurotrophic factor (BDNF) in brain tissues as in cortex and hippocampus in spaceflight wild

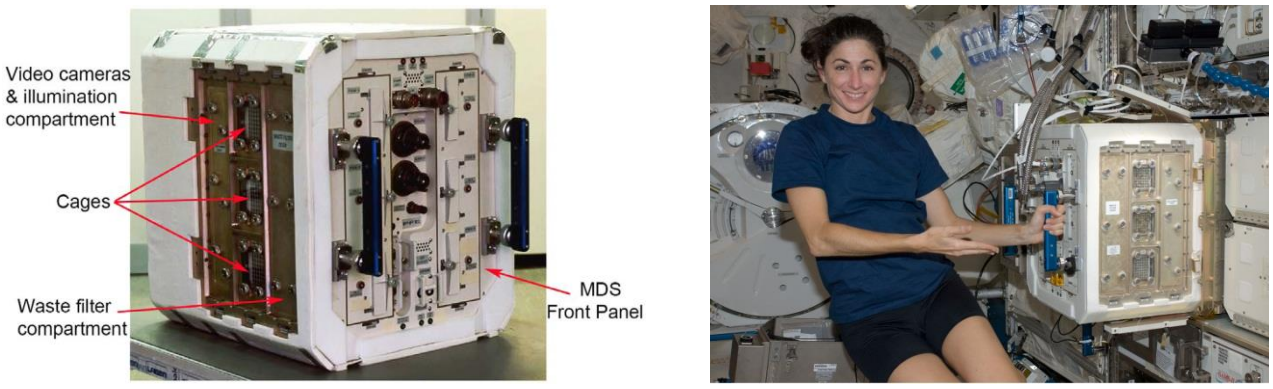

Figure 13: Mice Drawer System (MDS). Left the MDS model; right the MDS installed aboard the ISS

type animal compared to the controls [199]. Furthermore, proteins involved in long-term potentiation or in neurotransmitter release were up-regulated in the whole brain of mice exposed to ISS environment [199].

4.2. CNS and cosmic radiation

During spaceflight astronauts being continuously exposed to radiations could be affected by the Acute Radiation Syndrome (ARS) due to acute radiations in space. Note that radiation syndromes can also appear after chronic exposure, although it is uncommon. It is named chronic radiation syndrome (CRS) [200]. ARS, on the other hand, manifests with different symptoms such as nausea, vomiting, fatigue, skin injury, etc. whereas CRS can lead to neuroregulatory disorders, moderate marked leukopenia, thrombocytopenia and to sometime severe anemia cases [200].

During a stay in the ISS, astronauts are exposed to around 160-200 µGy per day of cosmic radiations. For a travel to Mars, every cell nucleus of the astronaut body would be hit by a protons or secondary particles every few days and by an HZE ion about once a month [201]. Whole-body doses of 1–2 mSv per day accumulate in interplanetary space and about 0.5–1 mSv per day on planetary surfaces [202]. It has been estimated that the travel to and from Mars would take about 400 days and that the complete Mars mission would be around 560 days. Finally, the estimated total dose to which the astronauts would be exposed would be around 1400 mSv. Therefore, the exposure of the crew to cosmic radiations is one of the most important barriers for traveling to Mars.

Due to the highly differentiated and non-cycling nature of neurons, it is assumed that they are more radioresistant than other cell types. Studies in this topic have reported effects of ionizing radiation on neurons at the cellular and molecular levels. Nevertheless, *in vivo* studies indicate that low doses of HZE particles such as Fe and Ar, are capable of producing morphological, neurochemical and behavioural alterations [203-206]. Investigations on

dopaminergic functions in the CNS and correlated motor behaviour of rats reported an alteration after exposure to 0.1 Gy Fe particles [203]. Additionally, these data suggested that rats exposed to Fe ions showed important alterations in neuronal signal transduction in the striatum, and in the motor behaviour parameters [203]. These deficits were characterized by losses in sensitivity of muscarinic receptors to stimulation [203]. Finally, it appears that Fe exposure induces decrements in motor behaviour due to cell loss and deficits in signal transduction in the striatum, the mechanisms of this alteration being attributed to changes in membrane signal transduction parameters [203].

Adult mice exposed to 1.5 Gy high-LET ^{56}Fe beams showed memory impairment 30 days after irradiation [207]. Nevertheless, in behavioural tests (water maze) trained mice attained a baseline value of latencies and the score of success for mice trained to find a hidden platform, after 14 day training was about 45% [207]. Moreover, increase of cell death in Purkinje cells and increase of DNA fragmentation in cerebellum tissue was reported in irradiated mice [207]. Investigation on X-irradiated mice reported a substantial impairment of memory and motor activities [208]. Furthermore, encephalic oxidative stress was observed in mice irradiated with heavy particles or X-rays [207-209]. Investigations on hippocampal plasticity and post-synaptic potential reported an impairment after ^{56}Fe irradiation [167]. Functional assessment of glutamate transport after proton irradiation revealed an increase uptake activity in neurons, whereas, on the contrary, transporter activity in astrocytes decreased [210]. Interestingly, as well, neurogenesis investigation in ^{56}Fe radiation of rodents reported a dose-dependent reduction of neuron generation in the dentate subgranular zone [211].

Finally, *in vivo* studies on radiation countermeasures reported that the use of molecules as lipopolysaccharides, melatonin, α-lipoic acid and superoxide dismutase can consistently reduce the previously described effect induced by radiation [208, 212].

4.3. Concluding remarks

Single cell studies reported morphological changes and motility reduction that occurred during exposure to space conditions. Furthermore, studies in the neuroscience field showed that the CNS is forced to change during spaceflights throughout a modification of its morphological as well as metabolic and functional activities. Therefore, it is important to characterise the neurological risks associated to spaceflight before a long-term space mission such as toward Mars to avoid neurological disorder to occur during or after long-term space mission.

Chapter II | Aim of the thesis

Aim of the thesis

One of the main concerns in space research is to estimate the astronaut health risk during space travel, especially whether the CNS can be damaged by microgravity and/or cosmic radiations exposure inducing behavioural changes, neurodegenerative disorders and learning or memory impairments. As previously observed, real and simulated microgravity, as well as ionizing radiations, can affect cell motility and cytoskeletal protein organization. The remodelling of mature neuronal networks due to environmental changes includes neuroplasticity, synaptic plasticity and neurogenesis; these neuronal functions are regulated by cell motility roles in particular by the activity of the outgrowth cone at the extremity of neurites. Therefore, it might be that exposure of non-connected or well-connected neurons to space conditions could affect the plasticity of these cells inducing neuronal dysfunctions or, in extreme cases, neurodegeneration.

In particular, the main aim of this thesis was to investigate the effects of space conditions on neuronal network remodelling by:

I. studying cell motility in adherent cells (monocytes and neurons) exposed to microgravity;
II. investigating gene expression in *in vitro* well-connected neurons exposed to microgravity;
III. evaluating the correlation between the effects induced by exposure to single or combined space conditions in well-connected neuronal network;
IV. determining the influence of microgravity on DNA repair dynamics in mature neurons during or after ionizing radiation exposure.

The opportunity to perform biological experiments in space is scarce due to the limited access to ISS and associated high cost. Hence, ground based facilities like the Random Positioning Machine (RPM) to reproduce microgravity as well as X-rays for low and high acute

dose radiation exposures and Californium-252 as a source for low dose chronic radiations were used in our laboratories to simulate space conditions.

The first part of this thesis was to select appropriate models and high content analysis methods to investigate neuronal plasticity in microgravity. To this end, this objective was divided into three main tasks. Firstly, we investigated the effects of real space conditions on adherent cell motility and cytoskeleton, using the monocyte/macrophage cell line J-111 as adherent cell model (**chapter III**). These experiments were performed within the "Motion and InterAct" (MIA) experiment carried out aboard the ISS in the framework of the Kubik Bio 1 mission of the European Space Agency. Secondly, we analysed the effects of simulated microgravity on the neuronal network in well-connected neuron cultures after short-, middle- or long-term exposure and to monitor whether the induced changes were permanent or reversible after restoring ground gravitational force (**chapter V**). To this end, dense neuronal networks obtained by culturing mouse primary neurons for 10 days were selected as an *in vitro* model. Thirdly, we selected or developed a toolkit for high content analysis of dense neuronal networks in well-connected mature neuron cultures (**chapter IV**). Fourthly, gene expression was evaluated on well-connected primary mature neurons exposed for short- or long-term to simulated low gravity (**chapter V**).

The second part of this PhD was to investigate the effects of simulated space conditions on neuronal networks and well-connected primary neurons with a particular emphasis on DNA damage/repair dynamics and neuroplasticity. To this end, X-rays were used as model of acute irradiation, while Californium-252 was used for low dose chronic irradiation with high LET neutrons and low LET γ-rays. Finally, we used the RPM as model of simulated microgravity. This particular investigation was divided into 4 tasks. In **chapter VI**, well-connected neuron cultures were exposed to simulated microgravity after X-irradiation to low and high doses with a high dose rate in order to investigate the neuronal network plasticity and mature neuron morphology. Then, in **chapter VI**, well-connected neurons were

concomitantly exposed to simulated low gravity and to chronic low doses of neutrons and γ-rays, simulating space conditions, to determine changes in neuronal network plasticity and neuron morphology. Thereafter, DNA repair efficiency was studied in altered gravity after acute, low or high doses of X-rays and, finally, during exposure to simulated space conditions (**chapter VII**).

Combining all results obtained within this PhD helps to better evaluate correlations between *in vitro* adherent cell models, real and simulated space conditions as well as difference between single and combined space conditions. Additionally, it may help to decipher the effects of combined space conditions on neuroplasticity and connectivity in the brain and to better evaluate the health risks encountered by astronauts during long-term or interplanetary space missions.

Chapter III | Space flight affects motility and cytoskeletal structures in human monocyte cell line J-111

MIA spaceflight hardware (page 59)

*Modified from "Meloni M., Galleri G., **Pani G.**, Saba A., Pippia P., Cogoli-Greuter M. Space flight affects motility and cytoskeletal structures in human monocyte cell line J-111. In: Cytoskeleton, 68:2(2011), p. 125-137.- ISSN 1949-3592". Meloni, Galleri, Pani have made equal contributions to this work.*

Space flight affects motility and cytoskeletal structures in human monocyte cell line J-111

Abstract

Certain functions of immune cells in returning astronauts are known to be altered. A dramatic depression of the mitogenic in vitro activation of human lymphocytes was observed in low gravity. T-cell activation requires the interaction of different type of immune cells as T-lymphocytes and monocytes. Cell motility based on a continuous rearrangement of the cytoskeletal network within the cell is essential for cell-cell contacts. In this investigation on the International Space Station we studied the influence of low gravity on different cytoskeletal structures in adherent monocytes and their ability to migrate. J-111 monocytes were incubated on a colloid gold substrate attached to a cover slide. Migrating cells removed the colloid gold, leaving a track recording cell motility. A severe reduction of the motility of J-111 cells was found in low gravity compared to 1g in-flight and ground controls. Cell shape appeared more contracted, whereas the control cells showed the typical morphology of migrating monocytes, i.e. elongated and with pseudopodia. A qualitative and quantitative analysis of the structures of F-actin, β-tubulin and vinculin revealed that exposure of J-111 cells to low gravity affected the distribution of the different filaments and significantly reduced the fluorescence intensity of F-actin fibers. Cell motility relies on an intact structure of different cytoskeletal elements. The highly reduced motility of monocytes in low gravity must be attributed to the observed severe disruption of the cytoskeletal structures and may be one of the reasons for the dramatic depression of the in vitro activation of human lymphocytes.

1. Introduction

Twenty five years of research in space and in modeled low gravity on ground, provided either by a fast rotating 2D clinostat or a Random Positioning Machine, have clearly shown that mammalian cells are showing alterations in their structure and function after exposure to altered gravity conditions [35, 213]. Cells of the immune system are the most severely affected. Investigations on the effect of gravity on peripheral blood lymphocytes have been triggered by reports in the early 70ties that the responsiveness of lymphocytes from cosmonauts and astronauts towards mitogens was remarkably reduced after spaceflight [214, 215].

A first space experiment with isolated human lymphocytes in culture revealed that their proliferative response to the mitogen Concanavalin A (Con A) was suppressed by more than 90% compared to the ground control [37]. An intensive follow-on research clearly showed that exposure of T lymphocytes in culture to low gravity conditions is accompanied by a major inhibitory effect, remarkably reducing their mitogenic activation process and severely altering growth rate, signal transduction, cytokines production, gene expression, cytoskeletal structures and motility [35, 40, 213, 216-218]. Human lymphocytes have been found to undergo apoptosis by exposure to modeled low gravity [39]. Furthermore it has been clearly demonstrated that factors other than low gravity (i.e. accelerations and vibrations during launch and cosmic radiation) can be excluded to be responsible for the depressed activation of lymphocytes.

The mechanism of T cell activation is very complex and still not yet fully understood. Three signals are required for full T cell activation. The first signal is delivered to the TCR/CD3 complex either by the antigen presenting cell, or by anti-CD3, or by the mitogen Con A. The second signal is a costimulatory signal delivered either by accessory cells - usually monocytes - via B7/CD28 interaction [219] or by anti CD28. Many cell surface receptors are able to enhance signaling through the TCR/CD3 complex, but CD 28 is the most efficient [Acuto and Michel, 2003]. After stimulation of the TCR/CD3 complex and CD28 the signal is transferred to the

nucleus, resulting in the synthesis of Interleukin-2 (IL-2) [220]. IL-2, acting as third signal, is secreted and bound to its receptor (IL-2R). This induces further synthesis of IL-2 and its receptor, resulting finally in full activation [221].

The activation process consists of several steps in which specific cytokines are secreted, locomotion of T cells is reduced and the structure of different cytoskeletal elements is altered before the onset of cell division. Conceivably, gravitational forces may interact with cell organelles and structures like the cytoskeleton, having significant density differences [222].

So far it is still not known which structures or mechanisms might act as "gravity responders" in lymphocytes, but there is increasing evidence suggesting that inhibition of lymphocyte proliferation is due to alterations occurring within the first few hours of exposure to low gravity [223, 224]. Recently it has been discovered that an impaired induction of early genes regulated primarily by transcription factors NF-κB, CREB, ELK, AP-1 and STAT contribute to T cell inhibition in modeled low gravity [225]. Furthermore PKA signal transduction was found to be down-regulated in modeled low gravity, whereas the PI3-K and PKC signals were not inhibited.

Cell-cell interaction and aggregate formation are important means of cell communication and signal delivery in the mitogenic in vitro activation of human T lymphocytes. Especially the interaction between T cells and monocytes is essential for the delivery of the costimulatory signal. Lack of the costimulatory signal results in anergy, a condition in which T cells can no more be stimulated. In earlier flight investigations we observed in real time that lymphocytes in the presence of Con A were highly motile and formed aggregates [226], but no dates are available so far on the motility of monocytes in low gravity. During locomotion, the cytoskeletal structures within the cells are subjected to repeated cycles of reassembly processes. The observed changes in activation and signal transduction as well as motility and aggregate formation of lymphocytes in low gravity may be related also to structural changes in the cytoskeleton due to gravity unloading. Marked alterations in the structure of the intermediate

filaments of vimentin [227] as well as in the microtubules network [228] were observed in Jurkat cells - a T cell line - after exposure to low gravity.

In the present investigation on the International Space Station we studied the motility of adherent human monocytes J-111 and alterations in the cytoskeletal structures of F-actin, β-tubulin and vinculin in these cells in low gravity. As we had found that suspended T lymphocytes are highly motile in low gravity, we hypothesized that an impaired motility of human monocytes could hinder the delivery of the costimulatory signal to activate the B7/CD28 pathway, and thus could be one of the reasons of the observed loss of T cell activation in low gravity. This hypothesis is further supported by the findings that a co-stimulation of CD3-activated cells by CD28 antibodies in modeled low gravity results in a normal T cell activation [229].

Monocytes play an important role in the adaptive immune defense, where they act as antigen-presenting cells and deliver the costimulatory signals essential for a full activation of T lymphocytes. Because of their phagocytic activity monocytes are also fundamental for the innate immune system. Furthermore monocytes migrate from the blood into other tissues and differentiate into macrophages and dendritic cells.

In preparation for this experiment we have investigated the motility of monocytes and changes in their cytoskeletal structure, specifically F-actin, β-tubulin and vinculin, in modeled low gravity conditions provided by the Random Positioning Machine using a similar protocol as for the flight experiment [38].

2. Materials and methods

The space experiment MIA has been performed on the International Space Station in the frame of the Kubik Bio 1 mission of the European Space Agency (ESA). Kubik is an incubator for space experiments manufactured by Comat Aerospace (Toulouse, France). A simultaneous control experiment was done at 1g in space (Kubik centrifuge). Furthermore a ground control experiment was performed with the same batch of cells.

2.1. Experimental hardware

The MIA Hardware has been developed and constructed by EMPA (Dübendorf, Switzerland) and Doctor Dany Lightweight (Urdorf, Switzerland). Each MIA unit (40x13.3x20 mm) can hold one glass cover slide (23x12 mm) covering a culture chamber (volume: 980 µl) and contains culture medium and fixative in their respective special compartments (volume: 270 µl each) [Cogoli-Greuter et al., 2005]. By a special manual mechanism the fixative was brought into contact with the medium in the culture chamber. All parts of the units have been proven to be fully biocompatible in tests with J-111 cells.

2.2. Cell line and cell culture

J-111 is a monocyte/macrophage cell line derived from human acute monocytic leukemia, obtained from "Sperimental Zooprofilatic Institute", Brescia (Italy). The cells display a good adhesion capacity and a certain extent of epithelial morphological polymorphism related to different functional and metabolic status of the cell. The cells were grown in RPMI-1640 medium GlutaMAX containing 10% FCS, HEPES 20mM, sodium bicarbonate 5mM, gentamycin 50 µg/ml and were subcultured every 3 days using 0.25% trypsin/EDTA (all obtained from GIBCO, Invitrogen, Carlsbad, CA). The cells for experiment MIA were transported in culture flasks at 37°C from Sassari to Baikonour.

2.3. "Experiment sequence test"

In order to test the flight protocol proposed by the space agency we have performed an experiment sequence test in modeled low gravity using the Random Positioning Machine (RPM). Two identical set of samples (cells in the MIA hardware) were exposed at 25°C for 60h to modeled low gravity, simulating the transfer of the cells to the International Space Station, followed by 24h at 37°C either at modeled low g (simulating 0g in space) or 1g (simulating in-flight 1g control; 1gSF). Ground Control samples (GC) were incubated first for 60h at 25°C followed by 24h at 37°C. Viability of the cells was evaluated with Trypan Blue and the state of nuclei with DAPI staining (Table II). All values, viability and state of nuclei of single cells, are expressed in percentage on total amount of cells. The counting was performed manually under inverted microscope for viability and on fluorescence images for state of nuclei. For the evaluation of the state of the nuclei we counted only cells with the correct circularity of nuclei.

2.4. Locomotion assay

A quantitative assay for the motility of spreading mammalian cells in culture, which are associated with large surface extensions i.e. lamellipodia and filopodia (microspikes) has been described by Albrecht-Buehler and Lancaster, 1976. In short, freshly suspended cells, plated on top of a gold particle-coated microscope glass slide, produce various surface protrusions and remove the particles within a ring around each cell [230]. During their spreading the cells begin to move while cleaning more particles out of their way. The particles around the cells are mostly cleaned out by surface protrusions during the 1st h after plating and become partly internalized (phagocytosed) and partly accumulated on the cell surface in big clumps without being phagocytosed [230]. To distinguish locomotion on plain surfaces from this combination of phagocytosis and cellular displacement we better indicate this phenomenon as "phagokinetics" and the particle free tracks conveniently visualized as "phagokinetic tracks". In order to observe

and quantify the motile behavior of monocytes under different gravity conditions we plated J-111 cells onto microscope glass cover slides coated with colloidal gold (according to Albrecht-Buehler and Lancaster, 1976 [230]). Exposure of the cells to gold particles had no obvious toxic effects as proven by preliminary viability tests using trypan blue dye exclusion test (Sigma Aldrich, St. Louis, MO). J-111 cells showed normal growth and spreading on gold coated glass slides.

2.5. Gold coating

Glass cover slides were first incubated with BSA (10mg/ml tridistilled H_2O) at room temperature for 10 min, then quickly washed with ethanol 100% and exposed to 85°C for 10 min. Subsequently 5ml of the gold suspension ($AuCl_4H$ 1.45 mM, (Sigma Aldrich, St. Louis, MO)) at 60-80 °C were added. After 45 min of incubation, the slides were washed in normal salt solution (113 mM NaCl, 3 mM KCl, 1 mM $MgCl_2$, 15 mM Na-phosphate, ph 7.8 in tridistilled H_2O), and then inserted into the MIA units. The units were brought to Baikonour at room temperature.

2.6. Pre-flight activities in Baikonour

For the MIA experiment 3 identical sets have been prepared: one set for exposure to low gravity, the second for the 1g control in space and the third for the ground control. Each set contained 2 units with gold-coated glass cover slides for the evaluation of cell motility. The other 4 units with uncoated glass cover slides were used for the investigation of the influence of low gravity on different cytoskeletal structures. The culture chambers of all MIA units were filled at launch-2 days with J-111 cells resuspended in RPMI-1640 with 10% FCS (units with gold coated slides contained $6.4x10^3$ cells, the other $4x10^4$), reservoir 1 with culture medium and reservoir 2 with fixative paraformaldehyde (22.65%). The units were than incubated for 24 h at 37°C to allow the J-111 cells to adhere to the glass cover slide. The2 flight sets were handed over

14 h before launch and transferred into the Soyuz rocket. The samples were stored at room temperature during launch and ascent. The ground control set was brought to Moscow.

2.7. In-flight operations

On flight day 3, the samples were transferred into the Russian segment of the International Space Station and loaded into the KUBIK incubator, one set in static position (low gravity) and one on the centrifuge (in-flight 1g control). After an incubation of 24 h at 37°C all samples were fixed with paraformaldehyde (final concentration: 4%). The ground control experiment was performed in Moscow with a delay of 40 min. The samples were stored at 3-4°C (except for descent and landing) until analysis performed in Sassari. The temperature conditions of the space samples and of the ground controls were recorded with the help of a SmartButton data logger (Atal BV, The Netherlands) from launch-11 h (March 29, 2006) until sample return on April 9, 2006.

2.8. Post-flight processing

After landing the samples were delivered at 4°C to Moscow and transported to Sassari together with the samples from the ground control. The glass cover slides were taken out from each MIA unit and analysed either for migration tracks or the cytoskeletal structures of F-actin, β-tubulin and vinculin.

2.9. Quantitative analysis of migration tracks

To analyze the motility of the J-111 cells, migration tracks were visualized by Bright-field illumination differential interference contrast (Normansky) microscope (Olympus Optical, Hamburg, Germany) magnified with a 20X objective. To evaluate the cell displacement image data were collected using an F View II Image camera with CCD coupled to the software "ANALYSIS" (both from Soft Imaging System GmbH, Münster, Germany).

2.10. Statistical analysis

After grouping displacement ranks the frequency percentages (percentage of cells showing a displacement in the distinct group 1-11) and standard deviation have been calculated. Data were analysed by one-way analysis of variance following rank sum test using SIGMA STAT program (Systat software, San Jose, California). The presented data are the average from 50 cells per slide for each gravity condition (low gravity, 1g in-flight and ground control), whereby 2 slides per condition have been evaluated. Statistical significance was accepted at the $P \leq 0.0001$ level.

2.11. Analysis of cytoskeletal structures

Cytoskeletal structures of β-tubulin and vinculin were detected by indirect immunofluorescence technique whereas F-actin was revealed by direct fluorescence. After extensive washing and cell permeabilization with Triton X-100 (Sigma) 0.1% in PBS for 3 min, fluorescent staining was performed by exposing the slides either to monoclonal anti- β-tubulin clone TUB 2.1, (diluted 1:100 in PBSO, Sigma) or to monoclonal Anti-Human Vinculin clone hVIN-1 (diluted 1:100 in BSA-PBS, Sigma), both at 37 °C for 1h in a moist chamber. After washing in PBSO and PBS respectively, a second layer of anti-Mouse IgG FITC conjugated (diluted 1:100 in BSA-PBSO or BSA-PBS respectively), was applied for 45 min, at room temperature in the dark. For the cytochemical labeling of F-actin, permeabilized cells were stained with 5μg/ml Phalloidin-FITC or -TRITC conjugated (Sigma) solution in PBS, at 37°C for 15 min. Nuclei were stained with 4',6'-diamidine-2-phenylindole hydrochloride (DAPI, Böhringer Mannheim GmbH, Germany), (100 ng/ml in PBS) for 6 min. Slides were rinsed in PBS and mounted with Immu-Mount (Shandon, Pittsburgh, Pennsylvania, USA). Cytoskeletal structures were visualized by fluorescence inverted microscope (Olympus Optical, Hamburg, Germany) using an oil immersion 100X objective (NA 1.3-0.6). To support the qualitative

microscopic observations on cell morphology and cytoskeletal features quantitative analysis of cell surface area and fluorescence intensity of cytoskeleton components of F-actin and β-tubulin were performed on cell images in gray color (8 bit). To obtain not overexposed pictures with good depth of field for fluorescence intensity analysis, the objective iris diaphragm was set in order to have N.A. 1 and a statistical analysis about exposure time (data not shown) between all experimental points for β-tubulin and F-actin were fixed at 4.3 and 3.5 sec respectively.

The morphometric analysis on cytoskeletal structures was based on algorithm applicable to fixed and immunolabeled cells expressing fluorescently tagged cytoskeletal proteins [231]. Fluorescence intensity of filaments of F-actin and β-tubulin were detected by Data Analysis-algorithm, after background removal and cell perimetral and fluorochrome pixel selection. The data indicate the rate of labeled actin or tubulin filaments referred to the total cell surface and the quantitative extent of cytoskeletal filaments network. Simultaneously, on the same images, the surface areas of the cells were evaluated using a measurement function of the same software. The presented data were from at least 50 values per each experimental condition (low gravity, 1g in flight and ground control). Statistical analysis on the quantitative data consisted of a T- test to compare matched values and was supported by Mann Whitney test.

3. **Results**

For the MIA experiment 3 identical sets have been investigated. On the International Space Station one set was placed in the static position in the Kubik incubator and thus exposed to low gravity in order to evaluate the influence of weightlessness on the motility of J-111 cells and their different cytoskeletal structures. The second set was placed simultaneously on the Kubik centrifuge for the 1g control in space. The 1g control in space is very important in order to distinguish between the effect of low gravity and possible effects caused by other factors as accelerations and vibrations due to launch or cosmic radiation. The cells exposed to low gravity have the same history related to launch and cosmic radiation as the one at 1g in space. A ground control experiment with the same batch of cells (prepared in Baikonour) was performed in the MIA hardware with 40 min delay to the operations in space at the Institute of Biomedical Problems in Moscow.

3.1. Cell motility

The qualitative microscopic analysis of the migration tracks of J-111 monocytes on gold particle coated cover slides revealed a normal pattern of cell migration at 1g in-flight and in the ground control, similar to those described in the literature [232]. Cells had the typical morphology of migrating monocytes, elongated and with pseudopodia and areas around cells appeared completely cleaned out of gold particles (Fig. 14 b-c bottom). On the other hand, J-111 cells exposed for 24 h to low gravity in space showed only very short migration tracks (Fig. 14 a bottom). Thus the motility of monocytes is very much reduced under this condition.

A quantitative analysis of the migration tracks revealed a clear difference in the locomotion ability of the cells in low gravity compared to 1g in-flight and ground controls. Cells exposed for 24 h to low gravity moved with an average of 8 µm and the most frequent displacement (43%) was between 0-4 µm (Fig. 14a top), whereas in the in-flight 1g control an

average displacement of 31 µm was observed and the most frequent displacement (14%) was between 30-34 µm (Fig. 14b top). The cells in the ground control showed a displacement of 49 µm on average with the most frequent displacement (40%) of ≥ 50 µm (Fig. 14c top).

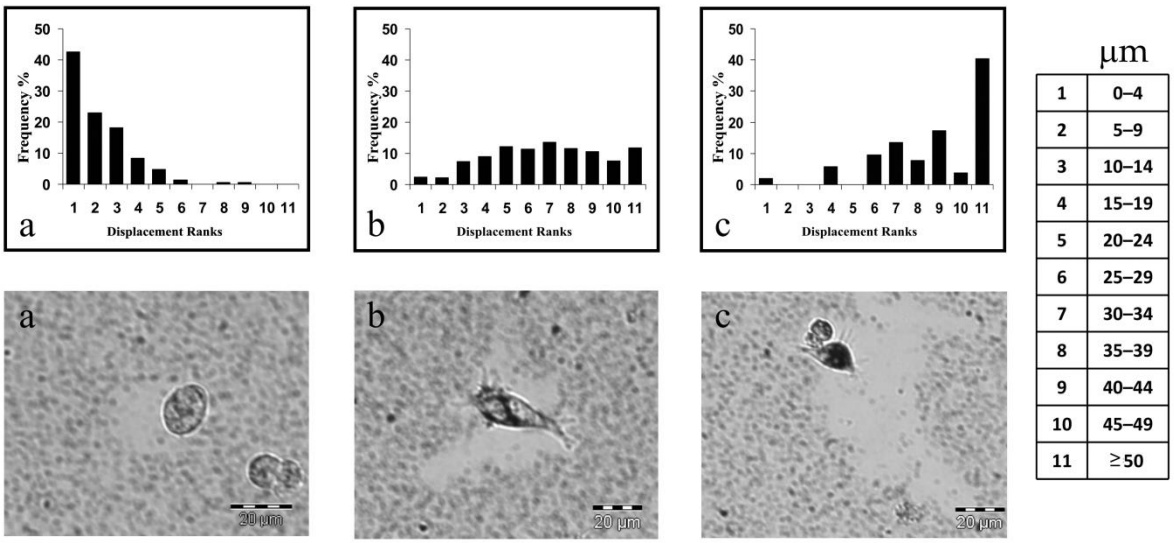

µm	
1	0–4
2	5–9
3	10–14
4	15–19
5	20–24
6	25–29
7	30–34
8	35–39
9	40–44
10	45–49
11	≥50

Figure 14: Migration tracks of J-111 on gold particle-coated slides.
a-c bottom. Migration tracks on gold particle-coated glass cover slides of J-111 cells observed with bright-field illumination differential interference contrast (Normansky) microscope after 24h of exposure to low gravity (a), 1g in-flight (b) and ground control (c). Very short migration tracks were observed at low gravity and cell shape appeared more contracted (a). Conversely 1g in-flight (b) and ground samples (c) showed areas around cell completely cleaned out of gold particles and the typical morphology of migrating cell, elongated and with pseudopodia. a-c top. Displacement frequencies (in %) of J-111 cells on gold particle-coated glass cover slides after 24 h of exposure to low gravity (a), to 1g in-flight (b) and in ground control (c). Cells exposed to low gravity moved between 0 and 4 µm with the most frequent displacement (43%) (a) compared to 1g in-flight control (b) with the most frequent displacement (14%) between 30 and 34 µm and to the ground control (c) with the most frequent displacement (40%) > 50 µm. The data are the average from 50 cells per slide for each gravity condition, whereby 2 slides per condition have been evaluated. Statistical significance was accepted at the P < 0.0001 level.

A remarkable difference of the motility of the cells in the in-flight 1g and the ground control was found. The most likely explanation for this discrepancy is that this is due to a memory effect of the cells as they have been exposed for 55.5 h to low gravity conditions during ascent and transfer into the International Space Station before they were placed on the 1g centrifuge. Similar phenomena have been observed by us [233] and other research teams [234] in human T lymphocytes and human monocyte cell line U937 in earlier spaceflight experiments.

The results from the MIA experiment on locomotion of J-111 monocytes exposed for 24 h to low gravity in space are comparable to those obtained in a previous ground based study in the Random Positioning Machine where the cells were exposed to modeled low gravity [38]. Again a normal pattern of monocyte locomotion was found in the control samples, whereas very short migration tracks were observed after 24 h of exposure to modeled low gravity (Table 2).

Table 2. Migration tracks of J-111 monocytes observed in low gravity in space and in modeled low gravity obtained on the RPM and respective controls

Gravity conditions	Average displacement	Most frequent displacement (%)
Space experiment		
0g	8 µm	43% between 0-4 µm
1gF	31 µm	14% between 30-34 µm
GC	49 µm	40% > 50 µm
Experiment on RPM*		
0g	8.7 µm	37% between 0-4 µm
GC	59.7 µm	62% > 50 µm

RPM - Random Positioning Machine
0g - low gravity in space and modeled low gravity
1gF - 1g in fight
GC - ground control
* Meloni et al., 2006

The quantitative measurement of the surface area of J-111 cells showed a significant difference between low gravity samples v/s in-flight 1g ($P = 0.0112$) and low gravity samples v/s ground control ($P = 0.0075$) revealing that the areas of the cells exposed for 24 h to low gravity conditions are significantly smaller than those of the controls (Fig. 15 b). In fact, the shape of the cells exposed to low gravity appeared more contracted, whereas the cells of the in-flight 1g and ground controls showed the typical morphology of migrating monocytes, i.e. elongated and with pseudopodia. Cells exposed to low gravity showed only in some cases very short protrusions.

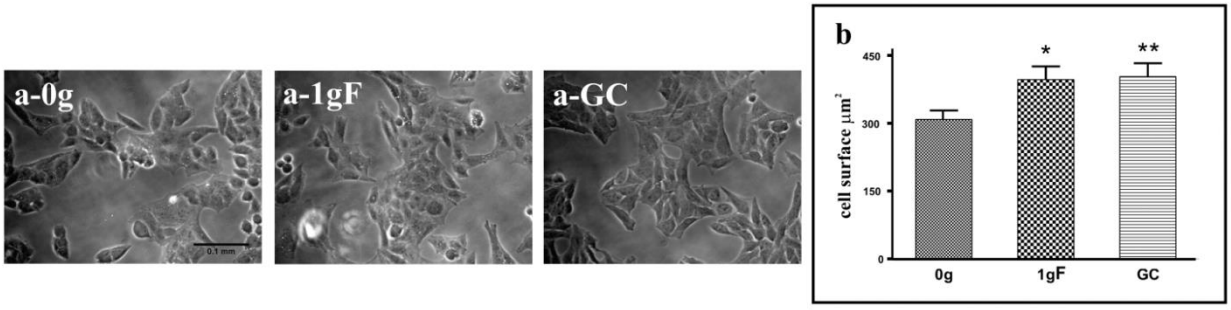

Figure 15: Monolayer of J-111 monocytes and analyses of cell surface.
a) Monolayer of J-111 monocytes from 3 different gravity conditions: low gravity (a-0g), 1g in-flight (a-1gF) and ground control (a-GC). Axiovert 25 Zeiss microscope with phase contrast. b) Quantitative analysis of J-111 cell surface area (µm2) after 24 h of exposure to low gravity (0g), 1g in-flight (1g) and in ground control (GC). Significant differences were observed, by digital fluorescent microscope, between 0g v/s 1g in-flight (P = 0.0112) and 0g v/s GC (P = 0.0075). All values are expressed as MEAN ± SEM.

In order to assess cell adhesion and spreading of J-111 monocytes we examined visually samples from the different gravity conditions (Fig. 15, left panel). No significant differences concerning cell-substratum adhesion were observed between cells exposed to low gravity (Fig. 15; a-0g) and control samples (Fig. 15 a-1gF and a-GC), but the cells at 0g appeared smaller and more contracted. This is in agreement with the quantitative analysis of cell surface area (Fig. 15 b). In space no viability tests could be performed before fixation of the cells. Thus, in order to assess the state of the cells, we have analysed the morphology of the nuclei in the merged fluorescence images (Fig. 16). In all 3 experimental conditions, DAPI staining showed normal nuclei in about 80% (± 10% SE) of the cells. DAPI test performed on each culture supernatant showed a nearly total absence of detached cells. These findings are in agreement with the previous analysis on cell viability in the MIA units in an experiment sequence test performed in preparation of the space experiment (Table 3).

Table 3. Cell viability and state of nuclei of J-111 monocytes in space investigation and mission sequence test on RPM.

Gravity conditions	Viability Trypan blue test (%)	State of nuclei DAPI staining (%)
Space experiment		
0g	-------	76,3
1gF	-------	81,2
GC	-------	84,6
Mission sequence test on RPM		
0g	78,5	79,2
1gSF	80,5	85,4
GC	85,4	87,8

RPM, random positioning machine;
0g, low gravity in space and modeled low gravity;
1gF, 1g in flight;
1gSF, 1g simulated flight;
GC, ground control.

3.2. Cytoskeletal architecture

A 24 h exposure of J-111 cells to low gravity conditions in space resulted in severe alterations of the structures of F-actin, β-tubulin and vinculin. In 1g conditions (ground and in-flight 1g controls) the structures of all 3 different cytoskeletal elements showed a normal and well organized network.

3.2.1. Microfilaments: F-actin

In the in-flight 1g and ground controls the architecture of F-actin appeared normal with a well organized network of cytosolic bundles and elongated and extended filopodia (Fig. 16 a-1gF and a-GC). Conversely, a remarkable decrease of the density of the filamentous biopolymers of F-actin was observed in J-111 cells exposed to low gravity (Fig. 16 a-0g). The actin filaments showed a disappearance of the complex cytosolic network and appeared mostly localized close to the plasma membrane. Identical changes in the structure of F-actin were observed in cells exposed for 1 h to modeled low gravity on the Random Positioning Machine

[38]. After 24 h in modeled low gravity an initial reorganization of the actin network was observed.

3.2.2. Microtubules: β-tubulin

The microtubules of J-111 monocytes showed a normal structure in the ground as well as in the in-flight 1g control (Fig. 16 b-1gF and b-GC). They appeared orderly radiating from the perinuclear area throughout the cytoplasm toward the cell periphery. Incubation of J-111 cells in low gravity conditions resulted in a disruption of the β-tubulin architecture (Fig. 16 b-0g). The microtubules, responsible for cell division, did not display their typical radial array; they were highly disorganized, and showed a more evident thickening in perinuclear position and a surrounding arborization that appeared organized but with short and incomplete prolongations towards the plasma membrane. Very similar changes in the structure of microtubules were observed in cells which experienced modeled low gravity for 1 and 24 h in the Random Positioning Machine [38].

3.2.3. Vinculin

Vinculin is an anchor protein which specifically participates in the formation of a submembrane “plaque” structure (focal adhesion plaque) responsible for the attachment of actin filaments to the plasma membrane. Fluorescence images of J-111 monocytes provide profiles of vinculin spots localized in focal adhesion plaques. In the in-flight 1g and ground controls (Fig. 16 c-1gF and c-GC) endogenous vinculin appeared concentrated as streak-like structures exhibiting a normal radial orientation towards the cell membrane according to cell spreading and connected to actin filaments. Samples exposed to low gravity (Fig. 16 c-0g) showed vinculin proteins thickened close to the cell membrane as globular clusters, losing radial orientation and arranging parallel to cell membrane, concomitantly to the altered redistribution of actin filaments. This is in correlation with the cell morphology showing more contracted and round cells, as a consequence of the decrease of cell spreading. Vinculin spots appeared to be larger

and the accumulation of fluorescent protein-tagged vinculin in the focal adhesions was usually more prominent in control cells (Fig. 16 c-1gF and c-GC) than in cells submitted to low gravity (Fig. 16 c-0g). The number of focal adhesions per single cell and the spatial extent of each individual adhesion plaque appeared to be reduced in low gravity as compared to those in cells exposed to normal gravity. The percentage of cells with altered vinculin location was 73.8% ± 9% in low gravity, and was the average from 50 cells per slide, whereby 2 slides have been evaluated. On the contrary samples at in-flight 1g and in the ground control showed a normal vinculin distribution (93% ± 7% in-flight 1g and 97.8% ± 3% in the ground control, respectively).

A quantitative analysis revealed that exposure of J-111 cells to low gravity conditions for 24 h affected the cytoskeleton network not only in the distribution of the filaments but also in the fluorescence intensity of the cytoskeletal pattern of F-actin and β-tubulin when compared to in-flight 1g and ground controls. The morphometric analysis performed by measuring fluorescence intensity of F-actin or β-tubulin filaments and referred to the total cell surface area, showed a significant statistical difference between F-actin fluorescence intensity of cells exposed to low gravity conditions compared to in-flight 1g controls (0g v/s 1g in-flight, $P < 0.05$) (Fig. 16 a-I). The difference was even more evident between low gravity samples compared to ground controls (0g v/s GC, $P < 0.0001$). On the other hand, the fluorescence intensity of β-tubulin related to total cell surface area showed no statistical difference between β-tubulin fluorescence intensity of samples exposed to low gravity conditions compared to in-flight 1g controls as well as between in-flight 1g compared to ground controls, whereas low gravity samples showed a slight difference versus ground controls (0g v/s GC, $P < 0, 05$) (Fig. 16 b-I).

The data of this space experiment and the earlier one in the Random Positioning Machine [38] suggest that the reduced migration response in J-111 cells exposed to low gravity (real and modeled) is linked to changes of the cytoskeletal structures and focal adhesion plaques.

Figure 16: Immunofluorescence images of F-actin (a), β-tubulin (b) and vinculin (c) in J-111 cells cultured under different gravity conditions.
a) F-actin monochromatic and merge immunofluorescence images with F-actin (green color) and nuclei (blue color) in J-111 cells after 24h of exposure to low gravity (a-0g), 1g in-flight (a-1gF) and in ground control (a-GC). a-I) Fluorescence intensity of F-actin filaments at low gravity (0g), 1g in-flight (1gF) and in ground control (GC). A statistical significant difference was observed between F-actin fluorescence intensity of samples exposed to low gravity conditions compared to 1g in-flight (0g v/s 1gF, P=0.03) and mostly between 0g samples compared to ground controls (0g v/s GC, P<0.0001). All values are expressed as MEAN ± SEM. 3b) β-tubulin monochromatic and merge immunofluorescence images with β-tubulin (green color) and nuclei (blue color) in J-111 cells after 24 h of exposure to low gravity (b-0g), 1g in-flight (b-1gF) and ground control (b-GC). b-I) Fluorescence intensity of β-tubulin at low gravity (0g), 1g in-flight (1gF) and in ground control (GC). Statistical difference was not observed between β-tubulin fluorescence intensity of samples exposed to low gravity conditions (0g) compared to 1g in-flight (1gF), as well as between 1g in-flight compared to ground controls (GC), whereas low gravity samples showed a slight difference versus ground controls (P = 0.03). All values are expressed as MEAN ± SEM. c) Vinculin monochromatic and merge immunofluorescence images with Vinculin (green color), F-actin (red color) and nuclei (blue color) in J-111 cells after 24 h of exposure to low gravity (c-0g), 1g in-flight (c-1gF) and in ground control (c-GC).

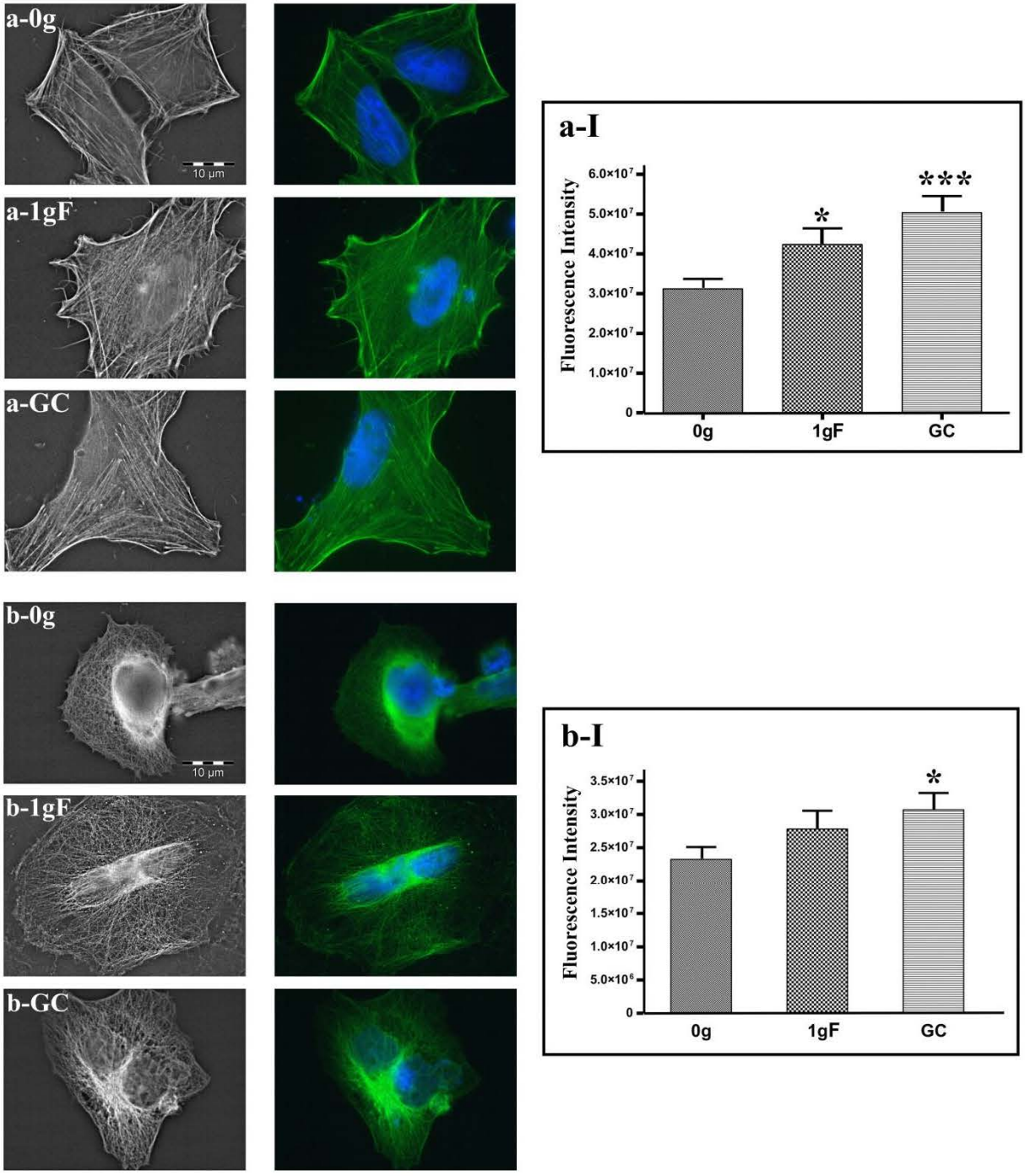
a-0g
10 μm
a-1gF
a-GC
a-I
Fluorescence Intensity
6.0×10⁷
5.0×10⁷
4.0×10⁷
3.0×10⁷
2.0×10⁷
1.0×10⁷
0
*
***
0g
1gF
GC
b-0g
10 μm
b-1gF
b-GC
b-I
Fluorescence Intensity
3.5×10⁷
3.0×10⁷
2.5×10⁷
2.0×10⁷
1.5×10⁷
1.0×10⁷
5.0×10⁶
0
*
0g
1gF
GC
c-0g
10 μm
c-1gF
c-GC

4. Discussion

The response of any organisms to gravity depends ultimately on functions at the cellular level, as single cell functions may be affected by gravity themselves. Still little is known about the effect of gravity at the scale of single cells, as research in cell biology in space has been rare and frequently unrepeated. More insight on the influence of low gravity on single cells comes from investigations performed in modeled low gravity on Earth using different simulation devices. As cells are sensitive to mechanical forces, low gravity might act on stress-dependent cell changes and specifically on the cytoskeleton. The cytoskeleton has been described to be the structure through which the cells sense gravity [60]. The cytoskeleton has an important role in the maintenance of the cell structure, cell movement and migration. Cell migration is an essential characteristic of many biological processes within an organism. In previous studies in modeled low gravity, several type of cells, such as T lymphocytes [235], human mesenchymal stromal precursor cells [236], vascular endothelium cells [237-239] and malignant human MCF-7 cells [240] showed reduced cell motility and migration. So far the basic mechanisms responsible for these phenomena in low gravity are still unclear.

On Earth, cells have evolved distinct mechanisms for generating cell movement. One mechanism responsible for cell motility and changes in the shape of a cell is a continuous rearrangement of cytoskeletal structures mostly by an assembly and disassembly of microfilaments and microtubules. Investigations in low gravity in space and in modeled gravity on ground revealed that different cytoskeletal structures, both in adherent and non-adherent cells, are highly sensitive to gravity changes. [56, 217, 228, 240-242].

Monocytes play an important role in the immune defense. Because of their phagocytic activity and their ability to differentiate into antigen-presenting cells monocytes participate in the innate as well as the adaptive immune response. As antigen presenting cell monocytes are involved in the activation of T lymphocytes, but they are also delivering the second signal - a

costimulatory signal - via B7/CD28 interaction [219]. Furthermore monocytes migrate from the blood into other tissues and differentiate into macrophages.

Migration of immune cells - lymphocytes and monocytes - is a crucial process during a multitude of physiological and pathophysiological conditions such as development, defense against infections and wound healing [232, 243].

In the present investigation performed on the International Space Station we found by a quantitative analysis that in low gravity the locomotion capability of J-111 cells on gold particle coated cover slides is remarkably reduced compared to the in-flight 1g and ground controls. The cell shape appeared more contracted, whereas the cells of the 1g in-flight and ground controls showed the typical morphology of migrating monocytes.

The different cytoskeletal structures are very important for cell motility. Recent findings highlight the cytoskeleton cross-talk during cell motility, coordination of membrane and actin cytoskeleton dynamics during filopodia protrusion and the importance of the intact networks of both cytoskeletal actin filaments and microtubule dynamics in cell movements [232, 244]. Cell migration begins with an initial protrusion or extension of the plasma membrane at the leading edge of the cell, driven by the polymerization of actin filaments, and stabilized through the formation of plasma membrane adhesive complexes, regulated by the combined microtubules activity. Actin polymerization plays also an important role in multiple and crucial aspects of the immune response including the antigen recognition, signal transduction, T cell proliferation, migration and adhesion [245]. Microtubules are also regulators of focal adhesion and turnover of focal complex. This is critical for the continued remodeling and reorganization of adhesion contacts during cell migration [246]. Microtubule fiber dynamics are required for the polarized protrusion of lamellipodia that drives the directional cell migration [247]. The acquisition of cell polarity induced by a reorganization of the different cytoskeletal elements is very important for migration, activation and apoptosis in leukocytes, i.e. in lymphocytes and monocytes [248].

The cytoskeleton is important for maintaining cell shape and coordinating cell motility. Furthermore it also locates organelles and cellular proteins in their proper spatial position with respect to each other and thus also plays a key role in signal transduction [182]. A disruption of the cytoskeletal network, caused for instance also by gravity changes, has an impact on signal transduction, cell growth and metabolism [249, 250]. In the present work we have observed severe alterations in the structure of F-actin, β-tubulin and vinculin in J-111 monocytes exposed for 24 h to low gravity conditions compared to in-flight 1g and ground controls.

The F-actin network showed a remarkable decrease in the filamentous biopolymers density. The microfilaments did not form into their usually strong bundles, with no preferential orientation and less lamellipodia. Concomitantly the normal polyhedral cell shape changed to a roundish one, the long filopodia were no longer present, and thus the cells appeared more contracted with only short protrusions. The layer of actin underneath the plasma membrane, responsible for the cell shape and the production of filopodia, was no longer continuous but interrupted at various places. The altered shape of the cells corresponded to the altered network of actin filaments.

Similar changes in the actin network, especially a disorganization and reduction of the stress fibers, in cells exposed to low gravity are also found in osteoblasts [251], human vascular endothelial cells [252], glial cells [56], HUVEC cells [69] and several other cells (for a review see [249]). Microfilaments in MCF-7 cells were not organized in bundles and the cells lacked lamellipodia [240].

The changes observed in the microtubules network of J-111 cells in space and in modeled low gravity [38] were similar to those observed by Lewis et al. [228] in Jurkat cells exposed to low gravity in space, showing that microtubule organizing centers were poorly defined. The intermediate filament network, responsible for the shape and position of the nucleus, was found to be disorganized, and the microtubules, lost their radial disposition. After 24 h exposure to modeled low gravity conditions an initial reorganization of the actin and tubulin network in J-

111 cells was taking place [38]. A similar reorganization of the microtubule network was also observed in Jurkat cells exposed to low gravity conditions [228]. But, despite the fact that the morphology of the microtubule network had a normal aspect, the functional state of the cells did not return to normal as the cells did not proliferate. In a cell free system, the self-assembly of microtubules was found to be inhibited in low gravity [253].

Vinculin is one of the most prominent membrane-cytoskeletal proteins in focal adhesion plaques and is involved in linkage of integrin adhesion molecules to the actin cytoskeleton. These adhesion sites serve as traction points for impellent forces that push the cell moving forward. Vinculin appears to facilitate the assembly of focal adhesion plaques by crosslinking and recruiting its various partners [254]. Vinculin's ability to interact with integrins to the cytoskeleton at the focal adhesion appears to be critical for control of cytoskeletal mechanics, cell spreading, and lamellipodia formation. Thus, vinculin appears to play a key role in shape control based on its ability to modulate focal adhesion structure and function [255, 256].

In J-111 cells exposed for 24 h to low gravity, we observed that the vinculin proteins are not evenly spread but thickened close to the cell membrane as globular clusters. Fewer and smaller focal adhesion plaques can induce a decrease of cell spreading and migration [257].

It is interesting to note that the structures of F-actin and β-tubulin of monocytes of the in-flight 1g samples are similar to those in the ground control, despite the fact that these cells have been exposed for 55.5 h to low gravity before they have been loaded on the 1g reference centrifuge in Kubik. Thus the structures of F-actin and β-tubulin in the J-111 cells have completely recovered within 24 h at 1g.

Based on our results – alterations in the structures of F-actin, β-tubulin and vinculin - and those of other authors it can thus be speculated that the impaired motility of adherent monocytes in low gravity on gold particle coated cover slides might be due to the disruption of the cytoskeletal network. The fact that the monocytes lost their ability to migrate may also be responsible for a hindered delivery of the costimulatory signal in T cell activation, important for

a full activation. Indeed, in several investigations we have found that the mitogenic activation of human lymphocytes is suppressed by more than 90% in low gravity [218].

The cytoskeleton has been described to be the structure through which the cells sense gravity [60]. In most cells, shape is determined and maintained by cytoskeleton polymerization forces, weaker in some cell types than in others and extension of microtubules to the cell membrane [258] to maintain mostly uniform cell surface tension. In the absence of gravity, very subtle cell volume changes may result from hydrostatic pressure shifts, potentially causing disjunction between the membrane and critical cytoskeletal elements [259]. Mechanical changes may be transduced into biochemical responses through the cytoskeletal scaffolding within the cell [260]. If cytoskeletal structures as F-actin and microtubules but also the intermediate filaments of vimentin are disrupted, molecular transport by cytoskeletal elements would be affected and cell surface, receptor-dependent signal transduction reactions could not occur. Besides the changes in the structures of F-actin and microtubules in monocytes, lymphocytes and other cells, reported by us and other authors we also have found significant changes in the structure of vimentin in Jurkat cells [227]. These alterations were observed already after an exposure of 30 seconds in low gravity and consisted in the formation of thick bundles compared to the fine network in the 1g control.

In the present investigation we have found that the motility of adherent monocytes is remarkably reduced in low gravity. Furthermore the cytoskeletal structures of F-actin, β-tubulin and vinculin are severely damaged. We thus speculate that the disruption of the 3 different cytoskeletal elements is the main reason for the loss of the ability of the J-111 cells to migrate. A disruption of the different cytoskeletal structures in monocytes may also have an influence on the differentiation of monocytes in low gravity and hence affect their role in the innate immune system.

Different cells of the innate immune system including monocytes are known to be sensitive to gravity changes. In blood samples of astronauts returning from space changes in the number

of monocytes and natural killer cells were observed depending on mission duration. After a 9-day missions, monocytes were increased while natural killer cells were decreased. However, monocytes were decreased after the 16-day missions whereas no change occurred in natural killer cells [261]. Furthermore, an increase in neutrophil granulocytes was found, but their phagocytic and oxidative functions significantly decreased [262]. In low gravity, monocytes lost their capability of secreting IL-1 [263] and expressing IL-2 receptor [223]. Space flight experiments revealed that the distribution, cellular quantity and kinetics of translocation of PKC- a key protein controlling growth and differentiation of monocytes into macrophages - are altered in U937 monocytes in low gravity [234, 264, 265]. Recently, the examination of gene expression of monocytes under low gravity demonstrated significant changes in gene induction associated with differentiation of monocytes into macrophages [266]. On the other hand, extensive studies in modeled and low gravity in space revealed that the cytotoxic effects of natural killer cells were not affected by gravity changes [267].

There are severe limitations in the number and type of experiments that can be conducted in low gravity in space. Therefore we have performed many studies with immune cells - lymphocytes and monocytes – in the Random Positioning Machine (RPM). The RPM is a device creating similar gravity conditions as obtained in space by randomizing the gravity vector. When we compare the data of the present investigation in space with the results obtained with the same cells - J-111 monocytes - in modeled low gravity [38] we can conclude that this is a suitable tool for gravity research on ground. Furthermore we also found a very good concordance of the results obtained with human lymphocytes in space as well as on ground in modeled low gravity [218].

Qualitatively, the results from space-flown immune cells in cultures, and cells exposed to modeled low gravity, are often similar to the effects space flight exerts on functional aspects of immune cells obtained from cosmonauts/astronauts after their return to Earth. The extensive research on immune cells in culture under different gravity conditions contributes significantly to

the understanding of growth responsiveness during space flight and may help in predicting potential compromise to immune functions in humans during long duration missions.

Chapter IV | MorphoNeuroNet, an automated method for dense neurite network analysis.

Modified from **“Pani G.**, De Vos W., Samari N., de Saint-Georges L., Baatout S., Van Oostveldt P., Benotmane M.A. MorphoNeuroNet, an automated method for dense neurite network analysis.” Conditionally accepted with major revision in Cytometry part A and revised version submitted in June 2013

MorphoNeuroNet, an automated method for dense neurite network analysis.

Abstract

High content cell-based screens are rapidly gaining popularity in the context of neuronal regeneration studies. To analyse neuronal morphology, automatic image analysis pipelines have been conceived, which accurately quantify the shape changes of neurons in cell cultures with non-dense neurite networks. However, most existing methods show poor performance for well-connected and differentiated neuronal networks, which may serve as valuable models for i.e. synaptogenesis.

Here, we propose a fully automated method for quantifying the morphology of neurons and the density of neurite networks, in dense neuronal cultures, which are grown for more than 10 days. MorphoNeuroNet, written as a script for ImageJ, Java based freeware, automatically determines various morphological parameters of the soma and the neurites (size, shape, starting points, fractional occupation). The image analysis pipeline consists of a multi-tier approach whereby the somas are segmented by adaptive region growing using nuclei as seeds, and the neurites are delineated by a combination of various intensity and edge detection algorithms.

Quantitative comparison showed a superior performance of MorphoNeuroNet to existing analysis tools, especially for revealing subtle changes in thin neurites, where the fluorescence intensity is low compared to the rest of the network.

The proposed method will help determining the effects of compounds on cultures with dense neurite networks, thereby gaining physiological relevance for cell-based assays in the context of neuronal diseases.

Keywords: Mature neuronal network, neurite tracing, neural morphology, ImageJ.

1. **Introduction**

The correct development of a neuronal network depends on neuron migration, regulated outgrowth of neurites (axon and dendrites) and connection with target cells (synaptogenesis) [268]. Cultured primary neurons are terminally differentiated and so they do not undergo mitosis. Neurogenesis can only occur if neuron progenitors are present in the culture and if they receive specific stimuli [269, 270]. Consequently, cultured neurons are able to create a network only by increasing neurite density and synaptic connections. The growth of the network is enhanced in the early stages of the culture until it reaches a plateau phase [176]. Based on the neurite density, two types of neuronal networks can be distinguished, non-dense and dense neurite networks. Non-dense neurite networks (NDN) are found in young cultures, grown for a max. of 3 days, with single immature neurons having short neurites with distinct tips and only a few connections. In dense neurite networks (DN) (after 8-10 days of culture), neurons have matured and they are intensively wired, with many neurites connecting various neuronal cells. Mature and immature neurons not only differ in structural aspects (number of synapses and neurite growth speed), but also in functional behaviour (action potential activities, spontaneous synaptic currents, synaptic protein distribution…) [175, 176]. Additionally, recent studies suggest that GABA and glycine neurotransmitters have inhibitory activity on mature but excitatory activity on immature cortical neurons [177, 178]. Furthermore, mature neurons are less sensitive to external compounds or agents than immature neurons [179, 180]. These differences can have important implications for clinical applications.

Modification of neuronal structures in response to environmental changes via the strengthening, weakening, pruning, or adding of synaptic connections is an intrinsic property of the neuronal network known as neuronal plasticity [154]. Understanding how the central nervous system reacts to potential therapeutic compounds or external impulses is one of the major challenges in neurobiology. *In vitro* assays on neurite outgrowth offer an attractive model for

studying biological or pharmacological effects on neuronal differentiation and re- or degeneration [271, 272]. This is done by measuring morphological features that portray the complexity of the neuronal network such as the branching of neurites. Whereas manual outlining of neurites is highly accurate and has successfully been applied to various small-scale screenings [273, 274], it is very laborious and not compatible with high-throughput screening methods. Hence dedicated image analysis pipelines are required that allow fully automated segmentation of neuronal network structures in combination with morphological feature extraction. Commercial solutions have been conceived by *inter alia* Imaris (Bitplane), Amira (Visage Imaging), HCA-Vision (CSIRO Biotech Imaging) but they are usually not openly for user customization and they are mainly available to large neuroscience groups. Open-source tools offer a cost-efficient alternative and can be adjusted more easily to the user demand, which is why developments in this field are ample. Indeed, several open-source tools for neurite outgrowth analysis have been devised for ImageJ, a popular and powerful open-source image analysis program [275]; to give a few examples, NeuronJ [276], NeuriteTracer [277], NeuronMetrics [278] and NeurphologyJ [279] are able to reliably trace neurites in non-dense neurite network cultures (NDN) and estimate their length with a good approximation (Table 4).

Given the important differences between mature and immature neuron cultures (cfr. above) and with an eye on gaining physiological relevance, one of the current challenges is to determine the effects of compounds/stressors on well-connected and differentiated neuronal cultures with DN (as opposed to routinely used early-stage NDN cultures). *In vitro* models with well-connected neurons are useful in investigating adult neurological diseases where events such as neuronal degeneration or regeneration are involved. In DN culture, neuronal morphology, connectivity and neuroplasticity can be monitored upon genetic, electrical or chemical perturbation. Despite their wide availability, none of the existing neurite tracing software packages designed for 2D analysis allows for performing a reliable detection of neurites in neuronal cultures with DN, (e.g. cultured for at least 10 days). This is because in DN, dendrites

and axons start to intersect and it becomes much more difficult to distinguish thin neurites due to the high density of the network. Hence, the main aim of this study was to design a tool that is capable of performing segmentation of DN in 2D in a fully automated manner, with a high accuracy in both neurite tracing and soma segmentation. The finality of this effort is the MorphoNeuroNet (MNN) package, which was conceived as a script for ImageJ/Fiji.

Table 4: Comparison of some features of ImageJ-based packages available for neurite tracing in two-dimensional images of non-dense networks (NDN).

Toolkit ImageJ based	**Operational mode**	**Morphological measurement**	**Required images/ Analysis speed per image**
NeuronJ	Manual	Neurite length per neuron Neurite branching	Neuron image/ Related to the image and the user
NeuroMetrics	Semi-automated	Neurite length per single neuron Neurite branching	Neuron image/ < 5 minutes
NeuroTracer	Automated	Neurite length per frame Soma number per frame	Neuron image stack Nuclei image stack /2.1 seconds
NeurphologyJ	Automated	Neurite length per frame Soma number and size per frame Neurite attachment points Neurite ending point per frame	Neuron image /1.7 seconds
MeasureNeurons	Automated	Neurite length per frame Soma number and size per frame Neurite attachment points Neurite ending point per frame Neurite branching per frame Segment length between branch points	Mask of soma Mask of neurites / 2.5 seconds (time for generating masks is not included)

2. Materials and Methods

2.1. Primary cortical neuron cultures

In this study, primary neuron cultures were initiated from brain cortex of 17 day-old mouse fetuses. All animal experiments were carried out in strict accordance with the recommendations of the Guide for the Care and Use of Laboratory Animals of the National Institutes of Health. The protocol was approved by the SCK•CEN (Belgian Nuclear Research Centre, Mol, Belgium) and VITO (Flemish Institute for Technological Research, Geel, Belgium) joint Ethical Committee on Laboratory Animal Experiments. Pregnant mice were sacrificed by cervical dislocation on day 17 after conception. Subsequently, brains from mouse fetuses were dissected and cortices were extracted. Neuronal cells were isolated by trypsinization, mechanical dissociation of tissue and cell centrifugation. Thereafter, cells were re-suspended in MEM medium (Gibco, Gent, Belgium) supplemented with 10% foetal serum (Gibco) and (0.1%) penicillin-streptomycin (Gibco) and seeded onto poly-D-lysine coated 4-well plates (Thermo Scientific, Erembodegem - Aalst, Belgium) at a density of 50,000 cell per cm^2. Neurons were incubated for 1 h at 37 °C and 5% CO_2 to remove non-neuronal small cells and to allow adherence. Thereafter, the medium was exchanged with Neurobasal medium (Gibco) supplemented with 2% B27 supplement (Gibco), HEPES 20 mM (Gibco) and penicillin-streptomycin (0.2%) (Gibco); this medium allowed selective growth of neuronal cells. In order to obtain a DN culture as an *in vitro* model, neurons were cultured for 20 days at 37 °C, 95% of humidity and 5% CO_2. After 5 days of culture, two thirds of medium was replaced by fresh medium every 2 days.

2.2. Immunofluorescence staining and image acquisition.

Neuronal cultures were stained with the neuronal marker β-tubulin 3 (β-tub 3) by means of indirect immunofluorescence. Briefly, the following protocol was applied: after fixation with 4%

paraformaldehyde (PFA) for 15 min at 4°C, cells were washed with phosphate buffered saline (PBS), permeabilized with PBS containing 0.1% Triton X-100 (Sigma, Bornem, Belgium) for 3 min and blocked for 30 min with 3% BSA. Next, samples were incubated with mouse monoclonal anti-β-tubulin 3 (T5076, Sigma-Aldrich), diluted 1:200 in 3% BSA in PBS, at 4 °C overnight. After washing three times in PBS, a secondary antibody FITC labelled anti-mouse (F2012, Sigma-Aldrich), diluted 1:200 in 3% BSA, was applied for 90 min in the dark at 37 °C. Nuclei were counterstained with Hoechst (B2883, Sigma-Aldrich), 1:400 in PBS, for 10 min. Wells were rinsed in PBS and finally in milliQ water.

Images were acquired with an automated inverted wide-field epifluorescence microscope (Nikon Eclipse Ti, Nikon Instruments, Paris, France) equipped with a metal halide lamp, motorized XYZ stage, automatically controlled Shutter and filter wheels with emission filters (387/11 for Hoechst and 485/20 for FITC) and excitation filters (452/45 for Hoechst and 536/40 for FITC) used in combination with a triple dichroic mirror (436/514/604) mounted in a filter cube at fixed position. Images were acquired with a 20x dry (Plan Fluor, NA 0.5) or a 40x oil (S Plan Fluor, ELWD, NA 0.6) objective using a Nikon DS-Qi1Mc camera and NIS-Elements software (Nikon Instrument Software; Nikon Instruments). To obtain a foreground/background between 5 and 10 for the healthy neuronal cells, the following acquisition settings were used: exposure time 100 ms for 20x and 150 ms for 40x. Pixel sizes were 0.320 µm x 0.320 µm for the 20x objective and 0.160 µm x 0.160 µm for the 40x objective and multiple axial planes were sampled at 1.4 µm intervals. Mosaic images were acquired with the "large image" method implemented in NIS Elements, which does automatic blended stitching, with an overlap of 25%. For the temporal follow-up of neuronal growth in culture, images were acquired at set time points of 1, 5, 10, 14, 20, 23 days. Per time point, a data set of 4 images was acquired with 40x magnification in mosaic (2x2) and 5 Z-positions.

2.3. Image processing and analysis

All image processing was performed in ImageJ freeware [280]. After acquisition, images were pre-processed to reduce background heterogeneity and artefacts generated during the acquisition by flat-field correction. In case of acquisition of a number of Z-slices, images were projected to a focused 2D image by an Extended Depth of Focus (EDF) algorithm available in NIS Elements software.

MorphoNeuroNet is conceived as a macro set for NIH's ImageJ (version 1.45s or higher) expanded with 3 additional plugins "Particle remover" (http://rsbweb.nih.gov/ij/plugins/index.html), "FeatureJ" (http://www.imagescience.org/meijering/software/featurej/) and "Analyze skeleton" (http://imagejdocu.tudor.lu/doku.php?id=plugin:analysis:analyzeskeleton:start). The software can be downloaded for free from the following URL: http://www.limid.ugent.be/downloads.htm.

MorphoNeuroNet architecture

MNN consists of four sequential analysis modules. The first step is the detection and sorting of nuclei, which are used in the second step as seeds for segmenting the cell bodies or somas. Subsequently, neurites are segmented, after which the different components of the neuronal network are connected and subsequently analysed to extract their morphological features. MNN is able to perform these operations in batch, making it ideally suited for high-content applications. The only requirement is for images to be placed in a single folder. The calibration of images is allowed to differ since, scale-dependent operations in the image-processing pipeline are expressed relative to the image calibration.

2.3.1. Detection and sorting of nuclei

Typically, in a DN culture 3 different cell populations are observed, which can be characterized by their nuclear signals (Figure 17A). The first population represents normal (presumably healthy) neurons with a well spread soma (area ~ 280 μm^2) and several neurites.

These cells have ellipsoid nuclei that contain a speckled chromatin pattern with ~5 chromocenters of ~1 µm in diameter. The second class of neurons has small somas (area < 150 μm^2) without any extensions. Their nuclei show more pronounced chromatin condensation with high fluorescence intensity concentrated in a few (3-4) blobs of large diameter (several microns). Finally the third class of cells demonstrates small (area < 35 μm^2) and completely condensed nuclei without soma. The two latter classes represent non-neuronal cells or different stages of cells undergoing apoptosis [281-283]. The difference in (mean) nuclear intensity between the first class and the other two was at least a factor 3. The acquisition settings were adjusted to maximize the nuclear signals for the healthy neurons, causing the signals from the apoptotic nuclei to become saturated (cfr. Immunofluorescence staining and image acquisition). In order to segment only the healthy nuclei (the first population), all nuclei were first enhanced by means of a Laplacian of Gaussian (LoG) filter (sigma=0.5 µm), followed by an automated thresholding procedure according to Huang's algorithm [284], resulting in a binary mask of nuclear regions. In this mask, nearby nuclei were separated by applying a watershed algorithm after which all nuclei were analysed for morphological and intensity parameters. Occasionally the watershed procedure split up nuclei in multiple parts, but we found this unwanted effect to be minimal (2%). Nuclei with high fluorescence intensity (higher than the mean intensity of all nuclei in the image), with over 50% of the nucleus area having condensed chromatin (being over 50% saturated pixels) and with projected area < 40 μm^2 were eliminated from the mask by filling the corresponding ROIs with background colour to obtain a final *nuclei mask.*

2.3.2. Soma detection

In a young neuronal culture, somas have higher (between 1.3 and 2 times) intensity than neurites. The most common method for segmenting somas is to apply a low pass filter such as a Gaussian blur filter followed by the application of an automated threshold [279]. In dense neurite network cultures, somas have different fluorescence intensities and neurons tend to cluster

making it difficult for such an approach to resolve adjacent somas. In order to discriminate touching somas, the nuclear masks are used as seeds in the segmentation process by applying an inverted skeletonization procedure. This allowed for obtaining discrete *soma regions* (Figure 17B).

To segment the actual somas, nuclear ROIs (region of interest) were isotropically expanded by 10-20 microns using the built-in 'Enlarge Selection' option from ImageJ (the extent need to be previously defined by measuring the maximum distance between nucleus and soma border) using the soma regions mask as boundaries (to prevent merging of touching somas). Next, the image contrast was normalized (allowing 1% saturation), followed by a Gaussian filtering (sigma of about 2 µm for an image acquired with a 40x) and finally a combined thresholding procedure was applied. First, the enlarged nuclear ROI was globally thresholded according to the IsoData algorithm (based on average of mean intensity of background and objects) [285], yielding preliminary soma ROIs. Subsequently, a local thresholding was applied by determining the optimal threshold in the preliminary soma ROI according to the Intermodes algorithm (based on determination of two maximal intensity peaks) [286]. The combination of these individual ROIs yielded the final *soma mask*. This mask was used to extract morphological parameters of individual somas (Figure 17B).

2.3.3. Neurite segmentation

In early stage (2-5 days) neuronal cultures, neurons are usually isolated and neurites well defined making segmentation rather straightforward. However, neurons cultured for longer periods (more than 10 days) create a dense neuronal network with variable contrast levels, making segmentation more challenging. To be specific, some parts are well defined and demonstrate strong fluorescence intensity, while other parts are thin and only weakly stained, especially at the tip ends of the neurites. To allow segmentation of the complete network, a three-tier approach was used (Figure 17C). General background intensity gradients were

removed by means of a background subtraction ("Rolling Ball" method, radius = 8 µm) after which the image was duplicated twice for multi-scale segmentation. In the first copy the high intensity parts of the image were extracted by an automated thresholding procedure (Moments algorithm [287]), creating a first mask, i.e. the *high intensity mask*. In the second copy, edge information was enhanced by means of an unsharp mask (Gaussian Blur: sigma = 2 µm) and subsequent thresholding (Moments algorithm [287]), creating a second mask, the *edge mask*. Finally, the weakest parts, the thinnest neurites, were segmented in the third copy image by applying a LoG filter (sigma = 0.25 µm) and automated thresholding according to the Moments algorithm [287], creating a third mask: the *LoG mask*. The sum of these three different binary images subtracted with the soma mask, generated a *neurite mask*, which was used to quantify the relative neurite area per image (Figure 17C).

2.3.4. Image reconstruction and analysis

In a final step the soma mask and neurite mask were combined to generate a *neuronal network mask*. Next, the *neurite mask* was skeletonized, as suggested by Kegl [288], after which branching points, end of neurites and segment lengths between branch points were determined per image. Soma morphology measured on the soma mask takes into account shape parameters such as size, roundness and circularity. To count the number of neurite attachment sites at the level of the soma, soma masks were dilated (3 pixel) after which the dilated regions were intersected with the skeleton of the *neurite mask*. Unique attachment points per soma were identified using a 'find maxima' operation (noise level=0) (Figure 17D).

Finally all masks were used to perform the actual measurements, including nuclei number, total projected area of nuclei per image, soma number and total soma area per image, neuron area, neurite area and neurite length. Normalized metrics were obtained by dividing the original metric per image by the number of nuclei. These results were saved as xls. format per image sorted by sample/folder identity.

2.4. Validation and statistical analysis

For the actual neuronal network analysis several ImageJ plugins were tested including NeuronJ, NeuroMetrics, NeuriteTracer, NeurphologyJ and CellProfiler's MeasureNeurons (Table 1). NeuronJ is a popular tool for manual neurite tracing and it has been used as reference package for testing 2D neuronal tracing automated software [276]. Given 2 points, one at the start and the other at the end of the neurite, NeuronJ traces the neurite by finding the optimal intensity path between them. NeurphologyJ is a package that can trace neurites automatically, but it does not provide any information on branching complexity. Additionally, NeurphologyJ measures number and size of somas, the total number of neurites attached to the somas (attachments points) and the total number of neurite tips (ending points) per image. CellProfiler, an open-source platform specifically conceived for high content image processing analyses [289], has a module named MeasureNeurons which allows to trace neurite and measure their length, as well as determine attachment points, end points, branching points and segment length between branch points. In contrast with ImageJ plugins, MeasureNeurons need to define a pipeline of functions to create soma and neurite masks before being applied (Supporting Table 1), so essentially it still requires many of the steps that we have implemented in our analysis.

Neuronal outlines obtained by NeuronJ-assisted manual tracing, were used as a ground truth. Based on a comparative analysis, NeurphologyJ proved to be the most useful and most accurate tool for automated tracing of neurites in NDN cultures (Table 5), which is why this tool was used as reference. Furthermore, the module MeasureNeurons, which requires a supporting pipeline of functions (Table 6) to generate soma and neurite masks, was used to evaluate the performance of this algorithm to skeletonize NDN as well as DN (Table 5).

Statistical analyses were performed in GraphPad Prism (GraphPad Software Inc., San Diego, USA) software, using the Pearson's correlation and paired Students T-test to compare neurite length, soma area and soma number between the automated tools and ground truth.

Additionally, one-way Anova was performed to observe variations in neurite area estimated by automated tools. Error rate and accuracy were calculated for the detected number of attachment points per soma. The error rate was estimated by dividing the difference between manually counted points (ground truth, M) and the automatically detected points (A) by the number of automatically detected points (Error rate % = (M-A)/A = D/A). The accuracy was estimated dividing the correctly detected points (A_C) by manual counted points (M) (Accuracy % = A_c/M) [279].

To determine the accuracy of MNN in soma segmentation, relative area per soma was calculated for 200 somas as follows: $\frac{Aa \cap Am}{An}$, whereby *Aa* represents the area of the automatically segmented soma and *Am* the area the manually segmented soma (ground-truth) [290].

To test the robustness of MNN Gaussian noise and Salt & Pepper (S&P) noise were added to original images. In order to obtain images with specific signal-to-noise ratio (SNR, dB), data sets of 15 images with Gaussian noise were generated by increasing the standard deviation (SD). Afterward, related signal-to-noise ratios (SNRs; dB) [291, 292] of image were determined per each SD by ImageJ plugin [293] as follow: $SNR = 10 * log_{10}\left[\frac{\sum_0^{n_x-1}\sum_0^{n_y-1}[r(x,y)]^2}{\sum_0^{n_x-1}\sum_0^{n_y-1}[r(x,y)-t(x,y)]^2}\right]$, whereby *r(x,y)* and *t(x,y)* represent single pixels of reference and modified images respectively. Furthermore, the correlation between SD and SNR was determined and the SD for SNR 25, 15, 7.5, 4 and 2 were calculated. Finally, Gaussian noise was applied to the original images and analyses performed (Fig. 22).

Figure 17: Workflow of the MNN neuronal analysis toolbox (see text for details).
Step A: Nuclei detection. Nuclei are segmented, using an automatic threshold and watershed-based separation, after which healthy neuronal nuclei are identified based on size and intensity parameters. Step B: Detection of somas. Using the healthy nuclei as seeds, somas are segmented by conditional dilation. Step C: Neurite segmentation. A combination of three different methods, one intensity-based and two edge-based, allow to distinguish the majority of neurites with variable thickness and fluorescence intensity. Step D: neuronal network reconstruction and image analysis. The final neuronal network mask is reconstructed by summing the neurite mask and the soma mask. Neurite length is obtained by analysing the skeleton of the neurite mask and neurite attachment points are detected by scoring the overlapping regions between the neurite mask and a dilated soma mask.

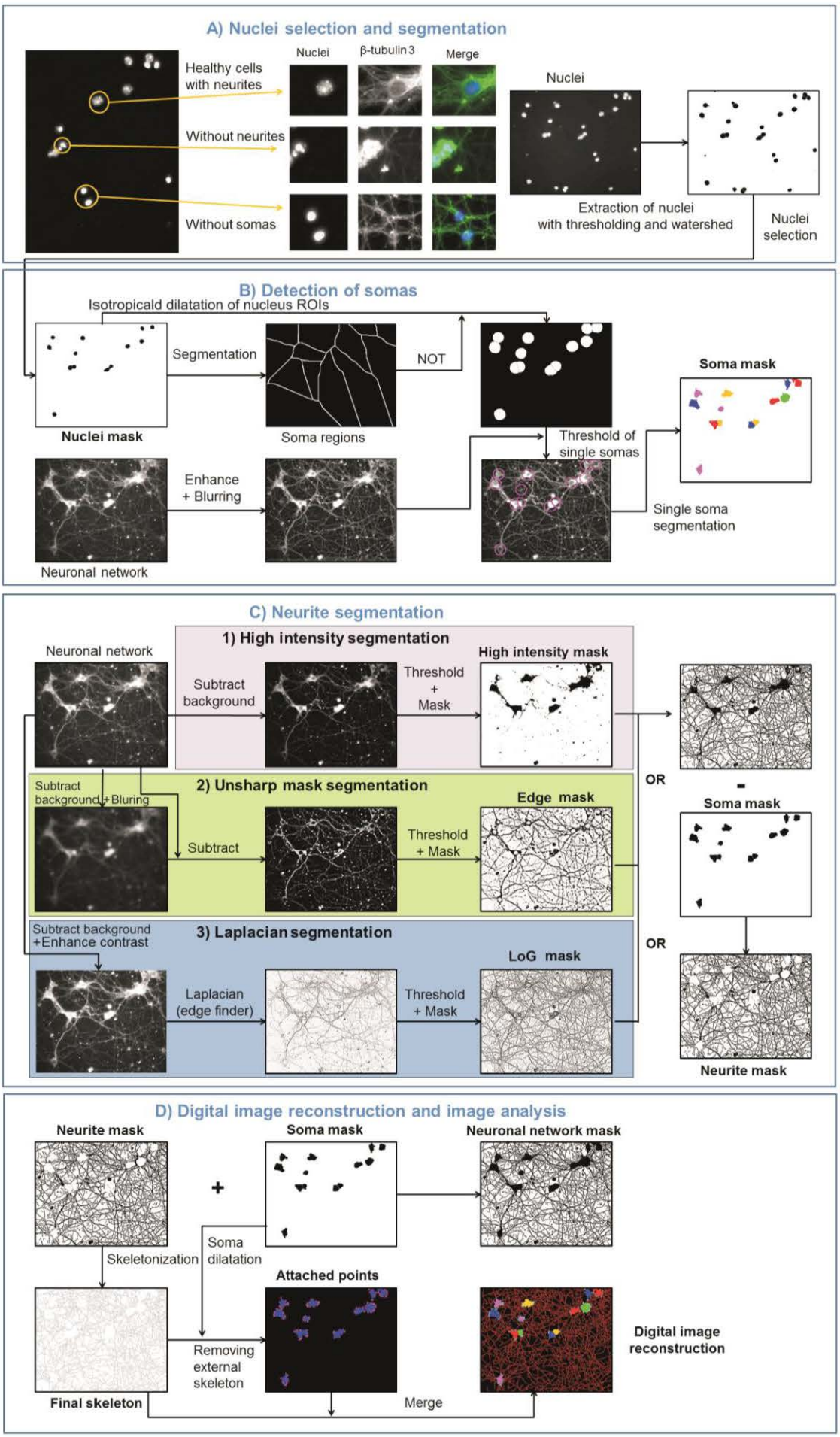
A) Nuclei selection and segmentation
Nuclei
β-tubulin 3
Merge
Healthy cells with neurites
Without neurites
Without somas
Nuclei
Extraction of nuclei with thresholding and watershed
Nuclei selection
B) Detection of somas
Isotropicald dilatation of nucleus ROIs
Segmentation
NOT
Soma mask
Nuclei mask
Soma regions
Threshold of single somas
Enhance + Blurring
Single soma segmentation
Neuronal network
C) Neurite segmentation
1) High intensity segmentation
Neuronal network
Subtract background
Threshold + Mask
High intensity mask
OR
Subtract background + Bluring
2) Unsharp mask segmentation
Subtract
Threshold + Mask
Edge mask
Soma mask
OR
Subtract background +Enhance contrast
3) Laplacian segmentation
Laplacian (edge finder)
Threshold + Mask
LoG mask
Neurite mask
D) Digital image reconstruction and image analysis
Neurite mask
Soma mask
Neuronal network mask
Skeletonization
Soma dilatation
Attached points
Removing external skeleton
Digital image reconstruction
Final skeleton
Merge

3. **Results**

To assess the performance of MorphoNeuroNet, we compared various parameters with the established neurite tracing tools NeuronJ [276], NeurphologyJ [279] and CellProfiler's MeasureNeurons on a data set of NDN cultures consisting of 20 mosaic images acquired with 20x magnification. Table 5 gives an overview of the parameters and accuracy of the four methods.

3.1. NDN culture analysis

We evaluated the accuracy of MNN in neurite tracing and in estimating morphological parameters in cortical neuron cultures cultured for 48 h. Parameters such as total neurite length per image, soma number per image and number of neurites (attachment points) per neuron were compared with the results obtained with manual tracing using NeuronJ, the automated tool NeurphologyJ and the automated CellProfiler module MeasureNeurons. Results obtained by manual neurite tracing with NeuronJ were considered as ground truth for performance assessments (Figure 18). All three automated methods showed a highly accurate and linear estimation of neurite length in 2 day-old NDN neuron cultures with a Pearson correlation coefficient close to 1 (NeurphologyJ R=0.98; CellProfiler R=0.93; MNN R=0.99) and the paired t-test showed no significant difference for the different methods from ground truth (NeurphologyJ p=0.19; CellProfiler p=0.72; MNN p=0.63). Notably, MNN was able to detect the weakest intensity parts of thin neurites, whereas this was not the case for the other two (Figure 18 A, yellow arrows).

Table 5: Comparison of MNN with manual and automatic neurite tracing packages designed for non-dense network (NDN) analysis.

Measurements (Functions, speed and accuracy)	**NeuronJ**	**NeurphologyJ**	**Pipeline to generate soma and neurite masks + MeasureNeurons**	**MorphoNeuroNet**
Required images	Neuronal network	Neuronal network	Neuronal network and nuclei	Neuronal network and nuclei
Number of nuclei	No	No	Yes	Yes
Soma numbers	No	Yes	Yes	Yes
Soma size	No	Yes	Yes	Yes
Soma shape parameters	No	No	Yes	Yes
Neuron size	No	No	Yes	Yes
Neurite size	No	No	Yes	Yes
Neurite length	Yes	Yes	Yes	Yes
Attachment points	Yes	Yes	Yes	Yes
Ending points	Yes	Yes	Yes	Yes
No. of images in one batch	Unlimited	Unlimited	Unlimited	Limited by memory
Analysis speed per image****	Related to neurite density and the user (50 - 200 min)	2.5 sec	1min 30 sec	50 sec
Correlation coefficient/*p*-value for neurite tracing in non-dense network *		R=0.99 / *p*=0.19	R=0.93 / *p*=0.72	R=0.98 / *p*=0.63
Correlation coefficient/*p*-value for soma area in non-dense network **		R=0.89 / *p*=0.11	R=0.98 / *p*=0.72	R=0.99 / *p*=0.82
Correlation coefficient/*p*-value for soma detection ***		R=0.95 / *p*=0.12	R=0.94 / *p*=0.82	R=0.99 / *p*=0.77
Correlation coefficient/*p*-value for neurite tracing in dense network *		R=0.67/*p*=0.049	R=0.43 / *p*=0.001	R=0.91 / *p*=0.63

* Manual tracing with NeuronJ used as a ground truth
** Manual tracing with NeuronJ used as a ground truth
*** Manual counting used as a ground truth
****The average processing time was measured on Intel Core 2 Duo, 2.40 GHz, 4 GB, 32-bit computer.

Whilst all three methods NeurphologyJ, MeasureNeurons and MNN are able to detect somas, thanks to the nuclear seeding procedure, MeasureNeurons and MNN are also capable of separating adjacent somas, where NeurphologyJ typically assigns them as one single soma (Figure 18 A). Comparison of the Pearson's correlation coefficient and a paired T-test of automated versus manual soma area per image showed that all methods were highly accurate, but MNN offered an additional advantage (NeurphologyJ R=0.89 p=0.11; CellProfiler R=0.98 p=0.78; MNN R=0.99 p=0.82) (Figure 18 C). By comparing the soma counts between programs, we found a strong correlation between the number of detected somas and the actual number of somas (based on manual identification) for all three methods (Pearson's correlation coefficients were R=0.95 for NeurphologyJ, R=0.94 for CellProfiler and R=0.99 for MNN). Nevertheless, MNN presented a higher correlation than NeurphologyJ and CellProfiler. Furthermore, a marked, but non-significant deviation from linearity for NeurphologyJ at the higher numbers of neurons (p=0.22 for soma nr >50) was observed (Figure 18 D). There was no significant difference in measured neurite area either (Figure 18 E). In neuronal re- or degeneration studies, it is important to accurately estimate the number of neurite attachment points. To determine accuracy and average error rate, attachment points of 20 neurons were manually counted as ground truth and compared with the number of attachment points estimated by NeurphologyJ and MNN. As reported in table 6 of supporting data, the error rate and the accuracy in NeurphologyJ were 5.02% and 98.38%, respectively. The error rate and the accuracy in CellProfiler were 4.64% and 95.3% and in MorphoNeuroNet were 4.35% and 97.41%, respectively.

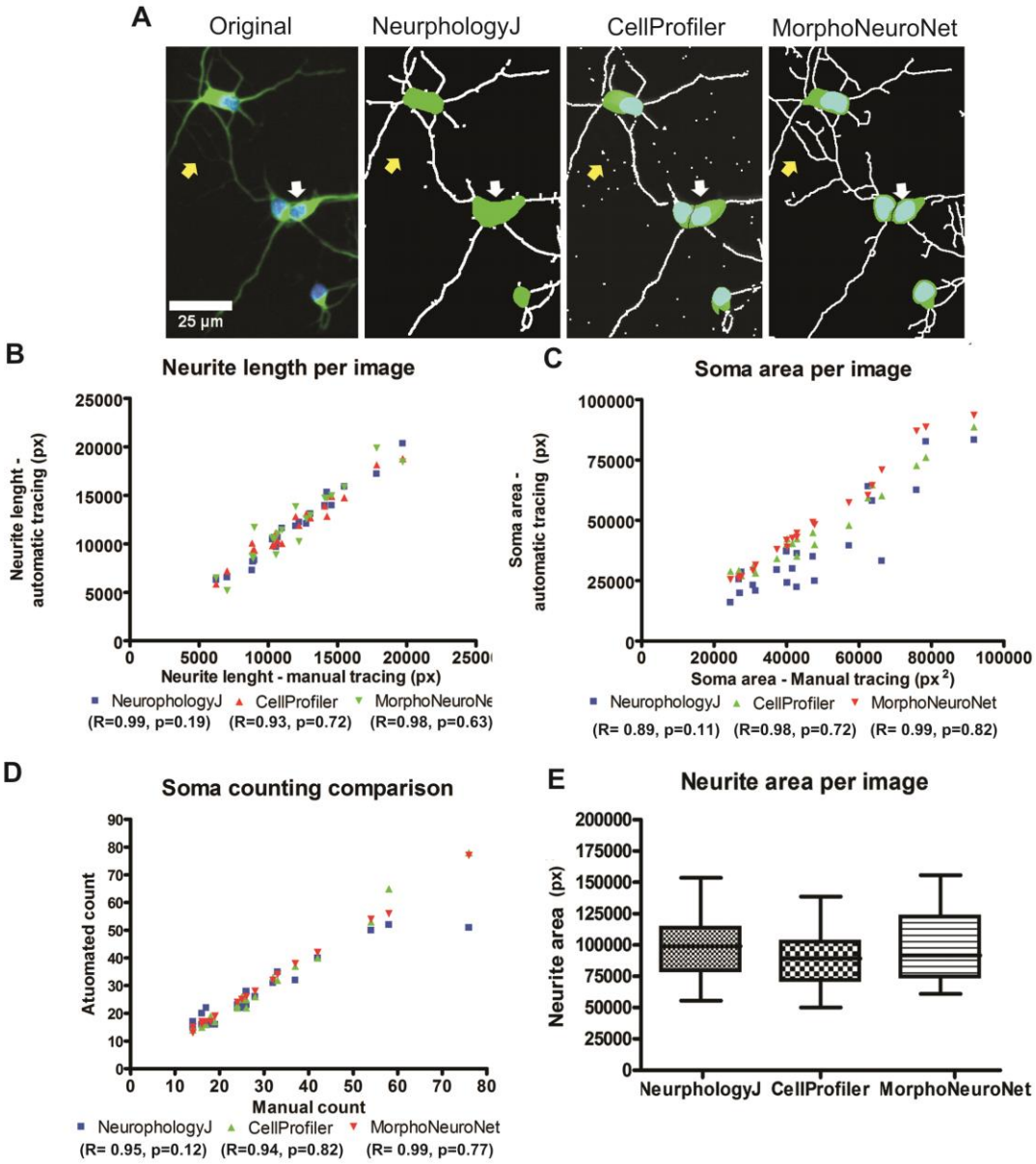

Figure 18: MNN accurately traces neurites and segments somas in NDN cultures.
(A) Example of mouse cortical neuron images analysed by NeurphologyJ, CellProfiler and MNN (nuclei in blue and β-tubulin 3 in green). In the binarized images, the skeleton of the neurites is represented in white, somas in green and nuclei in blue. White arrows indicate differences in soma segmentation whereas yellow arrows show segmentation of neurites with weak fluorescence intensity. (B-D) Quantitative comparison of performance of NeurphologyJ, CellProfiler and MNN with ground truth (manual tracing) in measuring (B) neurite length, (C) soma area, (D) soma number and (E) total neurite area. Pearson's correlation coefficients and p-values for the paired two-tailed Student's T-test are shown.

Table 6: Error rate and accuracy on automated counting of neurite per soma are calculated.
The error rate was estimated by dividing the difference between manually counted points (ground truth, M) and the automatically detected points (A) by the number of automatically detected points (A) (Error rate % = (M-A)/A = D/A). The accuracy was estimated dividing the correctly detected points (A_C) by manual counted points (M) (Accuracy % = A_c/M).

		NeurphologyJ				MeasureNeurons				MorphoNeuroNet			
Neuron ID	Manual (M)	Detected (A)	D*	Error rate (%) **	Ac ***	Accuracy (%) ****	Detected (A)	D*	Error rate (%) **	Ac ***	Accuracy (%) ****	Detected (A)	D*	Error rate (%) **	Ac ***	Accuracy (%) ****
1	6	6	0	0	6	100	6	0	0	6	100	6	0	0	6	100
2	5	4	1	25	4	80	6	1	16,7	5	100	5	0	0	5	100
3	6	8	2	25	6	100	5	1	20	5	83,3	8	2	25	6	100
4	6	6	0	0	6	100	6	0	0	6	100	6	0	0	6	100
5	5	5	0	0	5	100	5	0	0	5	100	5	0	0	5	100
6	6	6	0	0	6	100	6	0	0	6	100	6	0	0	6	100
7	6	6	0	0	6	100	6	0	0	6	100	7	1	14,3	6	100
8	5	5	0	0	5	100	5	0	0	5	100	6	1	16,7	5	100
9	6	7	1	14,3	6	100	6	0	0	6	100	6	0	0	6	100
10	8	8	0	0	8	100	8	0	0	8	100	8	0	0	7	87,5
11	5	5	0	0	5	100	5	0	0	5	100	5	0	0	5	100
12	8	9	1	11,1	7	87,5	9	1	11,1	8	100	8	0	0	8	100
13	6	6	0	0	6	100	6	0	0	6	100	6	0	0	6	100
14	6	8	2	25	6	100	6	0	0	6	100	7	1	14,3	6	100
15	5	5	0	0	5	100	5	1	20	4	80	5	0	0	5	100
16	5	5	0	0	5	100	4	1	25	3	60	5	0	0	5	100
17	7	7	0	0	7	100	7	0	0	7	100	6	1	16,7	6	85,7
18	3	3	0	0	3	100	3	0	0	3	100	3	0	0	3	100
19	6	6	0	0	6	100	6	0	0	5	83,3	6	0	0	6	100
20	4	4	0	0	4	100	4	0	0	4	100	4	0	0	3	75
Average				5,02		98,38			4,64		95,33			4,35		97,41

* D = M-A = Difference between manual counting and detected by the tool.
** Error rate %= D/A.
*** Ac = correctly detected by the tool.
**** Accuracy %= Ac/M

3.2. DN analysis

Similar to the NDN analysis, several tools such as NeuronJ [276], NeuriteTracer [277] and NeuroMetrix [278], were tested on DN. The two most suitable methods for tracing a neuronal network were NeurphologyJ and CellProfiler (MeasureNeurons), due to their accuracy and their capability to analyse the whole NDN images. Due to the high variability in fluorescence intensity between somas (Figure 19A) NeurphologyJ and CellProfiler were not able to correctly segment the somas. In an attempt to find the optimal equilibrium in threshold between somas with different intensity, NeurphologyJ increases the size of somas with high intensity and reduces the size of somas with low fluorescence intensity, creating highly inaccurate segmentation results. On the other hand, CellProfiler, which allowed for detecting somas using nuclei as seeds, showed an under-segmentation of the cell body. The capability of MNN to determine somas one by one, beginning from nuclei allows discriminating soma shape (Figure 19 D). In line with the results obtained for the NDN, CellProfiler and MNN are able to separate touching somas whereas NeurphologyJ is not (Figure 19 D).

Due to the high heterogeneity of DN immunofluorescence intensity, images should be acquired with a high-magnification (M>=40) and high-resolution objective (NA>0.6), to avoid loss of information at the level of thinnest neurites. As previously described by Shinn-Ying Ho [279], NeurphologyJ does not quantify neurite length correctly and the skeletonize function produces a tree-like skeleton in high resolution images. Due to the over- and under-sampling of somas, an incorrect skeletonization is generated, introducing an error in quantification of attachment points. In addition, due to the high variability in fluorescence intensity in the neurite network, thinner neurites with low intensity are not detected without an oversampling of neurites with high intensity (Figure 19 B-C-E). Less prominent but still present, a tree-like skeleton was observed in images processed with the CellProfiler's module MeasureNeurons (Figure 19 B-C-E). Thanks to its multi-tier approach, MNN is capable of handling strong intensity differences

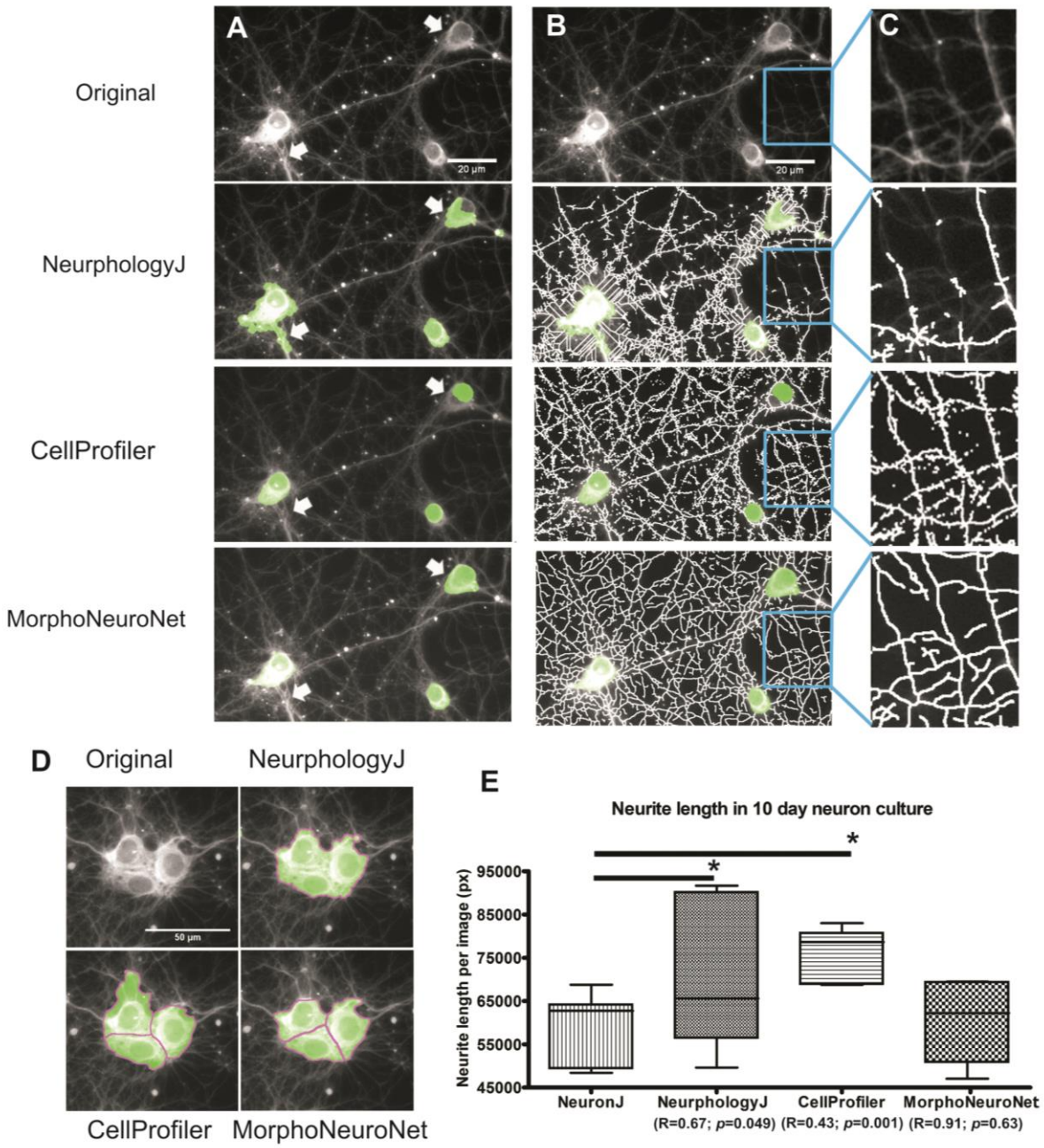

Figure 19: Automated neurite tracing and soma segmentation in DN cultures.
Example of (A-D) soma segmentation and (C-D) neurite tracing in 10 day old mouse cortical neuron images analysed by NeurphologyJ, CellProfiler and MNN. In binarized images the skeleton of neurites is represented in white, somas in green. (E) Box plot comparing total neurite length measured by NeurphologyJ, CellProfiler and MNN in 7 random frames (40X) of 10 day-old neuronal networks and compared with manual tracing. Total neurite area is expressed in pixels. Pearson's correlation coefficients and p-values for the paired two-tailed Student's T-test are shown.

between neurites and therefore allows for obtaining a more reliable estimation, with the neurite mask covering the majority of the visually discernible network without over-segmentation (Figure 19 B-C-E). Indeed, the comparison of neurite length per image between the three

automated methods with the ground truth showed statistically significant differences for NeurphologyJ (p=0.049) and CellProfiler's MeasureNeurons (p=0.001), which make an overestimation due to the incorrect skeletonization (Figure 19 E, table 2). In contrast, MNN showed a good Pearson correlation with the ground truth with 0.91 (p=0.63) (Figure 19 E, table 2).

3.3. Determining the neurite network by MNN throughout 23 days of culturing

Determining the length of neurites helps to estimate neuronal network development stage. To test the capability of MNN to trace neurites in very dense neuronal networks, cortical primary mouse neurons were cultured for 23 days and fixed and stained at day 1, 5, 10, 14, 20 and 23. Next, the analysis was applied to four randomly selected images per condition (Figure 20). Statistically significant differences were found for the average neurite length per neuron between 1 and 5 days (p=0.0039) and between 5 and 10 days (p=0.0274), but not between later time points. (Figure 20 A). Similar results were observed for total neuron size (soma + neurites) and total neurite size per neuron (Figure 20 B-C). Additionally, since neurites extend slower after 10 days showing a statistical difference only between 10 and 23 days, the reasonable stage of connectivity occurred around day 10. As expected, (since neurons do not divide in culture), no statistical difference was observed between soma numbers, (Figure 20 E) suggesting that the observed reduction of number of neurons within 23 days was not relevant and differences observed in neuronal network would mainly be due to plasticity activities (Figure 20 D).

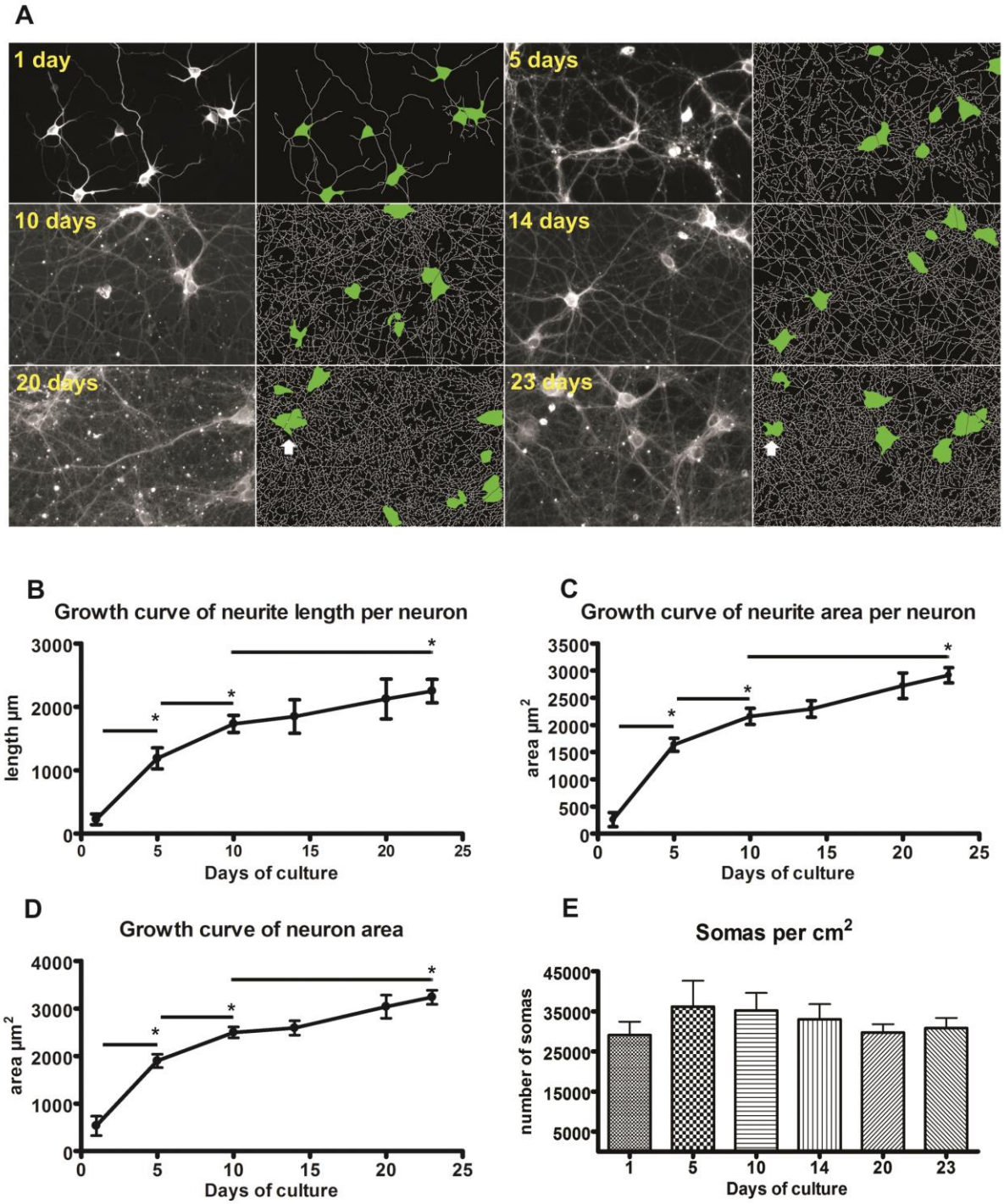

Figure 20: MNN traces neurites and segments somas throughout 23 days of culture.
*(A) Raw images and MNN-generated neuronal masks of primary mouse cortical neuron cultures at different time points. In binarized images, neurite skeletons are represented in white and somas in green. (B) Neurite length per neuron. (C) Average neurite area per neuron. (D) Average neuronal. (E) Average number of somas per cm2. Paired two-tailed Student's t-test was performed, significant differences are indicated with a *, error bars in the graphs represent the standard deviation. Arrows indicate non-accurate soma segmentation.*

3.4. Robustness of MNN

MNN is superior in segmentation performance of both neurite networks and somas, especially in DN cultures, the only drawback is the higher processing time, with an average of 50 sec per image (1500 x 1100 pixels) compared to 30 sec per image for NeurphologyJ (opening, analysis and saving). Since MNN is completely automated and opens, analyses and closes images without human assistance, this concession in time efficiency can be afforded.

In DN images, MNN might detect somas not as accurately when neurites with equal intensity are juxtaposed (Figure 20 A arrows). Furthermore, in order to separate adjacent nuclei, the watershed segmentation was used, which caused an over-segmentation error rate of about 2.3% (1 or 2 per image). Additionally, estimation of relative area of automated soma segmentation into manual segmentation showed an accuracy of about 93% (Fig. 21).

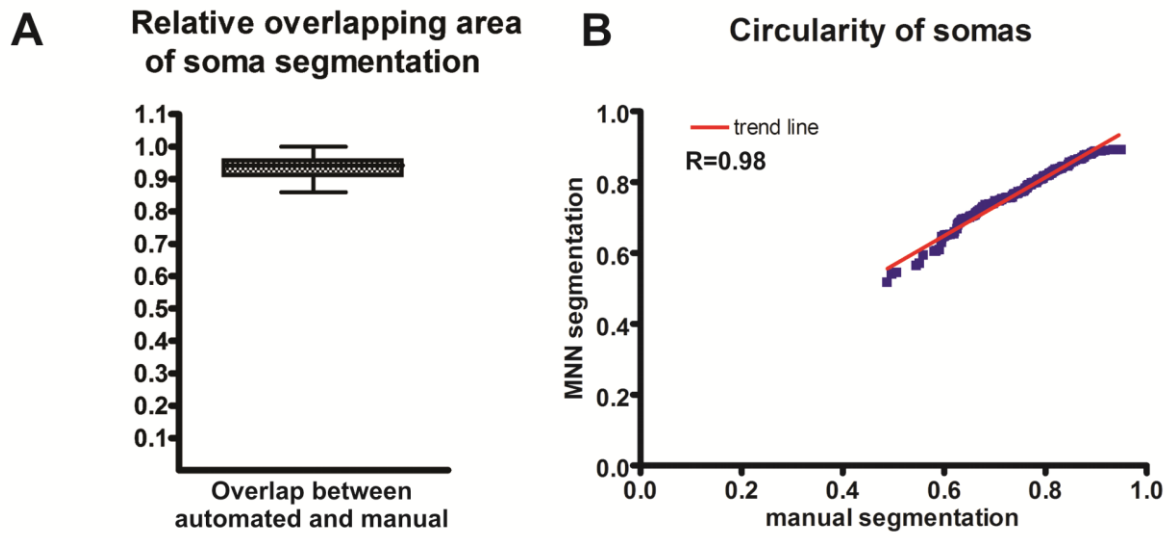

Figure 21: Soma segmentation accuracy of MNN.
(A) Relative overlapping area between automated and manual soma segmentation. (B) Comparison of soma circularity estimation performance between MNN and manual soma segmentation.

To test the robustness of MNN, the analysis was run on real images which were degraded by adding two types of noise: either additive Gaussian noise was applied in order to obtain the SNR between 25 (low noise) and 2 (high noise) or S&P noise (2.5%) up to 5 times. On a data set of 3 images, neuronal area, neurite area and length were estimated with MNN after noise application and compared with the original image to determine the percentage of error (obtained value/reference value*100). Results obtained with MNN on neuron area, neurite area and neurite length showed an increase of the error percentage in NDN images with SNR<=15 whereas the error percentage increased in DN images with SNR<=7.5 (Fig. 22). Furthermore, the error percentage was evident in both networks after applying twice (5%) the S&P noise (Fig. 22).

In order to determine if automated plugins are able to perform high throughput assays, sets of images of ten day-old cultures of primary neurons continuously exposed to low dose of high LET ionizing radiation for 5 days were analysed with MNN, CellProfiler and NeurphologyJ. Results on neurite length showed statistical difference between irradiated cultures and their respective controls (data not shown). Finally, the Z-factors [294], calculated on obtained neurite length per image, showed highest value for MNN (0.22) compared to CellProfiler (0.15) or NeurphologyJ (<0) (data not shown).

Figure 22: MNN performance in tracing neurites in images degraded with noise.
(A) Gradual increase of Gaussian noise in NDN images acquired with 20x and in DN images acquired with 20x and 40x. The Gaussian noise was applied in order to obtain a SNR (dB) of 25, 15, 7.5, 4 and 2. (B-D) The error percentages estimated on neuron area, neurite area and neurite length images with gradual increase of Gaussian noise. (E) Gradual increase in Salt & Pepper noise (2.5%) on the same images (F-H) Estimation of the error percentages increasing the Salt & Pepper noise estimating neuron area, neurite area and neurite length images.
(Page 107).

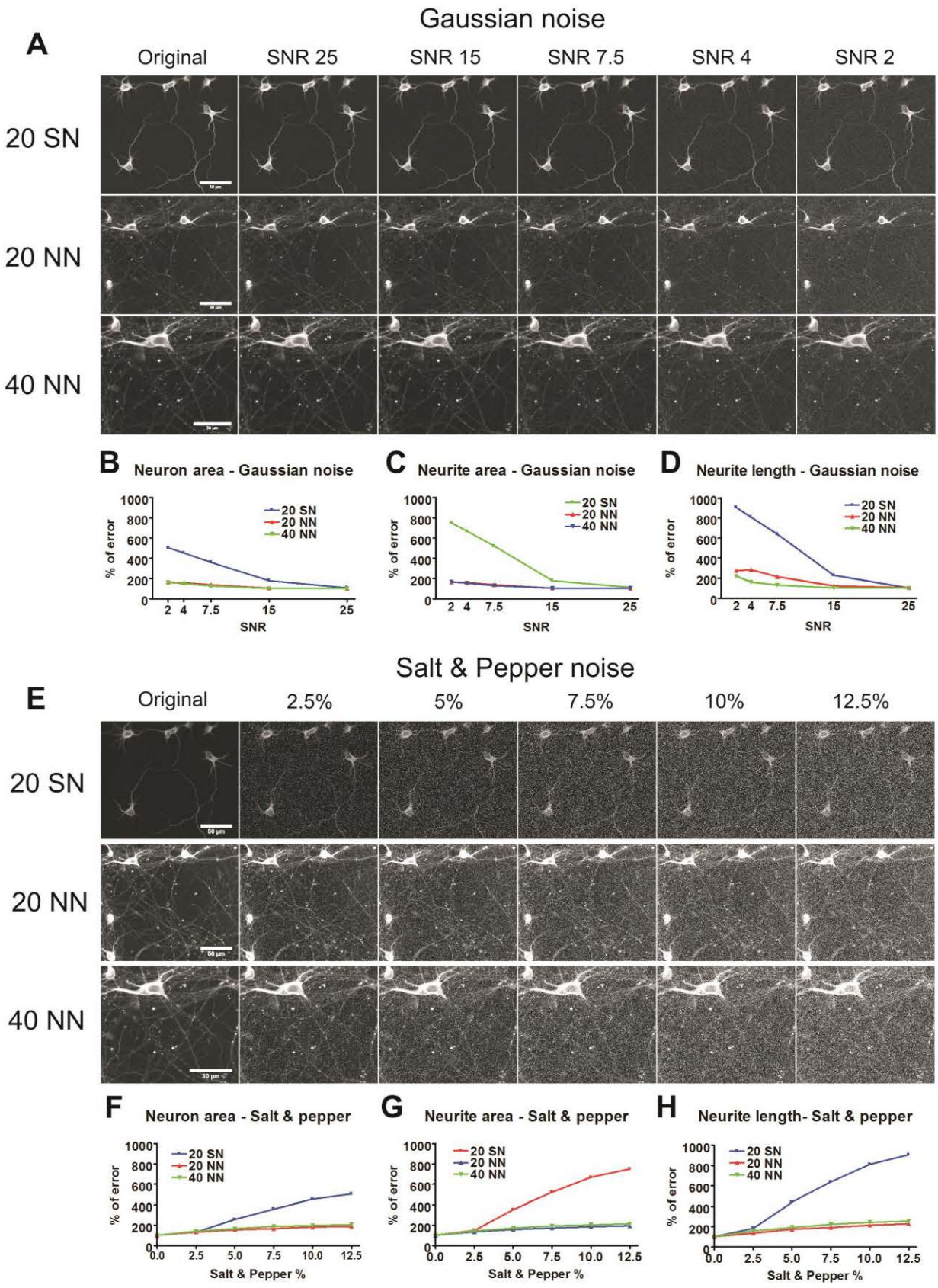
A
Gaussian noise
Original
SNR 25
SNR 15
SNR 7.5
SNR 4
SNR 2
20 SN
20 NN
40 NN
B
Neuron area - Gaussian noise
C
Neurite area - Gaussian noise
D
Neurite length - Gaussian noise
% of error
SNR
20 SN
20 NN
40 NN
E
Salt & Pepper noise
Original
2.5%
5%
7.5%
10%
12.5%
F
Neuron area - Salt & pepper
G
Neurite area - Salt & pepper
H
Neurite length- Salt & pepper
Salt & Pepper %

4. Discussion

In recent years, high content screens have revolutionized cell biological studies by giving phenotypical observations a statistically relevant and quantitative foundation. In line with this, the bottleneck has shifted from acquiring the images to analysing the image data sets in an automated and objective manner [117]. In the context of neuronal regeneration studies, several automated image analysis pipelines have been conceived, which accurately quantify the shape changes in NDN cell cultures [276-279]. However, most existing methods show limited performance for well-connected and differentiated neuronal networks. Nevertheless, these DN cultures may serve as valuable models for instance for investigating neuronal network remodelling in the presence of stress factors, thus demanding an appropriate analysis. To cater for this need, we developed MNN as a macro set for ImageJ to enable automated tracing of neurites in both NDN and DN images. During the development phase, the accuracy (in comparison with the ground truth), the speed (faster than manual reconstruction) and the broad applicability of the algorithms to different data sets were used as criteria to evaluate the performance, in analogy with other works [295, 296]. MNN shows a strong accuracy in neurite tracing and soma segmentation in culture conditions, measuring neurites in cultures grown for up to 23 days.

MNN allowed for detecting subtle changes in the neuronal network on multiple levels (neuron size, areas and length of neurite, size and shape of somas and attachment points to somas), in particular at the level of thin neurites, where the fluorescence intensity is low compared to the rest of the network. This capability is due to a multi-tier approach that combines intensity and edge information in the segmentation process, instead of using only one method as in NeuriteTracer [277], NeuronMetrics [278] or NeurphologyJ [279]. MNN performed well on different image data sets acquired at different resolutions and was robust to relatively high levels of noise. Finally, but not less important, the speed to analyse NDN cultures was about 60 times

faster than the manual tracing, and more than 200 times for 10 day-old neuronal networks. Using the MNN method, we found that neurites extend fast until they reach the stage of reasonable connectivity, after which the neuronal network grows slower, consistently with earlier data [176]. There are still improvements that can be made in terms of processing speed or segmentation performance. For instance, solutions could be implemented to prevent or recover erroneous separation of nuclei caused by the watershed algorithm. This could be done by *a posteriori* re-joining or model fitting based on a library of expected shapes [297, 298].

Thanks to the aforementioned advantages, the use of MNN holds promise in neurological research to estimate subtle changes in long-term neuron cultures used as *in vitro* mature nervous system model. It is known that cognitive dysfunction and memory impairment at adult age might be induced by neurological disease as well as external events like toxic compounds or radiation. *In vivo* [208] as well as *in vitro* [299] studies showed that ionizing radiation at low or high doses induce neuronal death. Analysis of DN neurite cultures continuously exposed for 5 days to ionizing radiations were performed with MNN. The calculated Z-factor [294] for MNN (0.22) suggested that our toolkit has a potential for high content analyses and with a few implementation could be useful also for high throughput screens. Recently, valuable efforts have been made to enable segmentation of neuronal networks in 3D. In the context of the DIADEM (Digital Reconstruction of Axonal and Dendritic Morphology) Challenge [295, 296], several algorithms have been developed, among which one that sequentially detects the neurite centre line and merges individual branches into trees to reconstruct 3D neurons [300] and one that is based on 3-D open-curve active contours for tracing and reconstructing neurites [301]. Whilst these methods show strong performance and high accuracy in individual neuron reconstruction, these algorithms require high-resolution images and high computational power for calculations, rendering them at this point in time less attractive for high content applications. Moreover, not all applications require that amount of detail. In many high-content and high-throughput screenings the purpose is to derive a simple yet accurate phenotypical indicator of a biological

effect. As we have shown, neuronal network density is one such valuable parameter, which can be efficiently measured in 2D and thus lends itself to implementation in such screening with much lower computational requirements and therefore higher capacity for multiplexing.

Another potential bottleneck in high content applications is the staining procedure, which is time consuming and has low multiplexing capability. Options to expand the number of markers include the use of Quantum dots but this still leaves the large number of samples that remains to be processed in parallel. To avoid this, fluorescently labelled neurons can be obtained by transgenic mice [302, 303]. Impressive solutions to allow resolving individual neurons in dense neuronal networks have been proposed by the Lichtman group (cfr. Brainbow, cre-lox approaches…) [302]. In addition, a mix of differently labelled neuronal cultures (e.g. from different transgenic strains) could allow resolving neuronal characteristics in different settings.

In conclusion, the toolbox that we have developed adds a new analytical strategy in the rapidly growing field of neurological research, by allowing accurate and robust estimation of the density of neuronal networks. This can be useful for high content analysis and compound screening of well-connected neuronal cultures and thereby opens new venues for neuronal research.

Chapter V | Morphological and physiological changes in mature *in vitro* neuronal networks towards exposure to short-, middle- or long-term simulated microgravity

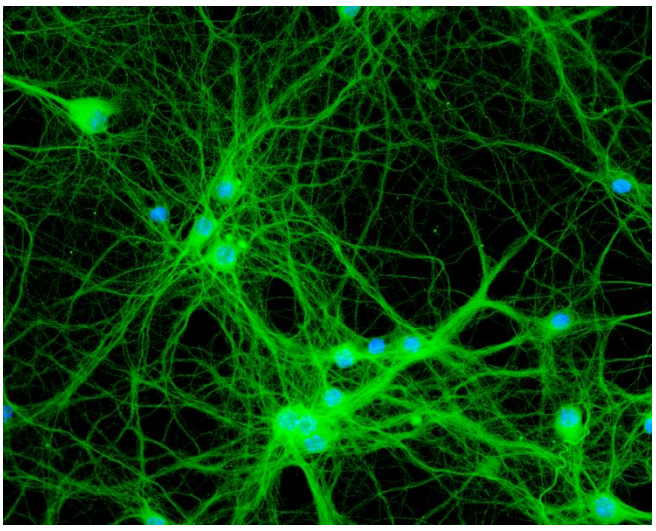

Modified from **"Pani G.**, Samari N., Quintens R., de Saint-Georges L., Meloni M.A., Baatout S., Van Oostveldt P., Benotmane M.A. Morphological and physiological changes in mature in vitro neuronal networks towards exposure to short-, middle- or long-term simulated microgravity." Conditionally accepted in PlosOne with minor revisions on May 30.

Morphological and physiological changes in mature *in vitro* neuronal networks towards exposure to short-, middle- or long-term simulated microgravity

Abstract

One of the objectives of the current international space programmes is to investigate the possible effects of the space environment on the crew health. The aim of this work was to assess the particular effects of simulated microgravity on mature primary neuronal networks and specially their plasticity and connectivity. For this purpose, primary mouse neurons were first grown for 10 days as a dense network before being placed in the Random Positioning Machine (RPM), simulating microgravity. These cultures were then used to investigate the impact of short- (1h), middle- (24 h) and long-term (10 days) exposure to microgravity at the level of neurite network density, cell morphology and motility as well as cytoskeleton properties in established two-dimensional mature neuronal networks.

Image processing analysis of dense neuronal networks exposed to simulated microgravity and their subsequent recovery under ground conditions revealed different neuronal responses depending on the duration period of exposure. After short- and middle-term exposures to simulated microgravity, changes in neurite network, neuron morphology and viability were observed with significant alterations followed by fast recovery processes. Long exposure to simulated microgravity revealed a high adaptation of single neurons to the new gravity conditions as well as a partial adaptation of neuronal networks. This latter was concomitant to an increase of apoptosis. However, neurons and neuronal networks exposed for long-term to simulated microgravity required longer recovery time to re-adapt to the ground gravity.

In conclusion, a clear modulation in neuronal plasticity was evidenced through morphological and physiological changes in primary neuronal cultures during and after

simulated microgravity exposure. These changes were dependent on the duration of exposure to microgravity.

Keywords: Mature neuronal network; neuroplasticity; neuronal morphology; simulated microgravity; short-term exposure; long-term exposure

1. **Introduction**

In an orbital spaceflight, astronauts are exposed to the orbital gravity (10^{-2} - 10^{-6} x *g*), also called microgravity, which is a continuous free-fall condition, resulting from the Earth's gravitational pull and the centrifugal forces from the spacecraft's propulsion. Microgravity is one of the main stressful components of the space environment since it is well known that it induces physiological changes in astronauts such as skeletal muscle atrophy [304], bone loss [305], immune system impairment [216, 263] and shifts of body fluids from the lower extremities to the upper body [306]. Moreover, cognitive deficits, sensory-motor alterations, changes in sleep-wake regulation as well as vegetative disorders can also occur during long-term space flight, affecting human performance [307]. It is also known that organisms exposed to microgravity undergo physiological, cellular as well as metabolic changes. For instance, cellular motility, morphology, cytoskeleton [59], proliferation [35], apoptosis [68, 308] as well as other physiological systems are known to be altered following exposure to modified gravitational fields.

When astronauts and/or animals are exposed to microgravity, a particular number of neurological disorders, such as space adaptation syndrome (SAS), space motion sickness (SMS), postural illusion, visual disturbances, nausea and headaches, neuromuscular fatigue and weakness as well as postural imbalance and ataxia may appear and persist until return to Earth [309]. These pathological changes affect both motor and sensory functions, and the effects can be long lasting. Furthermore, it has been suggested that these changes could be the signs of an active process of neuroplasticity [310]. However, the nature of the functional and structural mechanisms involved in these changes is currently not well understood.

Basically, the term "neuroplasticity" is related to the neuronal capability to modify some functional processes in response to the alterations in incoming information [153]. It is an intrinsic property of the nervous system maintained throughout life that allows physiological

modifications of neuron functions and structures in response to environmental changes via the strengthening, weakening, pruning or the addition of synaptic connections and/or the promotion of neurogenesis [154]. Increases in neuroplastic activity seem also to be linked to pain hypersensitivity and to headaches [154, 311]. Furthermore, it has been previously shown that environmental changes can alter cognition and behaviour by modifying connections between existing neurons in the hippocampus, cortex and other parts of the brain [155].

Several experiments on cell morphology and motility have been performed in real and simulated microgravity. In these experiments loss of cell adhesion, reduced cell surface, decrease in the number of filopodia and reduced motility were reported [38, 59]. These functions are mainly regulated by cytoskeletal activities and the observed alterations concern in particular the distribution and organization of microtubules, microfilaments and the structure of adhesion proteins [38, 51, 59]. Alterations of microtubule and microfilament organization under simulated microgravity have already been evidenced in neuron outgrowth cones [188]. It was also reported that glial cells showed morphological alterations already after 30 minutes of simulated microgravity, and after 20-32 h, presented an elevated cell death rate [56]. Moreover, neurons, exposed to simulated microgravity before plating, showed cell clustering and abnormal shapes after 24 h of culture in ground conditions [57]. Experiments on neuronal connections in simulated microgravity also suggested that synapse formation is sensitive to the gravitational vector [58, 312].

Apoptosis, or programmed cell death, occurs in all multicellular organisms and the initiation is induced by various stimuli such as changes in cellular homeostasis, binding of particular ligands to cell surface receptors, radiation and many other external stress factors [283]. In the brain, apoptosis is known to be partly induced by cytoskeleton disruption in hippocampal cells [313]. Apoptosis induced by microgravity, both *in vivo* and *in vitro*, was also described in several experiments related to the central nervous system (CNS) [67, 68].

As previously described, microgravity can directly influence several parts of the CNS inducing a re-organization of neuron connections in order to codify the new inputs coming from the sensory system. However, it is still unknown whether microgravity also exerts an effect on the CNS areas that are not directly involved with either the sensing or the response to gravity. In these CNS areas microgravity could induce alterations at the cellular level affecting thereafter events involved in neuronal plasticity and connectivity [307]. However, although some experiments reported morphological alterations in neurons cultured in altered gravity force [57, 58, 188, 196], until now only few *in vivo* and *in vitro* studies on mature nervous system models have been conducted to investigate the effects of real or simulated microgravity on adult neural plasticity processes [58, 196]. Results from the few *in vivo* studies on the effects of real or simulated space conditions on the CNS plasticity suggest that exposure to gravity alterations, both during microgravity as well as after return to Earth, induce changes in the mature nervous system [193]. During the Cosmos 1514 flight, pups were exposed to space conditions *in utero* and brains were thereafter morphologically and histochemically examined [168]. Ultrastructural studies revealed some delay in neuroblastic differentiation as well as in cytoskeletal changes in unmyelinated fibers and in outgrowth cones of axons and dendrites in the hypothalamic supraoptic nuclei [168]. Furthermore, experiments performed on rat during the Space Flight Science 1 and 2 reported changes in ribbon synaptic plasticity. In particular it was demonstrated that gravity sensor hair cells have an extraordinary ability to change number, type and distribution of synapses [165]. Recently, a payload for rodents, named Mice Drawer System (MDS) was built to house mice aboard the International Space Station (ISS) for investigating the long-term adaptation to space conditions [198]. A reduced expression of neuron growth factor (NGF) and brain-derived neurotrophic factor (BDNF) was reported in brain regions such as cortex and hippocampus of spaceflown as compared to ground control animals [199]. The same study revealed that genes involved in long-term potentiation, axon guidance, neuronal growth,

cone collapse, cell migration, dendrite branching and dendritic-spine morphology were up-regulated in the whole brain of mice exposed for 91 days to the ISS environment [199].

In this study we investigated the effects of simulated microgravity using the Random Positioning Machine (RPM) on *in vitro* dense mature neuronal networks obtained from primary mouse neurons with a particular emphasis on neuronal network morphology and cell death during short-, middle and long-term exposure to simulated microgravity.

2. Materials and method

2.1. Primary cell culture and adult neuronal network model

In this study, primary neuron cultures were initiated from brain cortex of 17 day-old mouse foetuses. All animal experiments were carried out in strict accordance with the recommendations from the Guide for the Care and Use of Laboratory Animals of the National Institutes of Health (USA). The protocol was approved by the SCK•CEN (Belgian Nuclear Research Centre, Mol, Belgium) and VITO (Flemish Institute for Technological Research, Geel, Belgium) Ethical Committee for Laboratory Animal Experimentation (Permit Number: 08-001). Three pregnant BALB/c mice, one per replicate, were sacrificed by cervical dislocation at day 17 post-conception. Subsequently, brains from mouse foetuses were dissected and cortices were extracted. Brain cortices of *foeti* from the same pregnant female were pooled and considered as one replicate. Treatment with 0.1% trypsin (cat n° 15400, Gibco, Belgium) and 10µg/ml DNAse I (cat n° 18068015, Gibco, Belgium) in phosphate buffered saline solution allowed to isolate single neuronal cells which were then collected after centrifugation. Finally, neurons from the three replicate pools were plated each in 18 4-well plates (54 4-well plates in total) (cat n° 76740, Thermo Scientific, Belgium) and in 18 flasks (15 cm^2) (54 flasks in total) (Thermo Scientific, Belgium) at a density of 50,000 cells per cm^2. Neurons were plated in poly-D-lysine pre-coated wells (cat n° P0899, Sigma-Aldrich, Belgium) with MEM medium (cat n° 31095, Gibco, Belgium) supplemented with 10% foetal serum (cat n° 10437, Gibco) and penicillin-streptomycin (0.1%) (cat n° 15140, Gibco, Belgium) and incubated for 1 h at 37°C and 5% CO_2 to allow adherence of neuron cells to the coated support. The medium was then exchanged for Neurobasal Medium (cat n° 10888-022, Gibco, Belgium) supplemented with 2% B27 supplement (cat n° 17504-044, Gibco, Belgium), HEPES 20 mM (cat n° 15630, Gibco, Belgium)

and 0.2% penicillin-streptomycin. This selective medium stimulated the growth of neuronal cells present in the culture and not the other brain cell types.

In order to obtain adult neuronal networks as *in vitro* model, neurons were cultured for 10 days at 37 °C, 95% of humidity and 5% CO_2. At days 5 and 7 of culture, 2/3 of each culture medium was replaced with fresh medium.

2.2. *In vitro* experimental layout

To study the morphological effects of simulated microgravity on dense neuronal networks as well as on well-connected neurons, at day 9 of neuron culture, plates and flasks were prepared to be exposed to the desktop RPM (Dutch Space) for 1 hour (short-time exposure), 24 hours (middle-term exposure) and 10 days (long-term exposure). The complete experiment required fifty-four 4 well-plates and fifty-four flasks, eighteen plates/flasks per replicate (9 GC and 9 RPM), which were fully filled with complete neurobasal medium and sealed with sterile parafilm. Bubbles were removed with a syringe. At day 10, 3x9 plates and 3x9 flasks were exposed to the RPM at 60°/s (0.03-0.008 x g) [314] for 1 h, 24 h or 10 days. For every time point, the three remaining plates and flasks were positioned on the static RPM bar as ground controls (GC). After 1 h, 24 h and 10 days of exposure, one plate per condition was fixed with 4% paraformaldehyde whereas cells in flask were lysed with lysis buffer from Qiagen AllPrep DNA/RNA/Protein Mini Kit. Remaining two plate and flasks per experimental point were kept for 24 or 72 h at normal ground conditions to further investigate the neuronal recovery after simulated microgravity. The experimental layout is described in supplementary figure 23.

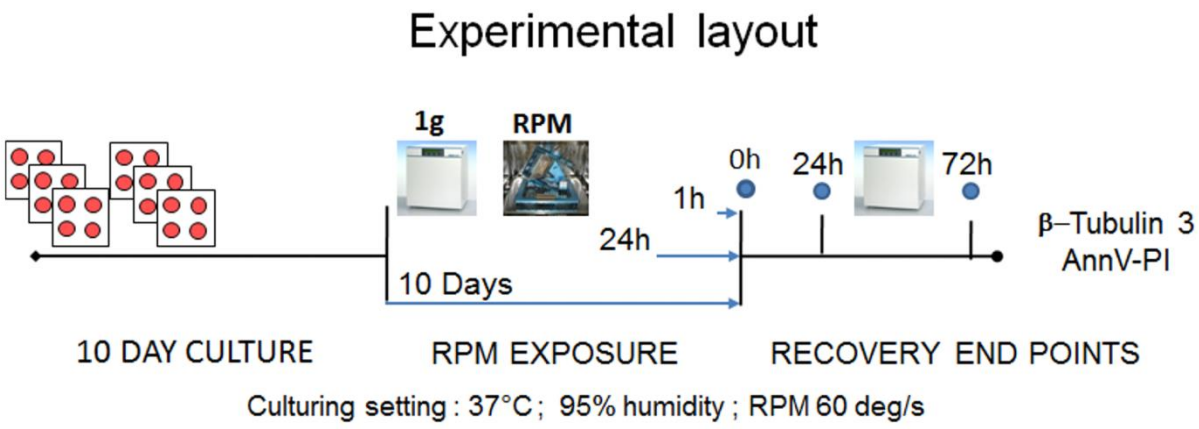

Figure 23: Experimental layout.
Ten day old neuron cultures used for different times of exposure to RPM or ground conditions (GC) for 1 h, 24 h and 10 days. Cells were then fixed immediately after (0 h) or after 24 and 72 h of recovery in GC.

2.3. Immunostaining of neuronal network

Neuronal networks were stained for the neuronal marker β-tubulin 3 (β-tub 3) using indirect immunofluorescence, whereas nuclei were revealed by direct fluorescence. After washing with phosphate buffered saline (PBS), cells were permeabilized with PBS-Triton X-100 (Sigma, Belgium) 0.1% for 3 min and blocked for 30 min with PBS-BSA 3%. Fluorescent staining was performed by exposing the samples to mouse monoclonal anti-β-tubulin 3 (cat n° T5076-200UL, Sigma-Aldrich, Belgium), diluted 1:200 in PBS (Sigma, Belgium), at 4 °C overnight. After washing in PBS, a second layer of fluorescein isothiocyanate (FITC)-conjugated anti-Mouse IgG (cat n° F2012, Sigma-Aldrich) antibody, diluted 1:200 in PBS, was applied for 90 min, at 37 °C in the dark. Nuclei were then stained with Hoechst (cat n° B2883, Sigma-Aldrich), 1:400 in PBS, for 10 min. Wells were then rinsed three times in PBS and twice in H_2O.

2.4. Image acquisition and neuronal network analysis.

Images were acquired with a Nikon Eclipse Ti (automated inverted wide-field epifluorescence microscope) equipped with a 40x magnification (S PLAN FLUR, ELWD 40x / 0. 6) dry objective and a Nikon DS-Qi1Mc camera controlled by a NIS-Elements software.

Per each condition, three mosaic regions of 3 by 3 images (27 bi-dimensional images, in total) with five focus positions were randomly acquired and compressed in a 2D in focus image by Extended Depth of Focus (EDF) NIS-Elements module. Data obtained from the 3 mosaics were summed and considered as a single large image.

The neuronal network image processing analyses were performed by a home-made tool for ImageJ (Rasband, W.S., N.I.H, USA, http://rsb.info.nih.gov/ij/) by merging known functions available in the freely available plugin [274, 278, 279, 315]. The high performance of this new tool came from an appropriate soma segmentation originating from nuclei and from an elegant multi-tier segmentation after image enhancing and edge detection, segmenting even the thinner neurites. Thereafter, morphological processes could be easily applied for the determination of the total neuron area, the total neurite area and length, the neurite attachment points, the soma counting and soma characteristics. Data related to area and length of neurites per image were determined to specifically investigate the effects of simulated microgravity on the neurite network density *in toto*. Finally, morphological values per single neuron were obtained dividing image parameters by number of neurons per image in order to obtain an average per cell.

In order to better understand the distribution of β-tub 3, the mean intensity of fluorescence was determined in somas and neurites. Calculating the ratios between mean intensities of somas and neurites allowed us to determine the distribution of tubulin into neurons.

Each experiment was performed in triplicates. A significant difference from the control conditions was determined by paired *t*-test or two-way ANOVA (Graph Pad Software Inc., San Diego, USA) and a p value <0.05 was considered significant.

2.5. Apoptosis

Apoptosis was estimated by Annexin V (Ann V) assay on adherent neurons using the Ann V-FITC apoptosis detection kit II (cat n° BMS500FI/300CE, eBioscience, Belgium) combined with an additional fluorescence staining of nuclei by Hoechst dye. Ann V-FITC was used to

quantitatively estimate the percentage of dead cells in the neuron cultures. The AnnV-FITC$^-$/PI$^-$/Hoechst$^+$ population was considered as normal healthy cells, while Ann V-FITC$^+$/PI$^-$/Hoechst$^+$ (Ann V$^+$-PI$^-$) and Ann V-FITC$^+$/PI$^+$/Hoechst$^+$ (AnnV$^+$-PI$^+$) cells were taken as an estimation of early apoptosis and late apoptosis or necrosis, respectively (Fig. 32 F). Image processing analysis is described in figures 24 and 25 (Fig. 24; Fig. 25). Primary neuron cultures are not 100% pure cultures as a small number of non-neuron cells (negative to β-tub 3) with small nuclei and condensed chromatin were observed after nuclei and neuron marker staining. This type of cells that were positive for PI and negative for Ann V staining were not taken into account in the viability estimation since they could induce a relative error in the counting of late apoptosis/necrosis neuron cells.

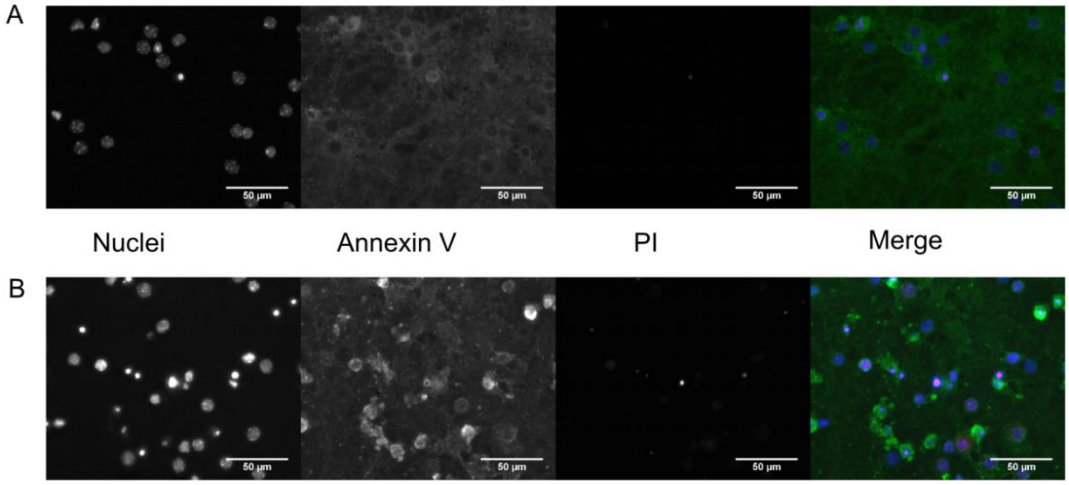

Figure 24: Annexin V – PI staining on neuronal networks.
From left to right: nuclei staining, Annexin V staining, propidium iodide (PI) staining and merge. (A) Neuronal network without Ann V positive neurons. (B) Neuronal networks with Ann V positive neurons are highlighted in bright green.

For statistical analysis, 36 images were randomly acquired with 40x objective and an average of 530±130 cells per condition were taken into account. Ann V$^-$-PI$^-$ cells as well as the specific Ann V$^+$-PI$^-$ and Ann V$^+$-PI$^+$ cells were counted and the percentages of Ann V$^+$-PI$^-$ and Ann V$^+$-PI$^+$ neurons on total cell number were then calculated. To estimate the relative level of total Ann V$^+$ (Ann V$^+$-PI$^-$ + Ann V$^+$-PI$^+$) neurons exposed to simulated microgravity, the percentage of total Ann V$^+$ neurons in culture exposed to the RPM were divided by the

percentage obtained in control cultures. Based on nucleus counterstaining of adherent neurons, the same apoptosis analysis image sets of neuron cultures exposed for short-, middle- or long-term to RPM were used to estimate the density of cells per cm^2. This allowed to compare neuron cultures exposed to the RPM vs. their respective controls. Additionally, comparison between 1 h GC and 10 days RPM was performed to observe the loss of cells over the whole experiment. For comparison between conditions, we used the paired *t*-test and a *p*-value <0.05 was considered significant.

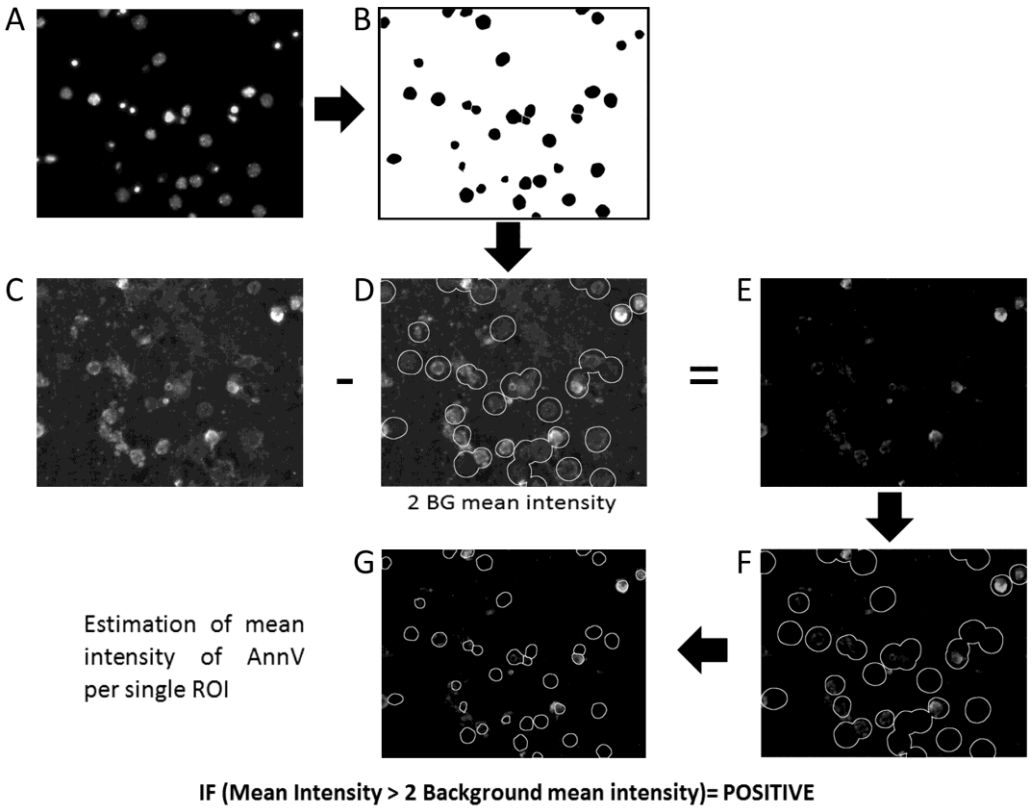

Figure 25: Image processing analysis of Annexin V – PI staining on neuronal networks.
From images of nuclei (A) regions of interest (ROI) related nuclei (B) were determined and counted. From Ann V images (C) neurite network mean intensity, related to the background, was determined after enlarging all ROI's of nuclei and inverting the obtained selection (D). Twice the background mean intensity was removed from the Ann V images in order to obtain a clear image of Ann V staining into somas (E). To determine if somas were positive or negative for Ann V staining, the external background was determined as previously described (F) and finally mean intensity related to each soma was estimated. As shown in image F, if the mean intensity related to each soma was higher than twice the background mean intensity, somas were considered as positive.
Similar procedure was performed to determine negative or positive neurons to propidium iodide staining. Finally, cells were divided in:
1) AnnV-FITC$^-$/PI$^-$/Hoechst$^+$ named Ann V negative, which characterizes normal neurons.
2) AnnV-FITC$^+$/PI$^-$/Hoechst$^+$ named Ann V positive, which characterizes neurons in early apoptosis.
3) AnnV-FITC$^+$/PI$^+$/Hoechst$^+$ named Ann V-PI positive, which characterizes neurons in late apoptosis or necrosis.
4) AnnV-FITC$^-$/PI$^+$/Hoechst$^+$ named PI positive, which characterizes neurons in necrosis or non-neuron cells or decreases.

2.6. RNA extraction

RNA was extracted from *in vitro* neuron cultures using the Qiagen AllPrep DNA/RNA/Protein Mini Kit according to the manufacturer's instructions. Concentration and purity of RNA were assessed using the Nanodrop spectrophotometer (Thermo Scientific, USA) while RNA integrity was determined using the RNA Integrity Number (RIN) (Agilent's lab-on-chip Bioanalyzer 2100, Agilent Technologies, USA). All samples had a RIN number above 8.0 and were used for further processing.

2.7. Microarray hybridization

The total RNA was quantified and used for synthesis of the first strand cDNA, followed by the synthesis of second strand-cDNA. The double stranded cDNA was then *in vitro* transcribed into cRNA. A second cycle of cDNA synthesis was performed followed by a purification and fragmentation step of the cDNA. The fragmented second cycle cDNA was then labelled and hybridized to Affymetrix Mouse Gene 1.0 ST Arrays (Affymetrix, Santa Clara, USA). All the steps of amplification, transcription and labelling were performed using the Ambion® WT Expression Kit according to the manufacturer's instructions (Life Technologies Ltd, Paisley, UK). For every time point following irradiation, the chips were all scanned in three steps. In total, 18 chips were prepared for *in vitro* samples exposed to 1 h RPM and 18 chips were prepared for *in vitro* samples exposed to RPM for 10 days.

2.8. Microarray data analysis

Microarray data were analysed using Partek Genomics Suite 6.6 Beta (version 6.13). Data were imported at exon level using a customized RMA algorithm (pre-background adjustment for probe sequence, default settings for RMA background correction, quantile normalization, Log2 transformation of the estimated probe signal intensities and median polish probe set

summarization). For summarization of exon signals to gene signals, a one-step Tukey's biweight summarization method was used. Since the transcriptional changes were quite small, we considered genes with a p-value <0.005 between the experimental conditions and the representative controls as being differentially expressed. Additionally, threshold of 1.4 in fold changes was set.

2.9. Panther classification system and gene set description

Gene classification of biological processes, cellular components and involved pathways were performed on gene lists from three different analyses (i.e. *in vitro* short-term exposure, *in vitro* long term exposure and *in vivo* exposure to microgravity) using the Panther 8 software (www.pantherdb.org) [316]. Gene ontology functional classification was performed to identify the number of modulated genes in biological processes. Additionally, gene ontology of biological processes was performed. Afterwards, based on previous analyses, tables of genes related to apoptosis, cell adhesion, cell communication and transition processes were generated. Finally, on the complete gene lists, pathway analysis was performed to identify which pathways were modified in microgravity conditions.

3. **Results**

3.1. Behaviour of neurons in culture

For all experiments primary neurons were cultured under ground conditions up to 23 days in a neuron-selective medium as described in the section Materials and Methods. The growth of the neuronal network was monitored and allowed us to determine at which stage a sufficient connectivity between neurons occurred which was indicating a good maturation of the neuronal network as previously demonstrated in other studies [176]. As shown in figure 26 we observed that during the first ten days of culture the neuronal network grew fast; thereafter the growth rate slowed down. Therefore, we decided to use 10-day old cultures for subsequent experiments.

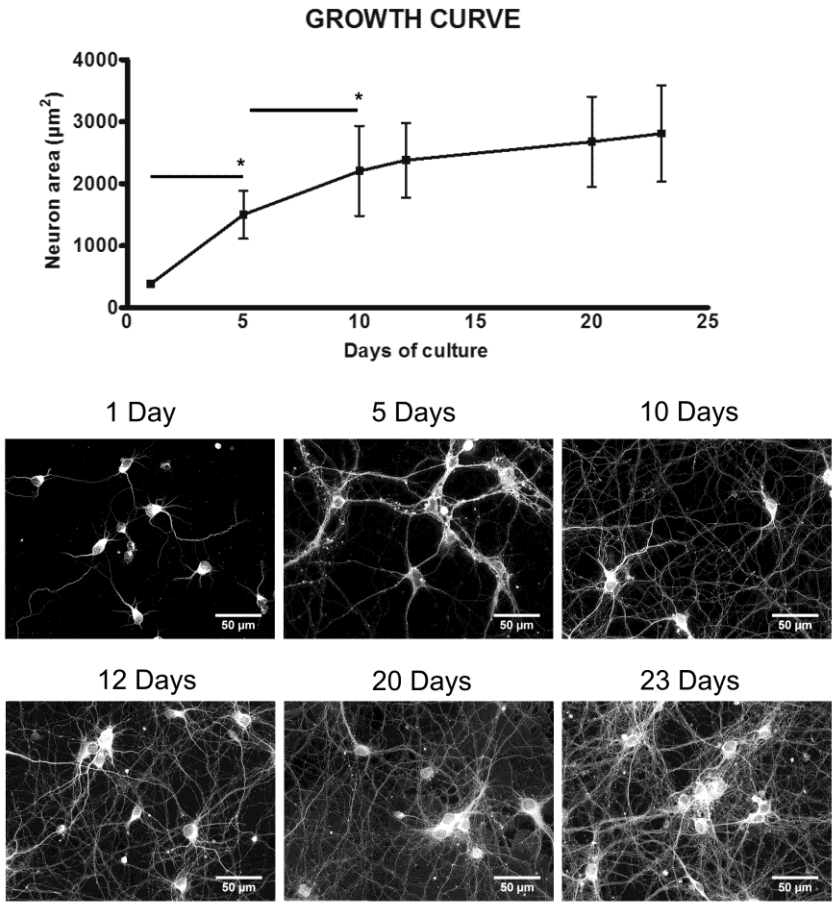

Figure 26: Neuronal network growth under ground conditions.
Growth curve of the neuronal area (upper panel) within a period of 23 days with representative images at selective time points (lower panel). Values are expressed as the average of single neuron areas and bars represent standard deviation. Paired t-test was performed to determine differences between two close experimental points and obtained results showed significant differences between 1 day vs. 5 days (P=0.046) and 5 days vs. 10 days (P=0.041) but not between the following time points.

3.2. Behaviour of the neuronal networks under simulated microgravity

To investigate the effects of simulated microgravity on dense neuronal networks, 10-day cultures were exposed for short-, middle- and long-terms to the RPM. Immunostaining of β-tub 3 as a specific marker of neurons was used to analyse the changes in the neuronal network.

3.2.1. Changes of neuron area and neurite area and length under simulated microgravity

Neurons cultured for 10 days under ground conditions and afterwards exposed to the RPM for 1 h showed an area reduction of 24% per neuron compared to their respective controls, whereas neurons exposed for 24 h showed a significant area reduction of 14% (Fig. 27 A, B and H) per neuron. In neurons exposed for 10 days the 6% area reduction was not significant (Fig. 27A, B and H). Similar effects of microgravity exposure were observed on the neurite area and length per neuron, both of which were significantly reduced after short- to middle-term exposures, but not after long-term exposure (Fig. 27C, D and H). These data therefore indicate that from the initial reduction in neuron/neurite area, which occurred during the first hour of RPM exposure, cells adapted to the new gravity condition over time. Additionally, analyses on neurite network density, estimated as neurite area or neurite length per image, showed a decrease in network density after exposure to the RPM for 1h or 24 h, whereas networks exposed for 10 days showed partial adaptation (Fig. 27 A, E, F and H). Interestingly, in both single neurons and neurite networks the adaptation of the neurite length in simulated microgravity was delayed (Fig. 27 H) indicating that the recovery of the neurite area after 24 h should be the result of partial thickening of the neurites (Fig. 28). Furthermore, analysis on neuron density determined in number of neurons per cm^2 did not show major change over the different exposure times to simulated microgravity compared to the respective controls.

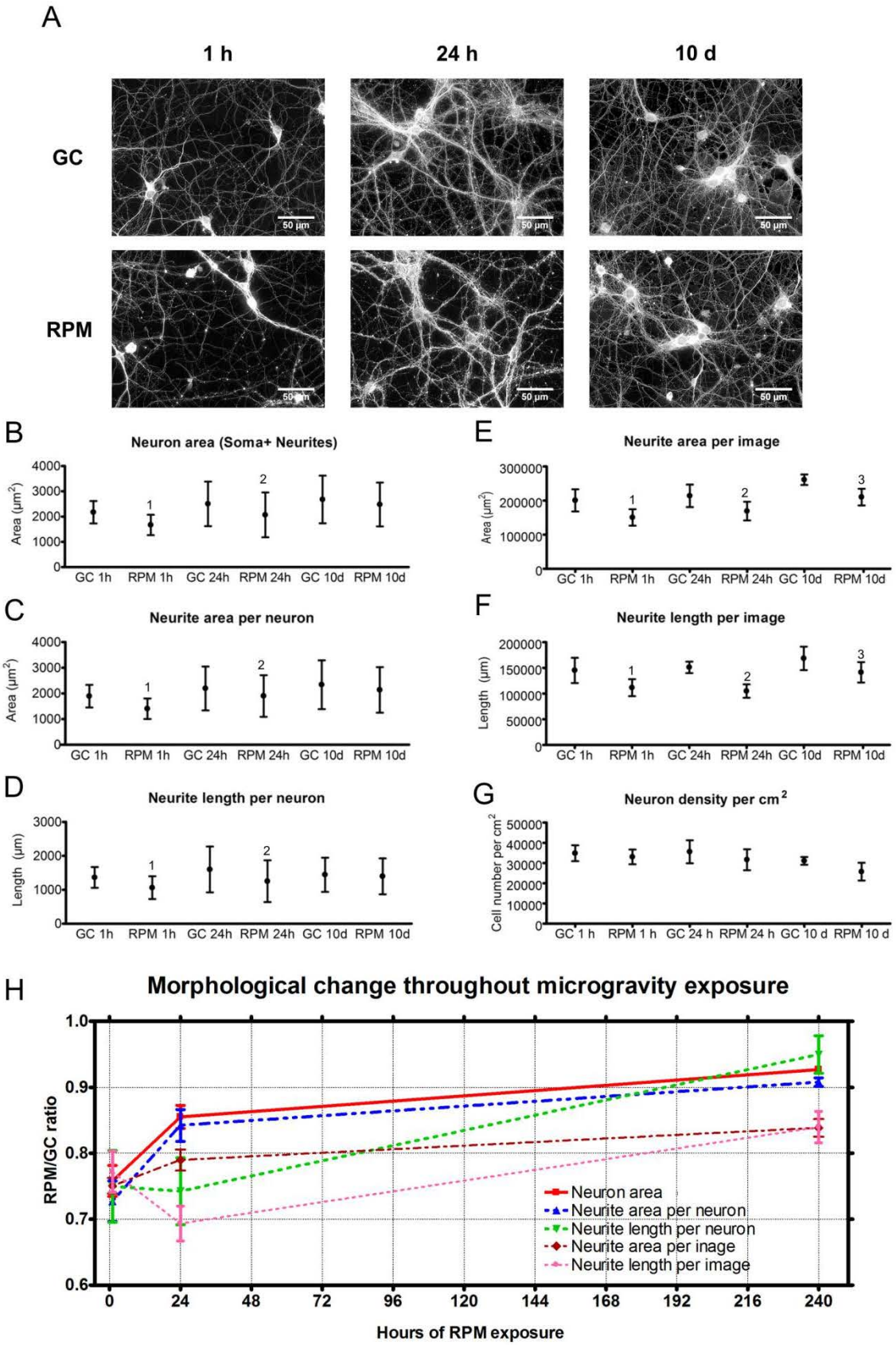
A
1 h
24 h
10 d
GC
RPM
50 µm
B
Neuron area (Soma+ Neurites)
Area (µm²)
E
Neurite area per image
C
Neurite area per neuron
F
Neurite length per image
Length (µm)
D
Neurite length per neuron
G
Neuron density per cm²
Cell number per cm²
GC 1h
RPM 1h
GC 24h
RPM 24h
GC 10d
RPM 10d
H
Morphological change throughout microgravity exposure
RPM/GC ratio
Hours of RPM exposure
Neuron area
Neurite area per neuron
Neurite length per neuron
Neurite area per inage
Neurite length per image

Figure 28: Effects of simulated microgravity on single neurons as well as on neuronal networks .
(A) First line: neuronal networks cultured in ground control conditions (GC 1h - 24h - 10 days); Second line: neuronal networks exposed to simulated microgravity (RPM 1h - 24h - 10 days). (B) Neuron area (soma + neurites) in neuronal network cultures exposed to RPM for 1h, 24h or 10 days and the respective controls. (C) Neurite area per neuron in neuronal network cultures exposed to RPM for 1h, 24h or 10 days and the respective controls. (D) Neurite length per neuron in neuronal network cultures exposed to RPM for 1h, 24h or 10 days and the respective controls. (E) Neurite area per image in cultures exposed to RPM for 1h, 24h or 10 days and the respective controls. (F) Neurite length per image in cultures exposed to RPM for 1h, 24h or 10 days and the respective controls. (G) Neuronal density per cm2; 10 day RPM vs. 1h GC : P=0.055. (H) RPM vs. Ground condition ratios of neuron area, neurite area and neurite length show how neurons adapt to simulated microgravity throughout the exposure time. Paired two-tailed Student's t-test and standard deviation bars are shown. 1, P < 0.05 RPM 1 h compared to GC 1 h; 2, P < 0.05 RPM 24 h compared to GC 24 h; 3, P < 0.05 RPM 10 days compared to GC 10 days. GC= ground condition; RPM=Random Positioning Machine

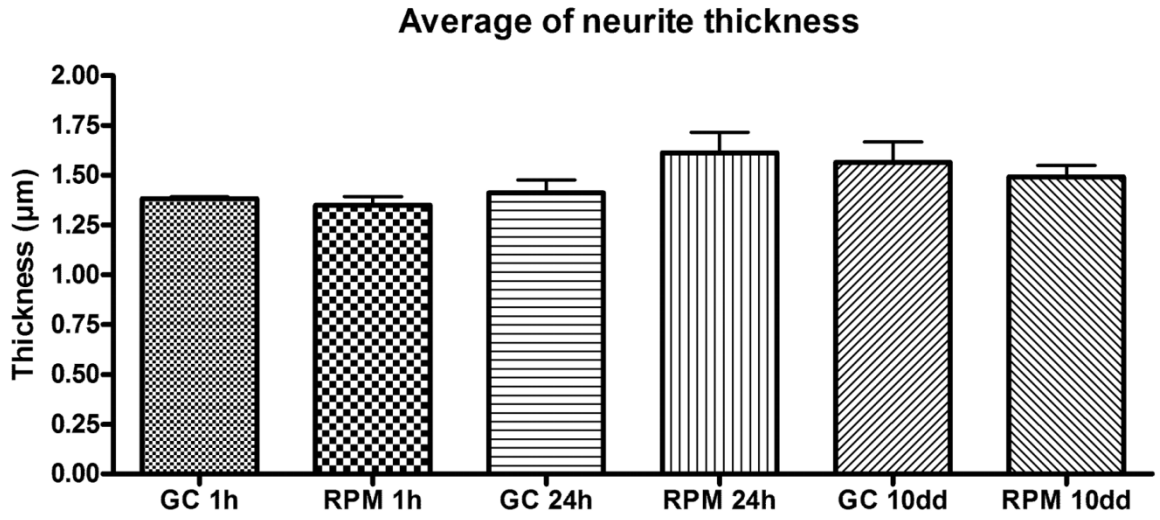

Figure 28: Neurite thickness.
Average of neurite thickness determined dividing neurite area by neurite length. No statistical difference was observed with Paired two-tailed Student's t-test and bars represent standard deviation.

3.2.2. Changes in soma morphology and β-tubulin isotype 3 distribution in neurons

Microtubules are cytoskeleton elements organized in substructures as protofilaments made by α- and β- tubulin monomers. They are involved in the internal transport, locomotion and cell shape. In particular, microtubules together with microfilaments and intermediate filaments determine the cell architecture which explains how cell shape and other mechanisms are controlled and respond to mechanical forces [185]. Microtubules are under a continuous turn-over of polymerisation and depolymerisation of their arborisation, also known as "treadmilling",

and the dynamic activity is linked to the cell function or to the intracellular or extracellular environment. Staining the cells for the β-tub 3, one of the components of microtubules, allowed us to analyse the distribution of the cytoskeletal protein into neurons exposed to simulated microgravity and therefore estimate variations in the protein distribution between somas and neurites.

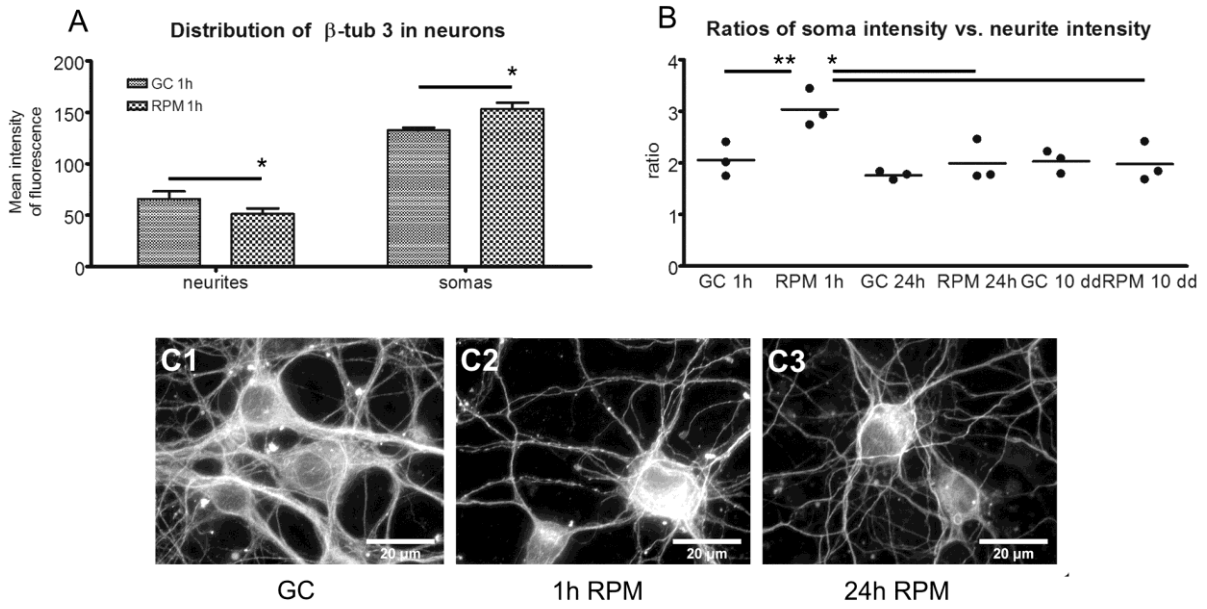

Figure 29: Distribution of β-tubulin isotype 3 (β-tub 3) under simulated microgravity.
(A) Distribution of β-tub 3 between somas and neurites in neurons exposed for 1 h to RPM (neurite p = 0.029; soma p = 0.038). (B) Soma intensity vs. neurite intensity ratios in neurons exposed for 1 hour, 24 hours and 10 days to the RPM compared to the respective ground condition controls. Statistical analysis show a difference between GC 1h vs. RPM 1h (P = 0.0012) and RPM 1h vs. rpm 24h vs. RPM 10 days (P < 0.05). (C 1-2-3) Higher magnification of neurons show the morphological and fluorescence intensity differences at the soma and neurite levels between exposed and non-exposed samples. One way Anova, Paired two-tailed Student's t-test and standard deviation bars are shown. GC= ground condition; RPM=Random Positioning Machine.

Typically, in neurons exposed to ground conditions, β-tub 3 mean intensity in somas was twice as high as in the neurites (Fig. 29A-B-C). However, after exposure to the RPM for 1 h, the mean intensity of the fluorescence signal decreased in the neurites (P = 0.029) whereas it increased in the soma (P = 0.039) (Fig. 29A-C) which suggests a redistribution of microtubules in the cells upon short-term exposure to microgravity. In contrast, cells exposed for 24 h or 10 days did not show any difference in β-tub 3 distribution compared to their respective controls indicating that the cells had adapted to their new environment (Fig. 29B-C).

Since a redistribution of microtubules may affect the cellular morphology, we also measured the size as well as the shape of the somas. We observed that, at all time points, exposure to microgravity led to a significant reduction of the soma size (Fig. 30A). The shape of each somas was attributed a certain roundness coefficient (ratio between longest and smallest diameter used to determine how far from a perfect circle the shape is), and we found that the roundness was reduced in short-term exposed cells, whereas it was increased in middle- and long-term exposed cells (Fig. 30B).

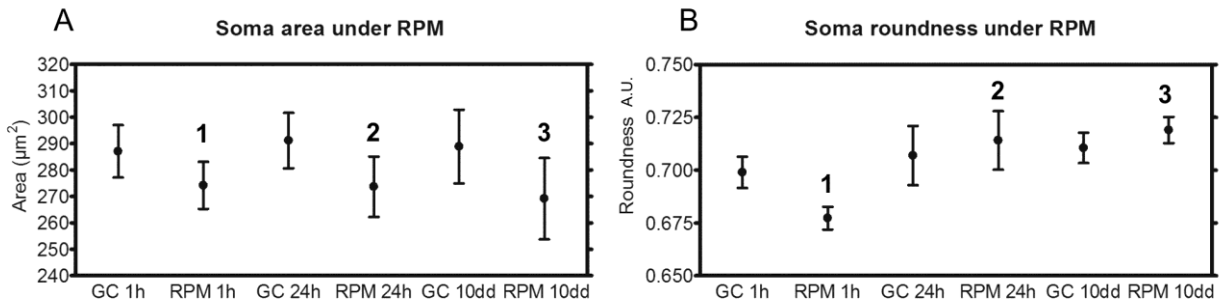

Figure 30: Soma characteristics in neurons exposed for 1 hour, 24 hours and 10 days to the RPM compared to their respective controls.
(A) Size of somas in neuron cultures exposed to RPM for 1, 24 hours or 10 days and their respective controls. (B) Roundness of somas in neuron cultures exposed to RPM for 1, 24 hours or 10 days and their respective controls. Paired two-tailed Student's t-test and standard deviation bars are shown. 1, P < 0.05 RPM 1 h compared to GC 1 h; 2, P < 0.05 RPM 24 h compared to GC 24 h; 3, P < 0.05 RPM 10 days compared to GC 10 days. GC= ground condition; RPM=Random Positioning Machine.

3.3. Neuronal network recovery after simulated microgravity

3.3.1. Neuron and neurite recovery after simulated microgravity

In order to understand whether microgravity induces permanent or temporary morphological changes, neuronal network cultures were exposed again to ground conditions for 24 and 72 hours after having been exposed to simulated microgravity. We analysed the neuron area, the neurite area and length per image and per neuron as well as the morphological parameters of the somas (size and roundness) to evaluate the recovery after RPM exposure.

Neurons exposed to simulated microgravity for 1 h showed a significant area increase from 75 to 90 % of the respective controls in 24 h of recovery in ground conditions. In the following

hours of recovery they reached 96% of their respective controls (Fig. 31A). Similar area increase was also observed in neurons previously exposed to the RPM for 24 h. Neurons exposed for 10 days to RPM did not show any statistical area increase. Also the area of neurites of single neurons exposed for 1 h and 24 h to the RPM showed a significant increase in the first 24 h of recovery in ground conditions, whereas neurons exposed to simulated microgravity for 10 days showed a statistical reduction of 4% (from 91% to 87%) in neurite area per neuron within the first 24 h of recovery and reaching 95% of the corresponding controls 72 h after RPM (Fig 31B). Similar behaviour was observed on neurite length per single neurons (Fig. 31C). Furthermore, analyses of neurite network density per image, expressed in neurite area and length, showed a similar recovery such as single neurons (Fig. 31 D, E). Additionally, neurite networks having recovered in re-established ground conditions after exposure to simulated microgravity for 10 days showed statistical difference in area and length compared to the respective controls (Fig. 31 D, E).

Figure 31: Recovery in re-established ground conditions of neuronal networks and neurons previously exposed to simulated microgravity.
(A) Recovery dynamics of area of single neurons after RPM as expressed in ratios of RPM vs. ground control exposed cultures. (B) Recovery dynamics of neurite area per neuron after RPM as expressed in ratios of RPM vs. ground control exposed cultures. (C) Recovery dynamics of neurite length per neuron after RPM as expressed in ratios of RPM vs. ground control exposed cultures. (D) Recovery dynamics of neurite network area per image after RPM as expressed in ratios of RPM vs. ground control exposed cultures. (E) Recovery dynamics of neurite metwork length per image after RPM as expressed in ratios of RPM vs. ground control exposed cultures. (F) Size of somas in neuron cultures previously exposed to RPM and having recovered for 24 hours in ground conditions and their respective controls. (G) Roundness of somas in neuron cultures previously exposed to RPM and having recovered for 24 hours in ground conditions and their respective controls. Paired two-tailed Student's t-test and standard deviation bars are shown., P<0.05 raw data 72 h RPM vs. raw data 72 h GC 1, P < 0.05 24 h vs 0 h of neuron area after 10 days of RPM; 2, P < 0.05 24 h vs 0 h of neurite area after 24 h of RPM; 3, P < 0.05 24 h vs 0 h of neurite length after 1 h of RPM; 4, P < 0.05 72 h vs 24 h of neuron area after 10 days of RPM; 5, P < 0.05 72 h vs 24 h of neurite area after 24 h of RPM; 6, P < 0.05 72 h vs 24 h of neurite length after 1 h of RPM. GC= ground condition; RPM=Random Positioning Machine. (page 136)*

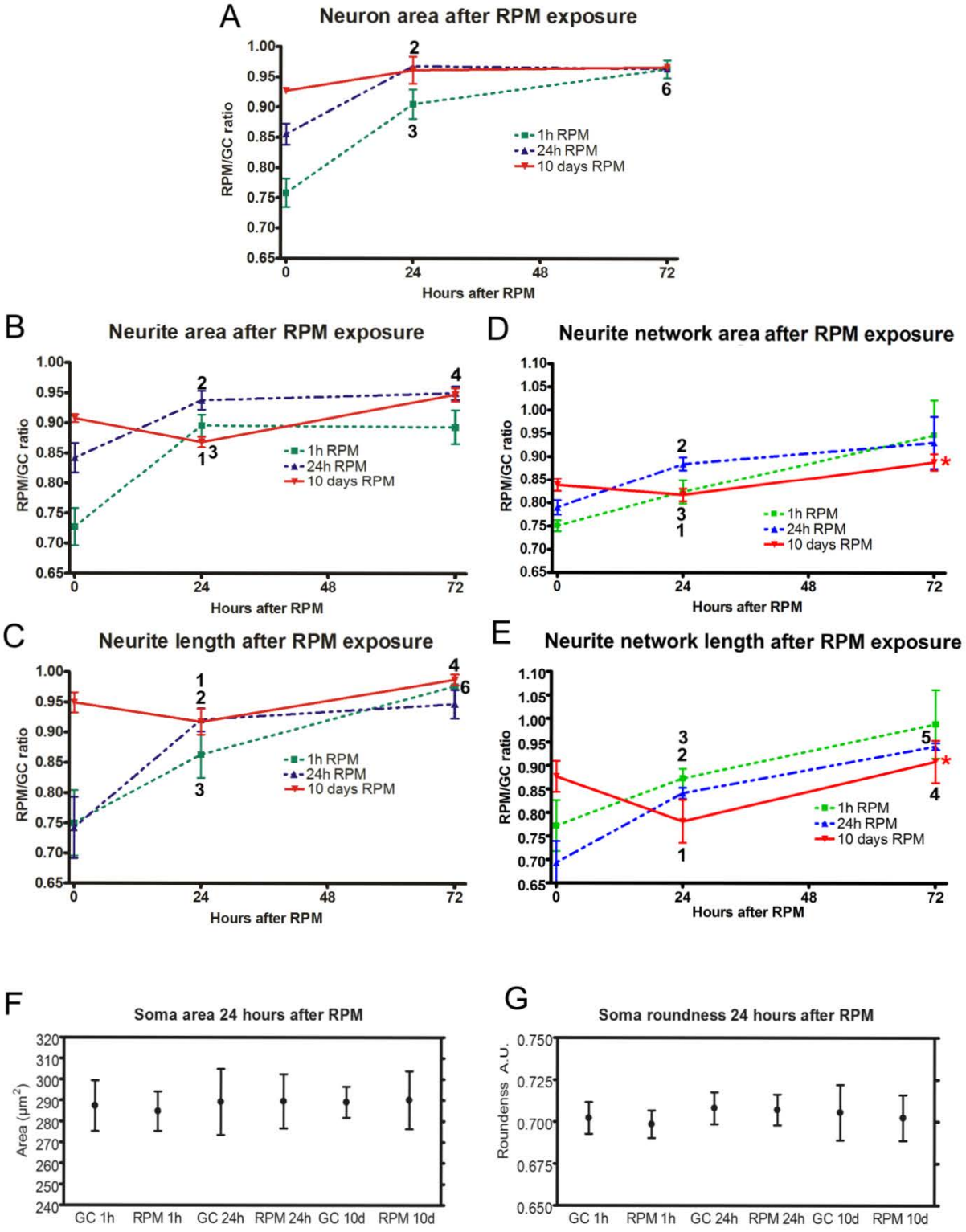
A
Neuron area after RPM exposure
RPM/GC ratio
Hours after RPM
1h RPM
24h RPM
10 days RPM
B
Neurite area after RPM exposure
C
Neurite length after RPM exposure
D
Neurite network area after RPM exposure
E
Neurite network length after RPM exposure
F
Soma area 24 hours after RPM
Area (µm²)
G
Soma roundness 24 hours after RPM
Roundenss A.U.
GC 1h
RPM 1h
GC 24h
RPM 24h
GC 10d
RPM 10d

1.1.1. Morphology of somas after simulated microgravity

As previously mentioned, somas of neurons exposed to simulated microgravity presented morphological alterations such as a reduction in size and changes in roundness. After being exposed to ground conditions for 24 h following simulated microgravity, these effects were completely reversed for short-, middle- as well as long-term exposed neuronal cultures (Fig. 31F, G), indicating a fast full recovery of the soma morphology.

3.4. Changes in cell viability

It is known that apoptosis can be induced by stress when cells are exposed to different physiological conditions. In order to understand whether neuron viability was altered by exposure to simulated microgravity and throughout the following recovery in ground conditions, neuron cultures were analysed using the Ann V - PI assay.

The percentages of total Ann V positive neurons (tot Ann V^+ = Ann V^+-PI^- +Ann V^+-PI^+) in cultures exposed to RPM for 1 h, 24 h and 10 days was between 1.5 and 2 times the respective controls (Fig. 32A-B). Interestingly, in cultures exposed for 10 days to RPM conditions the number of Ann V^+-PI^+ neurons was 3 times more elevated than the controls (Fig. 32A). This increase in Ann V^+-PI^+ cells was not observed in cultures exposed for 1 and 24 hours to the RPM (Fig. 6A). Furthermore the rate of tot Ann V^+ neurons (RPM/GC) did not change between short-, middle- and long-term exposure to simulated microgravity (Fig. 32A).

Neuron cultures exposed to the RPM and having recovered for 24 h showed an increase in percentage of tot Ann V^+ cells over 2 times more elevated than the respective controls. Furthermore, an increase in percentage of late apoptotic or necrotic (Ann V^+-PI^+) cells was observed in neuron cultures previously exposed for 1 h 24 h and 10 days to RPM (Fig. 32C). Seventy-two hours after exposure to RPM, only neurons exposed for 10 days still showed statistical differences in both tot Ann V^+ and only Ann V^+-PI^+ positive cells compared to the controls (Fig. 32D).

Moreover, it was observed that RPM/GC ratios of total Ann V^+ showed a statistical decrease between 24 and 72 hours after 1 h RPM exposure (Fig. 32E).

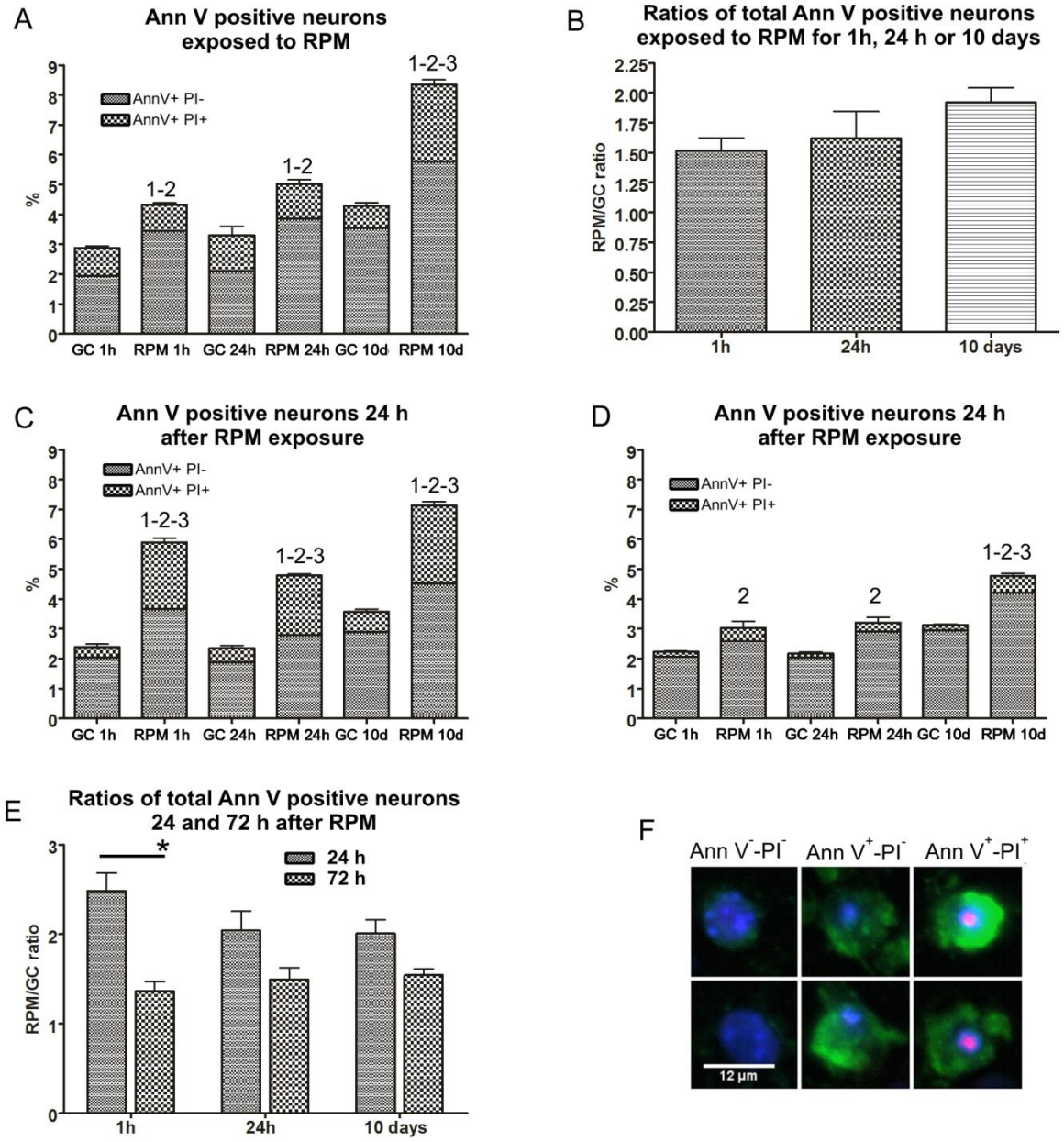

Figure 32: Altered viability induced during and after simulated microgravity exposure.
*(A) Percentage of Ann V+-PI- and Ann V+-PI+ cells in neuronal network induced after 1 hour, 24 hours or 10 days of simulated microgravity. (B) RPM/GC ratios of tot Ann V+ percentages of neuron cultures exposed and not exposed to simulated microgravity. (C) Percentages of Ann V+-PI- and Ann V+-PI+ cells in neuron cultures exposed to RPM and having recovered for 24 h in ground conditions. (D) Percentages of Ann V+-PI- and Ann V+-PI+ cells in neuron cultures exposed to RPM and having recovered for 72 h in ground conditions. (E) RPM/GC ratios of tot Ann V+ percentages of neuron cultures recovered for 24 and 72 hours after simulated microgravity exposure. * = P<0.05 24h compared to 72h. (F) Neurons stained with Annexin V-FITC/PI/Hoechst (green/red/blue) and observed under fluorescence microscope. Ann V-FITC-/PI-/Hoechst+ are considered healthy cells, V-FITC+/PI-/Hoechst+ are considered early apoptotic cells and Ann V-FITC+/PI+/Hoechst+ are considered late apoptotic or necrotic cells. Paired two-tailed Student's t-test and standard deviation bars are shown. 1, P < 0.05 Ann V+-PI- RPM compared to GC; 2, P < 0.05 Ann V+-PI+ RPM compared to GC; 3, P < 0.05 tot Ann V+ RPM compared to GC. GC= ground conditions; RPM=Random Positioning Machine.*

3.5. Gene expression changes in mature neuronal cultures after short-term exposure to simulated microgravity

Exposure of mature neuronal cultures to simulated microgravity for 1 h (1h RPM + 0h GC) resulted in 25 genes being significantly modulated ($p < 0.005$ compared to controls and ±1.4 fold changes) (Fig. 33). These genes are mainly involved in Wnt signalling, the gonadotropin-releasing hormone receptor pathway and the p53 pathway (Table 7). During the first 24 h of recovery after 1h RPM exposure (1h RPM + 24h GC) the number of modulated genes was 11 times higher (271 genes) than RPM exposed samples without recovery (1h RPM + 0h GC). The amount of significant genes decreased down to 140 within 72 h of recovery in re-established ground gravity (1h RPM + 72h GC). The change in the number of modulated genes provided a first indication about the neuron response during recovery in ground conditions after RPM exposure. Pathway analysis of up and down-regulated genes after 24 h of recovery underlined changes in genes involved in cytoskeleton related, axonal guidance, adrenaline and noradrenaline biosynthesis, apoptosis, Alzheimer's, Parkinson's and Huntington's diseases and neurotransmitter receptor signaling pathways (Table 7). Genes modulated after 72 h were,

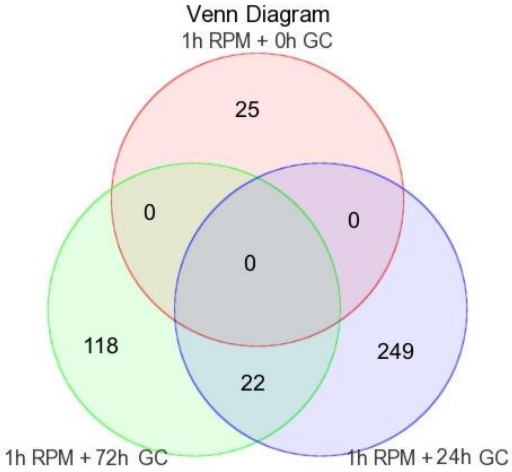

Figure 33: Venn diagram of regulated genes after 1h of RPM and during 24 and 72 h of recovery after restored ground conditions.
Statistical significance is considered when $p<0.001$. "1h RPM + 0h GC": cultures only exposed to 1 h of RPM; "1h RPM + 24h GC": cultures exposed to 1 h of RPM followed by 24h of recovery in ground conditions (GC); "1h RPM + 72h GC": cultures exposed to 1 h of RPM followed by 72h of recovery in ground conditions.

among others, involved in neurotransmitter receptor-mediated pathways, in cytoskeletal regulation by Rho GTPase, in integrin signaling, in the gonadotropin-releasing hormone receptor pathway as well as in neurotransmitter receptor signaling and in Huntington's disease-related pathways (Table 7). The up-regulation of few genes involved in axonal guidance is confirming the morphological observations delineating an increase in neurite area and length during recovery after simulated microgravity.

Table 7. Pathways involved after 1 h of RPM or in the following 24 and 72 h of recovery in GC. "1h RPM + 0h GC": cultures only exposed to 1 h of RPM; "1h RPM + 24h GC": cultures exposed to 1 h of RPM followed by 24h of recovery in ground conditions (GC); "1h RPM + 72h GC": cultures exposed to 1 h of RPM followed by 72h of recovery in ground conditions. D=down-regulated genes; U=up-regulated genes.

	1h RPM + 0h GC	**1h RPM + 24h GC**	**1h RPM + 72h GC**
Cadherin signaling pathway		D	
Cytoskeletal regulation by Rho GTPase			U
Integrin signalling pathway		D	U
Notch signaling pathway		U	
Axon guidance mediated by netrin			U
Axon guidance mediated by semaphorins		D	
Axon guidance mediated by Slit/Robo		U	U
Apoptosis signaling pathway		D	
p53 pathway	U	D	U
Alzheimer disease-amyloid secretase pathway		D	
Alzheimer disease-presenilin pathway		D	
Huntington disease		U D	U
Parkinson disease		U	
Ras Pathway		U D	
Synaptic vesicle trafficking			U
Adrenaline and noradrenaline biosynthesis		D	
Oxidative stress response		U	U
Gonadotropin-releasing hormone receptor pathway	U	U D	U D
5HT2 type receptor mediated signaling pathway		D	U
Beta1 adrenergic receptor signaling pathway		D	
Beta2 adrenergic receptor signaling pathway		D	
Nicotinic acetylcholine receptor signaling pathway		D	U
Oxytocin receptor mediated signaling pathway		D	U
Wnt signaling pathway	D	D	U D

Functional classification based on biological processes from the gene ontology database indicate that cell communication, metabolic and cellular processes appeared to be the most involved processes with a high number of genes during 1 hour of RPM and the following 24 and 72 hours of recovery in restored ground conditions (Figs 34-35). Interestingly, the high number of genes involved within the first 24 h of recovery after RPM exposure suggest that short-term exposure to microgravity could induce a relevant response in neuronal cells.

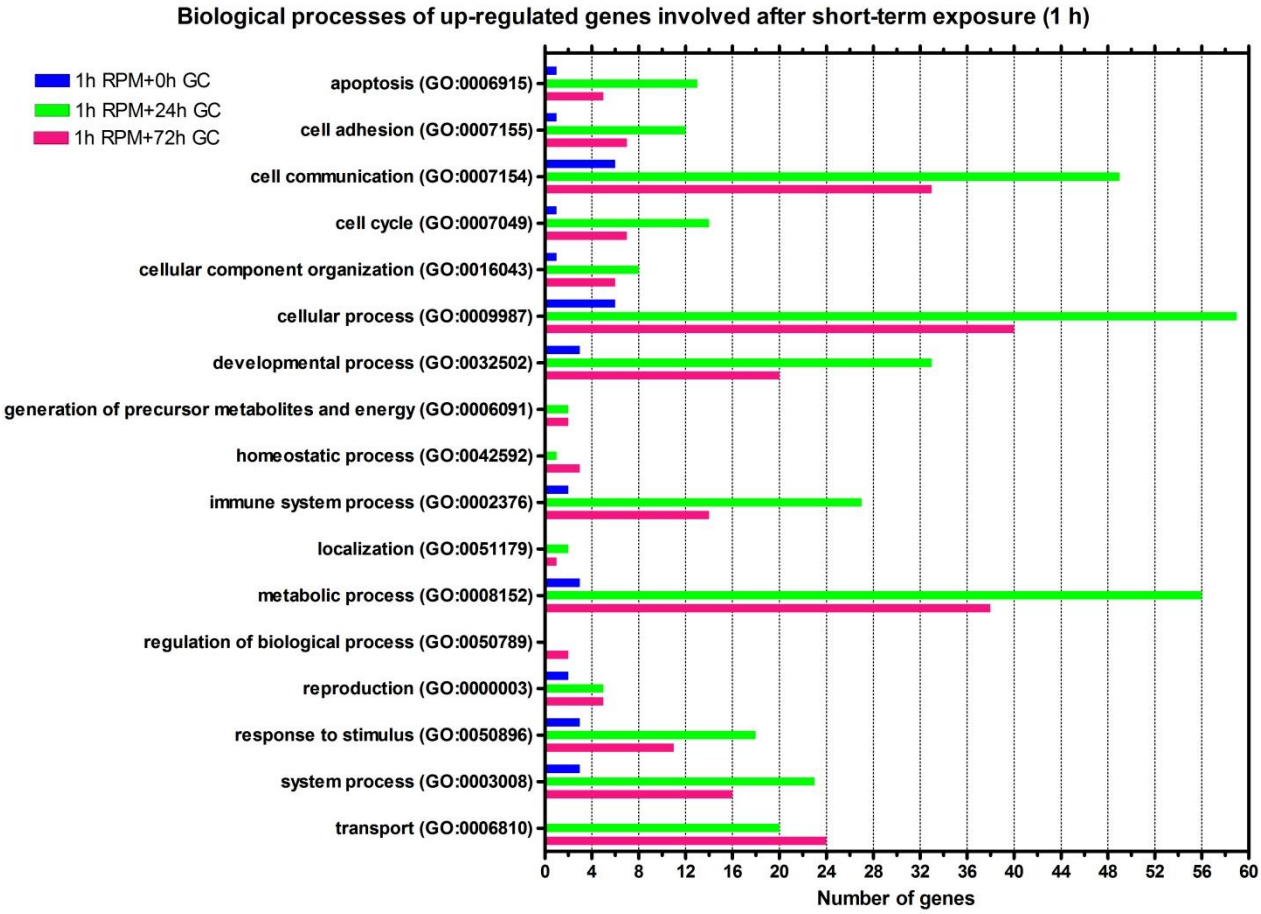

Figure 34:. Modulated biological processes related to up-regulated genes expressed in mature neuronal cultures exposed to RPM for 1h (1h RPM + 0h GC) and the following recovery in restored ground conditions (GC), 24h (1h RPM + 24h GC) and 72h (1h RPM + 72h GC) after RPM exposure.

Evaluation of gene expression changes involved in biological processes as apoptosis, cell adhesion, transport and cell communication showed that in *in vitro* mature neurons exposed to simulated microgravity, for instance, few genes as Gadd45b (involved in growth arrest and DNA

damage), Klra5 (involved in cell-cell adhesion and signal transduction), Rbp7 (involved in neuronal apoptosis) and Rassf1 (involved in signal transduction) were modulated (Tables 9-12).

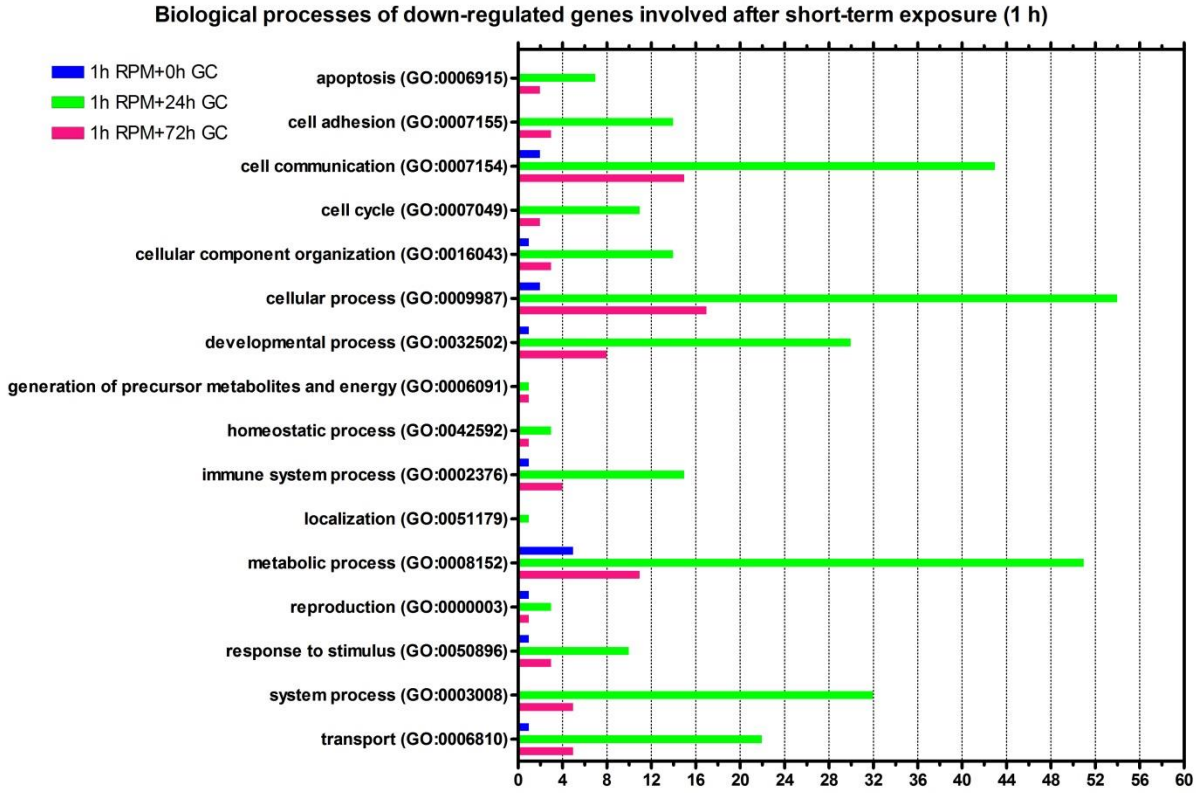

Figure 35: Modulated biological processes related to down-regulated genes expressed in mature neuronal cultures exposed to RPM for 1h (1h RPM + 0h GC) and the following recovery in restored ground conditions (GC), 24h (1h RPM + 24h GC) and 72h (1h RPM + 72h GC) after RPM exposure.

During the first 24 h of recovery after RPM exposure, several cytoskeleton and synapsis related genes (Cadm1, Cdh8, Col6a1, Glt25d2, Adamts1. Gpr50, Ntsr1, Svc2, Syn3, Enc1, Dnm3, Sh3gl3, Ezr, Tuba8, Myo1 and more) involved in cell adhesion, transport or cell communication were modulated as response to re-established ground gravity. Additionally, some structural components of cytoskeleton or involved in cell adhesion as α-tubulin 8, collagen α1, Procollagen-lysine,2-oxoglutarate 5-dioxygenase 2, pleckstrin and others were still highly expressed within 72 h of recovery (Tables 9 and 11). Nevertheless, for highly expressed gene, a similar pattern was observed with a maximum of expression at 24 h of recovery delineating a high similarity with the morphological changes (neurite area and length and apoptosis) showing also a maximum of change at 24 h.

3.6. Gene expression changes in mature neuronal cultures after long-term exposure to simulated microgravity

Interestingly, long-term exposure to simulated microgravity also induced a moderate effect on gene expression levels in mature neuronal cultures. After 10 days RPM exposure, 17 genes with a fold change of ±1.4 were significantly changed compared to ground controls (Fig. 36). Pathway analysis showed that these genes involved in P53 pathway and Gonadotropin-releasing hormone receptor pathways were up-regulated whereas genes involved in Huntington's disease and cytoskeleton regulation pathway were down-regulated. The number of modulated genes after 24 h of recovery (10d RPM + 24h GC) was 2.5 times higher (46 genes) as compared to the RPM exposed samples without recovery (10d RPM + 0h GC). After 72 h of recovery (10d RPM + 72h GC) the number of modulated genes increased up to 75 genes. The difference in the number of modulated genes provided us with a first indication about the neuron response to RPM exposure and the time-dependent recovery in ground conditions.

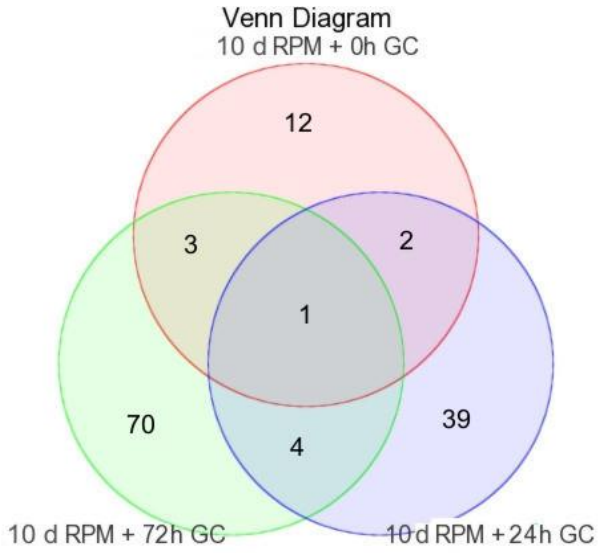

Figure 36: Venn diagram of regulated genes after 10 days of RPM and during 24 and 72 h of recovery after restored ground conditions.
Statistical significance is considered when p<0.001. "10 d RPM + 0h GC": cultures only exposed to 10 days of RPM; "10 d RPM + 24h GC": cultures exposed to 10 days of RPM followed by 24h of recovery in ground conditions (GC); "10 d RPM + 72h GC": cultures exposed to 10 days of RPM followed by 72h of recovery in ground conditions.

Pathway analysis of the modulated genes after 24 h of recovery underlined down-regulation of genes involved in adrenaline, noradrenaline and serotonin biosynthesis, apoptosis, Parkinson's and Alzheimer's diseases and inflammation (Table 8). Genes modulated after 72 h were, among others, involved in neurotransmitter receptor-mediated pathways, in cytoskeletal regulation by Rho GTPase, in serotonin degradation, in the gonadotropin-releasing hormone receptor pathways as well as in Parkinson's, Huntington's and Alzheimer's disease-related pathways.

Table 8. Pathways involved after 10 days of RPM or in the following 24 and 72 h of recovery in GC.
"10 days RPM + 0h GC": cultures only exposed to 10 days RPM; "10 days RPM + 24h GC": cultures exposed to 10 days of RPM followed by 24h of recovery in ground conditions (GC); "10 days RPM + 72h GC": cultures exposed to 10 days of RPM followed by 72h of recovery in ground conditions. D=down-regulated genes; U=up-regulated genes.

	10 day RPM + 0h GC		**10 day RPM + 24h GC**		**10 day RPM + 72h GC**	
Cytoskeletal regulation by Rho GTPase						D
Cytoskeletal regulation pathway		D		D		D
Notch signaling pathway				D		D
p53 pathway	U					
5-Hydroxytryptamine biosynthesis				D		
5-Hydroxytryptamine degredation					U	
Adrenaline and noradrenaline biosynthesis				D		
Nicotine pharmacodynamics pathway				D		
Gonadotropin-releasing hormone receptor pathway	U				U	D
Histamine H1 receptor mediated signaling pathway						D
Metabotropic glutamate receptor group II pathway						D
Metabotropic glutamate receptor group III pathway						D
Muscarinic acetylcholine receptor 1 and 3 signaling pathway						D
Nicotinic acetylcholine receptor signaling pathway						D
Alzheimer disease-amyloid secretase pathway						D
Alzheimer disease-presenilin pathway				D		D
Huntington disease		D			U	
Parkinson disease				D		
Wnt signaling pathway					U	D

Gene ontology analyses based on biological processes revealed that metabolic and transport processes were the most involved pathways after 10 days of RPM exposure (Fig. 37,

38). Time-dependent recovery over 24 and 72 hours post simulated microgravity exposure, revealed metabolic, cellular, and developmental processes as well as cell communication, cell adhesion, cellular component organization and transport as the main representative biological processes (Fig. 37, 38). Interestingly, most of the involved genes over the recovery period after 10 days RPM were down-regulated and could play a role in re-adaptation to the established gravity condition (Fig. 38).

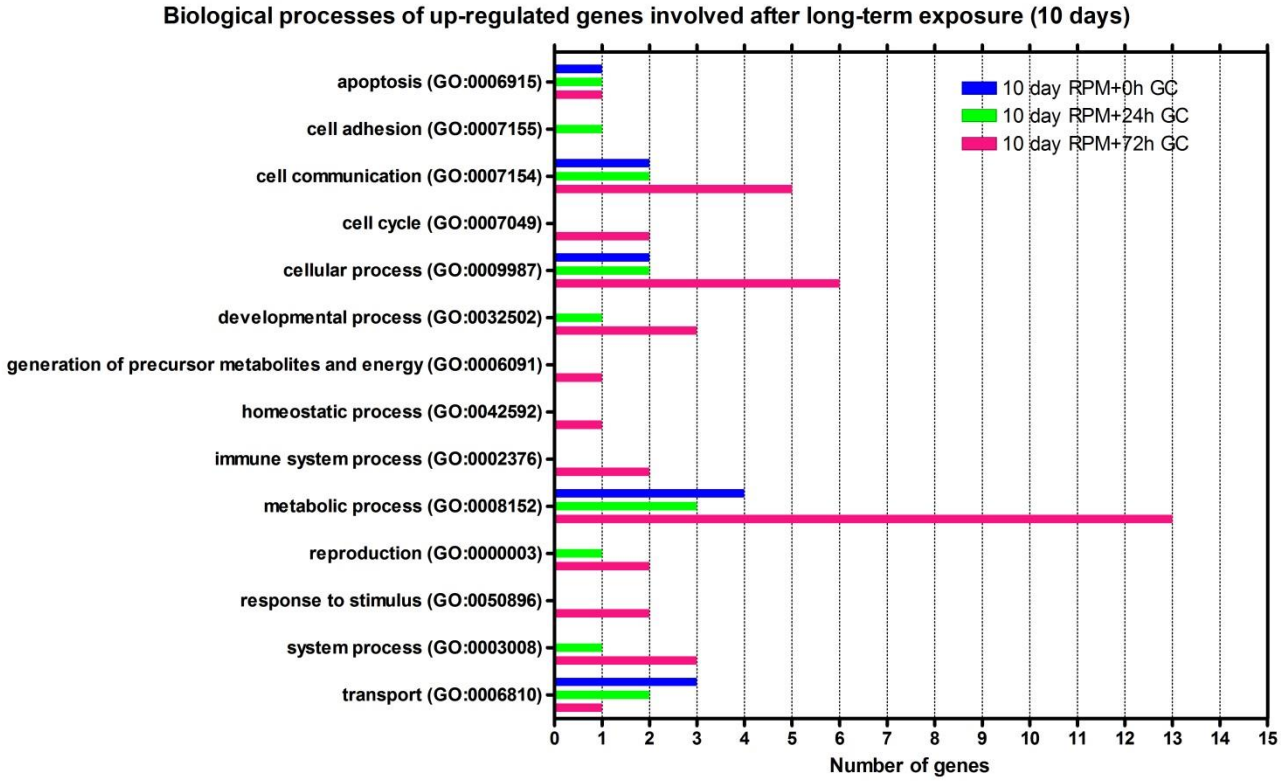

Figure 37: Modulated biological processes related to up-regulated genes expressed in mature neuronal cultures exposed to RPM for 1 h (10 days RPM + 0 h GC) and the following recovery in restored ground conditions (GC) 24h (10 days RPM + 24 h GC) and 72h (10 days RPM + 72 h GC) after RPM exposure.

Evaluation of gene expression changes in *in vitro* mature neurons exposed to simulated microgravity for 10 days and that recovered for 24 and 72 hours showed that not many genes were modulated in apoptosis and cell adhesion biological processes, although an increase in apoptosis coupled with a reduction of network density was observed at 24 h of recovery. Furthermore, transport and cell communication related genes were mainly down-regulated, suggesting a partial recovery of the neuronal network. Indeed, few genes involved in cell-matrix,

cell-cell adhesion, cell motion and membrane trafficking as tubulin-specific chaperone D, kinesin-like protein KIF3C, myosin-III b and calcium/calmodulin-dependent protein kinase type 1 were still down-regulated only 72 h of recovery after long-term exposure to RPM indicating a continuous recovery of the network (Tables 13-16).

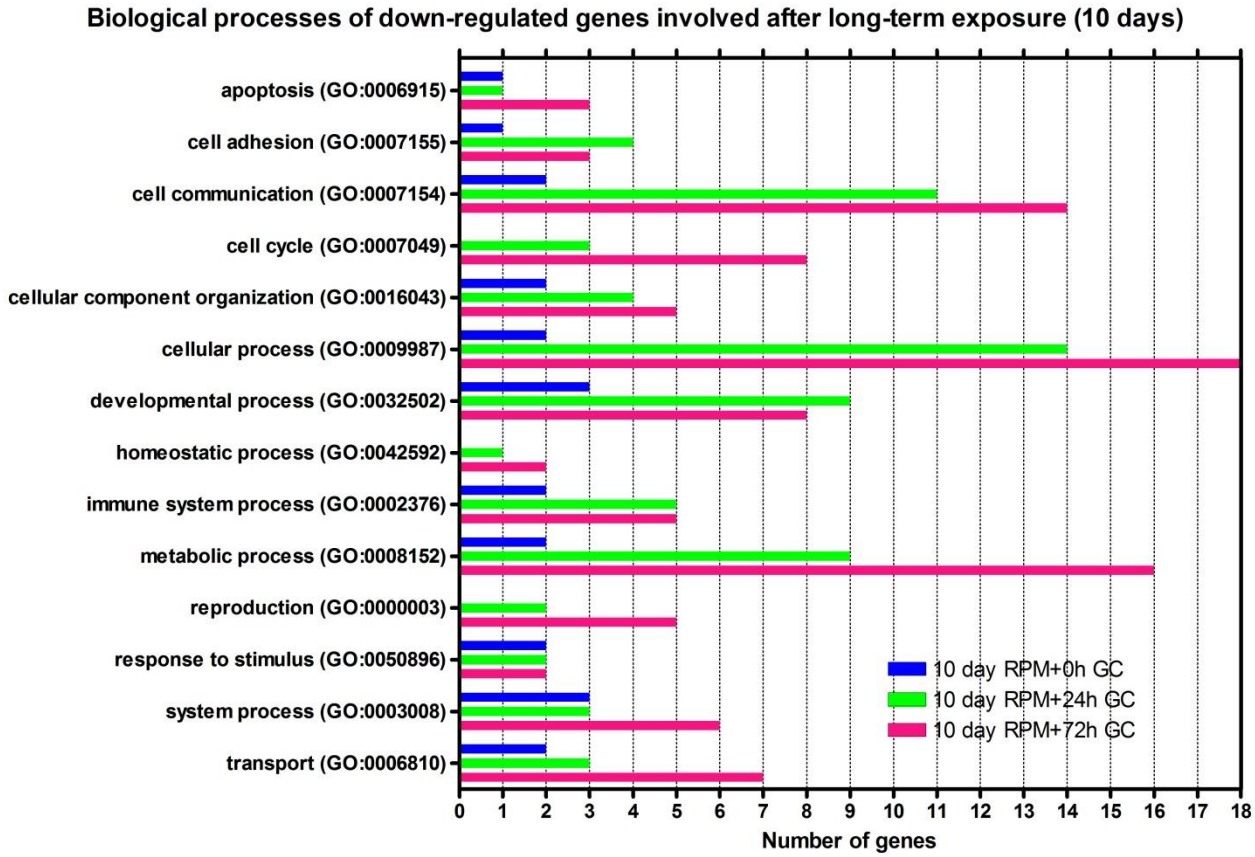

Figure 38: Modulated biological processes related to down-regulated genes expressed in mature neuronal cultures exposed to RPM for 1h (10 days RPM + 0 h GC) and the following recovery in restored ground conditions (GC) 24h (10 days RPM + 24h GC) and 72h (10 days RPM + 72h GC) after RPM exposure.

4. Discussion

In this study, we investigated morphological and molecular changes of well-connected primary neuronal networks cultured under simulated microgravity conditions using the RPM to test whether simulated microgravity can affect neuronal morphology and physiology in order to establish a possible link with physiological changes observed in astronauts during space flight.

4.1. Cellular and neurite network response to the modified gravity

In our study we observed that, within the first hour of simulated microgravity exposure, cultured single neurons exhibited a reduction of neurite length, size and roundness of somas indicating shrinkage of the cell. Concomitantly, the area and the length of neurite networks were also affected by the RPM environment. Moreover, β-tub 3 fluorescence intensity analyses showed that 1 h of exposure to microgravity induced changes in the microtubule distribution from the neurites to the soma. This is in accordance with other investigations on the cytoskeleton of cells exposed to short-term microgravity conditions, which described changes of microtubules, microfilaments and intermediate filaments [38, 51, 64]. Additionally, concomitant to microgravity-induced cytoskeletal changes [38, 51], cell area reduction occurred as well [59]. Furthermore, the observed reduction of the roundness of somas, which occurred within the first hour of simulated microgravity, seems to be a transitive stage before reaching the final stage in which neuron bodies of cells subjected to simulated microgravity were rounder compared to the controls already at 24 h of RPM.

Studies on cell motility reported a drastic reduction of cell locomotion [38, 59]. On the contrary, in our neuronal cultures, one of the responses observed in modulated gravity is that these cells do not lose their intrinsic property to extend neurites and search for contacts with other neurons. In fact, neurons as well as neuronal networks are initially affected by simulated microgravity and they reacted by increasing area and length of neurites throughout long RPM

exposure (Fig. 28 B-H). Despite the high neuron adaptation to simulated microgravity during long-term RPM exposure, the partial adaptation of neurite network to simulated microgravity could be explained by the observed increase of apoptosis over long-term exposure.

Within this study, we observed in both single neurons as well as neurite networks that most of the effects of short-term exposure to microgravity are attenuated in middle- and long-term exposed neurons, indicating that the cells adapt to the new gravity conditions. On the other hand, neuron recovery after long-term exposure showed a different re-adaptation to the ground conditions compared to short- and middle-term RPM exposure. After long-term RPM exposure (10 days) we observed in both single neurons and neurite networks an initial decrease in the area and the length of neurites during the first 24 hours of recovery followed by an increase after 72 hours of recovery reaching again almost the normality (Fig. 31 B, C).

The observed morphological changes are in line with the gene expression modulation. The guidance of axons is mediated by extracellular cues that modulate cytoskeletal dynamics in axonal growth cones during the organization of the neuronal network [317, 318]. According to literatures [319, 320] and to our results microgravity modulate changes in cytoskeleton structure distribution and organization resulting in alteration of cytoskeleton gene expression. In our experiments we observed that short-term exposure to microgravity induce retraction of neurites, which recover within a few days when the gravitational forces are re-established. As described by Guan and Hubert [317, 318], the observed down-regulation of Plexin-A1, gene involved in axon guidance collapse, together with up-regulation of Netrin-1, Rhoj and UNC5B, which are involved in attractive and repulsive functions during neurites extension, modulate the axonal guidance during the re-establishment of the neuronal network. Furthermore, no changes in genes involved in axonal guidance were observed over long-term exposure to simulated low gravity suggesting an adaptation to the new condition as observed from morphological analysis.

4.2. Viability of mature neurons under gravitational changes.

As reported in several studies, apoptosis and neuroplasticity (neurogenesis and neuronal network remodelling) are in stable equilibrium. An increase in one may trigger the other and *vice versa* [321]. *In vivo* studies reported that environmental as well as endogenous factors not only decrease neurogenesis but can also induce apoptosis [322, 323]. Indeed, several experiments showed that simulated microgravity induces apoptosis in different cell types [59, 67, 68, 324]. Within our experiments, cell death investigation revealed an increase of total Ann V^+ cells after exposure to simulated microgravity.

The observed increase of cells positive for the apoptosis markers (total Ann V^+) within 24 h of recovery after short and middle-term exposure to microgravity (Fig. 33C) might be due to the fact that, under simulated microgravity, some neurons may have lost their connections as a consequence of the reduction in neurite length. Furthermore, an increase of late apoptotic and necrotic (Ann V^+-PI^+) neurons was observed within the first 24 h of recovery after RPM which might induce gaps in the networks. Nevertheless, the number of apoptosis marker positive cells (total Ann V^+) decreased 72 h after RPM exposure (Fig. 33D, 1-24 h) allowing to re-establish the equilibrium between cell death and neuroplasticity.

Despite the neuron adaptation to simulated microgravity during long-term exposure, we observed an increase in Ann V^+-PI^+ neurons in long-term exposed cultures (Fig. 33A), but not in short- or middle-term exposed cultures. These results suggest that the increased percentage of late apoptosis could be the cause of the partial adaptation of neurite networks to simulated microgravity during long-term exposure. Within the first 24 h of recovery after long-term RPM exposure, neuronal networks showed reduction in neurite length and area (Fig. 32A, B), while the level of tot Ann V^+ cells was still higher than the control after 72 h of recovery. Furthermore, the higher percentage of late apoptotic or necrotic cells observed within the 24 h of recovery in ground conditions after RPM (Fig. 32C) might be linked to neuronal network changes observed

at the same time point, inducing a delay in the neuronal network recovery observed 72 h after RPM (Fig. 32A, B). Similar effects were reported in studies on skeletal muscles of rat exposed 12.5 days to real space conditions, where fiber necrosis and degeneration of motor innervation were observed a few days after landing [325].

According to the obtained data, up-regulation of genes involved in apoptosis, as well as in p53, growth arrest and DNA damage pathways were observed in mature neurons exposed to simulated microgravity for short- and long-term. In particular, increase of involved genes within the first 24h of recovery after short-term exposure to RPM suggested an initial impact of gravitational changes in well-connected neurons. Interestingly, induction of apoptosis and stress-related genes as well as genes involved in DNA damage/repair (Gadd45b and Gadd45g) and p53 pathways [326], after 1h RPM exposure and within the first 24 h of recovery (Table 9) is in line with the observed increase in apoptosis. Obtained results suggest a change in neuronal physiology due to the re-adaptation to the re-established Earth gravity conditions, as also observed in rat motor neurons which undergo apoptosis or neurodegeneration after microgravity exposure [325].

4.3. Neuroplasticity and possible links with physiological disorders in space

It was reported that environmental changes increase the activity of neuroplasticity. In fact, during the first days in space, the nervous system of astronauts is forced to develop new interpretations of the stimuli and to develop alternative adjustment strategies to compensate for the altered incoming stimuli [327]. In this study we provided new data on *in vitro* neuronal network changes during short- and middle-term exposure to simulated microgravity and on their partial adaptation over a period of 10 days. This seems to be in agreement with the behavioural tests performed on mice exposed for 91 days to the ISS environment and in which a quick learning in how the mice dealt with the new gravity conditions using the grid to grasp and direct their movements was reported [199]. In this study, we observed an increased level of apoptotic

neurons within 10 days of RPM, probably due to the stress induced by simulated microgravity, which might induce a reduction of the neurite network density resulting in an increase of neuroplasticity activity in order to re-establish the lost connections. These results could be the response to an increase of neuroplasticity activity in the neuronal network as reported by the up-regulation of genes related to axonal guidance, branching of neurites and long-term potentiation observed in genome expression analyses on the whole brain tissue of mice recently exposed to ISS environment [199] as well as in *in vitro* mature neuron culture exposed to RPM, as observed in our studies. The observed neuroplasticity (network remodelling and/or apoptosis) might be a factor contributing to changes in brain homeostasis. We provided here molecular and cellular evidence of neuronal network remodelling and neuron adaptation following a stress due to changes in gravity conditions such as the ones experienced by astronauts in space, although neuron cells represent just one piece of the puzzling central nervous system. Nevertheless, we believe that our system is an appropriate model for testing the effects of different space conditions and to better understand the related mechanisms that may compromise the structure and function of the neuronal network.

In conclusion, obtained results within this investigation underline two different responses related to simulated microgravity exposure time. First, short-term (1 h) exposure to simulated microgravity induces stress in neurons. Reduction in neurite network density, neuron size, alteration in β-tubulin isotype 3 distributions and increase of apoptotic cells are observed in neurons exposed to the RPM for only 1 hour. During recovery post short-term exposure to simulated microgravity, a fast restoration almost reaching the ground morphological state coupled with up-regulation of many genes involved in axonal guidance, cytoskeleton and cell motility occurred in the neurite network as well as in neurons. Furthermore, the response observed after short-term exposure to reduced gravity might influence the connectivity

stimulating neurons to increase the network by producing new neurites to establish new connections over time.

On the contrary, a second type of response was observed during long-term exposure where neurons reached a high degree of adaptation to simulated microgravity conditions, in which the neurite network was partially adapted, most probably due to increase of apoptosis. Additionally, the neuron recovery post long-term exposure to RPM appeared slower and the neuronal networks partially recovered. The neuronal network seems to acquire a different physiological state under microgravity conditions requiring a long re-adaptation period during recovery under ground conditions. This response clearly indicates that the highly adapted neurons to simulated microgravity (10 day exposure to RPM) exhibit different physiological cell state than in normal ground control conditions.

Most of the space motion sickness and the space adaptation syndrome symptoms are related to the nervous system which is forced to develop new strategies to interpret the opposite inputs coming from environmental sensors. This adaptation is probably partly based on neuroplasticity activity. In the light of the obtained results, *in vitro* neuronal networks seem to partially adapt to the reduced gravity conditions during long-term exposure. However, to confirm the physiological changes, complementary studies on metabolic pathways, neuronal connectivity and neuronal network activities should be performed. Investigations on mature neuronal networks exposed to both conditions, microgravity and radiation, are necessary to help deciphering the related health risks for the central nervous system in the context of long and deep space travels.

Table 9. Apoptosis-involved genes in neuron cultures exposed to 1 h RPM and having recovered for 24 and 72 h in ground conditions. Fold change threshold was 1.4 and p-value 0.005. Genes statistically different compared to the controls are highlighted in yellow.

Gene bank	Symbol	Full name gene	p-value – Fold-Change (RPM * 0 h vs. GC * 0 h)		p-value – Fold-Change (RPM * 24 h vs. GC * 24 h)		p-value – Fold-Change (RPM * 72 h vs. GC * 72 h)	
NM_011785	Akt3	RAC-gamma serine/threonine-protein kinase	0,6559	1,0	0,0006	-1,4	0,0288	-1,2
NM_013863	Bag3	BAG family molecular chaperone regulator 3	0,1255	1,3	0,0034	1,7	0,1473	1,3
NM_028967	Batf2	Basic leucine zipper transcriptional factor ATF-like 2	0,8759	-1,0	0,0003	1,7	0,0230	1,3
NM_001159557	Cd36	Platelet glycoprotein 4	0,9524	1,0	0,5281	-1,2	0,0001	-3,7
NM_007727	Cntn1	Contactin-1	0,9266	-1,0	0,0010	-1,5	0,1765	-1,1
NM_010143	Ephb3	Ephrin type-B receptor 3	0,6802	1,0	0,0010	1,6	0,0847	1,2
BC024332	Fam195a	Protein FAM195A	0,6996	1,1	0,0019	1,6	0,2542	1,2
NM_008655	Gadd45b	Growth arrest and DNA damage-inducible protein GADD45 beta	0,0031	4,1	0,0178	2,9	0,2113	1,7
NM_011817	Gadd45g	Growth arrest and DNA damage-inducible protein GADD45G	0,0170	2,5	0,0038	3,3	0,7104	1,1
NM_133849	Hrh3	Histamine H3 receptor	0,4899	1,2	0,0009	-2,7	0,3472	-1,2
NM_198610	Igsf21	Immunoglobulin superfamily member 21	0,9329	-1,0	0,0012	-1,6	0,3314	1,1
NM_008506	Mycl1	Protein L-Myc-1	0,1160	-1,1	0,0195	-1,2	0,0003	-1,5
NM_010850	Mycs	Protein S-Myc	0,7171	-1,1	0,0023	-2,1	0,2115	-1,3
NM_008872	Plat	Tissue-type plasminogen activator	0,8311	1,0	0,0011	1,8	0,0048	1,6
NM_008654	Ppp1r15a	Protein phosphatase 1 regulatory subunit 15A	0,5034	1,1	0,0045	2,0	0,4077	1,2
NM_019713	Rassf1	Ras association domain-containing protein 1	0,8568	-1,0	0,0039	1,6	0,7845	-1,0
NM_177073	Relt	Tumor necrosis factor receptor superfamily member 19L	0,9120	-1,0	0,0015	1,6	0,1333	1,2
NM_001004173	Sgpp2	Sphingosine-1-phosphate phosphatase 2	0,8627	1,0	0,4660	1,2	0,0016	2,9
NM_007706	Socs2	Suppressor of cytokine signaling 2	0,8799	-1,0	0,0009	-2,0	0,0759	-1,4
NM_213659	Stat3	Signal transducer and activator of transcription 3	0,8275	1,0	0,0027	1,7	0,5430	1,1
NM_011518	Sykb	Tyrosine-protein kinase SYK	0,7436	-1,0	0,1055	1,2	0,0011	1,6
NM_019913	Txn2	Thioredoxin, mitochondrial	0,9879	1,0	0,0026	1,5	0,4248	1,1
NM_029770	Unc5b	Netrin receptor UNC5B	0,3172	1,2	0,0018	1,8	0,0016	1,8
NM_173016	Vat1l	Synaptic vesicle membrane protein VAT-1 homolog-like	0,9631	-1,0	0,0035	-1,5	0,4560	-1,1

Table 10. Cell adhesion-involved genes in neuron cultures exposed to 1 h RPM and having recovered for 24 and 72 h in ground conditions. Fold change threshold was 1.4 and p-value 0.005. Genes statistically different compared to the controls are highlighted in yellow.

Gene bank	Symbol	Full name gene	p-value – Fold-Change (RPM * 0 h vs. GC * 0 h)		p-value – Fold-Change (RPM * 24 h vs. GC * 24 h)		p-value – Fold-Change (RPM * 72 h vs. GC * 72 h)	
NM_009621	Adamts1	A disintegrin and metalloproteinase with thrombospondin motifs 1	0,2804	1,5	0,0044	3,3	0,1108	1,8
NM_175314	Adamts9	Protein Adamts9	0,7899	-1,0	0,0013	1,7	0,2290	1,2
NM_011923	Angptl2	Angiopoietin-related protein 2	0,8293	1,1	0,0043	2,6	0,0387	1,9
NM_207675	Cadm1	Cell adhesion molecule 1	0,9635	-1,0	0,0037	-1,7	0,0979	-1,3
NM_178793	Ccbe1	Collagen and calcium-binding EGF domain-containing protein 1	0,8049	-1,1	0,0007	-2,8	0,0490	-1,6
NM_001159557	Cd36	Platelet glycoprotein 4	0,9524	1,0	0,5281	-1,2	0,0001	-3,7
NM_009853	Cdh8	Cadherin 8	0,7330	-1,1	0,0014	4,1	0,0137	2,7
NM_007954	Ces1c	Carboxylesterase 1C	0,4869	-1,1	0,0022	2,0	0,1600	1,3
NM_007689	Chad	Chondroadherin	0,1788	1,2	0,0032	-1,5	0,9158	-1,0
NM_007727	Cntn1	Contactin-1	0,9266	-1,0	0,0010	-1,5	0,1765	-1,1
NM_009933	Col6a1	Collagen alpha-1(VI) chain	0,8026	1,0	0,5195	1,1	0,0004	1,9
NM_029636	Ctsq	Cathepsin Q	0,9393	1,0	0,2135	1,2	0,0025	1,6
NM_001081084	Cubn	Cubilin	0,8479	-1,0	0,9771	1,0	0,0002	2,1
NM_007862	Dlg1	Disks large homolog 1	0,8435	1,0	0,0040	1,5	0,0955	1,2
NM_153078	Ehbp1	EH domain-binding protein 1	0,7085	-1,0	0,0001	-1,5	0,0985	-1,1
NM_010143	Ephb3	Ephrin type-B receptor 3	0,6802	1,0	0,0010	1,6	0,0847	1,2
NR_028267	Fcho1	FCH domain only protein 1	0,7834	-1,0	0,0007	-1,6	0,6212	-1,1
NM_177756	Glt25d2	Procollagen galactosyltransferase 2	0,7221	1,1	0,0025	2,0	0,0389	1,5
NM_198610	Igsf21	Immunoglobulin superfamily member 21	0,9329	-1,0	0,0012	-1,6	0,3314	1,1
NM_010593	Jup	Junction plakoglobin	0,5569	-1,1	0,0014	-1,6	0,8978	-1,0
NM_008463	Klra5	Killer cell lectin-like receptor 5	0,0019	2,1	0,3241	-1,2	0,5497	1,1
NM_010733	Lrrn3	Leucine-rich repeat neuronal protein 3	0,5776	-1,1	0,0019	-1,4	0,0047	-1,3
NR_027323	Lrrtm4	Leucine-rich repeat transmembrane neuronal protein 4	0,4429	1,1	0,8825	1,0	0,0042	-1,6
NM_023061	Mcam	Cell surface glycoprotein MUC18	0,5460	-1,1	0,0050	1,5	0,0207	1,3
NM_008594	Mfge8	Lactadherin	0,8608	-1,0	0,1029	-1,2	0,0010	-1,6
NM_019671	Net1	Netrin-1	0,5269	1,1	0,0016	1,5	0,1892	1,2
NM_001081324	Neto2	Neuropilin and tolloid-like protein 2	0,6538	-1,0	0,0000	-1,5	0,0004	-1,4
NM_001142916	Plod2	Procollagen-lysine,2-oxoglutarate 5-dioxygenase 2	0,7182	1,1	0,0074	1,8	0,0032	1,9
NM_172874	Podn	Podocan	0,7148	1,1	0,9350	-1,0	0,0011	2,5
NM_027514	Pvr	Poliovirus receptor-related protein 2	0,6649	-1,1	0,0000	2,6	0,0016	1,9
NM_011351	Sema6c	Semaphorin-6C	0,5574	1,1	0,0000	-1,8	0,0147	-1,3
NM_021286	Sez6	Seizure protein 6	0,8941	1,0	0,0027	-1,5	0,0175	-1,3
NM_011518	Sykb	Tyrosine-protein kinase SYK	0,7436	-1,0	0,1055	1,2	0,0011	1,6
NM_001168541	Tsku	Tsukushin	0,2813	-1,1	0,0040	1,5	0,0125	1,4
NM_173007	Tspan12	Tetraspanin-12	0,2390	1,1	0,0021	1,4	0,0048	1,4

Table 11. Cell communication-involved genes in neuron cultures exposed to 1 h RPM and having recovered for 24 and 72 h in ground conditions. Fold change threshold was 2 and p-value 0.005. Genes statistically different compared to the controls are highlighted in yellow.

Gene bank	Symbol	Full name gene	p-value – Fold-Change (RPM * 0 h vs. GC * 0 h)		p-value – Fold-Change (RPM * 24 h vs. GC * 24 h)		p-value – Fold-Change (RPM * 72 h vs. GC * 72 h)	
NM_009621	Adamts1	A disintegrin and metalloproteinase with thrombospondin motifs 1	0,2804	1,5	0,0044	3,3	0,1108	1,8
NM_011923	Angptl2	Angiopoietin-related protein 2	0,8293	1,1	0,0043	2,6	0,0387	1,9
NM_178793	Ccbe1	Collagen and calcium-binding EGF domain-containing protein 1	0,8049	-1,1	0,0007	-2,8	0,0490	-1,6
NM_001159557	Cd36	Platelet glycoprotein 4	0,9524	1,0	0,5281	-1,2	0,0001	-3,7
NM_007389	Chrna1	Acetylcholine receptor subunit alpha	0,7906	1,1	0,5127	1,2	0,0031	2,9
NM_009946	Cplx2	Complexin-2	0,9734	-1,0	0,0016	-2,3	0,0243	-1,7
NM_001081084	Cubn	Cubilin	0,8479	-1,0	0,9771	1,0	0,0002	2,1
NM_177914	Dgkk	Protein Dgkk	0,8772	1,1	0,0090	3,5	0,0002	8,7
NM_001085390	Dusp5	Dual specificity protein phosphatase	0,1641	1,3	0,0105	1,8	0,0032	2,1
NM_021306	Ecel1	Endothelin-converting enzyme-like 1	0,8837	-1,0	0,0221	2,2	0,0006	4,0
NM_008655	Gadd45b	Growth arrest and DNA damage-inducible protein GADD45 beta	0,0031	4,1	0,0178	2,9	0,2113	1,7
NM_011817	Gadd45g	GADD45G	0,0170	2,5	0,0038	3,3	0,7104	1,1
NM_008082	Galr1	Galanin receptor type 1	0,6478	-1,2	0,0074	2,9	0,0001	6,1
NM_177350	Gldn	Gliomedin	0,4151	1,1	0,3385	1,1	0,0001	2,2
NM_001010941	Gpr12	G-protein coupled receptor 12	0,2479	-1,2	0,0032	-2,0	0,0137	-1,7
NM_010340	Gpr50	Melatonin-related receptor	0,9766	1,0	0,0021	5,0	0,0389	2,6
NM_022427	Gpr88	Probable G-protein coupled receptor 88	0,9006	1,0	0,0038	-2,6	0,0036	-2,6
NM_019518	Grasp	General receptor for phosphoinositides 1-associated scaffold protein	0,7535	1,1	0,0560	1,6	0,0035	2,3
NM_016719	Grb14	Growth factor receptor-bound protein 14	0,8973	-1,0	0,0003	-2,5	0,0117	-1,7
NM_133849	Hrh3	Histamine H3 receptor	0,4899	1,2	0,0009	-2,7	0,3472	-1,2
NM_008463	Klra5	Killer cell lectin-like receptor 5	0,0019	2,1	0,3241	-1,2	0,5497	1,1
NM_010850	Mycs	Protein S-Myc	0,7171	-1,1	0,0023	-2,1	0,2115	-1,3
NM_181072	Myo1e	Unconventional myosin-Ie	0,9270	1,0	0,0031	2,2	0,0788	1,5
NM_018766	Ntsr1	Neurotensin receptor type 1	0,8058	1,1	0,0014	-3,7	0,6434	-1,2
NM_172874	Plekhh3	Pleckstrin homology domain-containing family H member 3	0,7148	1,1	0,9350	-1,0	0,0011	2,5
NM_015817	Podn	Podocan	0,5089	1,2	0,0031	2,2	0,0014	2,4
NM_027514	Prl2b1	Prolactin-2B1	0,6649	-1,1	0,0000	2,6	0,0016	1,9
NM_022020	Rassf1	Ras association domain-containing protein 1	0,0004	-1,5	0,5669	-1,0	0,4831	1,1
NM_011267	Relt	Tumor necrosis factor receptor superfamily member 19L	0,9642	-1,0	0,0006	3,0	0,0267	1,8
NM_001004173	Sez6	Seizure protein 6	0,8627	1,0	0,4660	1,2	0,0016	2,9
NM_007706	Slc6a15	Sodium-dependent neutral amino acid transporter B(0)AT2	0,8799	-1,0	0,0009	-2,0	0,0759	-1,4
NM_146028	Sp100	Nuclear autoantigen Sp-100	0,8239	1,1	0,5297	1,2	0,0021	2,9
NM_011491	Stac2	SH3 and cysteine-rich domain-containing protein 2	0,7213	-1,1	0,0013	3,5	0,0576	1,9
NM_013722	Sv2c	Synaptic vesicle glycoprotein 2C	0,7218	1,1	0,0001	-2,5	0,7609	-1,0

Table 12. Transport-involved genes in neuron cultures exposed to 1 h RPM and having recovered for 24 and 72 h in ground conditions. Fold change threshold was 1.6 and p-value 0.005. Genes statistically different compared to the controls are highlighted in yellow.

Gene bank	Symbol	Full name gene	p-value – Fold-Change (RPM * 0 h vs. GC * 0 h)		p-value – Fold-Change (RPM * 24 h vs. GC * 24 h)		p-value – Fold-Change (RPM * 72 h vs. GC * 72 h)	
NM_019785	Actr10	Actin-related protein 10	0,9981	-1,0	0,0026	-1,4	0,3204	-1,1
NM_011923	Angptl2	Angiopoietin-related protein 2	0,8293	1,1	0,0043	2,6	0,0387	1,9
NM_138652	Atp12a	Potassium-transporting ATPase alpha chain 2	0,2763	-1,3	0,5868	-1,1	0,0049	-2,1
NM_178793	Ccbe1	Collagen and calcium-binding EGF domain-containing protein 1	0,8049	-1,1	0,0007	-2,8	0,0490	-1,6
NM_001159557	Cd36	Platelet glycoprotein 4	0,9524	1,0	0,5281	-1,2	0,0001	-3,7
NM_009853	Cd68	Macrosialin	0,7330	-1,1	0,0014	4,1	0,0137	2,7
NM_007389	Chrna1	Acetylcholine receptor subunit alpha	0,7906	1,1	0,5127	1,2	0,0031	2,9
NM_007390	Chrna7	Neuronal acetylcholine receptor subunit alpha-7	0,9243	-1,0	0,0010	1,7	0,7133	1,0
NM_009933	Col6a1	Collagen alpha-1(VI) chain	0,8026	1,0	0,5195	1,1	0,0004	1,9
NM_001081084	Cubn	Cubilin	0,8479	-1,0	0,9771	1,0	0,0002	2,1
NM_011180	Cyth1	Cytohesin-1	0,2321	-1,2	0,0014	-1,7	0,0150	-1,4
NM_001038619	Dnm3	Dynamin-3	0,8568	1,0	0,0011	-1,7	0,0750	-1,3
NM_133838	Ehd4	EH domain-containing protein 4	0,8295	-1,0	0,0079	1,6	0,0038	1,7
NM_010143	Ephb3	Ephrin type-B receptor 3	0,6802	1,0	0,0010	1,6	0,0847	1,2
NM_020488	Gabrq	Gamma-aminobutyric acid receptor subunit theta	0,5354	-1,1	0,5783	1,1	0,0013	1,8
NM_177350	Gldn	Gliomedin	0,4151	1,1	0,3385	1,1	0,0001	2,2
NM_001033354	Hba-x	Hemoglobin subunit zeta	0,9400	1,0	0,1373	1,1	0,0001	1,6
NM_134090	Kcnq4	Potassium voltage-gated channel subfamily KQT member 4	0,9738	1,0	0,0390	1,8	0,0012	2,8
NM_008594	Lmbr1	Limb region 1 protein	0,8608	-1,0	0,1029	-1,2	0,0010	-1,6
NM_181072	Mfge8	Lactadherin	0,9270	1,0	0,0031	2,2	0,0788	1,5
NM_008872	Pitpnm2	Membrane-associated phosphatidylinositol transfer protein 2	0,8311	1,0	0,0011	1,8	0,0048	1,6
NM_024413	Plat	Tissue-type plasminogen activator	0,1984	1,2	0,0005	1,7	0,0088	1,4
NM_024413	Plekhf1	Pleckstrin homology domain-containing family F member 1	0,1984	1,2	0,0005	1,7	0,0088	1,4
NM_146030	Plekhh3	Pleckstrin homology domain-containing family H member 3	0,9402	-1,0	0,0048	1,6	0,3998	-1,1
NM_022020	Rbp7	Retinoid-binding protein 7	0,0004	-1,5	0,5669	-1,0	0,4831	1,1
NM_023275	Rhoj	Rho-related GTP-binding protein RhoJ	0,1879	1,2	0,0028	1,5	0,0008	1,7
NM_145495	Rin1	Ras and Rab interactor 1	0,7551	1,1	0,0086	2,0	0,0047	2,1
NM_027530	Rufy3	Protein RUFY3	0,3765	-1,1	0,0009	-1,8	0,3576	-1,1
NM_178227	Scn3b	Sodium channel subunit beta-3	0,8010	1,0	0,0043	-1,8	0,4005	-1,2
NM_001171010	Slc14a1	Urea transporter 1	0,6414	1,1	0,2081	-1,2	0,0001	2,0
NM_009196	Slc16a1	Monocarboxylate transporter 1	0,6338	1,1	0,0001	2,5	0,0017	1,8
NM_011400	Slc2a1	Solute carrier family 2, facilitated glucose transporter member 1	0,6229	1,1	0,0000	3,3	0,0018	2,0
NM_001135151	Slc39a14	Zinc transporter ZIP14	0,5856	1,1	0,0015	1,6	0,2210	1,2
NM_175328	Slc6a15	Sodium-dependent neutral amino acid transporter B(0)AT2	0,8386	1,0	0,0029	-1,6	0,6477	-1,1
NM_021471	Slco1c1	Solute carrier organic anion transporter family member 1C1	0,8661	1,0	0,0046	1,7	0,0023	1,8
NM_029068	Snx16	Sorting nexin-16	0,7050	-1,0	0,0004	-1,6	0,0039	-1,4
NM_007706	Socs2	Suppressor of cytokine signaling 2	0,8799	-1,0	0,0009	-2,0	0,0759	-1,4
NM_011518	Sykb	Tyrosine-protein kinase SYK	0,7436	-1,0	0,1055	1,2	0,0011	1,6
NM_013722	Syn3	Synapsin-3	0,7218	1,1	0,0001	-2,5	0,7609	-1,0
NM_019636	Tbc1d1	TBC1 domain family member 1	0,5046	1,1	0,0000	1,7	0,0003	1,5
NM_001081499	Tbc1d8b	TBC1 domain family member 8B	0,6067	-1,1	0,0001	3,3	0,0007	2,5
NM_030731	Trim23	E3 ubiquitin-protein ligase TRIM23	0,7243	1,0	0,0019	-1,6	0,2628	-1,2
NM_017379	Tuba8	Tubulin alpha-8 chain	0,8468	-1,0	0,0017	2,2	0,0002	2,9

Table 13. Apoptosis-involved genes in neuron cultures exposed to 10 days RPM and having recovered for 24 and 72 h in ground conditions. Fold change threshold was 1.4 and p-value 0.005. Genes statistically different compared to the controls are highlighted in yellow.

Gene banck	Symbol	Full name gene	p-value – Fold-Change (RPM * 0 h vs. GC * 0 h)		p-value – Fold-Change (RPM * 24 h vs. GC * 24 h)		p-value – Fold-Change (RPM * 72 h vs. GC * 72 h)	
NM_153397	Adam32	Disintegrin and metalloproteinase domain-containing protein 32	0,0030	1,1	0,0023	1,5	0,5631	-1,1
BC024332	Fam195a	Protein FAM195A	0,0005	1,5	0,2106	1,1	0,0021	1,4
NM_019752	Htra2	Serine protease HTRA2, mitochondrial	0,2281	-1,2	0,1485	-1,2	0,0006	-1,7
NM_001162884	Igsf10	Immunoglobulin superfamily member 10	0,0635	-1,5	0,0129	-1,7	0,0017	-2,1
NM_001190911	Kirrel3	Kin of IRRE like 3 (Drosophila), isoform CRA_b	0,0396	1,0	0,0031	-1,9	0,4968	-1,1
NM_153099	Prss42	Serine protease 42	0,0022	-1,6	0,6579	-1,1	0,9380	-1,0
NM_001039146	Vmn1r90	Protein Vmn1r90	0,3516	-1,1	0,7508	-1,0	0,0003	-1,5

Table 14. Cell adhesion-involved genes in neuron cultures exposed to 10 days RPM and having recovered for 24 and 72 h in ground conditions. Fold change threshold was 1.4 and p-value 0.005. Genes statistically different compared to the controls are highlighted in yellow.

Gene bank	Symbol	Full name gene	p-value – Fold-Change (RPM * 0 h vs. GC * 0 h)		p-value – Fold-Change (RPM * 24 h vs. GC * 24 h)		p-value – Fold-Change (RPM * 72 h vs. GC * 72 h)	
NM_153397	Adam32	Disintegrin and metalloproteinase domain-containing protein 32	0,0030	1,1	0,0023	1,5	0,5631	-1,1
NM_010818	Cd200	CD200 antigen	0,0009	-1,3	0,0008	-1,6	0,0012	-1,5
NM_001162884	Igsf10	Immunoglobulin superfamily member 10	0,0635	-1,5	0,0129	-1,7	0,0017	-2,1
NM_001190911	Kirrel3	Kin of IRRE like 3 (Drosophila), isoform CRA_b	0,0396	1,0	0,0031	-1,9	0,4968	-1,1
NR_027323	Lrrtm4	Leucine-rich repeat transmembrane neuronal protein 4	0,0007	-1,3	0,0000	-2,4	0,1272	-1,2
NM_010769	Matn1	Cartilage matrix protein	0,0046	-1,4	0,8907	-1,0	0,2748	1,1
NM_011216	Ptpro	Receptor-type tyrosine-protein phosphatase O	0,0001	-1,4	0,0001	-2,1	0,0001	-1,9

Table 15. Cell communication-involved genes in neuron cultures exposed to 10 days RPM and having recovered for 24 and 72 h in ground conditions. Fold change threshold was 1.4 and p-value 0.005. Genes statistically different compared to the controls are highlighted in yellow.

Gene bank	Symbol	Full name gene	p-value – Fold-Change (RPM * 0 h vs. GC * 0 h)		p-value – Fold-Change (RPM * 24 h vs. GC * 24 h)		p-value – Fold-Change (RPM * 72 h vs. GC * 72 h)	
NM_153397	Adam32	Disintegrin and metalloproteinase domain-containing protein 32	0,0030	1,1	0,0023	1,5	0,5631	-1,1
NM_133926	Camk1	Calcium/calmodulin-dependent protein kinase type 1	0,0339	-1,4	0,0634	-1,3	0,0042	-1,6
NM_144817	Camk1g	Calcium/calmodulin-dependent protein kinase type 1G	0,0122	-1,2	0,0047	-1,8	0,0087	-1,7
NM_009914	Ccr3	Probable C-C chemokine receptor type 3	0,5731	1,1	0,8040	1,0	0,0003	1,6
NM_010818	Cd200	CD200 antigen	0,0009	-1,3	0,0008	-1,6	0,0012	-1,5
NM_194446	Cdk10	Cyclin-dependent kinase 10	0,1517	-1,2	0,1801	-1,2	0,0036	-1,5
NM_009142	Cx3cl1	Fractalkine	0,0074	-1,2	0,0027	-1,5	0,0152	-1,4
NM_007873	Doc2b	Double C2-like domain-containing protein beta	0,1800	-1,3	0,0209	-1,6	0,0004	-2,3
NM_007892	E2f5	Transcription factor E2F5	0,0319	1,2	0,9849	-1,0	0,0015	1,4
BC024332	Fam195a	Protein FAM195A	0,0005	1,5	0,2106	1,1	0,0021	1,4
NM_133248	Glmn	Glomulin	0,1995	-1,1	0,0256	-1,3	0,0040	-1,4
NM_013531	Gnb4	Guanine nucleotide-binding protein subunit beta-4	0,1973	-1,6	0,0383	-2,3	0,0029	-3,7
NM_145552	Gnl2	Nucleolar GTP-binding protein 2	0,0362	-1,3	0,4957	-1,1	0,0038	-1,6
NM_027543	Gpr173	Probable G-protein coupled receptor 173	0,3450	-1,1	0,2449	-1,2	0,0001	-2,1
NM_019752	Htra2	Serine protease HTRA2, mitochondrial	0,2281	-1,2	0,1485	-1,2	0,0006	-1,7
NM_026298	Ift172	Intraflagellar transport protein 172 homolog	0,0395	-1,3	0,0093	-1,3	0,0006	-1,6
NM_001162884	Igsf10	Immunoglobulin superfamily member 10	0,0635	-1,5	0,0129	-1,7	0,0017	-2,1
NM_031252	Il23a	Interleukin-23 subunit alpha	0,0127	1,2	0,0015	1,5	0,5486	-1,1
NM_001190911	Kirrel3	Kin of IRRE like 3 (Drosophila), isoform CRA_b	0,0396	1,0	0,0031	-1,9	0,4968	-1,1
NR_027323	Lrrtm4	Leucine-rich repeat transmembrane neuronal protein 4	0,0007	-1,3	0,0000	-2,4	0,1272	-1,2
NM_008552	Mas1	Proto-oncogene Mas	0,0490	1,0	0,0040	-1,8	0,4492	-1,1
NM_010769	Matn1	Cartilage matrix protein	0,0046	-1,4	0,8907	-1,0	0,2748	1,1
NM_177376	Myo3b	Myosin-IIIb	0,3786	-1,2	0,3863	-1,2	0,0035	-2,0
NM_008747	Ntsr2	Neurotensin receptor type 2	0,0094	2,4	0,4369	1,3	0,0001	4,7
NM_011057	Pdgfb	Platelet-derived growth factor subunit B	0,0179	1,0	0,0030	-1,6	0,0266	-1,4
NM_011216	Ptpro	Receptor-type tyrosine-protein phosphatase O	0,0001	-1,4	0,0001	-2,1	0,0001	-1,9
NM_080793	Setd7	Histone-lysine N-methyltransferase SETD7	0,0072	1,3	0,0231	1,2	0,0008	1,4
NM_017400	Sh3gl3	Endophilin-A3	0,0035	-2,1	0,4084	-1,2	0,1595	-1,4
XM_003086051	Syngap1	Ras GTPase-activating protein SynGAP	0,0144	-1,1	0,0011	-1,7	0,1718	-1,2
NM_018803	Syt10	Synaptotagmin-10	0,0970	-1,6	0,0104	-2,2	0,0035	-2,5
NM_009377	Th	Tyrosine 3-monooxygenase	0,0078	-1,3	0,0021	-2,4	0,0259	-1,8
NM_144549	Trib1	Tribbles homolog 1	0,0294	1,0	0,0047	-1,5	0,1149	-1,2
NM_009528	Wnt7b	Protein Wnt-7b	0,0039	1,5	0,4570	1,1	0,0843	1,2

Table 16. Transport-involved genes in neuron cultures exposed to 10 days RPM and having recovered for 24 and 72 h in ground conditions. Fold change threshold was 1.4 and p-value 0.005. Genes statistically different compared to the controls are highlighted in yellow.

Gene banck	Symbol	Full name gene	p-value – Fold-Change (RPM * 0 h vs. GC * 0 h)		p-value – Fold-Change (RPM * 24 h vs. GC * 24 h)		p-value – Fold-Change (RPM * 72 h vs. GC * 72 h)	
NM_175550	Ap4e1	AP-4 complex subunit epsilon-1	0,0082	-1,1	0,0003	1,5	0,9153	1,0
NM_007873	Doc2b	Double C2-like domain-containing protein beta	0,1800	-1,3	0,0209	-1,6	0,0004	-2,3
NM_145552	Gnl2	Nucleolar GTP-binding protein 2	0,0362	-1,3	0,4957	-1,1	0,0038	-1,6
NM_026298	Ift172	Intraflagellar transport protein 172 homolog	0,0395	-1,3	0,0093	-1,3	0,0006	-1,6
NM_001111028	Kctd9	BTB/POZ domain-containing protein KCTD9	0,0339	1,2	0,0028	1,6	0,8057	-1,0
NM_008445	Kif3c	Kinesin-like protein KIF3C	0,5058	-1,1	0,0181	-1,3	0,0033	-1,4
NM_177376	Myo3b	Myosin-IIIb	0,3786	-1,2	0,3863	-1,2	0,0035	-2,0
NM_023409	Npc2	Epididymal secretory protein E1	0,0144	1,3	0,0024	1,4	0,0001	1,6
NM_153099	Prss42	Serine protease 42	0,0022	-1,6	0,6579	-1,1	0,9380	-1,0
NM_011216	Ptpro	Receptor-type tyrosine-protein phosphatase O	0,0001	-1,4	0,0001	-2,1	0,0001	-1,9
NM_026991	Sat2	Sodium-coupled neutral amino acid transporter 2	0,0057	-1,2	0,0008	-1,5	0,0424	-1,3
NM_017400	Sh3gl3	Endophilin-A3	0,0035	-2,1	0,4084	-1,2	0,1595	-1,4
NM_001040459	Shroom4	Protein Shroom4	0,0168	-1,1	0,0023	-1,4	0,7043	-1,0
NM_172577	Slc25a21	Mitochondrial 2-oxodicarboxylate carrier	0,0036	1,5	0,6837	1,0	0,3052	1,1
NM_134420	Slc26a6	Protein Slc26a6	0,0044	1,5	0,2062	1,2	0,0050	1,4
NM_018803	Syt10	Synaptotagmin-10	0,0970	-1,6	0,0104	-2,2	0,0035	-2,5

Chapter VI | Combined exposure to simulated microgravity and acute or chronic radiation reduces neuronal network integrity.

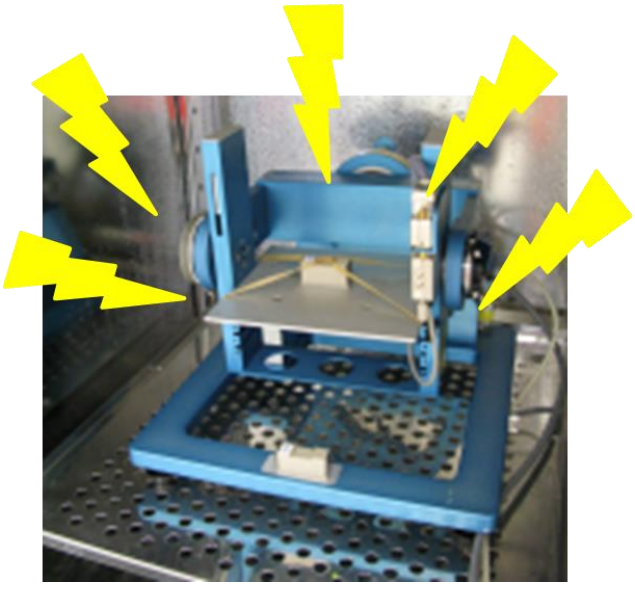

Modified from "**Pani G.**, Samari N., Quintens Q, de Saint-Georges L., Baatout S., van Oostveldt P., Benotmane. M.A. Combined exposure to simulated microgravity and acute or chronic radiation reduces neuronal network integrity." This manuscript is in final preparation to be submitted to PlosOne journal.

Combined exposure to simulated microgravity and acute or chronic radiation reduces neuronal network integrity.

Abstract

During orbital or interplanetary space flights, astronauts are exposed to cosmic radiations and microgravity. In order to estimate the potential health risks of astronauts during their permanence in space, the effects of these two conditions are usually investigated separately. This study aimed at assessing the effects of the combined conditions on neuronal plasticity. In particular, we investigated the effects of simulated microgravity during or after exposure to low dose ionizing radiations on the neuronal network density, cell morphology and cell viability in well-connected primary mouse cortical neuron cultures. To this end, we used the Random Positioning Machine (RPM) to simulate microgravity, X-rays for low and high acute dose radiation exposure and Californium-252 as a source for chronic low dose radiations.

High content image analysis of well-connected cortical neurons after exposure to acute or chronic radiation showed a delay in the outgrowth of neuronal extensions whereas simulated microgravity affected neurite area and length. Moreover, we showed that cell death was induced by high acute radiation dose, by low dose of chronic radiations as well as by microgravity. Nevertheless, when combining both simulated space conditions, we observed an enhanced effect on neuronal network density, neuron morphology and apoptosis.

In conclusion, our results provide evidence of enhanced effects of combined space conditions on the neuronal network integrity.

Keywords: Mature neuronal network; neuroplasticity; neuronal morphology; simulated microgravity; chronic irradiation; acute irradiation; simulated space conditions.

1. Introduction

Cosmic radiations and microgravity, combined with workload, confinement, hypoxia and psychological stress, are the main stressful components which affect astronauts during space flights. It is well known that microgravity induces physiological changes in human body such as bone loss [305], skeletal muscle atrophy [304], immune system impairment [216, 263], shifts of body fluids from the lower extremities to the upper body [306] and space motion sickness (SMS). Moreover, cognitive deficits, sensory-motor alterations, changes in sleep-wake regulation as well as vegetative disorders, which are SMS-related, may also occur during long-term spaceflights, affecting human behaviour and performance [307]. It has been reported that organisms exposed to low gravity undergo physiological, cellular as well as metabolic changes. In particular, reduced cellular motility, altered morphology, altered distribution in cytoskeletal proteins [59], reduced proliferation [35], delayed cell cycle [328] increased apoptosis [68, 308] are also known effects due to the exposure to modified gravitational fields. Cosmic radiations are an heterogeneous pool of ionizing radiations with a wide range of charges and energies produced mainly by galactic cosmic rays and solar particle events [78]. Approximately 91% of the particles composing cosmic radiations are protons, 8% α-particles and 1% are particles heavier than helium as high-Z and high-energy (HZE) particles [329]. Aboard the International Space Station (ISS), the average dose rate of cosmic radiation is around 0.0083 mSv/h or 0.2 mSv/day [77] but can increase during solar activities generating then a peak of higher dose rate for a short period. Furthermore, neutrons are one of the most produced secondary particles originating from the interaction of primary particles with the spacecraft skin [78, 86, 330]. It is known that chronic radiation exposure can lead to neuroregulatory disorders, moderate to marked leukopenia, thrombocytopenia and sometimes even severe anemia [200]. At the cellular level, radiations can cause increased oxidative stress [66, 331], DNA damage [332, 333], cell cycle

arrest [334], changes in cell motility, cytoskeleton distribution [102, 142-144], apoptosis and senescence [139, 140].

During embryonic development, neuron precursors are able to move from the ventricular zone to their final destination in the neocortex where they mature by extending neurites to establish synapses with target cells. Additionally, plasticity is the final phenomenon which occurs in the developing brain whereas neuroplasticity is an ability of the adult brain to remodel the network by contracting and re-extending neurites and to reorganize connections between neurons in response to environmental changes [154]. The neurite outgrowth motility involves several cytoskeletal proteins, in particular stable microtubules along the extensions, cortical actin and integrins at the periphery of the outgrowth cone.

Studies on real or simulated low gravity reported that cytoskeletal alterations observed during exposure may lead to reduced motility of adherent cells [38, 59]. Furthermore, gene expression analyses on the brain of mice exposed to the hindlimb-upload method to simulate low gravity showed a down regulation of Itga3. This gene codes for the alpha3 subunit of the transmembrane heterodimeric integrin complex which is important for adhesion, locomotion and organization of the sub-membrane actin cytoskeleton [197]. Recent *in vivo* experiments on mice exposed to the International Space Station (ISS) environment for 91 days reported a possible reduced expression of neuron growth factor (NGF) and brain derived neurotrophic factor (BDNF) in brain tissues as in cortex and hippocampus in wild-type animals exposed to spaceflight environment compared to the controls [199]. Furthermore, proteins involved in long-term potentiation or in neurotransmitter release were up-regulated in the whole brain of mice exposed to ISS environment [199]. Additionally, short-term exposure of well-connected neurons to simulated microgravity showed a reduction in neurite length and area and changes at the level of somas (Pani et al., unpublished results, chapter V). Investigations on neurons exposed to ionizing radiations have reported effects at the cellular and molecular levels. Indeed, analysis on spine numbers and synapsis clusters showed an alteration 14 days after high dose exposure

[335]. *In vitro* investigation on apoptosis induced by ionizing radiation exposure reported that low doses of X-rays (0.2 Gy) increase NMDA receptor-mediated cell death in maturing neurons [299]. *In vivo* studies on laboratory animals indicated that low doses of HZE particles such as Fe and Ar, are capable of producing morphological, neurochemical and behavioural alterations [203-206]. Investigations on dopaminergic functions in the CNS and correlated motor behaviour of rats also reported an alteration after exposure to 0.1 Gy of Fe particles [203]. Additionally, these data showed that rats exposed to Fe ions exhibited important alterations in neuronal signal transduction in the striatum and in motor neuron behaviour parameters [203]. Evident correlation was also reported between neurodegenerative diseases and heavy ion exposure in mouse model [336].

Three different theories have been proposed to describe 3 effects induced by radiation coupled with microgravity: additive [145], antithetical [337] and non-correlative effects. Only a few experiments have been performed combining both conditions, and in all of them samples were exposed to simulated microgravity after acute irradiation. One investigation reported a decreased apoptosis in foetal fibroblasts cultured for 24 h in the RPM after exposure to moderate (0.5 Gy) and high doses (1 Gy) of X-rays [337]. On the contrary, experiments on DNA repair efficiency and apoptosis in peripheral lymphocytes cultured in the Rotating Wall Vessel (RWV) after exposure to high doses of gamma irradiation showed an addictive effect with a delay in DNA repair kinetics and an increased apoptosis compared to cultures which had only been irradiated [145].

Concerning the *in vitro* neuronal network models, it has been reported that non-connected neurons and well-connected neurons differ in their action potential activities, spontaneous synaptic currents, number of synapses and neurite growth speed [175, 176]. It has also been described that synaptic protein distribution and associated vesicles are partially dependent on the acquisition of functional synapses [175]. Additionally, GABA or glycine neurotransmitters have

opposite activity in two developmental stages [177, 178] and neurons are less sensitive to external agents over maturation [179, 180].

Since no study had so far been performed exposing neuron cultures to both conditions, we investigated the effects of exposure of well-connected primary mouse neuron cultures to microgravity either after acute (X-rays) or during chronic (neutrons) irradiation. Within this study morphological parameters as well as death of neurons in neuronal network cultures were investigated in simulated space conditions.

2. Materials and methods

2.1. Primary cell cultures and mature neuronal network model

In this study, primary neuron cultures were initiated from the brain cortex of 17 day-old mouse fetuses. All animal experiments were carried out in strict accordance with the recommendations of the Guide for the Care and Use of Laboratory Animals of the National Institutes of Health. The protocol was approved by the Belgian Nuclear Research Centre (SCK•CEN, Mol, Belgium) and the Flemish Institute for Technological Research (VITO, Geel, Belgium) joint Ethical Committee on Laboratory Animal Experiments. Pregnant mice were sacrificed by cervical dislocation on day 17 after conception. Subsequently, brains from fetuses were dissected and cortices were extracted. Neuronal cells were isolated by trypsinization, mechanical dissociation of tissue and cell centrifugation after which they were seeded onto poly-D-lysine coated 4-well plates (Thermo Scientific, Aalst, Belgium) at a density of 50,000 cells per cm^2. Neurons were grown in MEM medium (Gibco, Gent, Belgium) supplemented with 10% fetal bovine serum (Gibco) and 0.1% penicillin-streptomycin (Gibco) and incubated for 1 h at 37 °C and 5% CO_2 to remove non-neuronal small cells and to allow cell adherence. Thereafter, the medium was exchanged with Neurobasal medium (Gibco) supplemented with 2% B27 supplement (Gibco), 20 mM HEPES (Gibco) and 0.2% penicillin-streptomycin (Gibco); this medium allowed for selective growth of neuronal cells. In order to obtain a dense neuronal network as *in vitro* model, neurons were cultured for 10 days at 37°C, 95% of humidity and 5% CO_2. After 5 days of culture, two thirds of medium were replaced by fresh medium every 2 days.

2.2. *In vitro* experimental layout

To study the morphological effects of simulated microgravity on dense neuronal networks, at day 9 of the neuron culture, all 4-well plates (27 for acute irradiation or 15 for chronic irradiation) were completely filled with complete neurobasal medium, sealed with a first layer of

sterile parafilm and, if required, bubbles were removed with a syringe. Then, a second layer of parafilm was applied. At day 10, three replicates for each condition were ready for mounting on a desktop RPM (Dutch Space) in the framework of simulated space condition experiments.

2.3. RPM exposure after acute X-irradiations

In the acute exposure experiments, 10 day old neuron cultures were first irradiated with X-rays after which they were exposed to simulated microgravity. Cell cultures were irradiated at room temperature with 250 kV-15 mA, 1 mm Cu-filtered X-rays (Pentak HF420 RX machine), delivered at 5 mSv/sec. The Farmer 2570-EMI dosemeter was under the control of the Intercomparison Committee for Dosimetry. Cells were either exposed to a low dose of 0.1 Sv or to a high dose of 1.0 Sv of X-rays; non-exposed cells underwent identical manipulations. Immediately after irradiation, half of the samples were mounted on the RPM for simulated microgravity and the other half was kept in ground conditions (GC) as controls, both at 37°C, 95% of humidity and 5% CO_2. After 30 min, 2 h or 24 h of exposure to simulated microgravity or ground conditions, one plate per condition was fixed with 4% paraformaldehyde for subsequent β-tubulin 3 (β-tub 3) or AnnexinV-PI and Hoechst stainings (Fig. 39 A).

2.4. RPM exposure during neutron irradiation

In the chronic exposure experiments, cell cultures were irradiated with neutrons during RPM treatment. We used Californium-252 as source of neutrons and 2% of primary and secondary γ-rays obtaining a final dose rate of 2 or 20 mSv/day to simulate space radiation [338]. At day 10 of culture, plates were divided into 3 replicates per experimental condition which included (1) control cultures, (2) cultures exposed for 5 days to simulated microgravity, (3) cultures exposed for 5 days to neutrons under ground conditions at a dose rate of 20 mSv/day, (4) cultures exposed for 5 days to neutrons under ground conditions at a dose rate of 2 mSv/day, and (5) cultures exposed for 5 days to neutrons at a dose rate of 2 mSv/day in the RPM (Fig. 39

B). After 5 days of treatment, all plates were fixed with 4% paraformaldehyde and stained with β-tubulin 3 or AnnexinV-PI and Hoechst.

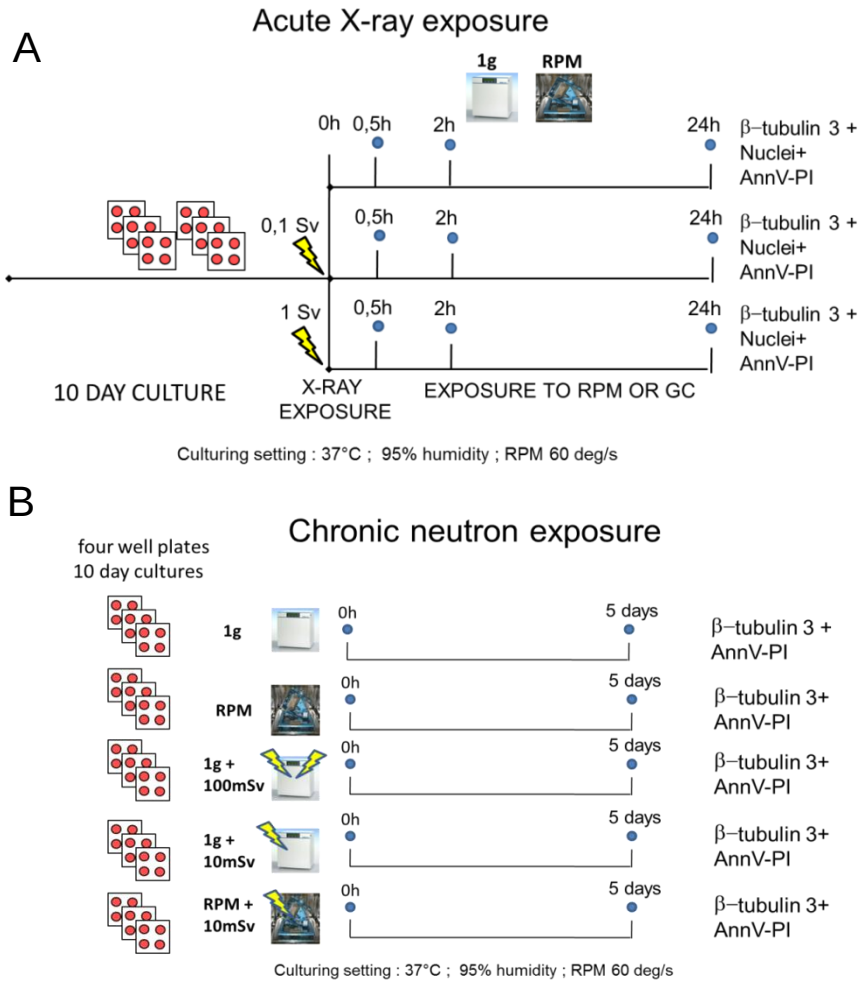

Figure 39: Experimental layouts of neuron cultures exposed to simulated space conditions.
A) Experimental layout of simulated low gravity coupled with X-ray exposure. Ten day neurons were exposed to ground conditions or RPM after low or high doses of X-irradiation. B) Experimental layout of simulated space condition exposure. Ten day neurons were exposed to neutron irradiation or concomitantly to RPM and neutrons for 5 days at a dose rate of 2 or 20 mSv/day.

2.5. Immunostaining of neuronal network

Neuronal networks were stained for the neuronal marker β-tubulin 3 using indirect immunofluorescence, whereas nuclei were revealed by direct fluorescence. After washing with phosphate buffered saline (PBS), cells were permeabilized with PBS containing 0.1% Triton X-100 (Sigma, Belgium) for 3 min and blocked for 30 min with PBS containing 3% BSA.

Fluorescent staining was performed by exposing the samples to mouse monoclonal anti-β-tubulin 3 (cat n° T5076-200UL, Sigma-Aldrich, Belgium), diluted 1:200 in PBS (Sigma, Belgium), at 4°C overnight. After washing in PBS, a second layer of fluorescein isothiocyanate (FITC)-conjugated anti-Mouse IgG (cat n° F2012, Sigma-Aldrich) antibody, diluted 1:200 in PBS, was applied for 90 min, at 37°C in the dark. Nuclei were then stained with Hoechst (1:400 in PBS, cat n° B2883, Sigma-Aldrich) for 10 min. Wells were then rinsed three times in PBS and twice in H_2O.

2.6. Image acquisition and neuronal network analysis.

Twenty-five mosaic regions of 2 by 2 images with five focus positions were acquired with a Nikon Eclipse Ti (automated inverted wide-field epifluorescence microscope) equipped with a 40x magnification (40x / 0.75) dry objective and a Nikon DS-Qi1Mc camera controlled by NIS-Elements software. Post-acquisition, images were compressed in a 2D in focus image by the Extended Depth of Focus (EDF) NIS-Elements module.

The neuronal network image processing analyses were performed using the MorphoNeuroNet, a home-made tool for ImageJ (Rasband, W.S., N.I.H, USA, http://rsb.info.nih.gov/ij/) (Pani et al., unpublished data, chapter IV). The high performance of this new tool comes from an appropriate soma segmentation originating from nuclei and from an elegant multi-tier segmentation after image enhancing and edge detection, segmenting even the thinner neurites. Thereafter, morphological analysis could be applied to determine total neuron area, total neurite area and length and soma counting. All the obtained data were referred to a single mosaic image to determine the neuronal network area, neurite network area and length per images that were afterwards normalized to single neuron, allowing to finally obtain an average of morphological values per single neuron.

Each experiment was performed in triplicates. Difference from controls was determined by paired *t*-test or two-way ANOVA (Graph Pad Software Inc., San Diego, USA) and a *p* value <0.05 was considered statistically significant.

2.7. Apoptosis

Apoptosis was estimated by Annexin V (Ann V)- propidium iodide (PI) assay on adherent neurons using the Ann V-FITC apoptosis detection kit II (cat n° BMS500FI/300CE, eBioscience, Belgium) with additional fluorescence staining of nuclei by Hoechst dye. Ann V-FITC was used to quantitatively estimate the percentage of dead cells in the neuron cultures. The AnnV-FITC$^-$/PI$^-$/Hoechst$^+$ (Ann V$^-$-PI$^-$) population was considered as normal healthy cells, while Ann V-FITC$^+$/PI$^-$/Hoechst$^+$ (Ann V$^+$-PI$^-$) and Ann V-FITC$^+$/PI$^+$/Hoechst$^+$ (AnnV$^+$-PI$^+$) cells were taken as an estimation of early apoptosis or late apoptosis/necrosis. Image processing analysis is described in chapter V (Fig. 31). Primary neuron cultures are not 100% pure cultures, since a small number of non-neuron cells (negative to β-tub 3) with small nuclei and condensed chromatin were observed after nuclei and neuron marker staining. This type of cells were positive to PI and negative to Ann V staining and were not taken into account in the viability estimation due to the high error in the evaluation of late apoptosis/necrosis staining that they can induce.

For statistical analysis, 25 images were acquired with a 20x objective and 500±150 cells per condition were taken into account. Ann V-PI negative cells as well as the specific Ann V and AnnV-PI positive cells were counted and the percentages of Ann V and AnnV-PI positive neurons and total cell numbers were then calculated. To estimate the relative level of Ann V and AnnV-PI positive neurons exposed to simulated low gravity, the percentage of positive neurons in cultures exposed to the RPM were divided by the percentages obtained in control cultures.

Furthermore, the same datasets of nucleus images were used for determining cell death. Fragmentation of nuclei into many small bodies with condensed chromatin is a characteristic of

apoptotic cells [67, 282, 283]; therefore, fragmented nuclei were counted and the respective percentage over the total number of nuclei was estimated. Nuclear fragmentation was defined by high fluorescence intensity (>20% of the nuclear pixels are saturated) and by the presence of two or more distinct nuclear lobes within a single nucleus. All three replicate conditions were compared using the paired *t*-test and a p-value <0.05 was considered significant.

3. **Results**

To evaluate the effects of simulated space conditions on well-connected mature neurons, 10 day cultures were exposed to simulated microgravity during chronic or after acute ionizing radiation. Immunostaining of β-tubulin 3 was used to investigate neurite network density and well-connected mature neuron morphology whereas AnnV- PI staining and nuclei fragmentation were assessed to determine the apoptotic cell rate. Additionally, neurite network area and length were monitored to observe the cumulative effects due to simulated space conditions and the induced apoptosis on the neuronal networks whereas the neuronal morphology was used to observe the effects on single neurons.

3.1. Simulated microgravity enhances the effects of acute radiation on well-connected neurons

Analysis of neurite network area and length in cultures exposed to 0.1 and 1 Sv of X-rays showed a dose-dependent reduction 24 h after irradiation. Furthermore, neuronal networks exposed for 2 hours to simulated microgravity after irradiation were shorter and less dense than the non-irradiated networks exposed to the RPM and the respective irradiated networks kept in ground conditions. This difference was higher in samples irradiated with high doses after 24 h of RPM exposure, suggesting an enhanced negative effect of combined conditions on total area and total length of the neurite network (Fig 40 A-B).

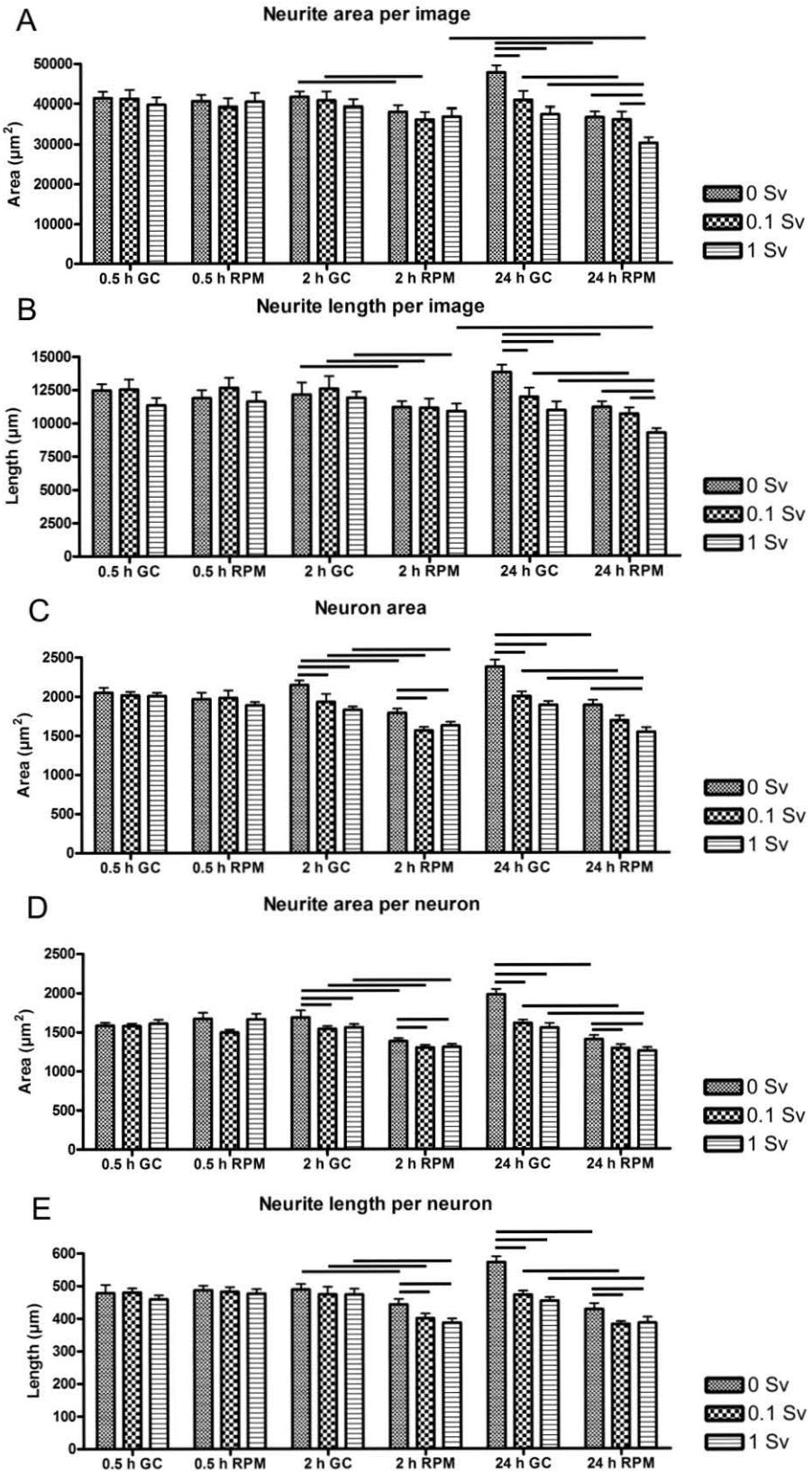

Figure 40: Effects of simulated microgravity after acute X-irradiation on well-connected mature neurons.
A) Average of neurite area per image. B) Average of neurite length per image. C) Average of neuron area (soma - neurites) per neuron. D) Average of neurite area per neuron. E) Average of neurite length per neuron. GC= Ground Conditions; RPM=Random Positioning Machine. Paired t-test was performed and $P<0.05$ were considered significant. Lines above the graphs represent significant difference between conditions or time points, error bars represent the SD.(page174)

Morphological analysis on 10 day cultures revealed that well-connected mature neurons exposed to low or high doses of X-rays decreased in size within the first 2 h after irradiation instead of growing like in the control conditions. Indeed, the areas of neurons and neurites were smaller than the non-irradiated neurons cultured in ground conditions after X-irradiation (Fig. 40 C-D). Additionally, neurite length was shorter than the controls only 24 h after exposure (Fig. 40 E). Concomitantly, an increase of neuron death was observed 24 h after X-ray exposure by quantification of fragmented nuclei with condensed chromatin (Fig. 41 A).

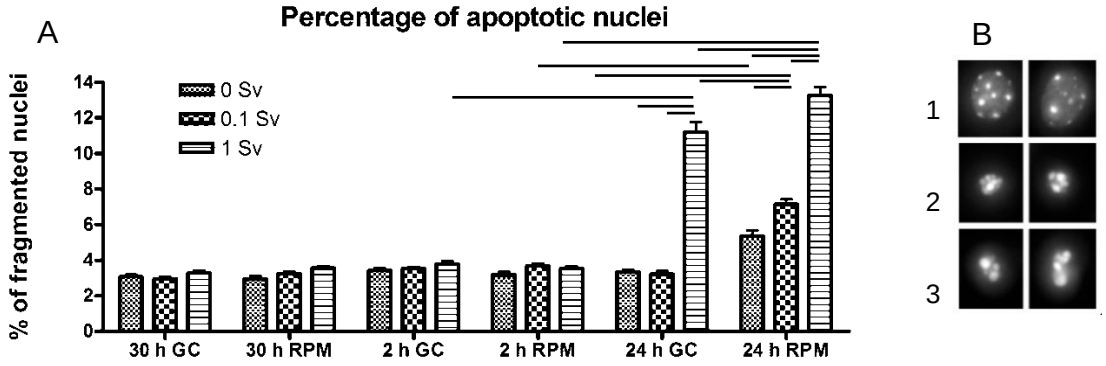

Figure 41: Fragmented nuclei due to radiation and/or simulated microgravity.
A) Percentage of fragmented nuclei with 2 or more distinct nuclear lobes within a single nucleus in neurons cultured in simulated microgravity after x-irradiation. Paired t-test was performed and P<0.05 were considered significant. GC= Ground Conditions; RPM=Random Positioning Machine. Lines above the graphs represent significant differences between conditions or time points, error bars represent the SD. B 1) Morphology of normal nuclei and (B 2-3) fragmentation of nucleus into many small bodies with condensed chromatin are characteristics of apoptotic nuclei.

As observed in a previous study (Pani et al., chapter V), simulated low gravity affected neuron morphology inducing a decrease of neuron area, as well as neurite length and area within the first hours (Fig 40 C-E). Well-connected mature neurons cultured in simulated low gravity for 2 hours after X-irradiation were smaller than the non-irradiated controls. Similar results were obtained with analysis on area and length of neurites. Interestingly, simulated microgravity enhanced the effects of both radiation doses within 2 h after irradiation; indeed, irradiated neurons cultured on the RPM had reduced neurite length compared to irradiated neurons cultured in ground conditions. Furthermore, a synergistic effect was also observed in cell death events 24 h after low doses of ionizing radiation exposure and enhanced after high doses (Fig 41 A).

3.2. Chronic irradiation and simulated low gravity affect neuron morphology

To better simulate conditions as they occur during space flights aboard the ISS, we exposed 10 day neuron cultures to simulated microgravity under continuous exposure to a source of Californium-252 emitting low doses of neutrons and γ-ray irradiation. We found that area and length of neurite networks decreased after exposure to low dose chronic radiations or RPM alone. Additionally, a synergistic effect was observed after exposure to combined conditions (Fig. 42 B,C). Furthermore, we observed that both neurite length and soma size were dose-dependently decreased with radiation alone. Also, simulated microgravity reduced the neurite length and soma size to the same level as was observed with the highest radiation dose (Fig. 42 D, E). On the contrary, neurons exposed to 2 mSv a day for 5 days (total dose 10 mSv) did not show any morphological differences compared to non-irradiated controls. Interestingly, the combination of simulated microgravity and chronic low dose rate neutron irradiation seemed to have an enhanced effect on neurite length and soma size reduction (Fig. 42 D-F). As previously observed, exposure of neuronal cultures to simulated microgravity, alone or in combination with ionizing radiation, increased the roundness of the somas. However, irradiation alone did not have any effect on the shape of the somas (Fig. 42 G, H).

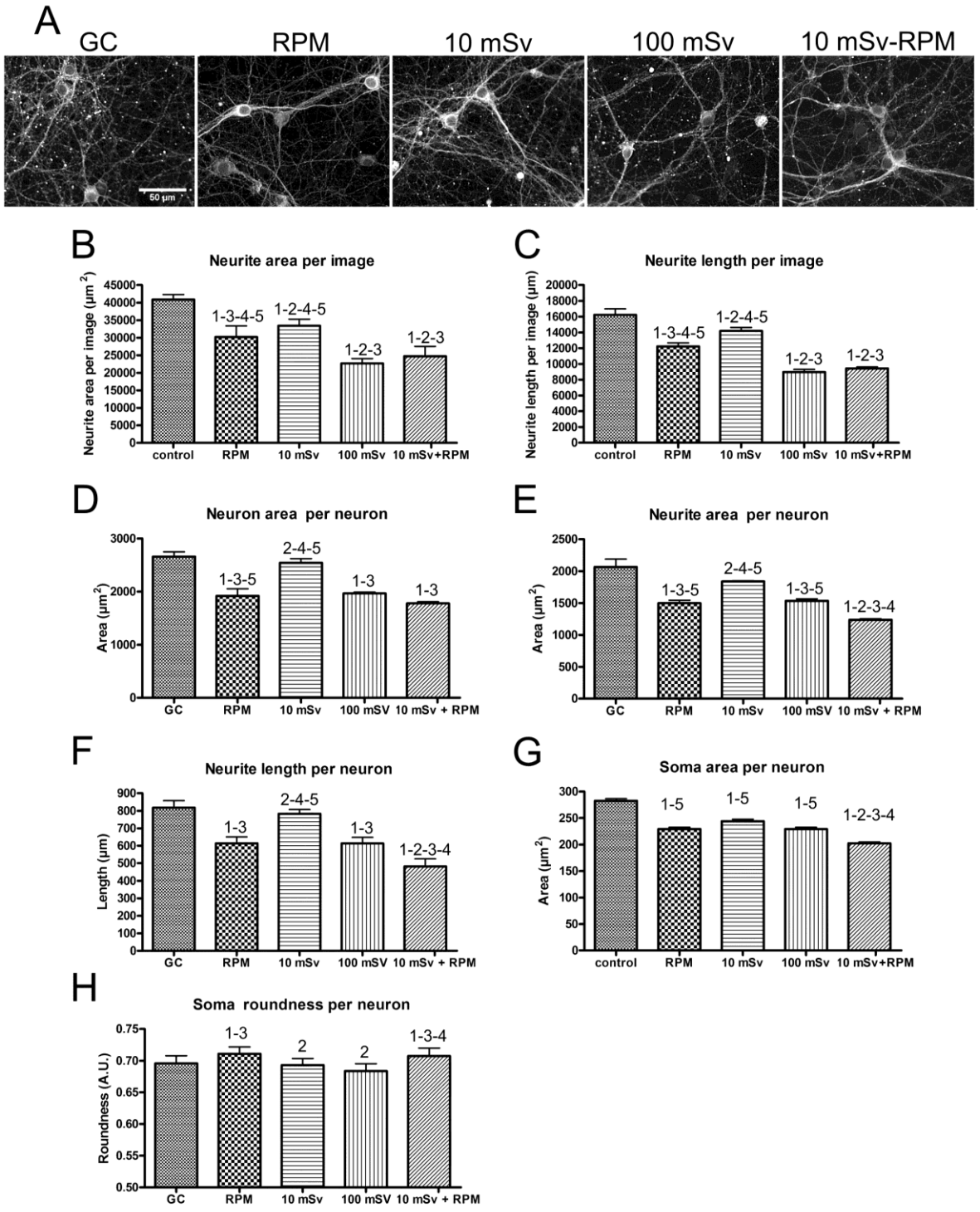

Figure 42: Effects of simulated space conditions on well-connected mature neurons after 5 days of exposure. A) Fluorescence images of neuronal cultures exposed to simulated space conditions. B) Average of neurite area per image. C) Average of neurite length per image. D) Average of neuron area (soma - neurites) per neuron. E) Average of neurite area per neuron. F) Average of neurite length per neuron. G) Average of soma areas. H) Soma shape expressed in average of roundness. GC = Ground Conditions; RPM = Random Positioning Machine; 10 mSv as a total dose in 5 days of exposure to neutron source with 2 mSv/day; 100 mSv as a total dose in 5 days of exposure with 20 mSv/day; 10 mSv + RPM is the combination of the two conditions. Paired t-test was performed and $P<0.05$ were considered significant. Statistical differences are indicated with 1 = X vs. GC; 2 = X vs. RPM; 3 X vs. 10 mSv; 4 = X vs. 100 mSv; 5 = X vs. 10 mSv + RPM. X means compared to any conditions.

Analysis of cell death using the AnnV-PI staining assay revealed that the number of total AnnV-PI positive neurons (total early + late apoptotic cells) was increased by 2-fold after 5 days of exposure to simulated microgravity alone (Fig. 43 A). A similar increase in total AnnV-PI positive neurons was observed in cultures exposed to chronic high dose rate neutron irradiation (20 mSv/day) or to the combination of chronic low dose rate irradiation (2 mSv/day) and simulated microgravity, whereas chronic low dose rate irradiation alone induced only a small, but significant increase in the number of total AnnV-PI positive neurons, indicating a dose-dependent effect (Fig. 43 A). Interestingly, as was observed on the morphological changes, the combined treatment of simulated microgravity and chronic irradiation had an enhanced effect on the number of AnnV-PI positive cells (late apoptotic/necrotic) (Fig. 43 A). This was in accordance with our analysis of fragmented nuclei showing a significant increase in the percentage of apoptotic nuclei with simulated microgravity and chronic low dose irradiation alone, an effect which was further increased when cells were exposed to the combined treatment (Fig. 43 B). Unlike the AnnV-PI staining, the analysis of apoptotic nuclei showed the strongest increase after treatment of neuronal cultures with chronic high dose irradiation (Fig. 43 B).

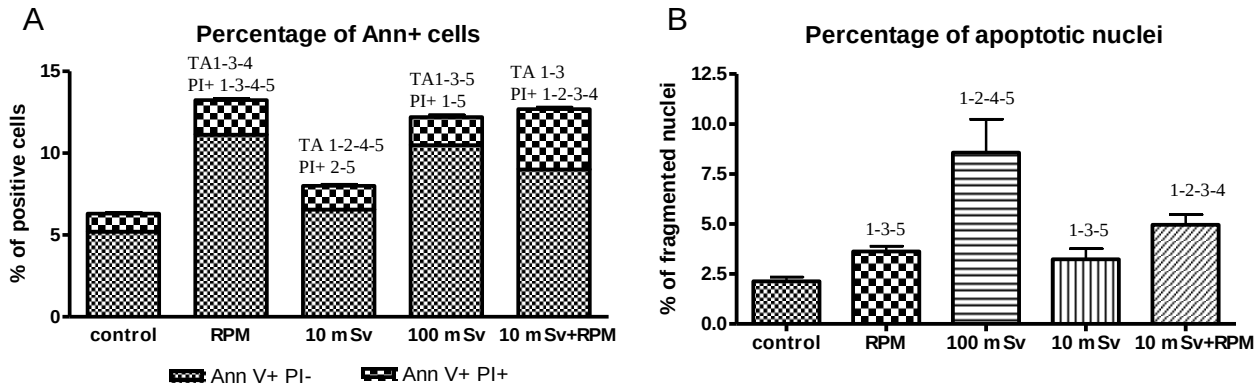

Figure 43: Altered viability induced by 5 days of exposure to simulated space condition exposure.
A) Percentage of Ann V^+-PI^- and Ann V^+-PI^+ cells in neuronal cultures. B) Percentage of fractionated nuclei with 2 or more distinct nuclear lobes within a single nucleus. GC= Ground Conditions; RPM=Random Positioning Machine; 10mSv as a total dose in 5 days of exposure to neutron source with 2 mSv/day; 100 mSv as a total dose in 5 days of exposure with 20 mSv/day; 10 mSv + RPM is the combination or the two conditions; TA= total Annexin V positive cells; PI+=Propidium iodide positive cells. Paired t-test was performed and $P<0.05$ were considered significant. Statistical differences are indicated with 1= X vs. GC; 2=X vs. RPM; 3=X vs. 10 mSv; 4 = X vs. 100 mSv; 5 = X vs. 10 mSv+ RPM. X means compared to any conditions.

4. Discussion

In this study, we evaluated the effects of simulated space conditions, exposure to acute or chronic ionizing radiation combined with simulated microgravity, on well-connected mature neuron cultures. In order to estimate the combined effect of both space conditions on well-connected mature neurons, neuronal network integrity was evaluated at different levels; neurite network density and cell morphology as well as cell death events in neurons cultured on the RPM after acute or during chronic ionizing radiation exposure.

Aboard the ISS, astronauts are exposed to around 0.2 mSv/day of an heterogeneous pool of radiations [77]. The impact of cosmic radiations with the spacecraft material produces secondary particles with lower energy and neutrons are one of the most produced particles [78, 86, 330]. In order to reproduce simulated space conditions aboard the ISS, Californium-252, a source of neutrons and γ-rays (2%), was used to obtain chronic low doses of ionizing radiation. Additionally, X-rays were used to generate acute low or high doses. We observed an altered neuronal network due to chronic low doses or acute doses of ionizing radiations which affected the neurite outgrowth cone motility and induced apoptosis. Furthermore, our data on acutely or chronically irradiated cultures showed dose dependent effects on neurite network density, neuron morphology and cell death events in well-connected primary mature neurons. These results are in agreement with studies on the effect of radiations on *in vitro* neuron and fibroblast cultures [299, 337] or in *in vivo* [339] investigations where ionizing radiation dose dependent effects were observed. Furthermore, low dose radiations with high or low dose rate affected neurite motility and soma size after exposure. Our data on the effects of radiations on cell motility activities are in agreement with several investigations on cancer radiation therapies which reported that ionizing radiation can affect cell adhesion to extracellular matrix and cell migration capability [141]. Furthermore, changes in the distribution as well expression of cytoskeletal proteins were observed in cells exposed to ionizing radiation [142-144]. Additionally, our data

showed that chronic low doses of ionizing radiation (2 mSv/day), equivalent to 10 time ISS dose, do not induce relevant effects on neurites in primary neuron cultures exposed for 5 days to ionizing radiation. Interestingly, the observed reduction of neurite network density after chronic irradiation might be mainly due to the increase of radiation-induced apoptosis instead of neurite morphological changes.

In our previous studies, we observed that well-connected mature neurons exposed for 10 days to simulated microgravity can adapt to the new gravity after initial morphological changes which were already observed within the first hour on RPM (chapter V). Within this study, we confirmed that the neurite network and neuron morphology changed within the first 24 hours of exposure to simulated microgravity. Furthermore, we observed that over 5 days of exposure to simulated microgravity, neuron adaptation to the new gravity condition has not yet occurred. These results are in line with other studies on cytoskeleton in microgravity indicating microfilament and microtubule changes due to the altered gravity [38, 51, 188] which might be linked to cell surface reduction [59]. The observed neuronal network and neuron morphology changes in well-connected mature neurons exposed to microgravity might also involve changes of NGF and BDNF which appeared reduced in cortex and hippocampus of wild type mice exposed to ISS environment for 91 days [199].

Space life investigators proposed three different theories on the effects of combined space conditions on cells or organisms: additive [145], antithetical [337] or non-correlative effects. In this study, we observed mainly an enhanced effect of low doses of ionizing radiation induced by simulated microgravity on neurite network density and length, areas of neurons, neurites and somas in well-connected neurons cultured on the RPM. Furthermore, we observed that the effects of the combined treatment with simulated space conditions on neurite motility and shape are bigger than the respective effects of single treatments, suggesting a synergistic effect of the combination of simulated microgravity with chronic ionizing radiation. It was also reported that radiation and microgravity can both induce apoptosis, whereas, the combination of the two

stressors on mitotic cells resulted in a decrease in radiation-induced apoptosis [146, 337] and cell cycle arrest in G2 phase [147, 337] upon low gravity exposure. Since post-mitotic neurons may enter in G1 phase, without going to the S phase, to repair the damaged DNA [340], they might not follow the response described for mitotic cells. Indeed, our results on cell death investigations showed a higher rate of apoptotic neurons after exposure to combined simulated space conditions than the rate observed after exposure to the two single conditions, RPM and ionizing radiation. The synergistic effects on the induction of apoptosis as observed in this study is in agreement with another investigation on the effect of the same simulated space conditions on the efficiency of DNA repair in post-mitotic neurons (Pani et al., chapter VII) or in peripheral blood lymphocytes (PBLs) exposed to simulated microgravity after γ-irradiation [149]. These results suggest that processes involved in neuronal network changes, observed in this study, and in non-well repaired DNA damage (Pani et al., chapter VII) in well-connected neurons cultured in simulated microgravity after or during exposure to radiations might contribute to induce apoptosis.

In conclusion, we showed that simulated low gravity affects the neuronal network integrity more than low dose radiation. Nevertheless, enhanced or synergetic effects were observed in well-connected mature neurons cultured in simulated low gravity after acute or during chronic ionizing radiations. Therefore, obtained results from our investigations on the effects of combined space conditions on neuronal network plasticity and neurite motility might help to better estimate the risks of astronauts during long-term space travel taking into account both conditions instead one per time.

Chapter VII | Simulated microgravity reduces the DNA repair efficiency in well-connected mature neurons after exposure to ionizing radiation.

Modified from "**Pani G.**, De Vos. W., Samari N., Quintens Q, de Saint-Georges L., Baatout S., van Oostveldt P., Benotmane. M.A. Simulated microgravity reduces the DNA repair efficiency in well-connected mature neurons after exposure to ionizing radiation. This article is in final preparation to be submitted to International Journal of Molecular Medicine.

Simulated microgravity reduces the DNA repair efficiency in well-connected mature neurons after exposure to ionizing radiation.

Abstract

Cosmic radiations and microgravity are the two main stressors to which crew members are exposed during space flights. The cellular response to ionizing radiation (IR) is highly dependent on environmental conditions (temperature, pH, vibration, etc.), implying a high interest for studying the correlated effect of co-exposures. This is important in the context of space research where numerous potential confounding factors can interfere, such as the reduced gravity. Indeed, various studies confer an important role for microgravity as a stress factor contributing in altering cell physiology and subcellular structure. This study aims at assessing the effect of simulated microgravity on the DNA repair efficiency in well-connected primary mature neurons after exposure to acute or chronic doses of IR. To this end, neuronal cell cultures were exposed to either X-rays (acute) or Californium-252 (chronic) radiation, whilst mounted onto a random positioning machine (RPM). High content analysis of γ-H2AX foci revealed an increased number of double stranded break foci in neurons cultured on RPM after acute or during chronic exposure to IR compared to ground controls (1g). Monitoring of the DNA repair efficiency over the time based on the kinetics of γ-H2AX foci reduction, acquired data showed a gravity and IR dose dependency. In addition, a higher rate of apoptosis was observed in cells under RPM six hours after exposure to IR. In conclusion, results suggest that simulated microgravity has a negative effect on IR-induced DNA repair and cell survival in neuronal cells.

Keywords: Mature neurons, microgravity, acute radiation, chronic radiation, low doses, high doses, γ-H2AX foci, DNA repair dynamics.

1. Introduction

One of the dominant risks in space missions, in particular during interplanetary travels, is the exposure of the crew members to cosmic radiations [341]. Cosmic radiations are an heterogeneous pool of ionizing radiations with a wide range of charges and energies which are produced mainly by galactic cosmic rays and solar particle events [78]. Approximately 91% of the particles composing cosmic radiations are protons, 8% α-particles and 1% are particles heavier than helium as high-Z and high-energy (HZE) particles [329]. The impact of primary particles with spacecraft materials generate secondary particles as knockout protons, neutrons and α-particles, as well as recoil heavy nuclei [78]. The major concern is that ionizing radiation induces DNA damage, which could damage tissues and increase cancer risk [342]. Upon infliction of DNA damage, the cell initiates a multifaceted response of gene induction and protein mobilization that leads to cell cycle arrest and DNA repair. Successful repair will allow the cell to resume its normal metabolism and continue with cell cycle progression. On the contrary, misrepair may induce genomic instability or mutations that can lead to tumorigenesis while irreparable damage may induce cell death [343]. Among all possible DNA lesions, the double strand break (DSB) is the most hazardous, being the most difficult to repair [332, 333]. One of the early steps following DSB formation is the rapid phosphorylation of the serine 136/139 residue of histone H2AX by members of the phosphatidylinositol-3-OH kinase (PI(3)K)-like family. Large stretches of phosphorylated H2AX surrounding the break region form ionizing radiation-induced foci (IRIF) or γ-H2AX foci that promote DNA repair by concentrating dedicated repair proteins. The number of γ-H2AX foci decreases with time after irradiation as DSBs are repaired [344].

When considering tissue damage that may arise from exposure to IR, the nervous system appears particularly vulnerable. Epidemiological data from Nagasaki and Hiroshima atomic bombings and from the Chernobyl accident reported effects on the brain due to exposure to

irradiations; therefore, it was suggested that neurodegenerative diseases may occur after ionising radiation exposure [345]. At the cellular level post-mitotic neurons were shown to activate the cell cycle to repair induced DNA damage [340, 346]. Furthermore, although DNA replication is lethal for post-mitotic neurons, they activate the G_0 to G_1 transition to repair induced DNA damage but do not enter S phase [340]. Since neurons are terminally differentiated cell types, they developed strategies to survive longer than other cells. Indeed, analysis on neocortex of 1, 7, 14 and 30 day-old mice X-irradiated with 8 Gy reported that IR-induced apoptosis of neurons decreases with ageing and therefore with the neuron maturation stage [347]. Furthermore, *in vitro* investigation on maturing neurons exposed to X-irradiation demonstrated an increase of DSBs and apoptosis 24 h after low and moderate dose exposures [299]. At the organismal level, *in vivo* experiments demonstrated memory impairment 30 days after irradiation in adult mice exposed to 1.5 Gy high-LET ^{56}Fe beams [207]. In the same experiments, an increase of cell death in Purkinje cells and an increase of DNA fragmentation in cerebellum tissue was reported in irradiated mice [207]. Studies on Alzheimer's disease in mice exposed to 100 cGy ^{56}Fe radiation showed an accumulation of Aβ plaques in hippocampus and cortex [336]. Furthermore, encephalic oxidative stress was observed in mice irradiated with heavy particles or X-rays [207-209].

During spaceflight, IR is not the only factor to take into account for estimating the risks. In fact, many factors may complicate the risk estimation and microgravity is one of the majors. Spaceflight studies and simulation experiments on Earth have shown that (simulated) microgravity affects cellular motility and cytoskeletal protein distribution [59], reduces cell proliferation and slows down cell cycle [35, 328], as well as increases apoptosis [68, 308] and oxidative stress [331] modulating activities of protein pathways. Recent *in vivo* experiments on mice exposed to International Space Station (ISS) environment for 91 days reported a reduced expression of neuron growth factor in brain tissues as in cortex and hippocampus in spaceflight wild-type animals compared to the controls [199]. Furthermore, proteins involved in long-term

potentiation or in neurotransmitter release were up-regulated in the whole brain of mice exposed to ISS environment [199] and biomarkers of oxidative stress in hypothalamus of mice were increased under simulated microgravity [348].

While several studies have been performed on the impact of IR on the central nervous system or neuron cultures, none of them included gravity as a possible influencing factor. With this study, we investigated the effects of combined conditions on *in vitro* mature and well-connected neurons with a particular emphasis on the DNA damage/repair dynamics in simulated microgravity after low or high exposure to acute X-irradiation or during exposure to low chronic neutron and γ-irradiation.

2. Materials and methods

2.1. Primary cell cultures and mature neuronal network model

In this study, primary neuron cultures were initiated from the brain cortex of 17 day-old mouse fetuses. All animal experiments were carried out in strict accordance with the recommendations of the Guide for the Care and Use of Laboratory Animals of the National Institutes of Health. The protocol was approved by the SCK•CEN (Belgian Nuclear Research Centre) and VITO (Flemish Institute for Technological Research, Geel, Belgium) joint Ethical Committee on the use of Laboratory Animal Experiments. Pregnant mice were sacrificed by cervical dislocation on day 17 after conception. Subsequently, brains from mouse fetuses were dissected and cortices were extracted. Neuronal cells were isolated by trypsinization, mechanical dissociation of tissue and cell centrifugation after which they were seeded onto poly-D-lysine coated 4-well plates (Thermo scientific, Erembodegem - Aalst, Belgium) at a density of 50,000 cells per cm^2. Neurons were grown in MEM medium (Gibco, Gent, Belgium) supplemented with 10% fetal bovine serum (Gibco) and (0.1%) penicillin-streptomycin (Gibco) and incubated for 1 h at 37 °C and 5% CO_2 to remove non-neuronal small cells and to allow cell adherence. Thereafter, the medium was exchanged with Neurobasal medium (Gibco) supplemented with 2% B27 supplement (Gibco), 20 mM HEPES (Gibco) and 0.2% penicillin-streptomycin (Gibco); this medium allowed selective growth of neuronal cells. In order to obtain a dense neuronal network as an *in vitro* model, neurons were cultured for 10 days at 37 °C, 95% of humidity and 5% CO_2. After 5 days of culture, two thirds of medium was replaced by fresh medium every 2 days.

2.2. *In vitro* experimental layout

To study the morphological effects of simulated microgravity on dense neuronal networks, at day 9 of neuron culture, three replicates were prepared for mounting on a desktop Random Positioning Machine (RPM, Dutch Space). To this end, 4-well plates were fully filled with

complete neurobasal medium, sealed with first layer of sterile parafilm and, if required, bubbles were removed with a syringe and a second layer of parafilm applied.

2.3. RPM exposure after acute X-irradiations

In the acute exposure experiments, 10 day-neuron cultures were first irradiated with X-rays after which they were exposed to simulated microgravity. To this end, X-irradiation was performed at room temperature with 250 kV-15 mA, 1 mm Cu-filtered X-ray machine (Pentak HF420), at the dose rate of 5 mGy/sec. The Farmer 2570-EMI dosemeter was under the control of the Intercomparison Committee for Dosimetry. Cells were either exposed to 0.1 Sv X-rays or exposed to 1 Sv X-ray; non-exposed cells underwent identical manipulations. Immediately after radiation, half of the samples were transferred on the RPM and the other half was kept in ground conditions (GC) as control, both at 37° C into the incubator. After 30 min, 2 h and 24 h of exposure to simulated microgravity or ground conditions, one plate per condition was fixed with 4% paraformaldehyde for subsequent γ-H2AX staining (Fig. 44).

2.4. RPM exposure during neutron irradiation

In the chronic exposure experiments, cell cultures were irradiated with neutrons during RPM treatment. At day 10 plates were divided in 3 groups. The first group was the control, the second group was exposed for 65 h to neutrons in ground conditions and the third group was exposed for 65 h concomitantly to neutrons and RPM. After 65 h of exposure to simulated space conditions (radiation or combined) or ground conditions all plates were fixed with 4% paraformaldehyde (Fig. 44) and stained with the DSB marker γ-H2AX. In our laboratories space radiations was simulated using Californium-252 as source of neutrons and 1% of secondary γ-rays obtaining a final dose rate of 20 mSv/day. To better simulate space conditions the RPM was coupled with chronic neutron irradiation.

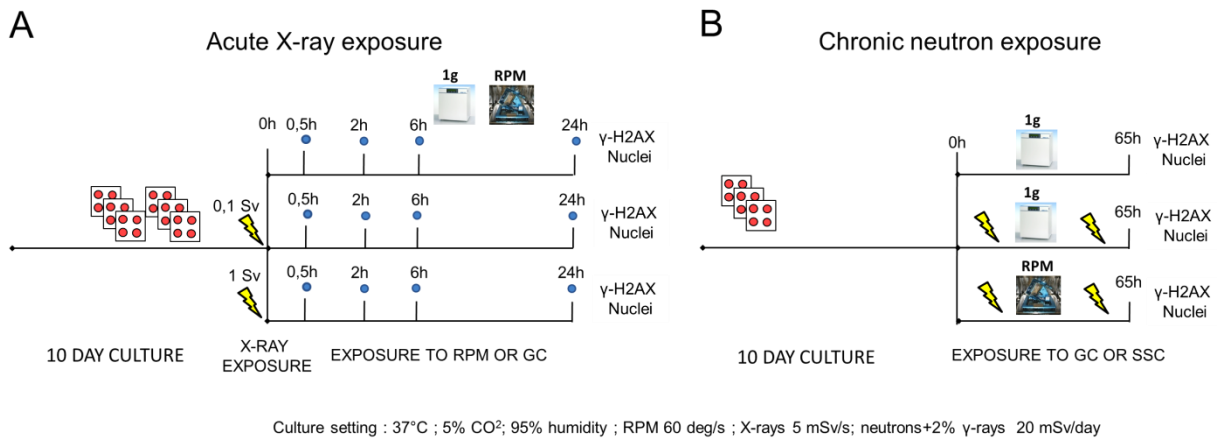

Figure 44: Experimental layouts of neuron cultures expose to simulated space conditions.
A) Acute exposure experiment; cell cultures were first irradiated with X-rays after which they were exposed to simulated microgravity. B) In the chronic exposure experiments, cell cultures were irradiated with neutrons during RPM treatment.

2.5. Immunofluorescence staining and automated γ-H2AX analysis.

DNA damage was visualized in fixed neurons by means of indirect immunofluorescent staining of the DSB marker γ-H2AX. Briefly, after fixation with 4% paraformaldehyde (PFA) for 15 min at 4°C, the bottom of the wells were carefully removed and the following immunostaining protocol was applied: cells were washed with phosphate buffered saline (PBS), permeabilized with PBS containing 0.25% Triton X-100 (Sigma-Aldrich, Bornem, Belgium) for 3 min and blocked for 30 min with 3% BSA. Next, samples were incubated with a primary mouse monoclonal antibody against the phosphorylated form of the histone H2AX (γ-H2AX) (Abcam, Cambridge, UK) diluted 1:300 in 3% BSA in PBS and incubated at 4 °C overnight. After washing three times in PBS, a secondary antibody FITC labeled anti-mouse (F2012, Sigma-Aldrich) diluted 1:300 in 3% BSA was applied for 60 min in the dark at 37 °C. Nuclei were counterstained with Hoechst (B2883, Sigma-Aldrich) 1:400 in PBS and incubated for 10 min. Wells were rinsed in PBS and finally in milliQ water; thereafter, they were mounted on large coverslips.

Images were acquired with an automated inverted wide field epifluorescence microscope (Nikon Eclipse Ti) equipped with a metal halide lamp, 40X Plan Fluor oil objective (NA 1.3) and Nikon DS-Qi1Mc camera (Nikon Instruments, Paris, France). Image pixel size was 0.16 µm. For high content analysis, a mosaic of 25 images was acquired at 13 Z-positions per sample. γ-H2AX foci were quantified using a dedicated macro-set written for open-source ImageJ, which allows fully automated measurement of nuclei and γ-H2AX spot parameters (size, shape, intensity, number…) [117]. Estimation of number of positive cells to γ-H2AX is important to determine the level of damage in the whole culture, therefore, neuron nuclei were considered positive when cells had at least 3 foci per nucleus due to the presence of DSBs in non-irradiated samples.

The same dataset of nucleus images was used for determining cell death. Fragmentation of nucleus into many small bodies with chromatin condensation is a characteristic of apoptotic cells [67, 282, 283]; therefore, fragmented nuclei were counted and their respective percentages on the total nuclei was estimated. Nuclear fragmentation was defined by high fluorescence intensity (>20% of the nuclear pixels are saturated) and by the presence of two or more distinct nuclear lobes within a single nucleus.

Each experiment was performed in triplicates and 150±50 cells per condition were taken into account. A significant difference from the controls was determined by paired t-test or one-way ANOVA (Graph Pad Software Inc., San Diego, USA) and a *p*-value <0.05 was considered significant. In non-linear correlation analysis for reduction of DSBs per nucleus and percentage of γ-H2AX positive neurons, the equation “one phase exponential decay” “Y=Span*exp(-K*X)+ Plateau” suggested by Graph Pad was used for the best fit of the curves.

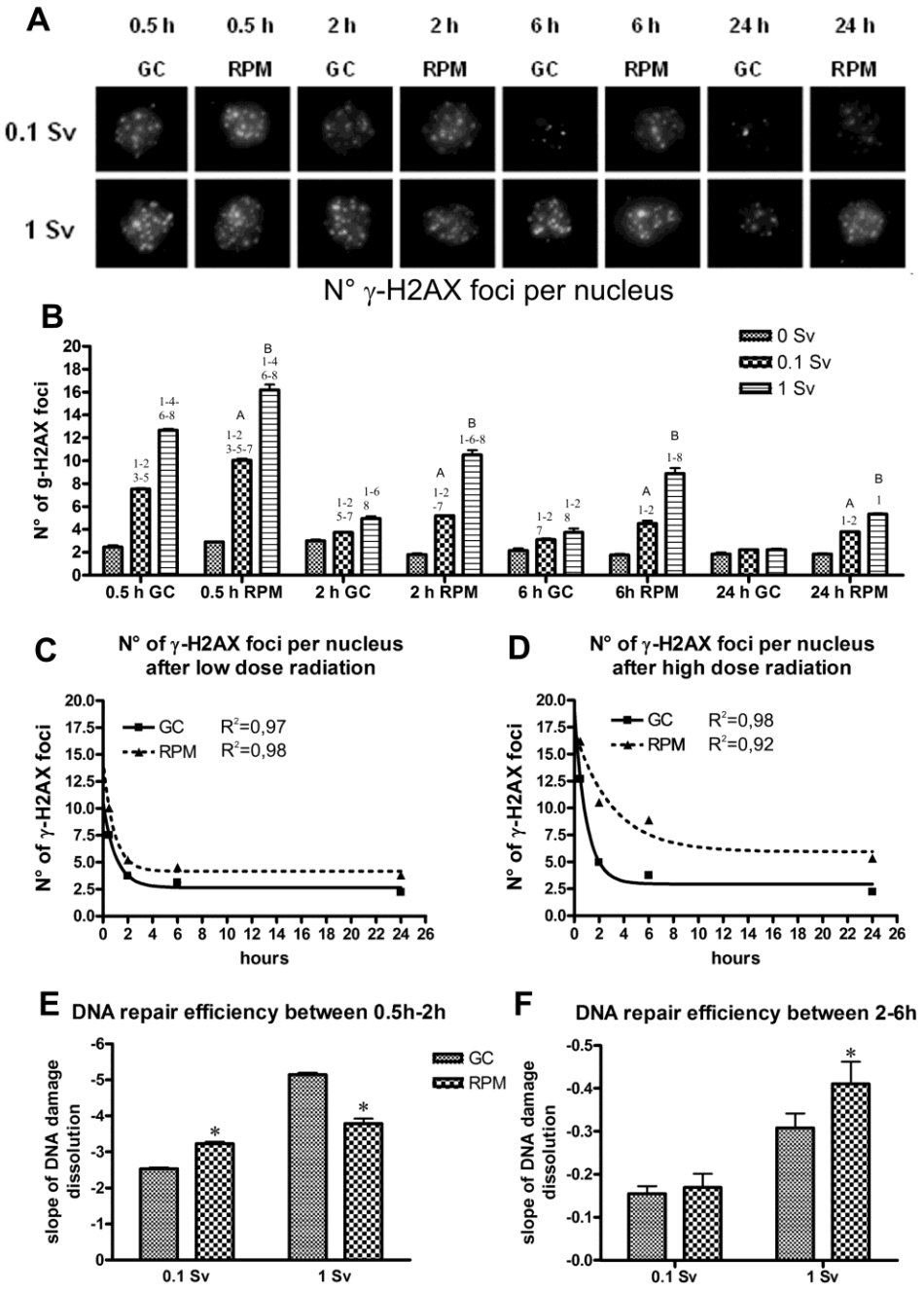

Figure 45: DNA damage/repair dynamics after low and high acute doses of X-rays.
A) Immunofluorescence of γ-H2AX foci in neurons cultured for 0.5, 2, 6, 24 h in both gravity conditions after low or high dose x-ray exposure. B) Number of γ-H2AX foci in neurons cultured in ground conditions (GC) or on the Random Positioning Machine (RPM) after low or high dose radiation exposure. Paired t-test was performed and P<0.05 were considered significant; numbers indicate difference between time points with equal gravity condition (GC or RPM): 1 - irradiated vs. respective control; 2 – 0.1 Sv vs. 1 Sv; 3 – X vs. 0.1 Sv 2 h; 4 – X vs. 1 Sv 2h; 5 – X vs. 0.1 Sv 6h; 6 – X vs. Sv 6h; 7 – X vs. 0.1 Sv 24h; 8 – X vs. 1 Sv 24h; letters indicate differences between gravity condition irradiated with equal dose and time points: A – 0.1 Sv RPM vs. 0.1 Sv GC; B – 1 Sv RPM vs. 1 Sv GC. C-D) DNA repair dynamics in both gravity conditions after low or high dose exposure. E) Linear regression analysis between 0.5 and 2 hours in neuron cultured in both gravity conditions after low (slope 0.1 Sv-GC=-2.53 ± 0.067; slope 0.1 Sv-RPM=-3.22 ± 0.10 P<0.001) and high dose radiation exposures (slope 1 Sv-GC=-5.140 ± 0.09092; slope 1 Sv-RPM=-3.781 ± 0.2368; P<0.001). G) Linear regression analysis between 2 and 6 hours in neurons cultured in both gravity conditions after low (slope 0.1 Sv-GC=-0.15 ± 0.03; slope 0.1 Sv-RPM=-0.17 ± 0.06) and high dose radiation exposures (slope 1 Sv-GC=-0.3079 ± 0.05799; slope 0.1 Sv-RPM=-0.4101 ± 0.08975; P<0.001). Error bars represent SD.

3. **Results**

3.1. DNA damage/repair kinetics in simulated microgravity after acute radiation

The DNA damage/repair dynamics in well-connected mature neurons were monitored in control and simulated microgravity conditions by immunofluorescence staining of γ-H2AX foci after low and high doses of X-irradiation. Automated analysis of foci in mature neurons cultured in both ground and simulated microgravity conditions for 30 minutes after irradiation confirmed dose-dependent increase of DSBs (Fig. 45 B). Indeed, a statistically significant increase of foci number was observed between 0.1 and 1 Sv irradiated cells and respectively in both compared to non-irradiated controls (Fig. 45 B). Interestingly, neurons cultured for 30 minutes on the RPM after irradiation showed an increased average of γ-H2AX foci per nucleus compared to the irradiated samples cultured in ground conditions. Indeed, the mean number of foci per nucleus went from 7.5 (GC) to 10 (RPM) after exposure to 0.1 Sv and from 12.6 (GC) to 16.2 (RPM) after 1 Sv. A statistically significant (P-value <0.05) decrease of foci number was observed at 2 h after irradiation with respect to the 30 min time point, suggesting initial repair of DSBs. Twenty-four hours after exposure to both X-ray doses, no significant difference was observed from the control conditions, suggesting complete repair (Fig. 45 B). While neurons exposed for 24 h to the RPM after irradiation exhibited an incomplete recovery compared to both controls, ground conditions and RPM (Fig 45 B). Notably, there were no statistical differences between non-irradiated neurons cultured in ground conditions or simulated microgravity (Fig 45 B). Analysis on DNA repair efficiency showed not only a dose and time-dependent kinetics (Fig 45 C-D) but also a clear involvement of the gravity component in the repair kinetics. Within the first 2 hours the DNA repair kinetics in microgravity after high dose exposure was slower than the controls; on the contrary, it was slightly faster after low dose irradiation (Fig 45 E). In the following 4 hours, DNA repair efficiency in simulated microgravity was faster than in control conditions

after high dose exposure, while low dose irradiated culture did not show any difference (Fig 45 F). Furthermore, comparing the percentage of γ-H2AX positive neurons exposed to low or high doses, the mean value after irradiation was significantly higher in simulated microgravity than in ground conditions throughout the whole experiments ($P<0.05$). Non-linear correlation analysis showed that there were similar dissolution kinetics in both control and simulated microgravity conditions after low dose exposure (Fig 46 A), whereas the decrease of γ-H2AX positive neurons cultured in simulated microgravity cells after high dose exposure was significantly slower than the respective controls (Fig 46 B).

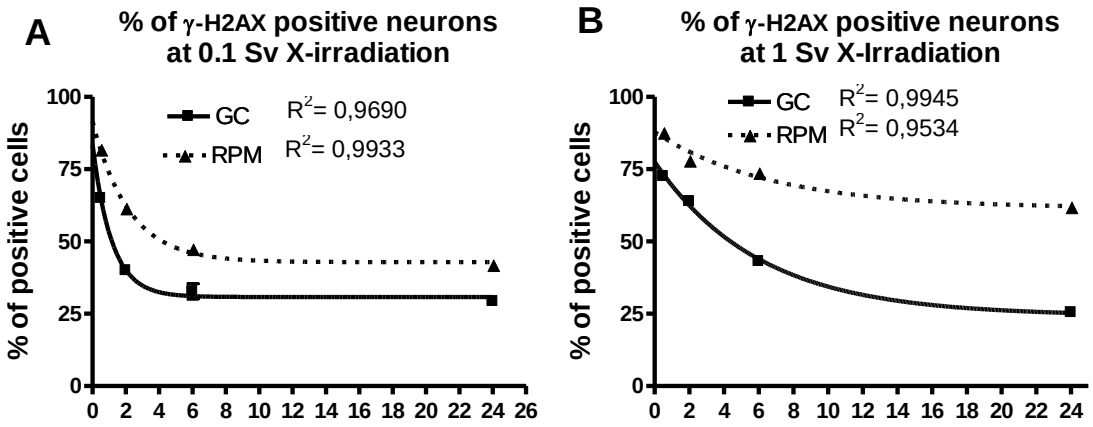

Figure 46: Non-linear correlation analysis of the percentage of γ-H2AX positive neurons cultured in both gravity conditions after low and high doses.
*Equation: one phase exponential decay "Y=Span*exp(-K*X)+ Plateau". Bars represent SD.*

We then estimated the apoptotic fractions (Fig. 47) by determining the percentage of cells with highly condensed chromatin in fractionated nuclei [283]. No difference in apoptotic nuclei was observed between control conditions and simulated microgravity (3±0.5) at 30 minutes and 2 hours. On the contrary, statistical increase was observed in 6 and 24 h RPM exposed cultures. At six and twenty-four hours after X-ray exposure in ground control conditions (6-24 h GC), the fraction of apoptotic cells in high dose irradiated neurons was higher than in the non-irradiated cells. The percentage of apoptotic cells in cultures exposed to RPM after irradiation with the high X-ray dose (1 Sv-6/24 h RPM) was higher than the respective controls (0 Sv-6/24 h RPM) and the low dose irradiated (0.1 Sv-6/24 h RPM) samples at 6 and 24 h after irradiation. The

percentage of fractionated nuclei in cultures exposed to RPM after high dose exposure was also higher than the earlier time point exposed to RPM (1 Sv-6 h RPM) and the ground control high dose irradiated (1 Sv-24 h GC) cultures. Furthermore, neuron cultures exposed to low radiation followed by simulated microgravity showed an increase when compared to the respective irradiated cells in ground conditions (0.1 Sv RPM vs. 0.1 Sv GC). Additionally, statistical increase was observed between neurons cultured for 24 h on RPM after low dose X-irradiation and the respective controls (0 Sv-24 h RPM) as well as the previous time point (0.1 Sv-6 h RPM) (Fig 47).

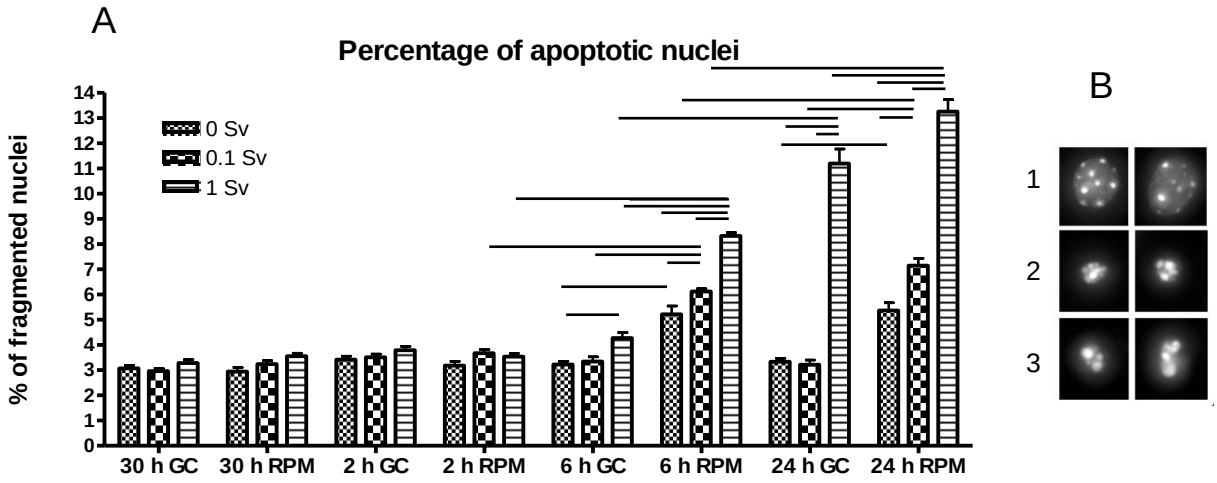

Figure 47: Altered nuclei due to radiation and/or simulated microgravity.
Paired t-test was performed and differences with a P-value < 0.05 were considered significant and showed as lines between different samples. Data ±SD are showed in the graph B) Representative images of nuclear morphology of normal (1) and apoptotic (2-3) nuclei. Apoptotic nuclei can be further categorized by the absence (2) or presence (3,4) of fragmentation. Bars represent SD.

3.2. DNA damage increases in simulated microgravity during chronic irradiation.

Neuron cultures were also exposed to chronic low doses using a natural source of neutrons and γ-rays (1%) while cultured in simulated microgravity (RPM) as a simulation for space conditions. Exposure to chronic radiations (total dose of 55 mSv during 65 h) in ground conditions caused 2-fold more DNA double-strand breaks and the fraction of DSB marker positive neurons exposed to neutrons in ground conditions was 2.5-fold more than the controls (Fig 48 A, B). Furthermore, the mean number of γ-H2AX foci in neurons exposed to simulated

space conditions was statistically higher than in control conditions as well as in the samples exposed only to radiation (Fig 48 A). The fraction of positive cells in cultures exposed to simulated space conditions was 4.1-fold more than the controls and 1.7 fold more than the neurons exposed only to radiation (Fig 48 B). The percentage of fractionated nuclei with highly condensed chromatin was 2.4 times than in the controls in cultures exposed to neutrons in ground conditions and 4.3 times more in cultures exposed to simulated space conditions (neutron IR and RPM) (Fig 48 C).

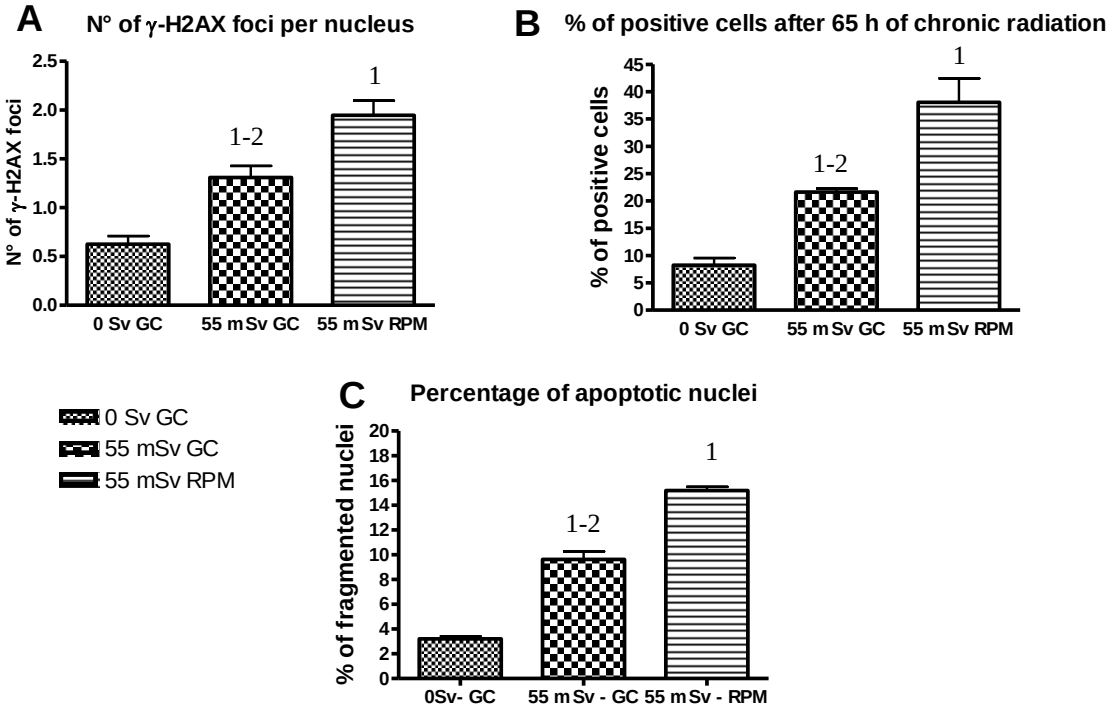

Figure 48: Effects of 65 h of simulated space conditions on DNA repair dynamics in well-connected neurons. A) average of γ-H2AX foci per nucleus. B) percentage of γ-H2AX positive cells. C) percentage of altered nuclei. Paired t-test was performed and P<0.05 were considered significant. 1 - irradiated vs. respective controls; 2 – 0.1 Sv vs. 1 Sv. Bars represent SD.

4. Discussion

In this study, we tried to illustrate the synergistic effects of the two main stressors present in space conditions on established neuronal networks. Namely, cosmic radiations are made of a heterogeneous pool of ionizing radiations and microgravity is a continuous state of free fall condition during orbital space flight. It is now widely established that ionizing radiation induces DNA damage, including DSBs [349]. Generally, cells respond to the DNA damage by activating cell cycle checkpoints and DNA repair machinery. Whereas the ideal outcome is full repair, in some severe cases, irreparable DNA damage induces apoptosis, or incorrect repair causes genome instability [350]. Our previous investigation on maturing neurons exposed to low and moderate X-ray doses showed a dose-dependent DSB and dose-dependent cell death [299].

In this study we investigated the DNA repair efficiency in simulated microgravity after high or low acute dose or during chronic low dose exposure to ionizing radiations. In our experiments well-connected mature neurons showed an increased average of γ-H2AX foci per nucleus 30 minutes after low and high dose X-ray exposure. In both cases, DSBs were repaired after 24 h when cultured in ground conditions. Moreover, chronic exposure to low dose radiation caused a production of DSBs, generating 3 times more foci than the controls within 65 hours.

Additionally, we investigated DNA repair efficiency in simulated microgravity which exhibited a slower kinetic in the first 2 hours after acute high doses. This is in accordance with investigations reported on human PBL showing a slower DNA repair efficiency in simulated microgravity after high dose γ-irradiation (5 Gy) [145]. Within the four following hours, the repair efficiency in post-mitotic neurons became then faster. On the contrary, neurons cultured on the RPM after low dose exposure were faster repairing the DNA damage within the first 2 h followed by typical repair efficiency. The minimal DNA damage required to activate the DNA repair [351] might explain the higher efficiency in simulated microgravity after acute low doses in neuronal cells observed in our study. Since neurons activate the phase G_1 of cell cycle to

repair DSBs [340] and cell cycle in cycling cells is delayed by microgravity [35, 352], it might explain the higher level of IR-induced DNA damage observed in the first 30 minutes of simulated microgravity due to hypothesized delay in re-entering into the cell cycle. Additionally, the initial higher level of radiation-induced γ-H2AX foci observed in neurons exposed to the RPM persists over the whole experiments showing a non-restored genome 24 h after X-irradiation. The fraction of γ-H2AX positive cells in RPM compared to the ground control showed a proportional decrease in low dose irradiated neurons over the time, while in cells exposed to high acute doses the decrease is slower in simulated microgravity than in ground conditions resulting in two times less repaired DNA in RPM conditions than control conditions. Additionally, the increase of apoptotic nuclei in neurons cultured in simulated low gravity after acute irradiation suggests a synergistic effect on this process.

In order to evaluate astronaut risk during space travels, where chronic doses of ionizing radiation with high energy (0.2 mSv/day) are received [77], we exposed 10 day well-connected mature neuron cultures to 20 mSv/day of neutrons and γ-rays coupled to the RPM for 65 h to simulated space conditions. Again, a higher level of DNA damage and cell death was observed in RPM cultured cells versus the ground controls suggesting a synergistic effect due to the coupling of both space conditions.

In conclusion, we have shown that simulated microgravity acts synergistically with IR in neuronal cell cultures. The decreased DNA repair efficiency in microgravity may induce genomic instability in neurons. Therefore, caution is warranted when interpreting ground-based studies for estimating risks during space travel. Furthermore, our results might contribute to increase the knowledge and help in evaluating, during or after space missions, the risk of astronauts [84, 202, 336, 353] who are exposed for long periods to low dose cosmic radiations and microgravity. Both space conditions could induce genomic instability and neurodegeneration in the CNS that could lead to neurological disorders and thereafter cancer and neurodegenerative diseases.

Chapter VIII | General discussion.

General discussion

Thousand years of evolution allowed mankind to adapt to non-extreme Earth environment characterized by an atmosphere with oxygen, mean temperatures above 0° C, the presence of a gravitational field and very low levels of radiations. Nowadays, mankind has reached a high level of technological development which allowed to build spacecrafts and space stations for more than half of century. Since the beginning of space missions, several studies in physics allowed to define space environment which is characterised by an absence of oxygen, extremely low temperatures, reduced gravity and higher levels of natural radiations than on Earth. Therefore, researchers developed a wide variety of technological countermeasures for traveling in space; nevertheless, mankind is not yet ready to undertake long permanent stays in space due to the high level of astronaut health risk since the appropriate shielding and gravitational field generators are still under development. Indeed, several medical and biological studies have determined changes induced by the space environment inside the body, within the organs as well as at the cellular and molecular levels.

Microgravity and cosmic radiations are two main stress factors to which astronauts are exposed during spaceflights. Wide varieties of medical and biological investigations performed directly in space or on ground-based systems have reported several changes induced by space stressors. For example, muscular atrophy, decreased bone mass, immune system impairment, fluid shift, SMS are the main organ and tissue responses to microgravity observed in astronauts. In parallel, at the cellular level, cell cycle delay, reduced cell motility, change in cytoskeletal protein distribution, oxidative stress, up- or down-regulation of genes and cell death have all been reported after microgravity exposure. On the other hand, cosmic radiations can also induce effects at the cellular level such as oxidative stress, DNA damage, cell cycle arrest, cell death, senescence and cell motility reduction.

One of the main questions related to the astronaut health risk during space travel is whether the CNS can be damaged from microgravity and cosmic radiations that could induce behavioural changes as well as learning and memory impairments. The aim of this thesis was thus to investigate the effects of space conditions on neuronal plasticity and connectivity in mammalians. In particular, we aimed at estimating the effects induced by microgravity and/or ionizing radiation on the neuronal network remodelling by studying cell motility in adherent cells and in neurons, determining the influence of microgravity on DNA repair dynamics and evaluating the correlation between the effects induced by exposure to single conditions or their combination.

1. *In vitro* model for space condition studies.

In this study, two *in vitro* models were used in order to investigate the effect of space conditions (real *vs.* simulated) on adherent cells. Since we had the chance to collaborate to one spaceflight experiment, we studied the locomotion and cytoskeleton in microgravity conditions aboard the International Space Station (ISS). In 2006, we had the opportunity to perform the **experiment "Motion and InterAct" (MIA) carried out aboard the ISS** in the framework of the Kubik Bio 1 mission of the European Space Agency. For this investigation, a monocyte cell line was chosen for this first flight due to its property to adhere to the substrate and the fact that the cell movements are mainly triggered by chemotactic attraction. The objective of this "Motion" experiment was to investigate the distribution of the cytoskeleton structures such as F-actin, β-tubulin and vinculin as well as to analyse the locomotion capability of monocytes on colloidal gold substrate used to coat slides. Migrating cells removed the colloid gold, leaving tracks and allowing to record cell locomotion [230]. To achieve the aim of this experiment, we had to select a certain type of monocytes which already had the innate capability to adhere to the surface without any activation process and which showed a large surface allowing the further study of the cytoskeletal structure distribution. Therefore, J-111 monocytes were finally selected

for this experiment. J-111 is a monocyte/macrophage cell line originating from human acute monocytic leukemia. In this investigation, aboard the ISS, monocytes were cultured into the specific hardware named MIA which allowed to grow cells on coverslips in a larger chamber and fix cells by opening two secondary small chambers prefilled with fixative solution [59]. We finally studied the influence of microgravity on different cytoskeletal components in adherent monocytes and their ability to migrate on a colloid gold substrate.

Based on the results obtained from these previous experiments in real space conditions on board the ISS, that were indicating alterations of cytoskeleton structure and reduction in motility in monocytes, we decided to further investigate the *in vitro* **effects of simulated space conditions on neuronal network plasticity and connectivity**.

The first step was to determine the best neuronal model; thus, which type of neurons represented the most sensitive model to external stress factors. From literature studies, it appeared that cell lines, which can differentiate into neurons, are more resistant than primary neurons to external compounds [174]. The next step was to determine from which growth stage of the culture, neurons became well-connected having developed a typical mature network physiology in order to optimally be able to observe changes induced by space conditions. For that purpose, we investigated several *in vitro* models highlighting a wide variety of physiological differences between maturing and mature neurons. First of all, we observed that neurons needed to be well connected in order to be mature. Additionally, we noticed that synaptic protein distribution and associated vesicles were partially dependent on the acquisition of functional synaptic transition [175]. It was also reported that immature neurons and mature neurons differ in action potential activities, spontaneous synaptic currents, number of synapses and neurite outgrowth speed [175, 176]. Additionally, GABA and glycin neurotransmitters differed in inhibitory or excitatory activity in cortical neurons [177, 178] and the sensitivity to exogenous stressors (compounds, environmental factors and infections) was related to the neuronal ageing stage [179, 180]. Moreover, we had to determine at which stage the neuron cultures showed the

least changes possible in neurite network growth, neuronal connectivity and cell death related to the culture ageing. In the literature, it was reported that neurons grew longer and exponentially increased their connections until they reach a stage of reasonable connectivity, thereafter slowing down their growth rate [176]. The use of **mature neuronal networks allowed to simulate some structural and physiological functions as in the adult brain**. In conclusion, we chose to use mouse primary neurons from cortex plated with a density of 50-66,000 cells per cm^2 that were cultured for 10 days before exposure to simulated space conditions. High content microscopy analysis performed with MorphoNeuroNet (see chapter IV) on neuronal network density, neurite morphology and cell death revealed a certain rate of stability between 10 and 25 days of culture.

To perform high content microscopy analysis, our chosen *in vitro* neuronal network model presented a few disadvantages. The main characteristic of this model was the high density of the neurite networks with a high variability in β-tub 3 distribution along the neurites. In the context of neuronal studies, several automated image analysis toolkits had been conceived accurately enabling to quantify shape changes in non-dense neuronal network cultures [276-279]. For our purpose, a few of them were compared but due to the high costs coupled to a low number of analysed parameters or low accuracy in tracing dense neurite network we therefore finally decided to design a new toolkit for dense network analysis. In conclusion, for high content analysis of two-dimensional neuronal network fluorescence images, **MorphoNeuroNet** (see chapter IV), a fully automated toolkit for ImageJ was developed allowing an accurate segmentation of the neurites in neuronal networks, defining area and length and number of non-apoptotic nuclei, segmenting the respective somas as well as quantifying the related shape parameters. The peculiarity of this tool is that the neurite network is segmented **by a combination of various intensity and edge detection algorithms allowing to trace even neuron extension ends with low fluorescence intensity**. The final outputs of this tool were given in tables with labels and related parameters. Finally, we propose this method for high content analysis on the effects of compounds or stressors in dense neuronal networks thereby

gaining physiological relevance for cell-based assays in the context of neuronal diseases. In the future, this tool can be up-graded firstly by making it lighter and faster and secondly, by implementing new functions as to detect protein accumulation along neurites of the soma, protein distribution (see observations on β-tub 3 in chapter V) or even by tracking protein movement onto neurons and, why not, by evolving into a 3D analysis system.

Since neurons are adherent and that they cannot be detached from the substrate without breaking neurites, therefore damaging the plasma membrane and losing cytoplasmic material, analysis of apoptosis using flow cytometry could not be performed. In order to perform high content analysis on early and late stages of apoptosis, two function pipelines for ImageJ were developed to estimate the rate of death in neuronal cultures, based on AnnexinV-PI assay or nuclear fragmentation with condensed chromatin (see chapters V, VI and VII). These macros counted the number of positive cells by measuring nuclear or cytoplasmic signals of the used marker above a user-defined threshold relative to the background or the maximal image intensity. For nuclear markers, we delineated regions of interest (ROI) based on nuclear masks derived from a nuclear counterstain image or by conditional dilatation of the nuclear region for cytoplasm markers. In conclusion, we proposed these methods to be used for high content analysis when evaluating the effects of compounds or stressors that could potentially induce apoptosis in adherent cells.

In prospective of a future possible spaceflight of our neuronal network model, we designed a new spaceflight hardware which would allow to culture adherent cells on glass in a small volume of culture medium thanks to a gas permeable membrane disposed as a cover. A space flight culture chamber with such a design could allow oxygen exchange and microscopy observations. Supplementary tests that would include among others thermal shock, cryogenic conservation and vibration tests would still need to be performed in order to determine the stability of the cultures in those space simulated conditions.

2. **Spaceflight experiments aboard the ISS**

Within this project we had the opportunity to participate to 2 spaceflight experiments, the first was the **MIA experiment on monocytes in the framework of KUBIC BIO 1** directed by Dr. Marianne Cogoli-Greuter (Zero-g LifeTec Zürich, Switzerland) [59] and the second in the framework of the first flight of **the MDS payload developed for rodent studies in space** and directed by Dr. Ranieri Cancedda (DOBIG, University of Genova, Genova, Italy) [198].

Within the framework of the MIA experiment performed aboard the ISS, the obtained results on monocyte motility throughout measurements of tracks on colloid gold substrate allowed to underline a **severe reduction in locomotion ability** in cells exposed for 24 h to real microgravity compared to 1 *g* flight controls and the ground controls. Indeed, monocytes exposed to ISS environment moved below 4 µm within 24 h compared to 31-34 µm in 1*g* controls aboard the ISS (KUBIC centrifuge) and over 50 µm in ground controls.

As observed in other cell types, microgravity causes alterations in locomotion as well as in several functions and structures such as the cytoskeleton [38, 64, 188, 252]. Obtained results on monocyte J-111 cytoskeleton pattern showed a **gravisensitivity of cytoskeletal components like F-actin, β-tubulin and vinculin** underlining alterations in the structure and distribution in cells exposed to ISS environment compared to 1 *g* controls. Similar changes were observed in endothelial cells, osteoblasts and HUVEC cells [69] and in the outgrowth cones of neuroblastoma cells [188]. Additionally, comparing the observed changes in real microgravity with changes observed in simulated microgravity allowed to evaluate the reliability of the effects obtained under microgravity conditions reproduced with the RPM on adherent cells [38, 59].

In conclusion, since cytoskeleton plays an important role in cell motility, especially in adherent cells where motility is based on a continuous reorganization of the cytoskeletal network, **microgravity-induced alteration of cytoskeletal structures might be the reason of reduced cell locomotion and morphological changes.**

In order to determine how the mammalian adult brain could respond to long-term exposure to space conditions and in collaboration with Dr. Daniela Santucci (Istituto Superiore di Sanità, Behavioural Neurosciences Section, Department of Cell Biology and Neurosciences, Roma, Italy), we had access to the shared brains of mice exposed to ISS environment. In 2009, 3 wild-type and 3 pleiotrophin transgenic mice were housed on the ISS for 91 days "equivalent to 10 years for mankind life span". Aboard the ISS, mice were housed into the Mice Drawer System (MDS). Due to low number of survived animal, 1 wild-type and 2 transgenic mice, preliminary genomic analyses could be performed on transgenic mice. Preliminary gene expression analysis showed that 111 genes were involved in the cortex, 271 in the cerebellum and 415 in the medulla oblongata after a 91 day trip in ISS. Preliminary analysis on GO biological functions showed that most of the genes were involved in cellular and metabolic processes, in cell communication and transport as well in developmental processes in the three tissues. Additionally, pathway analyses revealed also changes in Huntington's disease and p53 pathways in the cortex whereas axon guidance, cytoskeleton regulation by Rho GTPase, integrin, inflammation, Alzheimer's disease and P53 pathways were modulated in the cerebellum. Furthermore, cadherin and integrin signaling, axon guidance mediated by netrin or semaphorins, inflammation, Alzheimer's disease, and a few neurotransmitter receptor pathways were modulated in the medulla oblongata by ISS environment.

In order to complete genomic analysis, we will try to participate in future mouse spaceflight or post flight "tissue sharing" of mice or to organize *in vivo* experiments using the facilities available at SCK•CEN where the hindlimb method (as a model to simulate microgravity on animals) could be coupled with chronic irradiation exposure.

3. **Simulated space conditions (RPM and IR)**

Based on the previous experiments (*in vitro* monocyte cell type and *in vivo* adult mouse brain) performed under real space conditions on board of ISS and due to the limited access to

flight experiments, we decided then to study the morphological and physiological changes as well as the molecular alterations of mature neuronal networks under simulated space conditions on Earth. Morphological investigations on **well-connected mature cortical neurons showed a reduced area and length of neurites and a reduced area of somas within short-term exposures to simulated low gravity**. On the contrary, mature neurons showed an increase in area and length of neurites that reached almost back the normality over **10 days under simulated microgravity, thus showing a great adaptation to the new gravity conditions** without losing their intrinsic property to search for contacts (chapter V). It is well known that cell motility is regulated by cytoskeletal structures as microfilaments and microtubules as well as by focal contacts and integrins. Since it is known that cells are sensitive to mechanical forces, microgravity might act on stress-dependent cell changes and specifically on the cytoskeleton. Indeed, the cytoskeleton has been described to be the structure through which the cells sense gravity [60, 252]. So far, the basic mechanisms responsible for these phenomena in low gravity are still unclear. In our studies, we reported that neuronal microtubules change their distribution within the first hours of exposure to simulated microgravity increasing the concentration into the soma with a consequent reduction of the neurites. Over the following hours, the physiological equilibrium of tubulin distribution between soma and neurites was re-established (chapter V). These data are in agreement with the data on β-tubulin distribution in monocytes exposed to RPM for 1h which reported an accumulation of this protein surrounding the nucleus and a low concentration close to the cell cortex where 24 h after, the microtubular network distribution was partially re-established [38]. Indeed, monocytes exposed for 24 h to the ISS environment did not show any statistical differences in tubulin intensities when compared to the respective 1 *g* flight controls [59]. Additionally, observations on gene expression on *in vitro* neuronal networks showed a lower number of representative genes related to cytoskeleton components after exposure to simulated microgravity with an increase of involved genes in the following hours (chapter V). From these results we could hypothesize that the body of neuron cells, where

cytoskeleton structures regulate cell motility and shape, is affected by microgravity as observed in monocytes. These results are supported also by the genomic analysis which showed a general higher number of genes related to axonal guidance and cell motility processes or cytoskeleton components at 24 h after 1 h of RPM and lower at 72 h. Additionally, it has been observed that most of the morphological and microtubule distribution changes in neurons appeared between 30 and 60 minutes (chapters V and VI); this might explain why not many genes related to cell motility and cytoskeleton are involved within 1 h of RPM. On the contrary, neurite network adaptation to the new gravity conditions over a longer period of 10 days might suggest that cellular extensions are less affected by changes in gravitational forces. It appears that the adapted neurons to the new gravitational conditions acquired a different physiology since they showed a slower recovery after a long exposure to the RPM, thus requiring longer time to re-establish typical ground physiology. Additionally, well-connected neurons exposed for 10 days to simulated low gravity had the highest number of changed gene expression with genes related to cell motility and cytoskeleton after 72 h of recovery in re-established Earth's gravity from RPM exposure.

Ionising radiation is the second main stressor in space conditions. It has been reported that irradiation affects the CNS as well as neuron cultures at the cellular and molecular levels [203, 207, 212, 299, 335, 336]. Our investigations on well-connected cortical mature neurons exposed to low and high doses of X-irradiation with high dose rate or low doses of neutrons with a low dose rate showed an increase of DNA damage and apoptosis concomitantly to a reduction in neurite network growth (chapters VI and VII). In particular 24 hours after 100 mSv of acute X-irradiation (dose rate 5 mSv/sec), neuronal networks and neurites were 2-5% smaller than the controls, the irradiation-induced DNA damage was repaired and no apoptosis was observed. On the other hand, well-connected neuron cultures exposed for 5 days to 100 mSv of neutrons and 2% γ-irradiation (dose rate 20 mSv/day) had a neuronal network 45% smaller than the controls and neurites were 25% smaller than the controls. Additionally, the apoptosis fraction and the

DNA damage were 3-fold higher than in non-irradiated cultures. These obtained results suggest that chronic **irradiation could induce higher damage in well-connected mature neurons than acute doses** maybe because X-rays are low LET and that sources of radiation like neutrons are high LET. In addition, the Relative Biological Effectiveness (RBE) of neutrons is 12 to 16 times higher than X-rays.

In the space environment, since microgravity and ionizing radiation coexist concomitantly, we chose as model, well-connected neuronal networks cultured on the RPM with a concomitant chronic exposure to neutrons or an exposure to acute X-irradiation with low and high doses (chapters VI and VII). **Well-connected neurons cultured in simulated space conditions showed an enhanced reduction in neurite area and length per neuron as well as neurite network density, thus an overall reduction in neuronal network integrity**. The rate of apoptosis in such cultures was increased in neurons exposed to high or low doses suggesting a synergistic effect of combined conditions. Additionally, the radiation-induced DNA damage per neuron such as the number of DSB γ-H2AX positive cells was higher whilst the efficiency of DNA repair was slowed down after exposure to the combination of both conditions.

Future analyses on neuronal network activity throughout calcium assay, electrophysiology-like assay as the multi-electrode array (MEA) could be performed to determine the functional integrity of the neuronal network after long-term exposure to simulated space conditions. In particular, multi-electrode array assay could be carried out on both well-connected neuron cultures and *ex-vivo* brain slices in order to analyse spontaneous activities or the propagation of induced excitation. Additionally, deeper investigations on ROS or neurodegenerative disease-related protein accumulation in *in vitro* neurons or in laboratory animal brain could help to better estimate the effects of space conditions on adult brain to the consequent risks.

In conclusion, we believe that simulated microgravity (RPM) enhances the DNA damage after exposure to ionizing radiation, which results in an increase of apoptosis and a reduction of the neuronal network integrity. In addition, the reduced DNA-repair kinetics

and the high amount of unrepaired damage up to 24 h observed with simulated microgravity (RPM) after or during exposure to ionizing radiation, suggest possible genomic instability due to non-well repaired DNA damage in simulated space conditions which could cause a longer delay in axon and dendrite growth and the consequent adaptation of the neuronal network to microgravity conditions over long-term exposure. Changes in the expression of cytoskeletal, transport or cell motility-related genes as well as axonal guidance-related genes in both *in vivo* and *in vitro* models and in space as well as simulated conditions indicate the sensitivity of these pathways to gravitational force changes. These observations are in good correlation with the morphological observations of the outgrowth cone motility involving cell motility and cytoskeleton adaptation to space conditions and the remodelling after recovery under ground conditions. Finally, alteration in *in vivo* gene expression in the medulla oblongata and the cerebellum compared to the *in vitro* changes in the neuronal network integrity indicate possible behaviour and cognition changes related to motor (cerebellum) and autonomous (medulla oblongata) functions. These results are of utmost interest in view of astronaut health risk assessment for long-term space travel.

Summary / Samenvatting

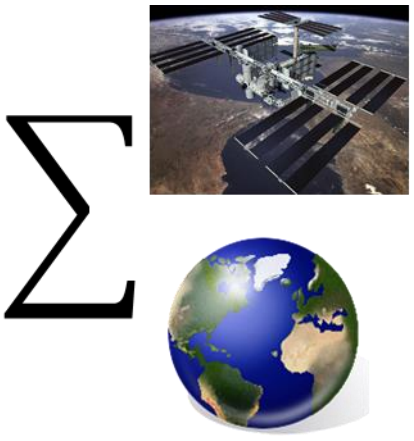

Summary

During orbital spaceflights, astronauts are exposed to various stressful factors such as microgravity and cosmic radiations. Therefore, one of the main objectives in space biology research is to understand the mechanisms involved in the adaptation of living organisms to the space environment. Together with the musculoskeletal, cardiovascular and immune systems, the central nervous system is forced to adapt to the space environment. The aim of this PhD thesis is to investigate the **effects of real and simulated space conditions** on *in vitro* adherent cells as monocytes and neurons with a particular emphasis on **cell motility and cytoskeleton organization** as well as **neuronal network plasticity and connectivity**. To achieve the objective of this PhD, we had the opportunity to participate to spaceflight experiments aboard the International Space Station. In the context of these real space condition experiments, we studied the effects on cell locomotion and cytoskeleton structures on *in vitro* adherent cells using the monocyte J-111 cell line as a model.

To study the plasticity and connectivity of mature neuronal networks, *in vitro* experiments were also performed with ground-based space condition systems. Well-connected mature neuron cultures were obtained from 17 day-old mouse foetus cortices that were cultured for 10 days in ground conditions. In our laboratories, we used, as ground-based space condition systems, on one hand, the Random Positioning Machine (RPM) to simulate microgravity, and on the other hand, low and high doses of X-rays and Californium-252 (source of neutrons) for acute and chronic irradiations, respectively. To determine the effects of space conditions on our *in vitro* model, toolkits for image analysis were developed; one to monitor neuronal network and neuron morphology changes and two others to estimate neuronal death by monitoring plasma membrane and nuclear morphology changes.

The obtained results showed an impaired locomotion of monocytes in real space conditions linked to the altered distribution of cytoskeletal structures. Experiments performed on *in vitro*

neuronal networks in ground-based space condition systems underlined an adaptation of mature cortical neurons over long periods of exposure to simulated microgravity after initial morphological and cytoskeletal changes due to the altered gravitational forces. Furthermore, neurons exposed for long periods of time to the RPM required longer periods to recover than under shorter exposures. These observations are in agreement with genome expression analyses on *in vitro* models in which the expression of cell motility, cytoskeleton as well as neurological and signal transmission-related genes was shown to be modulated. Moreover, a delay in neuronal network growth coupled to an increase in DNA damage and apoptosis were induced by low doses of chronic irradiations. Finally, when combining the two space simulated conditions, we observed an enhanced reduction of neuronal network and neuronal morphology changes as well as a synergistic increase in the DNA damage per neuron, number of Double Strand Break positive neurons and apoptosis.

We believe that microgravity induces impairment in the DNA repair efficiency during or after ionizing irradiation exposure. Additionally, the higher amount of unrepaired DNA damage suggests a possible genomic instability due to the impaired DNA repair efficiency which might thereafter causes a longer delay in neuronal network adaptation to space conditions. In conclusion, the observed *in vitro* changes in neuronal network integrity induced by space simulated conditions, might help in health risk evaluation and to develop countermeasures to prevent neurological disorders which could occur in astronauts over long-term space travels.

Samenvatting

Tijdens ruimtevaartmissies worden astronauten blootgesteld aan diverse stressfactoren aanwezig in de ruimte zoals een verminderde zwaartekracht en kosmische straling. Een belangrijk doel van ruimtevaartonderzoek is het begrijpen van de mechanismen die een rol spelen in de aanpassing van levende organismen aan deze ruimteomstandigheden. Het centrale zenuwstelsel, samen met het musculoskeletaal, cardiovasculair en immuunsysteem, moeten zich aanpassen aan de stressfactoren in de ruimte. In dit doctoraat onderzoeken we de **effecten van echte en gesimuleerde ruimteomstandigheden** op *in vitro* adherente cellen, zoals monocyten en neuronen waarbij de focus zowel op **cel motiliteit en cytoskeletale organisatie**, als op de **plasticiteit en connectiviteit van het neuronale netwerk** gelegd wordt. Om dit doel te bereiken hebben we de mogelijkheid gehad om deel te nemen aan experimenten in de ruimte aan boord van het Internationaal Ruimtestation ISS. In de context van deze echte ruimteomstandigheden bestudeerden we *in vitro* de effecten op cel voortbeweging en de structuur van het cytoskeleton van de adherente monocyte cellijn J-111. Om plasticiteit en connectiviteit in mature neuronale netwerken te bestuderen werden ook *in vitro* experimenten op aarde in ruimte-simulerende condities uitgevoerd. Hiervoor hebben we mature neuronen geïsoleerd uit de cortices van 17 dagen oude muis foetussen. Deze werden vervolgens gedurende 10 dagen in cultuur gebracht onder normale omstandigheden alvorens ze bloot te stellen aan gesimuleerde stressfactoren. Voor simulatie van de typische stressfactoren in de ruimte, hebben we enerzijds de 'Random Positioning Machine' (RPM) gebruikt om verminderde zwaartekracht na te bootsen en anderzijds lage en hoge dosissen van Californium-252 (een bron van neutronen) voor respectievelijk chronische en acute bestralingen als simulatie van kosmische straling. Om het effect van deze gesimuleerde stressfactoren op ons *in vitro* model te bepalen, hebben we specifieke computermodellen voor beeldanalyse ontwikkeld; één om het neuronale netwerk en morfologische veranderingen in de neuronen te bestuderen en twee andere gebaseerd op

morfologische veranderingen in het plasmamembraan en de celkern om dode neuronen te identificeren.

Onze resultaten van het eerste ISS experiment tonen een verzwakte motiliteit van monocyten aan die wordt gekoppeld aan veranderingen in de structuur van het cytoskelet. Een veranderde expressie van genen betrokken in celmotiliteit en cytoskelet alsook in de begeleide opbouw van zenuwuitlopers kon worden aangetoond in de drie hersendelen geïsoleerd uit de muizen die voor een lange tijd werden blootgesteld aan de omgeving in het ISS. Verder zien we dat genen betrokken bij zowel neurologische processen en signaaltransmissie als bij oxidatieve stress en neurodegeneratieve ziekten eveneens beïnvloed zijn door de omgeving in het ISS. Langdurige blootstelling van ons *in vitro* model aan gesimuleerde verminderde zwaartekracht in de RPM heeft aangetoond dat mature corticale neuronen zich aanpassen aan deze langdurige blootstelling door veranderingen in hun morfologie en het cytoskelet. Bovendien hebben langdurig blootgestelde neuronen meer tijd nodig om te herstellen dan neuronen die blootgesteld werden voor een korte tijd. Deze bevindingen zijn in overeenstemming met de resultaten van genexpressie analyse van de *in vivo* en *in vitro* modellen komende van de twee ISS experimenten, waarbij de expressie van genen betrokken in zowel celmotiliteit en cytoskelet als in neurologische processen en signaal transmissie veranderd is. Verder hebben we gezien dat de groei van het neuronale netwerk in ons *in vitro* model vertraagd is na chronische bestraling met lage dosissen. Dit is gekoppeld aan een toename in DNA schade en geprogrammeerde celdood. Tenslotte, wanneer we beide gesimuleerde stressfactoren combineren, zien we een uitgesproken afbraak van het neuronale netwerk die samengaat met morfologische veranderingen in de corticale neuronen. In deze neuronen werd eveneens een toename in DNA schade (dubbelstrengige breuken) en geprogrammeerde celdood waargenomen.

We veronderstellen dat een verminderde zwaartekracht de efficiëntie van het DNA herstel verminderd tijdens of na blootstelling aan ioniserende straling. Bovendien suggereert de toename in niet-herstelde DNA schade een mogelijk genomische instabiliteit als gevolg van een minder

efficiënt DNA herstel. Dit zal op termijn leiden tot een vertraagde aanpassing van het neuronale netwerk aan de typische omgeving in de ruimte. Ter conclusie, de *in vitro* geobserveerde veranderingen in de neuronale netwerk integriteit, geïnduceerd door gesimuleerde ruimtecondities, kan bijdragen tot de evaluatie van het gezondheidsrisico en de ontwikkeling van maatregelen tegen neurologische aandoeningen bij astronauten op lange-termijn ruimte reizen.

References

References

1. Newton I, M.A., Chittenden, N. W. , *Newton's principles: the mathematical principles of natural philosophy.* 1846 : Adee Daniel.
2. Brinckmann, E., *Biology in Space and Life on Earth.*
3. *ISS User's Guide-Release 2.0.*
4. Ceglia, E., *European User Guide to Low Gravity Platforms.* UIC-ESA-UM-0001, 2005(Issue 2 revision 0).
5. Drummer, C., et al., *Body fluid regulation in micro-gravity differs from that on Earth: an overview.* Pflugers Arch, 2000. **441**(2-3 Suppl): p. R66-72.
6. Jost, P.D., *Simulating human space physiology with bed rest.* Hippokratia, 2008. **12 Suppl 1**: p. 37-40.
7. Walton, K., *Postnatal development under conditions of simulated weightlessness and space flight.* Brain Res Brain Res Rev, 1998. **28**(1-2): p. 25-34.
8. Klaus, D.M., *Clinostats and bioreactors.* Gravit Space Biol Bull, 2001. **14**(2): p. 55-64.
9. Davis, J.R., et al., *Space motion sickness during 24 flights of the space shuttle.* Aviat Space Environ Med, 1988. **59**(12): p. 1185-9.
10. Lackner, J.R. and P. Dizio, *Space motion sickness.* Exp Brain Res, 2006. **175**(3): p. 377-99.
11. Graybiel, A. and J. Knepton, *Sopite Syndrome - Sometimes Sole Manifestation of Motion Sickness.* Aviation Space and Environmental Medicine, 1976. **47**(8): p. 873-882.
12. Dai, Z.Q., et al., *Simulated microgravity inhibits the proliferation and osteogenesis of rat bone marrow mesenchymal stem cells.* Cell Prolif, 2007. **40**(5): p. 671-84.
13. Kaplansky, A.S., et al., *The effect of microgravity on bone fracture healing in rats flown on Cosmos-2044.* Physiologist, 1991. **34**(1 Suppl): p. S196-9.
14. Caillot-Augusseau, A., et al., *Bone formation and resorption biological markers in cosmonauts during and after a 180-day space flight (Euromir 95).* Clin Chem, 1998. **44**(3): p. 578-85.
15. Carmeliet, G. and R. Bouillon, *The effect of microgravity on morphology and gene expression of osteoblasts in vitro.* FASEB J, 1999. **13 Suppl**: p. S129-34.
16. Tesch, P.A., et al., *Skeletal muscle proteolysis in response to short-term unloading in humans.* J Appl Physiol, 2008. **105**(3): p. 902-6.
17. Fitts, R.H., D.R. Riley, and J.J. Widrick, *Functional and structural adaptations of skeletal muscle to microgravity.* J Exp Biol, 2001. **204**(Pt 18): p. 3201-8.
18. Slentz, D.H., G.A. Truskey, and W.E. Kraus, *Effects of chronic exposure to simulated microgravity on skeletal muscle cell proliferation and differentiation.* In Vitro Cell Dev Biol Anim, 2001. **37**(3): p. 148-56.
19. Kalb, R. and D. Solomon, *Space exploration, Mars, and the nervous system.* Arch Neurol, 2007. **64**(4): p. 485-90.
20. Widrick, J.J., et al., *Effect of a 17 day spaceflight on contractile properties of human soleus muscle fibres.* J Physiol, 1999. **516 (Pt 3)**: p. 915-30.
21. Fitts, R.H., D.R. Riley, and J.J. Widrick, *Physiology of a microgravity environment invited review: microgravity and skeletal muscle.* J Appl Physiol, 2000. **89**(2): p. 823-39.
22. Edgerton, V.R., et al., *Human fiber size and enzymatic properties after 5 and 11 days of spaceflight.* J Appl Physiol, 1995. **78**(5): p. 1733-9.
23. Fitts, R.H., et al., *Models of disuse: a comparison of hindlimb suspension and immobilization.* J Appl Physiol, 1986. **60**(6): p. 1946-53.
24. Mano, T., *Autonomic neural functions in space.* Curr Pharm Biotechnol, 2005. **6**(4): p. 319-24.

25. Souvestre, P., Blaber, A., and Landrock, C., *<Space motion sickness_ The sensory motor controls and cardiovascular correlation.pdf>*. Acta Astronaut, 2008(63): p. 745–757.
26. Norsk, P., *Cardiovascular and fluid volume control in humans in space.* Curr Pharm Biotechnol, 2005. **6**(4): p. 325-30.
27. Leach, C.S., et al., *Regulation of body fluid compartments during short-term spaceflight.* J Appl Physiol, 1996. **81**(1): p. 105-16.
28. Blomqvist, C.G., et al., *Mechanisms of post-flight orthostatic intolerance.* J Gravit Physiol, 1994. **1**(1): p. P122-4.
29. Diedrich, A., S.Y. Paranjape, and D. Robertson, *Plasma and blood volume in space.* Am J Med Sci, 2007. **334**(1): p. 80-5.
30. Fuller, C.A., *Homeostasis and biological rhythms in the rat during spaceflight.* Physiologist, 1985. **28**(6 Suppl): p. S199-200.
31. Fritsch-Yelle, J.M., et al., *Microgravity decreases heart rate and arterial pressure in humans.* J Appl Physiol, 1996. **80**(3): p. 910-4.
32. Eckberg, D.L., et al., *Baroreflex modulation of sympathetic activity and sympathetic neurotransmitters in humans.* Acta Physiol Scand, 1988. **133**(2): p. 221-31.
33. Wallin, B.G., et al., *Simultaneous measurements of cardiac noradrenaline spillover and sympathetic outflow to skeletal muscle in humans.* J Physiol, 1992. **453**: p. 45-58.
34. Rykova M.P., et al., *Humoral and cellularimmunity in cosmonautsafter the ISS missions.* Acta astronautica, October–November 2008. **63**(7-10): p. 697–705.
35. Cogoli, A. and M. Cogoli-Greuter, *Activation and proliferation of lymphocytes and other mammalian cells in microgravity.* Adv Space Biol Med, 1997. **6**: p. 33-79.
36. Walther, I., et al., *Simulated microgravity inhibits the genetic expression of interleukin-2 and its receptor in mitogen-activated T lymphocytes.* FEBS Lett, 1998. **436**(1): p. 115-8.
37. Cogoli, A., A. Tschopp, and P. Fuchs-Bislin, *Cell sensitivity to gravity.* Science, 1984. **225**(4658): p. 228-30.
38. Meloni, M.A., et al., *Cytoskeleton changes and impaired motility of monocytes at modelled low gravity.* Protoplasma, 2006. **229**(2-4): p. 243-9.
39. Maccarrone, M., et al., *Creating conditions similar to those that occur during exposure of cells to microgravity induces apoptosis in human lymphocytes by 5-lipoxygenase-mediated mitochondrial uncoupling and cytochrome c release.* J Leukoc Biol, 2003. **73**(4): p. 472-81.
40. Cogoli, A., *Signal transduction in T lymphocytes in microgravity.* Gravit Space Biol Bull, 1997. **10**(2): p. 5-16.
41. Sonnenfeld, G., *The immune system in space and microgravity.* Med Sci Sports Exerc, 2002. **34**(12): p. 2021-7.
42. Gridley, D.S., et al., *Spaceflight effects on T lymphocyte distribution, function and gene expression.* J Appl Physiol, 2009. **106**(1): p. 194-202.
43. Baqai, F.P., et al., *Effects of spaceflight on innate immune function and antioxidant gene expression.* J Appl Physiol, 2009. **106**(6): p. 1935-42.
44. Chapes, S.K., et al., *Effects of spaceflight and PEG-IL-2 on rat physiological and immunological responses.* J Appl Physiol, 1999. **86**(6): p. 2065-76.
45. Mutsaers, S.E., et al., *Mechanisms of tissue repair: from wound healing to fibrosis.* Int J Biochem Cell Biol, 1997. **29**(1): p. 5-17.
46. Baum, C.L. and C.J. Arpey, *Normal cutaneous wound healing: clinical correlation with cellular and molecular events.* Dermatol Surg, 2005. **31**(6): p. 674-86; discussion 686.
47. Diegelmann, R.F. and M.C. Evans, *Wound healing: an overview of acute, fibrotic and delayed healing.* Front Biosci, 2004. **9**: p. 283-9.
48. Davidson, J.M., et al., *Sustained microgravity reduces intrinsic wound healing and growth factor responses in the rat.* FASEB J, 1999. **13**(2): p. 325-9.

49. Chouker, A., et al., *Effects of confinement (110 and 240 days) on neuroendocrine stress response and changes of immune cells in men.* J Appl Physiol, 2002. **92**(4): p. 1619-27.
50. Shearer, W.T., et al., *Immune responses in adult female volunteers during the bed-rest model of spaceflight: antibodies and cytokines.* J Allergy Clin Immunol, 2009. **123**(4): p. 900-5.
51. Sciola, L., et al., *Influence of microgravity on mitogen binding and cytoskeleton in Jurkat cells.* Adv Space Res, 1999. **24**(6): p. 801-5.
52. Grimm, D., et al., *How and why does the proteome respond to microgravity?* Expert Rev Proteomics, 2011. **8**(1): p. 13-27.
53. Bechler, B., A. Cogoli, and D. Mesland, *[Lymphocytes are sensitive to gravity]*. Naturwissenschaften, 1986. **73**(7): p. 400-3.
54. Takeda, M., et al., *Effects of simulated microgravity on proliferation and chemosensitivity in malignant glioma cells.* Neurosci Lett, 2009. **463**(1): p. 54-9.
55. Chen, J., R. Chen, and S. Gao, *Morphological characteristics and proliferation of keratocytes cultured under simulated microgravity.* Artif Organs, 2007. **31**(9): p. 722-31.
56. Uva, B.M., et al., *Clinorotation-induced weightlessness influences the cytoskeleton of glial cells in culture.* Brain Res, 2002. **934**(2): p. 132-9.
57. Crestini, A., et al., *Effects of simulated microgravity on the development and maturation of dissociated cortical neurons.* In Vitro Cell Dev Biol Anim, 2004. **40**(5-6): p. 159-65.
58. Gruener, R. and G. Hoeger, *Vector-free gravity disrupts synapse formation in cell culture.* Am J Physiol, 1990. **258**(3 Pt 1): p. C489-94.
59. Meloni, M.A., et al., *Space flight affects motility and cytoskeletal structures in human monocyte cell line J-111.* Cytoskeleton (Hoboken), 2011. **68**(2): p. 125-37.
60. Ingber, D., *How cells (might) sense microgravity.* FASEB J, 1999. **13 Suppl**: p. S3-15.
61. Servotte, S., et al., *Establishment of stable human fibroblast cell lines constitutively expressing active Rho-GTPases.* Protoplasma, 2006. **229**(2-4): p. 215-20.
62. Nichols, H.L., N. Zhang, and X. Wen, *Proteomics and genomics of microgravity.* Physiol Genomics, 2006. **26**(3): p. 163-71.
63. Nikawa, T., et al., *Skeletal muscle gene expression in space-flown rats.* FASEB J, 2004. **18**(3): p. 522-4.
64. Infanger, M., et al., *Simulated weightlessness changes the cytoskeleton and extracellular matrix proteins in papillary thyroid carcinoma cells.* Cell Tissue Res, 2006. **324**(2): p. 267-77.
65. Bucaro, M.A., et al., *The effect of simulated microgravity on osteoblasts is independent of the induction of apoptosis.* J Cell Biochem, 2007. **102**(2): p. 483-95.
66. Maccarrone, M., M. Taccone-Gallucci, and A. Finazzi-Agro, *5-Lipoxygenase-mediated mitochondrial damage and apoptosis of mononuclear cells in ESRD patients.* Kidney Int Suppl, 2003(84): p. S33-6.
67. Uva, B.M., et al., *Microgravity-induced apoptosis in cultured glial cells.* Eur J Histochem, 2002. **46**(3): p. 209-14.
68. Sun, X.Q., et al., *Simulated weightlessness aggravates hypergravity-induced impairment of learning and memory and neuronal apoptosis in rats.* Behav Brain Res, 2009. **199**(2): p. 197-202.
69. Carlsson, S.I., et al., *Endothelial stress by gravitational unloading: effects on cell growth and cytoskeletal organization.* Biochim Biophys Acta, 2003. **1642**(3): p. 173-9.
70. Mammone, T., D. Gan, and R. Foyouzi-Youssefi, *Apoptotic cell death increases with senescence in normal human dermal fibroblast cultures.* Cell Biol Int, 2006. **30**(11): p. 903-9.
71. Wang, J., et al., *Simulated microgravity promotes cellular senescence via oxidant stress in rat PC12 cells.* Neurochem Int, 2009. **55**(7): p. 710-6.

72. Todd P, *Current topics in space radiation biology. In: Tobias C, Todd P eds. Space radiation biology and related topics. pp. 1–18. Academic Press; New York and London.* 1974.
73. Millikan, R., *Electrons (+ and –), protons, photons, neutrons, mesotrons and cosmic rays.* University of Chicago Press; Chicago, Illinois, USA., 1947.
74. Van Allen, J. and L. Franck, *Radiation around the earth to a radial distance of 107,400 km.* Nature, 1959. **183**: p. 430.
75. Van Allen, J. and L. Franck, *Radiation measurements to 658,300 km with Pioneer IV.* Nature, 1959. **184**: p. 219.
76. Vanmarcke, H., H. Bosmans, and G. Eggermont, *Ionizing radiation exposure of the Belgian population in 2006.* Third European IRPA congress, 2010.(Helsinki,Finland.).
77. Maalouf, M., M. Durante, and N. Foray, *Biological effects of space radiation on human cells: history, advances and outcomes.* J Radiat Res, 2011. **52**(2): p. 126-46.
78. Benton, E.R. and E.V. Benton, *Space radiation dosimetry in low-Earth orbit and beyond.* Nucl Instrum Methods Phys Res B, 2001. **184**(1-2): p. 255-94.
79. Haffner, J., *Shielding Strategies for Human Space Exploration.* In. pp. Academic Press; City., 1967).
80. TH, J., *Evidence that protons are the primary particles of the hard component.* Review Modelling Physics, 1938. **11**: p. 208–210.
81. Freier P, e.a., *Evidence of heavy nuclei in the primary cosmic radiation.* Physics Reviews 1948). **74**: p. 213-217.
82. Comstock GM and e. al, *Energy spectra and abundances of the cosmic-ray nuclei helium to iron from the OGO-1 satellite experiment.* Astrophysics Journal, 1969. **155**: p. 609-617.
83. Reitz, G., *Characteristic of the radiation field in low Earth orbit and in deep space.* Z Med Phys, 2008. **18**(4): p. 233-43.
84. Durante, M. and F.A. Cucinotta, *Heavy ion carcinogenesis and human space exploration.* Nat Rev Cancer, 2008. **8**(6): p. 465-72.
85. Cucinotta FA, et al., *Space Radiation Cancer Risk Projections for Explorative Missions: Uncertainty Reductionand Mitigation.* NASA WashingtonDC:NASAJSCDocument(JSC-29295), 2001.
86. Maurer, R.H., et al., *Neutron production from polyethylene and common spacecraft materials.* IEEE Trans Nucl Sci, 2001. **48**(6): p. 2029-33.
87. La Tessa, C., et al., *Fragmentation of 1GeV/nucleon iron ions in thick targets relevant for space exploration.* Advances in Space Research, 2005. **35**(2): p. 223-229.
88. Zeitlin, C., *Shielding and fragmentation studies.* Radiation Protection Dosimetry, 2005. **116**(1-4): p. 123-124.
89. Hoffman, J., P. Fisher, and O. Batishchev, *Use of Superconducting Magnet Technology for Astronaut Radiation Protection.* Final Report for NIAC Phase I Contract CP 04-01, 2 May, 2005.
90. Reitz, G., *Space radiation dosimetry.* Acta Astronaut, 1994. **32**(11): p. 715-20.
91. Bidoli, V., et al., *The Sileye-3/Alteino experiment for the study of light flashes, radiation environment and astronaut brain activity on board the International Space Station.* J Radiat Res, 2002. **43 Suppl**: p. S47-52.
92. Vanhavere, F., et al., *DOsimetry of BIological EXperiments in SPace (DOBIES) with luminescence (OSL and TL) and track etch detectors.* Radiation Measurements, 2008. **43**(2-6): p. 694-697.
93. Hallil, A., et al., *MOSFET dosimetry mission inside the ISS as part of the Matroshka-R experiment.* Radiat Prot Dosimetry, 2010. **138**(4): p. 295-309.
94. ICRP, *ICRP 1991 Recommendations of the International Commission on Radiological Protection ICRP Publication 60.* Ann. ICRP 21: p. 1-3.

95. Tubiana, M., et al., *The linear no-threshold relationship is inconsistent with radiation biologic and experimental data.* Radiology, 2009. **251**(1): p. 13-22.
96. Blyth, B.J. and P.J. Sykes, *Radiation-induced bystander effects: what are they, and how relevant are they to human radiation exposures?* Radiat Res, 2011. **176**(2): p. 139-57.
97. Vilenchik, M.M. and A.G. Knudson, *Radiation dose-rate effects, endogenous DNA damage, and signaling resonance.* Proc Natl Acad Sci U S A, 2006. **103**(47): p. 17874-9.
98. Twardella, D. and J. Chang-Claude, *Studies on radiosensitivity from an epidemiological point of view - overview of methods and results.* Radiother Oncol, 2002. **62**(3): p. 249-60.
99. Turesson, I., et al., *Prognostic factors for acute and late skin reactions in radiotherapy patients.* Int J Radiat Oncol Biol Phys, 1996. **36**(5): p. 1065-75.
100. ICRP, *The 2007 Recommendations of the International Commission on Radiological Protection.* ICRP Publication 103, in Ann. ICRP 37, 2007.
101. Dieriks, B., et al., *Medium-mediated DNA repair response after ionizing radiation is correlated with the increase of specific cytokines in human fibroblasts.* Mutat Res, 2010. **687**(1-2): p. 40-8.
102. Fujita, M., et al., *Carbon-ion radiation enhances migration ability and invasiveness of the pancreatic cancer cell, PANC-1, in vitro.* Cancer Sci, 2012. **103**(4): p. 677-83.
103. Desai, N., et al., *High LET-induced H2AX phosphorylation around the Bragg curve.* Adv Space Res, 2005. **35**(2): p. 236-42.
104. Cucinotta, F.A., et al., *Effects of target fragmentation on evaluation of LET spectra from space radiations: implications for space radiation protection studies.* Radiat Meas, 1996. **26**(6): p. 923-34.
105. Decoursey, T.E. and E. Ligeti, *Regulation and termination of NADPH oxidase activity.* Cell Mol Life Sci, 2005. **62**(19-20): p. 2173-93.
106. Moreira, P.I., et al., *Oxidative stress: the old enemy in Alzheimer's disease pathophysiology.* Curr Alzheimer Res, 2005. **2**(4): p. 403-8.
107. Lankin, V.Z., et al., *Oxidative stress in atherosclerosis and diabetes.* Bull Exp Biol Med, 2005. **140**(1): p. 41-3.
108. Spitz, D.R., et al., *Metabolic oxidation/reduction reactions and cellular responses to ionizing radiation: a unifying concept in stress response biology.* Cancer Metastasis Rev, 2004. **23**(3-4): p. 311-22.
109. Wu, L.J., et al., *Targeted cytoplasmic irradiation with alpha particles induces mutations in mammalian cells.* Proc Natl Acad Sci U S A, 1999. **96**(9): p. 4959-64.
110. Wan, X.S., et al., *Protection against radiation-induced oxidative stress in cultured human epithelial cells by treatment with antioxidant agents.* Int J Radiat Oncol Biol Phys, 2006. **64**(5): p. 1475-81.
111. Borrelli, A., et al., *A recombinant MnSOD is radioprotective for normal cells and radiosensitizing for tumor cells.* Free Radic Biol Med, 2009. **46**(1): p. 110-6.
112. Dziegielewski, J., W. Goetz, and J.E. Baulch, *Heavy ions, radioprotectors and genomic instability: implications for human space exploration.* Radiat Environ Biophys, 2010. **49**(3): p. 303-16.
113. Xiao, M. and M.H. Whitnall, *Pharmacological countermeasures for the acute radiation syndrome.* Curr Mol Pharmacol, 2009. **2**(1): p. 122-33.
114. Desai, N., et al., *Immunofluorescence detection of clustered gamma-H2AX foci induced by HZE-particle radiation.* Radiat Res, 2005. **164**(4 Pt 2): p. 518-22.
115. Hakem, R., *DNA-damage repair; the good, the bad, and the ugly.* EMBO J, 2008. **27**(4): p. 589-605.
116. Rogakou, E.P., et al., *DNA double-stranded breaks induce histone H2AX phosphorylation on serine 139.* J Biol Chem, 1998. **273**(10): p. 5858-68.
117. De Vos, W.H., et al., *High content image cytometry in the context of subnuclear organization.* Cytometry A, 2010. **77**(1): p. 64-75.

118. Warmerdam, D.O. and R. Kanaar, *Dealing with DNA damage: relationships between checkpoint and repair pathways.* Mutat Res, 2010. **704**(1-3): p. 2-11.
119. Walworth, N.C., *Cell-cycle checkpoint kinases: checking in on the cell cycle.* Curr Opin Cell Biol, 2000. **12**(6): p. 697-704.
120. Bartek, J. and J. Lukas, *Pathways governing G1/S transition and their response to DNA damage.* FEBS Lett, 2001. **490**(3): p. 117-22.
121. Verheij, M. and H. Bartelink, *Radiation-induced apoptosis.* Cell Tissue Res, 2000. **301**(1): p. 133-42.
122. Udayakumar, T., et al., *The E2F1/Rb and p53/MDM2 pathways in DNA repair and apoptosis: understanding the crosstalk to develop novel strategies for prostate cancer radiotherapy.* Semin Radiat Oncol, 2010. **20**(4): p. 258-66.
123. Bree, R.T., et al., *The switch from survival responses to apoptosis after chromosomal breaks.* DNA Repair (Amst), 2004. **3**(8-9): p. 989-95.
124. Westwick, J.K., et al., *Ceramide activates the stress-activated protein kinases.* J Biol Chem, 1995. **270**(39): p. 22689-92.
125. Verheij, M., et al., *Requirement for ceramide-initiated SAPK/JNK signalling in stress-induced apoptosis.* Nature, 1996. **380**(6569): p. 75-9.
126. Yang, X., et al., *Daxx, a novel Fas-binding protein that activates JNK and apoptosis.* Cell, 1997. **89**(7): p. 1067-76.
127. Bossy-Wetzel, E., L. Bakiri, and M. Yaniv, *Induction of apoptosis by the transcription factor c-Jun.* EMBO J, 1997. **16**(7): p. 1695-709.
128. Miller, T.M., et al., *Bax deletion further orders the cell death pathway in cerebellar granule cells and suggests a caspase-independent pathway to cell death.* J Cell Biol, 1997. **139**(1): p. 205-17.
129. Shiah, S.G., et al., *Activation of c-Jun NH2-terminal kinase and subsequent CPP32/Yama during topoisomerase inhibitor beta-lapachone-induced apoptosis through an oxidation-dependent pathway.* Cancer Res, 1999. **59**(2): p. 391-8.
130. Hayflick, L. and P.S. Moorhead, *The serial cultivation of human diploid cell strains.* Exp Cell Res, 1961. **25**: p. 585-621.
131. Campisi, J., *Cancer, aging and cellular senescence.* In Vivo, 2000. **14**(1): p. 183-8.
132. Itahana, K., G. Dimri, and J. Campisi, *Regulation of cellular senescence by p53.* Eur J Biochem, 2001. **268**(10): p. 2784-91.
133. Shelton, D.N., et al., *Microarray analysis of replicative senescence.* Curr Biol, 1999. **9**(17): p. 939-45.
134. Schmitt, C.A., et al., *A senescence program controlled by p53 and p16INK4a contributes to the outcome of cancer therapy.* Cell, 2002. **109**(3): p. 335-46.
135. Kim Sh, S.H., P. Kaminker, and J. Campisi, *Telomeres, aging and cancer: in search of a happy ending.* Oncogene, 2002. **21**(4): p. 503-11.
136. Harley, C.B., A.B. Futcher, and C.W. Greider, *Telomeres shorten during ageing of human fibroblasts.* Nature, 1990. **345**(6274): p. 458-60.
137. Dimri, G.P., et al., *A biomarker that identifies senescent human cells in culture and in aging skin in vivo.* Proc Natl Acad Sci U S A, 1995. **92**(20): p. 9363-7.
138. Campisi, J., *Cellular senescence as a tumor-suppressor mechanism.* Trends Cell Biol, 2001. **11**(11): p. S27-31.
139. Tsai, K.K., et al., *Low-dose radiation-induced senescent stromal fibroblasts render nearby breast cancer cells radioresistant.* Radiat Res, 2009. **172**(3): p. 306-13.
140. Hong, E.H., et al., *Ionizing radiation induces cellular senescence of articular chondrocytes via negative regulation of SIRT1 by p38 kinase.* J Biol Chem, 2010. **285**(2): p. 1283-95.
141. Ogata, T., et al., *Particle irradiation suppresses metastatic potential of cancer cells.* Cancer Res, 2005. **65**(1): p. 113-20.

142. Woloschak, G.E., P. Felcher, and C.M. Chang-Liu, *Expression of cytoskeletal and matrix genes following exposure to ionizing radiation: dose-rate effects and protein synthesis requirements.* Cancer Lett, 1995. **92**(2): p. 135-41.
143. Wang, D. and D.J. Jang, *Protein kinase CK2 regulates cytoskeletal reorganization during ionizing radiation-induced senescence of human mesenchymal stem cells.* Cancer Res, 2009. **69**(20): p. 8200-7.
144. Olwell, P.M., et al., *Cytoskeletal reorganization and altered phagocytotic ability in primary cultures of rainbow trout hemopoietic tissue exposed to low-level ionizing radiation.* Radiat Res, 2005. **164**(1): p. 45-52.
145. Mognato, M., et al., *DNA repair in modeled microgravity: double strand break rejoining activity in human lymphocytes irradiated with gamma-rays.* Mutat Res, 2009. **663**(1-2): p. 32-9.
146. Risin, D. and N.R. Pellis, *Modeled microgravity inhibits apoptosis in peripheral blood lymphocytes.* In Vitro Cell Dev Biol Anim, 2001. **37**(2): p. 66-72.
147. Canova, S., et al., *"Modeled microgravity" affects cell response to ionizing radiation and increases genomic damage.* Radiat Res, 2005. **163**(2): p. 191-9.
148. Manti, L., *Does reduced gravity alter cellular response to ionizing radiation?* Radiat Environ Biophys, 2006. **45**(1): p. 1-8.
149. Mognato, M. and L. Celotti, *Modeled microgravity affects cell survival and HPRT mutant frequency, but not the expression of DNA repair genes in human lymphocytes irradiated with ionising radiation.* Mutat Res, 2005. **578**(1-2): p. 417-29.
150. Horneck, G., et al., *DNA repair in microgravity: studies on bacteria and mammalian cells in the experiments REPAIR and KINETICS.* J Biotechnol, 1996. **47**(2-3): p. 99-112.
151. Kandel, E.R. and J.H. Schwartz, *Principles of Neural Science*, ed. M.-H.E.-E.t.R. edition. 2000
152. Goodman, C.S. and C.J. Shatz, *Developmental mechanisms that generate precise patterns of neuronal connectivity.* Cell, 1993. **72 Suppl**: p. 77-98.
153. Shaw, C.A., R.A. Lanius, and K. van den Doel, *The origin of synaptic neuroplasticity: crucial molecules or a dynamical cascade?* Brain Res Brain Res Rev, 1994. **19**(3): p. 241-63.
154. Pascual-Leone, A., et al., *Characterizing brain cortical plasticity and network dynamics across the age-span in health and disease with TMS-EEG and TMS-fMRI.* Brain Topogr, 2011. **24**(3-4): p. 302-15.
155. Ponti, G., P. Peretto, and L. Bonfanti, *Genesis of neuronal and glial progenitors in the cerebellar cortex of peripuberal and adult rabbits.* PLoS One, 2008. **3**(6): p. e2366.
156. Harris, K.M. and S.B. Kater, *Dendritic spines: cellular specializations imparting both stability and flexibility to synaptic function.* Annu Rev Neurosci, 1994. **17**: p. 341-71.
157. Fischer, M., et al., *Rapid actin-based plasticity in dendritic spines.* Neuron, 1998. **20**(5): p. 847-54.
158. Kaech, S., H. Brinkhaus, and A. Matus, *Volatile anesthetics block actin-based motility in dendritic spines.* Proc Natl Acad Sci U S A, 1999. **96**(18): p. 10433-7.
159. Lendvai, B., et al., *Experience-dependent plasticity of dendritic spines in the developing rat barrel cortex in vivo.* Nature, 2000. **404**(6780): p. 876-81.
160. Bear, M.F. and R.C. Malenka, *Synaptic plasticity: LTP and LTD.* Curr Opin Neurobiol, 1994. **4**(3): p. 389-99.
161. Malenka, R.C., *Synaptic plasticity in the hippocampus: LTP and LTD.* Cell, 1994. **78**(4): p. 535-8.
162. Luscher, C., et al., *Synaptic plasticity and dynamic modulation of the postsynaptic membrane.* Nat Neurosci, 2000. **3**(6): p. 545-50.
163. Kauer, J.A. and R.C. Malenka, *Synaptic plasticity and addiction.* Nat Rev Neurosci, 2007. **8**(11): p. 844-58.

164. Citri, A. and R.C. Malenka, *Synaptic plasticity: multiple forms, functions, and mechanisms.* Neuropsychopharmacology, 2008. **33**(1): p. 18-41.
165. Ross, M.D. and J. Varelas, *Synaptic ribbon plasticity, ribbon size and potential regulatory mechanisms in utricular and saccular maculae.* J Vestib Res, 2005. **15**(1): p. 17-30.
166. Wiedemann, M. and W. Hanke, *Gravity sensing in the central nervous system.* J Gravit Physiol, 2002. **9**(1): p. P43-4.
167. Vlkolinsky, R., et al., *Effects of lipopolysaccharide on 56Fe-particle radiation-induced impairment of synaptic plasticity in the mouse hippocampus.* Radiat Res, 2007. **168**(4): p. 462-70.
168. Alberts, J.R., et al., *Early postnatal development of rats gestated during flight of Cosmos 1514.* Physiologist, 1985. **28**(6 Suppl): p. S81-2.
169. Manda, K., M. Ueno, and K. Anzai, *Space radiation-induced inhibition of neurogenesis in the hippocampal dentate gyrus and memory impairment in mice: ameliorative potential of the melatonin metabolite, AFMK.* J Pineal Res, 2008. **45**(4): p. 430-8.
170. Koh, S.H., et al., *Protective effects of statins on L-DOPA neurotoxicity due to the activation of phosphatidylinositol 3-kinase and free radical scavenging in PC12 cell culture.* Brain Res, 2011. **1370**: p. 53-63.
171. Yuyama, K., et al., *Resistance of PC12 cells against nitric oxide (NO)-induced toxicity in long-term culture: implication of neuronal NO synthase expression.* Neurosci Lett, 2001. **309**(3): p. 169-72.
172. Koike, T., *Molecular and cellular mechanism of neuronal degeneration caused by nerve growth factor deprivation approached through PC12 cell culture.* Prog Neuropsychopharmacol Biol Psychiatry, 1992. **16**(1): p. 95-106.
173. Guo, L., et al., *Differentiation of mesenchymal stem cells into dopaminergic neuron-like cells in vitro.* Biomed Environ Sci, 2005. **18**(1): p. 36-42.
174. Radio, N.M., et al., *Comparison of PC12 and cerebellar granule cell cultures for evaluating neurite outgrowth using high content analysis.* Neurotoxicol Teratol, 2010. **32**(1): p. 25-35.
175. Basarsky, T.A., V. Parpura, and P.G. Haydon, *Hippocampal synaptogenesis in cell culture: developmental time course of synapse formation, calcium influx, and synaptic protein distribution.* J Neurosci, 1994. **14**(11 Pt 1): p. 6402-11.
176. Lai, P.Y., L.C. Jia, and C.K. Chan, *Growth of cortical neuronal network in vitro: modeling and analysis.* Phys Rev E Stat Nonlin Soft Matter Phys, 2006. **73**(5 Pt 1): p. 051906.
177. Ben-Ari, Y., *Excitatory actions of gaba during development: the nature of the nurture.* Nat Rev Neurosci, 2002. **3**(9): p. 728-39.
178. Singer, J.H., et al., *Development of glycinergic synaptic transmission to rat brain stem motoneurons.* J Neurophysiol, 1998. **80**(5): p. 2608-20.
179. Vernon, P.S. and D.E. Griffin, *Characterization of an in vitro model of alphavirus infection of immature and mature neurons.* J Virol, 2005. **79**(6): p. 3438-47.
180. Mundy, W.R. and T.M. Freudenrich, *Sensitivity of immature neurons in culture to metal-induced changes in reactive oxygen species and intracellular free calcium.* Neurotoxicology, 2000. **21**(6): p. 1135-44.
181. Bretscher, M.S., *Getting membrane flow and the cytoskeleton to cooperate in moving cells.* Cell, 1996. **87**(4): p. 601-6.
182. Janmey, P.A., *The cytoskeleton and cell signaling: component localization and mechanical coupling.* Physiol Rev, 1998. **78**(3): p. 763-81.
183. Koyama, T., et al., *Hypergravity induces ATP release and actin reorganization via tyrosine phosphorylation and RhoA activation in bovine endothelial cells.* Pflugers Arch, 2009. **457**(4): p. 711-9.

184. Versari, S., et al., *Alterations of the actin cytoskeleton and increased nitric oxide synthesis are common features in human primary endothelial cell response to changes in gravity.* Biochim Biophys Acta, 2007. **1773**(11): p. 1645-52.
185. Ingber, D.E., *Tensegrity I. Cell structure and hierarchical systems biology.* J Cell Sci, 2003. **116**(Pt 7): p. 1157-73.
186. Cooper, G., *The Cell: A Molecular Approach. 2nd edition.*, S. Associates, Editor. 2000.
187. Cogoli, M., et al., *Lymphocytes on sounding rockets.* Adv Space Res, 1992. **12**(1): p. 141-4.
188. Rosner, H., et al., *Effects of altered gravity on the actin and microtubule cytoskeleton of human SH-SY5Y neuroblastoma cells.* Protoplasma, 2006. **229**(2-4): p. 225-34.
189. Paloski, W.H., et al., *Recovery of postural equilibrium control following spaceflight.* Ann N Y Acad Sci, 1992. **656**: p. 747-54.
190. Anderson, D.J., et al., *Dynamic posture analysis of Spacelab-1 crew members.* Exp Brain Res, 1986. **64**(2): p. 380-91.
191. Black, F.O., et al., *Vestibular plasticity following orbital spaceflight: recovery from postflight postural instability.* Acta Otolaryngol Suppl, 1995. **520 Pt 2**: p. 450-4.
192. Paloski, W.H., et al., *Vestibular ataxia following shuttle flights: effects of microgravity on otolith-mediated sensorimotor control of posture.* Am J Otol, 1993. **14**(1): p. 9-17.
193. Krasnov, I.B., *Gravitational neuromorphology.* Adv Space Biol Med, 1994. **4**: p. 85-110.
194. Ross, M.D., *Morphological changes in rat vestibular system following weightlessness.* J Vestib Res, 1993. **3**(3): p. 241-51.
195. Martinelli, L.K., et al., *Effect of microgravity on immune cell viability and proliferation: simulation using 3-D clinostat.* IEEE Eng Med Biol Mag, 2009. **28**(4): p. 85-90.
196. Gruener, R. and G. Hoeger, *Vector-averaged gravity alters myocyte and neuron properties in cell culture.* Aviat Space Environ Med, 1991. **62**(12): p. 1159-65.
197. Frigeri, A., et al., *Effect of microgravity on gene expression in mouse brain.* Exp Brain Res, 2008. **191**(3): p. 289-300.
198. Cancedda, R., et al., *The Mice Drawer System (MDS) experiment and the space endurance record-breaking mice.* PLoS One, 2012. **7**(5): p. e32243.
199. Santucci, D., et al., *Evaluation of gene, protein and neurotrophin expression in the brain of mice exposed to space environment for 91 days.* PLoS One, 2012. **7**(7): p. e40112.
200. Reeves, G.I. and E.J. Ainsworth, *Description of the chronic radiation syndrome in humans irradiated in the former Soviet Union.* Radiat Res, 1995. **142**(2): p. 242-3.
201. Cucinotta, F.A., H. Nikjoo, and D.T. Goodhead, *The effects of delta rays on the number of particle-track traversals per cell in laboratory and space exposures.* Radiat Res, 1998. **150**(1): p. 115-9.
202. Cucinotta, F.A. and M. Durante, *Cancer risk from exposure to galactic cosmic rays: implications for space exploration by human beings.* Lancet Oncol, 2006. **7**(5): p. 431-5.
203. Joseph, J.A., et al., *Possible "accelerated striatal aging" induced by 56Fe heavy-particle irradiation: implications for manned space flights.* Radiat Res, 1992. **130**(1): p. 88-93.
204. Rabin, B.M., W.A. Hunt, and J.A. Joseph, *An assessment of the behavioral toxicity of high-energy iron particles compared to other qualities of radiation.* Radiat Res, 1989. **119**(1): p. 113-22.
205. Philpott, D.E., et al., *The effect of high energy (HZE) particle radiation (40Ar) on aging parameters of mouse hippocampus and retina.* Scan Electron Microsc, 1985(Pt 3): p. 1177-82.
206. D'Amelio, F.E., et al., *Synaptic plasticity in the cerebral cortex of mice: effects of radiation and anesthesia.* J Hirnforsch, 1983. **24**(5): p. 479-83.
207. Manda, K., M. Ueno, and K. Anzai, *Memory impairment, oxidative damage and apoptosis induced by space radiation: Ameliorative potential of α-lipoic acid.* Behavioural Brain Research, 2008. **187**(2): p. 387-395.

208. Manda, K., et al., *Radiation-induced cognitive dysfunction and cerebellar oxidative stress in mice: Protective effect of α-lipoic acid.* Behavioural Brain Research, 2007. **177**(1): p. 7-14.
209. Denisova, N.A., et al., *Brain signaling and behavioral responses induced by exposure to (56)Fe-particle radiation.* Radiat Res, 2002. **158**(6): p. 725-34.
210. Sanchez, M.C., G.A. Nelson, and L.M. Green, *Effects of Protons and HZE Particles on Glutamate Transport in Astrocytes, Neurons and Mixed Cultures.* Radiation Research, 2010. **174**(6a): p. 669-678.
211. Rola, R., et al., *Indicators of hippocampal neurogenesis are altered by 56Fe-particle irradiation in a dose-dependent manner.* Radiat Res, 2004. **162**(4): p. 442-6.
212. Manda, K. and R.J. Reiter, *Melatonin maintains adult hippocampal neurogenesis and cognitive functions after irradiation.* Progress in Neurobiology, 2010. **90**(1): p. 60-68.
213. Lewis, M.L., *The cytoskeleton, apoptosis, and gene expression in T lymphocytes and other mammalian cells exposed to altered gravity.* Adv Space Biol Med, 2002. **8**: p. 77-128.
214. Konstantinova, I., et al., *Study of reactivity of blood lymphoid cells in crew members of the Soyuz-6, Soyuz-7 and Soyuz-8 spaceships before and after flight.* Space Biol Med 1973. **7**: p. 48-55.
215. Kimzey, S.L., et al., *Hematology and immunology studies: the second manned Skylab mission.* Aviat Space Environ Med, 1976. **47**(4): p. 383-90.
216. Cogoli, A., *The effect of hypogravity and hypergravity on cells of the immune system.* J Leukoc Biol, 1993. **54**(3): p. 259-68.
217. Cogoli-Greuter, M., *Effect of Gravity Changes on the Cytoskeleton in Human.* LGrav Space Bioymphocytes Bull Acad Natl Med, 2004. **17**: p. 27-37.
218. Cogoli A and C.-G. M., *Cells of the immune system in space (lymphocytes).* , in *Biology in Space and Life on Earth*, B. E, Editor. 2007, Wiley-VCH. p. 193-222.
219. Smith-Garvin, J.E., G.A. Koretzky, and M.S. Jordan, *T cell activation.* Annu Rev Immunol, 2009. **27**: p. 591-619.
220. Leonard, W.J. and J.J. O'Shea, *Jaks and STATs: biological implications.* Annu Rev Immunol, 1998. **16**: p. 293-322.
221. Bachmann, M.F. and A. Oxenius, *Interleukin 2: from immunostimulation to immunoregulation and back again.* EMBO Rep, 2007. **8**(12): p. 1142-8.
222. A, C., *Cell Biology*, in *Fundamental of Space Biology*, Clement G and S. K, Editors. 2006, Springer: Heidelberg. p. 121 - 170
223. Hashemi BB, et al., *T cell activation response are differentially regulated during clinorotation and in spaceflight.* FASEB J 1999. **13**: p. 2071-2082.
224. Hughes-Fulford, M., et al., *Early immune response and regulation of IL-2 receptor subunits.* Cell Signal, 2005. **17**(9): p. 1111-24.
225. Boonyaratanakornkit, J.B., et al., *Key gravity-sensitive signaling pathways drive T cell activation.* FASEB J, 2005. **19**(14): p. 2020-2.
226. Cogoli-Greuter, M., et al., *Movements and interactions of leukocytes in microgravity.* J Biotechnol, 1996. **47**(2-3): p. 279-87.
227. Cogoli-Greuter M, et al., *Influence of microgravity on mitogen binding, motility and cytoskeleton patterns of T lymphocytes and Jurkat cells – experiments on sounding rocket.* Jap J Aerospace Env Med, 1998. **35**: p. 27-39.
228. Lewis, M.L., et al., *Spaceflight alters microtubules and increases apoptosis in human lymphocytes (Jurkat).* FASEB J, 1998. **12**(11): p. 1007-18.
229. Vadrucci S, et al., *Effects of vector-averaged gravity on the response to different stimulatory signals in T cells.* J Gravit Physiol Behav, 2005. **12**: p. 177-178.

230. Albrecht-Buehler, G. and R.D. Goldman, *Microspike-mediated particle transport towards the cell body during early spreading of 3T3 cells.* Exp Cell Res, 1976. **97**(2): p. 329-39.
231. Lichtenstein, N., B. Geiger, and Z. Kam, *Quantitative analysis of cytoskeletal organization by digital fluorescent microscopy.* Cytometry A, 2003. **54**(1): p. 8-18.
232. Horwitz, A.R. and J.T. Parsons, *Cell migration--movin' on.* Science, 1999. **286**(5442): p. 1102-3.
233. Pippia, P., et al., *Activation signals of T lymphocytes in microgravity.* J Biotechnol, 1996. **47**(2-3): p. 215-22.
234. Hatton, J.P., et al., *Microgravity modifies protein kinase C isoform translocation in the human monocytic cell line U937 and human peripheral blood T-cells.* J Cell Biochem, 2002. **87**(1): p. 39-50.
235. Sundaresan, A., D. Risin, and N.R. Pellis, *Loss of signal transduction and inhibition of lymphocyte locomotion in a ground-based model of microgravity.* In Vitro Cell Dev Biol Anim, 2002. **38**(2): p. 118-22.
236. Gershovich, J.G., et al., *The effects of prolonged gravity vector randomization on differentiation of precursour cells in vitro.* J Gravit Physiol, 2007. **14**(1): p. P133-4.
237. Romanov, Y., N. Kabaeva, and L. Buravkova, *Simulated hypogravity stimulates cell spreading and wound healing in cultured human vascular endothelial cells.* J Gravit Physiol, 2000. **7**(2): p. P77-8.
238. Scheglovitova, O.N., et al., *The Effect of Smooth Muscle Cells and Leukocytes on HSV-1 Reproduction in Cultured Human Endothelial Cells.* Russ J Immunol, 2000. **5**(2): p. 133-140.
239. Vincent, L., et al., *Combretastatin A4 phosphate induces rapid regression of tumor neovessels and growth through interference with vascular endothelial-cadherin signaling.* J Clin Invest, 2005. **115**(11): p. 2992-3006.
240. Li, J., et al., *Modeled microgravity causes changes in the cytoskeleton and focal adhesions, and decreases in migration in malignant human MCF-7 cells.* Protoplasma, 2009. **238**(1-4): p. 23-33.
241. Schatten, H., M.L. Lewis, and A. Chakrabarti, *Spaceflight and clinorotation cause cytoskeleton and mitochondria changes and increases in apoptosis in cultured cells.* Acta Astronaut, 2001. **49**(3-10): p. 399-418.
242. Vassy, J., et al., *The effect of weightlessness on cytoskeleton architecture and proliferation of human breast cancer cell line MCF-7.* FASEB J, 2001. **15**(6): p. 1104-6.
243. Lauffenburger, D.A. and A.F. Horwitz, *Cell migration: a physically integrated molecular process.* Cell, 1996. **84**(3): p. 359-69.
244. Yang, C., et al., *Coordination of membrane and actin cytoskeleton dynamics during filopodia protrusion.* PLoS One, 2009. **4**(5): p. e5678.
245. Reicher, B. and M. Barda-Saad, *Multiple pathways leading from the T-cell antigen receptor to the actin cytoskeleton network.* FEBS Lett, 2010. **584**(24): p. 4858-64.
246. Enomoto, T., *Microtubule disruption induces the formation of actin stress fibers and focal adhesions in cultured cells: possible involvement of the rho signal cascade.* Cell Struct Funct, 1996. **21**(5): p. 317-26.
247. Hu, Y.L., et al., *Roles of microtubule dynamics and small GTPase Rac in endothelial cell migration and lamellipodium formation under flow.* J Vasc Res, 2002. **39**(6): p. 465-76.
248. Fais, S. and W. Malorni, *Leukocyte uropod formation and membrane/cytoskeleton linkage in immune interactions.* J Leukoc Biol, 2003. **73**(5): p. 556-63.
249. Ullrich, O., K. Huber, and K. Lang, *Signal transduction in cells of the immune system in microgravity.* Cell Commun Signal, 2008. **6**: p. 9.

250. Valitutti, S., et al., *Sustained signaling leading to T cell activation results from prolonged T cell receptor occupancy. Role of T cell actin cytoskeleton.* J Exp Med, 1995. **181**(2): p. 577-84.
251. Hughes-Fulford, M. and M.L. Lewis, *Effects of microgravity on osteoblast growth activation.* Exp Cell Res, 1996. **224**(1): p. 103-9.
252. Buravkova, L.B. and Y.A. Romanov, *The role of cytoskeleton in cell changes under condition of simulated microgravity.* Acta Astronaut, 2001. **48**(5-12): p. 647-50.
253. Papaseit, C., N. Pochon, and J. Tabony, *Microtubule self-organization is gravity-dependent.* Proc Natl Acad Sci U S A, 2000. **97**(15): p. 8364-8.
254. Cox, E.A. and A. Huttenlocher, *Regulation of integrin-mediated adhesion during cell migration.* Microsc Res Tech, 1998. **43**(5): p. 412-9.
255. Ezzell, R.M., et al., *Vinculin promotes cell spreading by mechanically coupling integrins to the cytoskeleton.* Exp Cell Res, 1997. **231**(1): p. 14-26.
256. Goldmann, W.H. and D.E. Ingber, *Intact vinculin protein is required for control of cell shape, cell mechanics, and rac-dependent lamellipodia formation.* Biochem Biophys Res Commun, 2002. **290**(2): p. 749-55.
257. Pirone, D.M., et al., *An inhibitory role for FAK in regulating proliferation: a link between limited adhesion and RhoA-ROCK signaling.* J Cell Biol, 2006. **174**(2): p. 277-88.
258. Osborn, M. and K. Weber, *Cytoplasmic microtubules in tissue culture cells appear to grow from an organizing structure towards the plasma membrane.* Proc Natl Acad Sci U S A, 1976. **73**(3): p. 867-71.
259. P., T., *Gravity-dependent phenomena at the scale of the single cell.* ASGSB Bull 1989. **2**: p. 95–113.
260. Ingber, D.E., *Tensegrity: the architectural basis of cellular mechanotransduction.* Annu Rev Physiol, 1997. **59**: p. 575-99.
261. Stowe, R.P., C.F. Sams, and D.L. Pierson, *Effects of mission duration on neuroimmune responses in astronauts.* Aviat Space Environ Med, 2003. **74**(12): p. 1281-4.
262. Kaur, I., et al., *Changes in monocyte functions of astronauts.* Brain Behav Immun, 2005. **19**(6): p. 547-54.
263. Cogoli, A., *The effect of space flight on human cellular immunity.* Environ Med, 1993. **37**(2): p. 107-16.
264. Hatton JP, et al., *The kinetics of translocation and cellular quantity of protein kinase C in human leukocytes are modified during spaceflight.* FASEB J, 1999. **13**: p. 23-33.
265. Schmitt, D.A., et al., *The distribution of protein kinase C in human leukocytes is altered in microgravity.* FASEB J, 1996. **10**(14): p. 1627-34.
266. Hughes-Fulford M and L.C. Chang T, *Effect of Gravity on Monocyte Differentiation.* J Grav Physiol 2008. **15**: p. 145-146.
267. L.B., B., G. O.V., and R. M.P., *The effect of microgravity on the in vitro NK cell function during six International Space Station Missions.* Microgravity Sci Technol 2007. **19**: p. 145-147.
268. Jessell, T., Cell migration and axon guidance. In: Kandel ER, Schwartz JH, Jessell TM, editors. Principles of neural science. New York, NY: Elsevier Science Publishing Co. Inc.; 1991. p. 908–28.
269. Raineteau, O., et al., *Neurogenesis in hippocampal slice cultures.* Mol Cell Neurosci, 2004. **26**(2): p. 241-50.
270. Perez-Gomez, A. and R.A. Tasker, *Enhanced neurogenesis in organotypic cultures of rat hippocampus after transient subfield-selective excitotoxic insult induced by domoic acid.* Neuroscience, 2012. **208**: p. 97-108.
271. Zanella, F., J.B. Lorens, and W. Link, *High content screening: seeing is believing.* Trends Biotechnol, 2010. **28**(5): p. 237-45.

272. Perlman, Z.E., et al., *Multidimensional drug profiling by automated microscopy.* Science, 2004. **306**(5699): p. 1194-8.
273. Laketa, V., et al., *High-content microscopy identifies new neurite outgrowth regulators.* Mol Biol Cell, 2007. **18**(1): p. 242-52.
274. Meijering, E., *Neuron tracing in perspective.* Cytometry A, 2010. **77**(7): p. 693-704.
275. Abramoff MD, M.P., Ram SJ, *Image processing with ImageJ.* Biophotonics Int 2004. **11**: p. 36–42.
276. Meijering, E., et al., *Design and validation of a tool for neurite tracing and analysis in fluorescence microscopy images.* Cytometry A, 2004. **58**(2): p. 167-76.
277. Pool, M., et al., *NeuriteTracer: a novel ImageJ plugin for automated quantification of neurite outgrowth.* J Neurosci Methods, 2008. **168**(1): p. 134-9.
278. Narro, M.L., et al., *NeuronMetrics: software for semi-automated processing of cultured neuron images.* Brain Res, 2007. **1138**: p. 57-75.
279. Ho, S.Y., et al., *NeurphologyJ: an automatic neuronal morphology quantification method and its application in pharmacological discovery.* BMC Bioinformatics, 2011. **12**: p. 230.
280. Schneider, C.A., W.S. Rasband, and K.W. Eliceiri, *NIH Image to ImageJ: 25 years of image analysis.* Nat Methods, 2012. **9**(7): p. 671-5.
281. Johnson, V.L., et al., *Effector caspases are dispensable for the early nuclear morphological changes during chemical-induced apoptosis.* J Cell Sci, 2000. **113 (Pt 17)**: p. 2941-53.
282. Gobbel, G.T., et al., *Response of postmitotic neurons to X-irradiation: implications for the role of DNA damage in neuronal apoptosis.* J Neurosci, 1998. **18**(1): p. 147-55.
283. Ziegler, U. and P. Groscurth, *Morphological features of cell death.* News Physiol Sci, 2004. **19**: p. 124-8.
284. Huang, L.-K.W., M-J J, <*Huang- Image thresholding by minimizing the measure of fuzziness4.pdf*>. Pattern Recognition 1995. **28**(1): p. 41-51.
285. Ridler, T.C., S, *Picture thresholding using an iterative selection method.* IEEE Transactions on Systems, Man and Cybernetics 1978. **8**: p. 630-632.
286. Prewitt, J.M. and M.L. Mendelsohn, *The analysis of cell images.* Ann N Y Acad Sci, 1966. **128**(3): p. 1035-53.
287. Tsai, W.C., *Moment-preserving thresholding: a new approach.* Computer Vision, Graphics, and Image Processing, 1985. **29**(377-393).
288. Kegl, B. and A. Krzyzak, *Piecewise linear skeletonization using principal curves.* IEEE Transactions on Pattern Analysis and Machine Intelligence, 2002.
289. Lamprecht, M.R., D.M. Sabatini, and A.E. Carpenter, *CellProfiler: free, versatile software for automated biological image analysis.* Biotechniques, 2007. **42**(1): p. 71-5.
290. Möller, M., L. Lymburner, and V. M., *The comparison index: A tool for assessing the accuracy of image segmentation.* International Journal of Applied Earth Observation and Geoinformation, 2007. **9**(3): p. 311–321.
291. Saffor, A., A.R. Ramli, and K.-H. Ng, *A COMPARATIVE STUDY OF IMAGE COMPRESSION BETWEEN JPEG AND WAVELET.* Malaysian Journal of Computer Science, 2001. **14**(1): p. 39-45.
292. Gonzalez, R.C. and R.E. Woods, *"Digital Image Processing," Third Edition, Prentice Hall2008. ISBN: 013168728.*
293. Daniel, S., *SNR, PSNR, RMSE, MAE.* http://bigwww.epfl.ch/sage/soft/snr/, 2011.
294. Zhang, J.H., T.D. Chung, and K.R. Oldenburg, *A Simple Statistical Parameter for Use in Evaluation and Validation of High Throughput Screening Assays.* J Biomol Screen, 1999. **4**(2): p. 67-73.
295. Liu, Y., *The DIADEM and beyond.* Neuroinformatics, 2011. **9**(2-3): p. 99-102.
296. Svoboda, K., *The past, present, and future of single neuron reconstruction.* Neuroinformatics, 2011. **9**(2-3): p. 97-8.

297. De Vylder, J., et al., *A novel dictionary based computer vision method for the detection of cell nuclei.* PLoS One, 2013. **8**(1): p. e54068.
298. Cheng, J. and J.C. Rajapakse, *Segmentation of clustered nuclei with shape markers and marking function.* IEEE Trans Biomed Eng, 2009. **56**(3): p. 741-8.
299. Samari, N., et al., *Non-conventional apoptotic response to ionising radiation mediated by N-methyl D-aspartate receptors in immature neuronal cells.* Int J Mol Med, 2013.
300. Chothani, P., V. Mehta, and A. Stepanyants, *Automated tracing of neurites from light microscopy stacks of images.* Neuroinformatics, 2011. **9**(2-3): p. 263-78.
301. Wang, Y., et al., *A broadly applicable 3-D neuron tracing method based on open-curve snake.* Neuroinformatics, 2011. **9**(2-3): p. 193-217.
302. Livet, J., et al., *Transgenic strategies for combinatorial expression of fluorescent proteins in the nervous system.* Nature, 2007. **450**(7166): p. 56-62.
303. Feng, G., et al., *Imaging neuronal subsets in transgenic mice expressing multiple spectral variants of GFP.* Neuron, 2000. **28**(1): p. 41-51.
304. Fuchs, H.S., *Man in weightlessness: physiological problems, clinical aspects, prevention and protection. Related bio-medical research in micro-gravity during the forecoming SPACELAB missions.* Riv Med Aeronaut Spaz, 1980. **43**(3-4): p. 332-46.
305. Nicogossian, A., et al., *Assessment of the efficacy of medical countermeasures in space flight.* Acta Astronaut, 1988. **17**(2): p. 195-8.
306. Moore, T.P. and W.E. Thornton, *Space shuttle inflight and postflight fluid shifts measured by leg volume changes.* Aviat Space Environ Med, 1987. **58**(9 Pt 2): p. A91-6.
307. Newberg, A.B., *Changes in the central nervous system and their clinical correlates during long-term spaceflight.* Aviat Space Environ Med, 1994. **65**(6): p. 562-72.
308. Battista, N., et al., *Effect of RNAlater on lipoxygenase activity and expression, and immune cell apoptosis: opening the gate to the "ROALD" experiment aboard the space shuttle.* J Gravit Physiol, 2007. **14**(1): p. P131-2.
309. Slenzka, K., *Neuroplasticity changes during space flight.* Adv Space Res, 2003. **31**(6): p. 1595-604.
310. Vazquez, M.E., *Neurobiological problems in long-term deep space flights.* Adv Space Res, 1998. **22**(2): p. 171-83.
311. Vein, A.A., et al., *Space headache: a new secondary headache.* Cephalalgia, 2009. **29**(6): p. 683-6.
312. Anken, R.H., M. Ibsch, and H. Rahmann, *Microgravity (STS-90 Neurolab-Mission) influences synapse formation in a vestibular nucleus of fish brain.* Adv Space Res, 2002. **30**(4): p. 843-7.
313. Kim, J.A., et al., *Cytoskeleton disruption causes apoptotic degeneration of dentate granule cells in hippocampal slice cultures.* Neuropharmacology, 2002. **42**(8): p. 1109-18.
314. Borst, A.G. and J.J.W.A. van Loon, *Technology and Developments for the Random Positioning Machine, RPM.* Microgravity Science and Technology, 2009. **21**: p. 287-292
315. Popko, J., et al., *Automated analysis of NeuronJ tracing data.* Cytometry A, 2009. **75**(4): p. 371-6.
316. Mi, H., A. Muruganujan, and P.D. Thomas, *PANTHER in 2013: modeling the evolution of gene function, and other gene attributes, in the context of phylogenetic trees.* Nucleic Acids Res, 2013. **41**(Database issue): p. D377-86.
317. Guan, K.L. and Y. Rao, *Signalling mechanisms mediating neuronal responses to guidance cues.* Nat Rev Neurosci, 2003. **4**(12): p. 941-56.
318. Huber, A.B., et al., *Signaling at the growth cone: ligand-receptor complexes and the control of axon growth and guidance.* Annu Rev Neurosci, 2003. **26**: p. 509-63.
319. Crawford-Young, S.J., *Effects of microgravity on cell cytoskeleton and embryogenesis.* Int J Dev Biol, 2006. **50**(2-3): p. 183-91.

320. Grosse, J., et al., *Short-term weightlessness produced by parabolic flight maneuvers altered gene expression patterns in human endothelial cells.* FASEB J, 2012. **26**(2): p. 639-55.
321. Uzbay, T., *Alzheimer disease and neuroplasticity: New approaches and new targets in pharmacotherapy.* Marmara Pharmaceutical Journal, 2012. **16**: p. 65-76.
322. Fuchs, E., et al., *Alterations of neuroplasticity in depression: the hippocampus and beyond.* Eur Neuropsychopharmacol, 2004. **14 Suppl 5**: p. S481-90.
323. Lucassen, P.J., E. Fuchs, and B. Czeh, *Antidepressant treatment with tianeptine reduces apoptosis in the hippocampal dentate gyrus and temporal cortex.* Biol Psychiatry, 2004. **55**(8): p. 789-96.
324. O'Brien, P.J., et al., *Cardiac troponin T is a sensitive, specific biomarker of cardiac injury in laboratory animals.* Lab Anim Sci, 1997. **47**(5): p. 486-95.
325. Riley, D.A., et al., *Skeletal muscle fiber, nerve, and blood vessel breakdown in space-flown rats.* FASEB J, 1990. **4**(1): p. 84-91.
326. Harris, S.L. and A.J. Levine, *The p53 pathway: positive and negative feedback loops.* Oncogene, 2005. **24**(17): p. 2899-908.
327. Blaber, E., H. Marcal, and B.P. Burns, *Bioastronautics: the influence of microgravity on astronaut health.* Astrobiology, 2010. **10**(5): p. 463-73.
328. Thiel, C.S., et al., *Rapid alterations of cell cycle control proteins in human T lymphocytes in microgravity.* Cell Commun Signal, 2012. **10**(1): p. 1.
329. Donald, R., *Radiation effects and shielding requirements in human missions to the moon and Mars.* Mars 2, 2006: p. 46-71.
330. Armstrong, T.W. and B.L. Colborn, *Predictions of secondary neutrons and their importance to radiation effects inside the International Space Station.* Radiat Meas, 2001. **33**(3): p. 229-34.
331. Rizzo, A.M., et al., *Effects of long-term space flight on erythrocytes and oxidative stress of rodents.* PLoS One, 2012. **7**(3): p. e32361.
332. Mills, K.D., D.O. Ferguson, and F.W. Alt, *The role of DNA breaks in genomic instability and tumorigenesis.* Immunol Rev, 2003. **194**: p. 77-95.
333. Olive, P.L., *The role of DNA single- and double-strand breaks in cell killing by ionizing radiation.* Radiat Res, 1998. **150**(5 Suppl): p. S42-51.
334. Lisby, M., et al., *Cell cycle-regulated centers of DNA double-strand break repair.* Cell Cycle, 2003. **2**(5): p. 479-83.
335. Okamoto, M., et al., *Effect of radiation on the development of immature hippocampal neurons in vitro.* Radiat Res, 2009. **172**(6): p. 718-24.
336. Cherry, J.D., et al., *Galactic cosmic radiation leads to cognitive impairment and increased abeta plaque accumulation in a mouse model of Alzheimer's disease.* PLoS One, 2012. **7**(12): p. e53275.
337. Beck, M., et al., *Simulated microgravity decreases apoptosis in fetal fibroblasts.* Int J Mol Med, 2012. **30**(2): p. 309-13.
338. Mastroleo, F., et al., *Experimental design and environmental parameters affect Rhodospirillum rubrum S1H response to space flight.* ISME J, 2009. **3**(12): p. 1402-19.
339. Mancuso, M., et al., *Dose and spatial effects in long-distance radiation signaling in vivo: implications for abscopal tumorigenesis.* Int J Radiat Oncol Biol Phys, 2013. **85**(3): p. 813-9.
340. Schwartz, E.I., et al., *Cell cycle activation in postmitotic neurons is essential for DNA repair.* Cell Cycle, 2007. **6**(3): p. 318-29.
341. Townsend, L.W. and R.J. Fry, *Radiation protection guidance for activities in low-Earth orbit.* Adv Space Res, 2002. **30**(4): p. 957-63.
342. Helleday, T., et al., *DNA double-strand break repair: from mechanistic understanding to cancer treatment.* DNA Repair (Amst), 2007. **6**(7): p. 923-35.

343. Jackson, S.P., *Sensing and repairing DNA double-strand breaks.* Carcinogenesis, 2002. **23**(5): p. 687-96.
344. Cucinotta, F.A., et al., *Biochemical kinetics model of DSB repair and induction of gamma-H2AX foci by non-homologous end joining.* Radiat Res, 2008. **169**(2): p. 214-22.
345. Manton, K.G., S. Volovik, and A. Kulminski, *ROS effects on neurodegeneration in Alzheimer's disease and related disorders: on environmental stresses of ionizing radiation.* Curr Alzheimer Res, 2004. **1**(4): p. 277-93.
346. Tomashevski, A., et al., *Cyclin-C-dependent cell-cycle entry is required for activation of non-homologous end joining DNA repair in postmitotic neurons.* Cell Death Differ, 2010. **17**(7): p. 1189-98.
347. Nakaya, K., et al., *Sensitivity to radiation-induced apoptosis and neuron loss declines rapidly in the postnatal mouse neocortex.* Int J Radiat Biol, 2005. **81**(7): p. 545-54.
348. Sarkar, P., et al., *Proteomic analysis of mouse hypothalamus under simulated microgravity.* Neurochem Res, 2008. **33**(11): p. 2335-41.
349. Jeggo, P. and M.F. Lavin, *Cellular radiosensitivity: how much better do we understand it?* Int J Radiat Biol, 2009. **85**(12): p. 1061-81.
350. Su, T.T., *Cellular responses to DNA damage: one signal, multiple choices.* Annu Rev Genet, 2006. **40**: p. 187-208.
351. Deckbar, D., P.A. Jeggo, and M. Lobrich, *Understanding the limitations of radiation-induced cell cycle checkpoints.* Crit Rev Biochem Mol Biol, 2011. **46**(4): p. 271-83.
352. Maier, J.A., *Impact of simulated microgravity on cell cycle control and cytokine release by U937 cells.* Int J Immunopathol Pharmacol, 2006. **19**(2): p. 279-86.
353. Durante, M., *Biomarkers of space radiation risk.* Radiat Res, 2005. **164**(4 Pt 2): p. 467-73.

Acknowledgements

Life is a long journey made of short trips which allow to grow up and become mature enough to share your knowledge, at the end or during each of its steps. These last four/five years have been the most amazing trip I have ever done, learning thinks that I never thought to learn and living in a multi-ethnic community. Therefore, I cannot close this trip without thanking all those people who supported, guided and taught me during this period far away from my native land.

First of all, I would like to thank **Prof. Sarah Baatout** and **Dr. MariAntonia Meloni**, since it is thanks to their cross collaboration that I got the opportunity to do this PhD. I would like to thank **Prof. Sarah Baatout** for welcoming me in her laboratory, for supervising my PhD over the whole period as SCK•CEN mentor initially and as promoter in the last period, for giving me the opportunity to participate in many conferences and courses, but also for contributing to improve my scientific work, especially in writing my articles and this PhD thesis, and for motivating me in these moments of doubt, *especially at the end*. I would also like to thank **Dr. Rafi Benotmane** for following me over the whole period of the PhD, for having spent long hours in discussions on experimental organization, on the results and discussion obtained and in the writing of articles and the PhD thesis. Finally, I want to also thank him for encouraging me every time that I had doubts on my reasoning or when the bad luck was persecuting me. I would like to thank also **Dr. Louis de Saint-Georges** for supporting me with his knowledge on radiation protection and for all the long discussions and suggestions related to the neuron behaviour and microscopy analysis specially during the development of the "MorphoNeuroNet" software. I would like to thank also my promoter **Prof. Patrick van Oostveldt** for accepting me as a PhD student at Ghent University and, despite his retirement two years ago, for supervising me until the end of this PhD.

I would also like to give particular thanks to **Dr. Winnok De Vos**, master in bio-imaging, for teaching me many microscopy analysis secrets and for following and reviewing the writing of articles on MorphoNeuroNet and DNA damage. I would like to express my gratitude to **Dr. Roel Quintens** for giving me his time, for helping me with the microarray analyses and for reading and commenting my texts. I would like to thank also those people who helped me practically in the laboratory such as **Liselotte Leysen** for the mouse mating and dissection management and her effort to meet sometimes very complex schedules as well as **Kevin Tabury** and **Bart Marlein** for helping to set the facility during the experiments in simulated space conditions. Many thanks also to **Arlette Michaux** and **Ann Janssen** for their precious help when extracting RNA and performing microarrays, and to **Mieke Neefs** and **Jasmine Buset** for helping me with neuronal cell culture.

When I arrived here, it was such an adventure! I had landed at Eindhoven airport on a Saturday morning at 7 and could only reach Boeretang at 1 pm due to the missing taxi at my arrival. When I realized that the taxi would not be coming to fetch me at the airport, my first questions were "Where am I?" and "Now, how can I reach Mol?". My luck was that MariAntonia had given me the phone number of **Dr. Felice Mastroleo** (thanks Felice) who was so kind to book the taxi to finally pick me up 1h later at the airport. I finally arrived to SCK•CEN where I found a welcoming committee composed of **Khalil Abouelaradat** and **Myriam Ghardi**, two PhD students in radiobiology at that time, who kindly helped me for the accommodation and the shopping over the weekend. Thank God, Khalil was there for explaining me all tips about Boeretang life and, on the following Monday, for accompanying me in the laboratory where, for the first time, I met Rafi. He kindly introduced me to the MCB group during the Monday lab meeting. At the time, **Michaël Beck** and **Nada Samari**, two other PhD students in radiobiology, were already there. I was appointed in the same office with all of them (on the GKD roof) and we shared a lot of unforgettable moments all together, in the laboratories as well as outside during conferences, courses or social activities. **Michaël** and I spent a lot of time discussing on two main topics: space and photography. During the social activities, we were always the picture guys immortalizing people with witness face or positions, in particular shooting **Myriam** who was always shouting immediately thereafter "Please Deleeeete !!!!!☺". Since **Nada** and I had complementary projects we always worked together sharing not only mice, materials and reagents but also lucky and unlucky periods in the lab, preparing neuron cultures until our dinner time (9 pm or over). I would like to thank her not only for teaching me how to dissect foetal brains but also for all those moments that we supported each other when something was going wrong. Later also **Hussein El Saghire** joined us initially as a stagiair and later as a PhD student. With him I spent great moments especially in the dormitories, discussing about a wide variety of serious topics as work, religion, politics and others as well as everyday life or complaining about these people who were loudly speaking at night in the kitchen, since he had a room close to the kitchen and that I was right below the kitchen. Within these years, I shared the roof office with **Aurélie Crabbé**, **Matthias D'huyvetter**, **Annelies Suetens** and **Sheridan Nicole**. After moving, **Tine Verreet** joined Annelies and me in the new office close to the GKD medical service. In, as well as out of office, I shared great and weak moments with all of them. I want to thank especially **Annelies** and **Tine** for the support during the writing of the thesis. My thanks also to **Charlotte Rombouts** for kindly translating the summary of this thesis to Ducth language and **Annelies** for the last minute changes. I would like to thank also all the other colleagues with whom I was pleased to share professional and social events during my PhD

such as **Dr. Paul Jacquet**, **Dr. Hanane Derradji**, **Dr. Marjan Moreels, Dr. An Aerts, Marlies Gijs**, **Hanène Badri**, **Salem Ben Hamouda** and **Tom Verbiest.** I would like to thank **Hans Vanmarcke** and **Frank Hardeman** for their kind support. My thanks also to **Betty Vandingelen** and **Sofie De Schynckel** for always be ready to help in administrative issues.

I would like to thank **Dr. Daniela Santucci** for opened collaboration, the possibility that she gave me to work on brains of mice which had been aboard the International Space Station and to have accepted to be a member of the jury for PhD defence. I will never forget the moments passed in and out the laboratory with **Miriam Mura** for preparing her master thesis at SCK•CEN. I also want also to thank **Dr.Marianne Cogoli-Greuter** and **Dr. Augusto Cogoli** as well as **Dr. Meloni MariaAntonia, Prof. Proto Pippia**, **Dr. Grazia Galleri**, **Dr. Angela Saba** and **Gavino Campus** for keeping the collaboration during my PhD.

Last, but not least, **my father** and **my mother** for their support over the whole PhD as well as my *nonna* **Nonna** who wished and prayed for me for all the best and for every single moment. My special thanks to my sweet heart **Irene** (**Dr. Briguglio**) with whom I shared great and weak moments, supporting each other over this period spent far away from my native land, for every time she fought against her flight phobia to stay together, for waiting for me until I was back and for replying "YES" when I asked to live together the rest of our life. Thanks also to **Graziella** and **Salvatore** who supported Irene and me during our doctorates. I will never forget all the best friends that I found in the "Boeretang Kingdom" as **Davide**, **Gabriella**, **Angela**, **Fernando**, **Annelies**, **Riccardo**, **Kevin**, **Hussein**, **Massimo**, **Fulvio**, **Evelien**, **Julie**, **Clarita**, **Nathalie**, **Alexey** and the **whole Italian team 2008-2013** (more than 40 people). *Dulcis in fundo,* I will never forget all "Boeretang Kingdom" people with whom I spent a lot of my free time enjoying social events.

Curriculum Vitae

CURRICULUM VITAE

GIUSEPPE PANI

Current address
Boeretang 204/42
2400 Mol
Belgium
0032-476056970 (Belgian mobile)
0039-3496087543 (Italian mobile)
giuseppe_pani@tiscali.it

Gender
Male

Education

- PhD in Applied Biological Sciences, Faculty of Bioscience Engineering, University of Ghent, Belgium, defence on June 19 2013.
- Master degree in Biological Sciences (Physiopathology), Faculty of Mathematics, Physics and Natural Sciences, University of Sassari, Italy. March 2008.

Honors and Awards

- PhD grant for 3 academic years (12/2008-12/2011) from the Sardinian government in the framework of the "Master and Back" programme.
- AWM PhD grant (01/2012-04/2013) from SCK•CEN and University of Ghent.
- ESA Education sponsorship to participate at the ELGRA Symposium 2009 "In the Footsteps of Columbus", Bonn, Germany. September 1-4, 2009. The funding covered the registration fees and a contribution towards travel and accommodation expenses.
- Travel grant to participate to the "9th European Workshop on Astrobiology" (EANA'09), Brussels, Belgium. October 12-14, 2009.
- Partial fee grant to participate at the CAREX (coordinated action on extreme environments) Conference on Life in Extreme Environments, Dublin, Ireland. October 18-20, 2011.
- 9th place at the "2008 European Sigma ANTIBODY Photo Award". Immunofluorescence competition for the first 10 best photos at the European level using Sigma secondary antibodies. The prize was the Photo Book "LIFE" of Lennart Nilsson. November, 2008.
- Chairman for the radiation session at ESA, ISGP, ISSBB, and ELGRA Joint Life Science Meeting: 'Life in Space for Life on Earth', Trieste, Italy, June 13-18, 2010.
- Poster Award at the "9th European Workshop on Astrobiology" for "Radiation and low gravity effects on neuronal cell cultures", authors **Pani G.**, Samari N., de Saint-Georges L., Meloni M.A., Baatout S., Van Oostveldt P., Benotmane M.A. EANA'09 Brussels, Belgium. October 12-14, 2009.
- Selected image of monocyte cytoskeleton for book cover of "Colture cellulari" (cell cultures) written by Meloni Mariantonia, Aracne Editor, 2012.
- Selected image of monocyte cytoskeleton by the European Space Agency for the brochure about Luca Palmittano's mission to ISS, 2013.
- Selected image of post-synaptic proteins in neuronal network for the semi-final (first 12) at the "International Antibody Image Contest 2013" organized by Sigma Aldrich (final result will be officialised after 15 of June)..

Reference experience

- Effects of space conditions on neuronal plasticity and connectivity, laboratories of Prof. Sarah Baatout and Prof. Patrick Van Oostveldt, Belgian Nuclear Research Center (SCK•CEN) and University of Gent, Belgium, November 2008- June 2013.
- Cytoskeleton recovery under simulated microgravity, Laboratory of Prof. Proto Pippia and Dr. Meloni Mariantonia, University of Sassari, Italy, April 2008.
- Investigation on cell locomotion and cytoskeleton in monocytes exposed to ISS environment, Laboratory of Prof. Proto Pippia and Dr. Meloni Mariantonia, University of Sassari, Italy, April 2005 – March 2008.

Teaching experience

- 15 hours of lectures and laboratory practice on space neurobiology, brain dissection, primary neuron cultures and immunostaining of DSBs and cytoskeletal structures to students following the European MSc in Radiation Biology, 2010-2013, SCK•CEN, Mol, Belgium.
- 4 hours of lectures and laboratory practice on space neurosciences and design of biological spaceflight experiments to students following the Course on Life Sciences and Biology in Space in the framework of the Advanced Master in Space Sciences, KUL-UGent, 2010-2011-2012, SCK•CEN, Mol, Belgium.
- Two lectures on microscope settings and capture of digital images at the Molecular Biology and Cytometry Course, Belgian Society for Analytical Cytometry, May 2009, May 2011, SCK•CEN, Mol, Belgium.

Follow-up of students

- Miriam Mura- *"Microtubule recovery in human monocytes during exposure to RPM after nocodazole treatment"*. University of Sassari, Italy, November 2008, Bachelor thesis.
- Miriam Mura- *"Cytoskeleton recovery in human monocytes after simulated space condition exposure"*. University of Sassari, April 2011, Italy, Master thesis.
- Christelle Meulepas- *"Rôle du gène TP53 dans la croissance des extensions neuronales"*. HELHA Haute Ecole Louvain en Hainaut, June 2012, Bachelor thesis.

Publications with Peer Review

- Meloni M., Galleri G., **Pani G**., Saba A., Pippia P., Cogoli-Greuter M. Space flight affects motility and cytoskeletal structures in human monocyte cell line J-111. In: Cytoskeleton, 68:2(2011), p. 125-137.- ISSN 1949-3592 (Meloni, Galleri, Pani have made equal contributions to this work)
- Samari N., de Saint-Georges L., **Pani G.**, Baatout S., Leyns L., Benotmane M.A. Non-conventional apoptotic response to ionising radiation mediated by N-methyl D-aspartate receptors in immature neuronal cells. International Journal of Molecular Medicine, 31(3) (March 2013), p.516-24. doi: 10.3892/ijmm.2013.1245. Epub 2013 Jan 15
- **Pani G.**, Samari N., Quintens R., de Saint Georges L., Meloni M.A., Baatout S., Van Oostveldt P., Benotmane M.A. Morphological and physiological changes in mature in vitro neuronal networks towards exposure to short-, middle- or long-term simulated microgravity. Conditionally accepted in PlosOne with minor revisions on May 30
- **Pani G.**, De Vos W., Samari N., de Saint Georges L., Baatout S., Van Oostveldt P., Benotmane M.A. MorphoNeuroNet, an automated method for dense neurite network analysis. Conditionally accepted with major revision in Cytometry part A and revised version submitted in June 2013
- Samari N., **Pani G**, Quintens R, Michaux A., Janssen A., de Saint-Georges L., Baatout S., Leyns L., Benotmane M.A.. Maturing neurons exhibit a delay in neurite outgrowth upon exposure to low and moderate doses of ionising radiation. Submitted to Radiation Research Journal and accepted with major revisions in October 2012

Oral presentations

- Pippia P., Galleri G., Meloni M.A., Saba A., **Pani G.**, Cogoli A. and Cogoli-Greuter M. Modelled microgravity conditions alter human monocytes motility and cytoskeleton pattern. Comunicazione al 1st Convegno Nazionale di Biomedicina e Spazio, Monte Porzio Catone, Italy. March 14-15, 2006. (presented by Pippia)
- Meloni M.A., Galleri G., Saba A., **Pani G.**, Pippia P., Cogoli-Greuter M. Microgravity affects immune cells. 4th European Congress Medicine in space and in extreme environments achievements for health care on earth. Berlin, Germany. October 24-26, 2007.
- **Pani G.** Effect of space conditions on neuronal plasticity and connectivity. WE-Heraeus Physics Winter School: Advanced Lectures on Protection of Humans and Their Environment Against Ionizing Radiation, Bad Honnef, Germany. February 9 – 18, 2009.
- Meloni M.A., **Pani G.**, Galleri G., Pippia P., Cogoli A., Cogoli-Greuter M. Recovery of microtubular network in simulated low gravity in human monocytes pretreated with nocodazole. ELGRA Symposium: "In the Footsteps of Columbus", Bonn, Germany. September 1-4, 2009.
- **Pani G**. Effect of space conditions on neuronal plasticity and connectivity. Day of the PhD. Mol, Belgium. October 29, 2009.
- Samari N., Abou-El-Ardat K., **Pani G.**, de Saint-Georges L., Baatout S., Leyns L., Benotmane MA. Low doses of irradiation on nervous cells impairs neurite outgrowth and causes neuronal degeneration. Third European IRPA congress. Helsinki, Finland. June 14-18, 2010.
- **Pani G.**, Samari N., de Saint-Georges L., Meloni M.A., Baatout S., Van Oostveldt P., Benotmane M. A. DNA damage/repair dynamics in neuronal networks after X-ray exposure under low gravity conditions. European Space Agency (ESA); International Society for Gravitational Physiology (ISGP); ISSBB Symposium; European Low Gravity Research Association (ELGRA) - Joint Life Science Meeting: 'Life in Space for Life on Earth'. Trieste, Italy. June 13-18, 2010.
- Benotmane R., Samari N., **Pani G.**, Quintens R., Janssen A., Michaux A., e.a. Molecular and cellular effects of embryonic irradiation on Cognitive functions. European Master in Radiation Biology. Mol, Belgium, February 14-25, 2011.
- **Pani G.**, Samari N., de Saint-Georges L., Meloni M.A., Baatout S., Van Oostveldt P., Benotmane M.A. Simulated low gravity effects on neuronal network plasticity. ELGRA 2011. Antwerp, Belgium. September 5-9, 2011.
- **Pani G.**, Mura M.M., Meloni M.A., Pippia P., Baatout S. Monocyte cytoskeleton recovery after simulated space conditions. ELGRA 2011. Antwerp, Belgium. September 5-9, 2011.
- Fortunati A., **Pani G.**, Vanhoudt N., Tassone P., Loreto F., Calfapietra C., Baatout S., Vandenhove H., Migliaccio F. Root growth pattern is altered by simulated space environment (SSE): effect of microgravity and radiations. CAREX Conference on Life in Extreme Environments. Dublin, Ireland. October 18-20, 2011.
- **Pani G.** Neuronal network analysis: MorphoNeuroNet.- Journal club. SCK•CEN, Mol, Belgium. February 3, 2012.
- **Pani G.**, Samari N., Quintens R., de Saint-Georges L., Meloni M., Baatout S., Van Oostveldt P., Benotmane M.A. Effect of space conditions on neuronal plasticity and connectivity. Day of the PhD's, SCK•CEN, Mol, Belgium. April 27, 2012.

Poster Presentations

- **Pani G.,** Meloni M. A., Galleri G., Saba A., Pippia P., CogoliA., Cogoli-Greuter M. Effect of space conditions on neuronal plasticity and connectivity. Italian Society for Space Biomedicine and Biotechnology 4th National Conference "Un mondo senza gravità", Santa Margherita Ligure, Italy. March 31 – April 2, 2009.
- **Pani G.**, Meloni M.A., Galleri G., Saba A., Pippia P., Cogoli A., Cogoli-Greuter M. Microtubular recovery in modelled low gravity conditions after nocodazole treatment of human monocytes. Italian Society for Space Biomedicine and Biotechnology 4th National Conference "Un mondo senza gravità", Santa Margherita Ligure, Italy. March 31 – April 2, 2009.
- Saba A., Larorsa D.R., Valenti G., Galleri G., **Pani G.**, Meloni M. A., Pippia P. *In vivo* rat experiments in Random Positioning Machine: Bone marrow cell mineralization and water transport. Italian Society for Space Biomedicine and Biotechnology 4° National Conference "Un mondo senza gravità", Santa Margherita Ligure, Italy. March 31 – April 2, 2009.
- Saba A., Galleri G., **Pani G.**, Pippia P., Meloni M.A. Effect of simulated microgravity conditions on talin binding to LFA-1 Integrin in Human T-lymphocytes. Italian Society for Space Biomedicine and Biotechnology 4th National Conference "Un mondo senza gravità", Santa Margherita Ligure, Italy. March 31 – April 2, 2009.
- Meloni M.A., **Pani G.**, Galleri G., Saba A., Pippia P., Cogoli-Greuter M. Microtubular network recovery in human monocytes in modeled low gravity after pretreatment with nocodazole. International Society for

Gravitational Physiology "30th Annual International Gravitational Physiology Meeting", Xi'an, China. May 24-29, 2009.

- Meloni M.A., Benotmane M.A., Mastroleo F., **Pani G.**, Abou-el-Ardat K., Janssen A. Leysen L., Vanhavere F., Leys L., Galleri G., Pippia P., Baatout S. Biological effect of simulated ISS ionizing radiation environment on Human T-lymphocytes. International Society for Gravitational Physiology "30th Annual International Gravitational Physiology Meeting", Xi'an, China. May 24-29, 2009.
- Saba A., Galleri G., **Pani G.**, Meloni M. A., Pippia P. *In vivo* physiological experiments in modeled microgravity (RPM) on rat bone marrow cell mineralization. International Society for Gravitational Physiology "30th Annual International Gravitational Physiology Meeting". Xi'an. China. May 24-29, 2009.
- **Pani G.**, Samari N., de Saint-Georges L., Meloni M.A., Baatout S, Van Oostveldt P., Benotmane M.A. Effect of space conditions on neuronal morphology. ELGRA Symposium: "In the Footsteps of Columbus", Bonn, Germany. September 1-4, 2009.
- Meloni M.A., Galleri G., **Pani G.**, SabaA., Pippia P., Cogoli-Greuter M. Human leucocytes in space: the "MIA" experiment. 81° SIBS conference and 4th ARNA conference "Nutrizione e Biologia Sperimentale nella Ricerca Umana e Animale, Cagliari, Italy. October 8-10, 2009.
- **Pani G.**, Samari N., de Saint-Georges L., Meloni M.A., Baatout S., Van Oostveldt P., Benotmane M.A. Radiation and low gravity effects on neuronal cell cultures. "9th European Workshop on Astrobiology" EANA'09 Brussels, Belgium. October 12-14, 2009.
- **Pani G.**, Meloni M. A., Baatout S., Saba A., Galleri G., Pippia P., Cogoli A., Cogoli-Greuter M. Human monocyte microtubular recovery in simulated low gravity after nocodazole exposure. "9th European Workshop on Astrobiology" EANA'09 Brussels, Belgium. October 12-14, 2009.
- **Pani G.**, Samari N., de Saint-Georges L., Meloni M.A., Baatout S., Van Oostveldt P., Benotmane M.A. Effects of radiation and low gravity on neuronal cell cultures. "BVAC/ABCA and NVC joint annual conference" Antwerp, Belgium. November 12-13, 2009.
- **Pani G.**, Meloni M. A., Baatout S., Saba A., Galleri G., Pippia P., Cogoli A., Cogoli-Greuter M. Effect of simulated low gravity on human monocyte microtubular recovery after nocodazole exposure. "BVAC/ABCA and NVC joint annual conference" Antwerp, Belgium. November 12-13, 2009.
- Samari N., **Pani G.**, de Saint-Georges L., Baatout S., Leyns L., Benotmane MA. Effect of low doses of radiation on neurite outgrowth and nervous network formation. The first joint meeting between the Belgian Society for Analytical Cytology (BVAC/ABCA) and the Dutch Society for Cytometry (NVC), Antwerpen, Belgium. November 12-13, 2009.
- **Pani G.**, Samari N., de Saint-Georges L., Meloni M., Baatout S., Van Oostveldt P., Benotmane MA. Effects of radiation and low gravity on neuronal cell cultures. 2009 first joint meeting between the Belgian Society for Analytical Cytology (BVAC/ABCA) and the Dutch Society for Cytometry (NVC), Antwerp, Belgium. October 12-13, 2009.
- Samari N., **Pani G.**, de Saint-Georges L., Baatout S., Leyns L., Benotmane MA. Effect of low doses of radiation on neurite outgrowth and nervous network formation. Second edition of the international conference on medical radiations: research and applications. Marrakech, Morocco. April 7-9, 2010.
- Samari N., **Pani G.**, de Saint-Georges L., Baatout S., Leyns L., Benotmane MA. Effect of low doses of radiation on neurite outgrowth and nervous network formation. PhD Research Day 2010. Vrije Universiteit Brussels (VUB), Belgium. May 28, 2010.
- Meloni M.A., **Pani G**., Benotmane M. A., Mastroleo F., Abou-el-ardat K., Janssen A., Leysen L., Vanhavere F., Leys N., Galler G., Pippia P., Baatout S. Effects of ISS equivalent ionizing radiation dose on Human T-lymphocytes. COSPAR 2010. Bremen, Germany. July 18-25, 2010.
- **Pani G.**, Meloni M., Galleri G., Saba A., Pippia P., Cogoli-Greuter M. Motility and cytoskeleton quantification in monocytes exposed to real low gravity aboard the International Space Station. Advanced Light Microscopy Symposium (ALM 2010), Ghent, Belgium. September 23-24, 2010.
- **Pani G.**, De Vos W., Samari N., de Saint-Georges L., Meloni M., Baatout S., e.a."DNA damage/repair dynamic in neuronal network after/during ionizing radiation exposure under low gravity conditions. Advanced Light Microscopy Symposium (ALM 2010), Ghent, Belgium. September 23-24, 2010.
- Samari N., Abouelaradat K., **Pani G.**, de Saint-Georges L., Baatout S., Leyns L., e.a. Low doses of irradiation on nervous cells impair neurite outgrowth and cause neuronal degeneration. DoReMi Wokshop meeting on Task 7.5, Mol, Belgium. September 29, 2010.
- Samari N., **Pani G.**, de Saint-Georges L., Baatout S., Leyns L., Benotmane R. Effect of low doses of radiation on neuronal plasticity and connectivity. Day of the PhD's. Mol, Belgium. October 28, 2010.
- Samari N., **Pani G.**, de Saint-Georges L., Baatout S., Leyns L., Benotmane R. Effect of low doses of radiation on neurite outgrowth and nervous network formation. The Belgian-Luxembourgish cytometry meeting 2010.- Luxembourg, Luxembourg. November 18-19, 2010.

- **Pani G.**, DeVos W., Samari N., de Saint-Georges L., Meloni M., Baatout S., e.a. DNA damage/repair dynamic in neuronal network after/during ionizing radiation exposure under low gravity conditions. The Belgian-Luxembourgish Cytometry Meeting 2010.- Luxembourg, Luxembourg. November 18-19, 2010.
- Samari N., **Pani G.**, de Saint-Georges L., Baatout S., Leyns L., Benotmane R. Effect of low doses of ionizing radiation on neurite outgrowth. 1st Periodic meeting of DoReMi. Brussels, Belgium. July 4-6, 2011.
- Samari N., **Pani G.**, de Saint-Georges L., Baatout S., Leyns L., Benotmane R. Effect of low doses of ionising radiation on neurite outgrowth. 8th IBRO World Congress of Neuroscience. Florence, Italy. August 14-18, 2011.
- **Pani G.**, Samari N., Quintens R., de Saint-Georges L., Meloni M., Baatout S., Van Oostveldt P., Benotmane M.A. Effect of space conditions on neuronal plasticity and connectivity. Day of the PhD's. Mol, Belgium. October 6, 2011.
- **Pani G.**, De Vos W.H., Samari N., de Saint Georges L., Meloni M.A., Baatout S., van Oostveldt P., Benotmane M.A. Effects of simulated low gravity on DNA damage/repair dynamics in neuronal network after/during ionizing radiation exposure. CAREX Conference on Life in Extreme Environments. Dublin, Ireland. October 18-20, 2011.
- **Pani G.**, Samari N., Quintens R., de Saint-Georges L., Baatout S., Van Oostveldt P., Van Oostveldt P., Benotmane M.A..- MorphoNeuroNet: an automated method for dense neuronal network analysis. 12th international meeting on advanced light microscopy. Leuven, Belgium. June 5-8, 2012.

Project proposals

- Proposal writing on “Morphological and molecular alterations on neuron cells during long exposure to space environment” under the supervision of SCK•CEN mentors: Drs. M.A. Benotmane, L. de Saint Georges and S. Baatout, Sassari University mentors: Dr. M.A. Meloni, Prof. P. Pippia. RIBES-Bion M1 mission, Space biological research opportunity. Submitted to ASI (Italian Space Agency) in June 2009 (Responsible: Dr. Meloni MariAntonia, Principal Investigator: PhD Student Pani Giuseppe)
- Participation in writing the proposal "Assessment of Neuronal Network Connectivity Under Space Conditions" ILSRA Announcement of Opportunity by ESA. Submitted to ESA in September 2009. (Coordinator: Dr. Abderrafi Benotmane).
- Participation in writing the proposal on "Effect of accelerated particles on neuronal network" . Announcement of opportunity for investigations into biological effects of radiation using the GSI accelerator facility (AO-10-IBER). Submitted to ESA in January 2011. (Coordinator: Dr. Abderrafi Benotmane).